

TRANSIENT DYNAMIC RESPONSE OF VISCOELASTIC CYLINDERS
ENCLOSED IN FILAMENT WOUND CYLINDRICAL COMPOSITES

A THESIS SUBMITTED TO
THE GRADUATE SCHOOL OF NATURAL AND APPLIED SCIENCES
OF
MIDDLE EAST TECHNICAL UNIVERSITY

BY

ÖZGE ŞEN

IN PARTIAL FULFILLMENT OF THE REQUIREMENTS
FOR
THE DEGREE OF DOCTOR OF PHILOSOPHY
IN
ENGINEERING SCIENCES

AUGUST 2005

Approval of the Graduate School of Natural and Applied Sciences

Prof. Dr. Canan ÖZGEN
Director

I certify that this thesis satisfies all the requirements as a thesis for the degree of Doctor of Philosophy.

Prof. Dr. M. Ruşen GEÇİT
Head of Department

This is to certify that we have read this thesis and that in our opinion it is fully adequate, in scope and quality, as a thesis for the degree of Doctor of Philosophy.

Prof. Dr. Doğan TURHAN
Supervisor

Examining Committee Members

Prof. Dr. Yusuf ORÇAN	(METU, ES)	<hr/>
Prof. Dr. Doğan TURHAN	(METU, ES)	<hr/>
Prof. Dr. Tekin GÜLTOP	(Gazi Un, CE)	<hr/>
Prof. Dr. Suha ORAL	(METU, ME)	<hr/>
Prof. Dr. Turgut TOKDEMİR	(METU, ES)	<hr/>

I hereby declare that all information in this document has been obtained and presented in accordance with academic rules and ethical conduct. I also declare that, as required by these rules and conduct, I have fully cited and referenced all material and results that are not original to this work.

Name, Last Name : Özge ŞEN

Signature :

ABSTRACT

TRANSIENT DYNAMIC RESPONSE OF VISCOELASTIC CYLINDERS ENCLOSED IN FILAMENT WOUND CYLINDRICAL COMPOSITES

Şen, Özge

Ph.D., Department of Engineering Sciences

Supervisor: Prof. Dr. Doğan Turhan

August 2005, 189 pages

In this study, transient dynamic response of viscoelastic cylinders enclosed in filament wound cylindrical composites is investigated. Thermal effects, in addition to mechanical effects, are taken into consideration. A generalized thermoelasticity theory which incorporates the temperature rate among the constitutive variables and is referred to as temperature-rate dependent thermoelasticity theory is employed. This theory predicts finite heat propagation speeds.

The body considered in this thesis consists of $n+1$ -layers, the inner layer being viscoelastic, while the outer fiber reinforced composite medium consist of n -different generally orthotropic, homogeneous and elastic layers. In each ply, the fiber orientation angle may be different. The body is a hollow circular cylinder with a finite thickness in the radial direction, whereas it extends to infinity in the axial direction. The multilayered medium is subjected to uniform time-dependent dynamic inputs at the inner and/or outer surfaces. The body is assumed to be initially at rest. The layers are assumed to be perfectly bonded to each other.

The case in which the inner surface of the viscoelastic cylinder is a moving boundary is further investigated in this study. This is similar to the solid

propellant rocket motor cases. The solid propellant is modelled as a viscoelastic material which in turn is modelled as standard linear solid; whereas, the rocket motor case is a fiber-reinforced filament wound cylindrical composite.

Method of characteristics is employed to obtain the solutions. Method of characteristics is suitable because the governing equations are hyperbolic. The method is amenable to numerical integration and different boundary, interface and initial conditions can be handled easily.

Key words: Filament wound cylindrical composites, viscoelasticity, standard linear solid, anisotropic elasticity, generalized thermoelasticity.

ÖZ

ELYAF SARGILI SİLİNDİRİK BİLEŞİK CİSİMLERLE ÇEVRELENMİŞ VİSKOELASTİK SİLİNDİRLERİN GEÇİCİ DİNAMİK DAVRANIŞI

Şen, Özge

Doktora, Mühendislik Bilimleri Bölümü

Tez Yöneticisi: Prof. Dr. Doğan Turhan

Ağustos 2005, 189 sayfa

Bu çalışmada, elyaf sargılı silindirik bileşik cisimlerle çevrelenmiş viskoelastik silindirlerin geçici dinamik davranışı incelenmektedir. Mekanik etkilere ek olarak ısı etkilere de gözönüne alınmaktadır. Bünye değişkenleri arasında sıcaklık değişim hızı da bulunan ve sıcaklık değişim hızına bağlı genelleştirilmiş termoelastisite teorisi olarak adlandırılan teori uygulanmaktadır. Bu teori sonlu ısı yayılma hızı içermektedir.

Bu tezde gözönüne alınan cisim $n+1$ tabakadan oluşmaktadır. En iç tabaka viskoelastik, dışındaki elyaf takviyeli bileşik ortam ise n farklı genel ortotrop, homojen ve elastik tabakadan oluşmaktadır. Her bir tabakada, elyaf doğrultu açısı farklı olabilmektedir. Cisim, içi boş bir dairesel silindir olup, radyal doğrultuda sonlu kalınlıkta, aksel doğrultuda ise sonsuza uzanmaktadır. Çok tabakalı ortamın iç ve/veya dış yüzeyleri zamana bağlı düzgün dinamik etkilere maruzdur. Cismin başlangıçta sükunet halinde olduğu varsayılmaktadır. Tabakalar birbirlerine mükemmel olarak yapıştırılmışlardır.

Viskoelastik silindirin iç yüzeyinin hareket eden bir sınır yüzeyi olması hali de bu çalışmada incelenmektedir. Bu durum katı yakıtlı roket motorundaki duruma

benzemektedir. Katı roket yakıtı viskoelastik malzeme ve viskoelastik malzeme de standart doğrusal katı olarak modellenirken, roket motor gövdesi elyaf sargılı silindirik bileşik cisim olarak alınmıştır.

Çözümleri elde etmek için karakteristikler yöntemi uygulanmaktadır. Davranışı tanımlayan alan denklemlerinin hiperbolik olmasından dolayı karakteristikler yöntemi uygundur. Yöntem sayısal integrasyonu kolaylıkla mümkün kılar ve değişik sınır, arayüzey ve başlangıç şartları kolaylıkla ele alınabilir.

Anahtar kelimeler: Elyaf sargılı silindirik bileşik cisimler, viskoelastisite, standart doğrusal katı, anizotrop elastisite, genelleştirilmiş termoelastisite.

To Hale and Öykü Doğa

ACKNOWLEDGMENTS

I would like to express my deepest gratitude and appreciation to my supervisor, Prof. Dr. Doğan TURHAN whose guidance, advice, criticism, encouragements and insight were invaluable in carrying out and completing this study.

I would also like to express my appreciation to thesis supervising committee members Prof. Dr. Suha ORAL and Prof. Dr. Turgut TOKDEMİR for their guidance, advice and helpful discussions we have made throughout the study.

This work has been supported by TÜBİTAK-SAGE. I would like to thank TÜBİTAK-SAGE for providing the technical support, computational power and literature sources which were enormously important for the study.

I would also like to give my special thanks to Dr. Mutlu D. CÖMERT, the coordinator of Weapon Systems and Control Technologies Group, Dr. Serkan GÖZÜBÜYÜK, Head of Structure Mechanics Division and the members of TÜBİTAK-SAGE Structure Mechanics Division for their help and understanding.

I wish to express my thanks to my parents, father-in-law and mother-in-law for their moral support, encouragement and continuous support all through this study.

Finally, my wife Hale and 5-years old daughter Öykü Doğa bore the brunt of this effort as much as I did myself. My thanks and love, now and always, to them.

TABLE OF CONTENTS

PLAGIARISM.....	iii
ABSTRACT	iv
ÖZ.....	vi
DEDICATION	viii
ACKNOWLEDGMENTS.....	ix
TABLE OF CONTENTS	x
LIST OF FIGURES.....	xiii
CHAPTER	
1. INTRODUCTION.....	1
2. MECHANICAL RESPONSE OF VISCOELASTIC CYLINDERS ENCLOSED IN FIBER-REINFORCED CYLINDRICAL COMPOSITES ..	13
2.1 Introduction	13
2.2 The Fundamental Equations of the Linear Theory of Elasticity for Orthotropic Materials and Viscoelasticity Theory for Isotropic Materials in Cylindrical Coordinates	14
2.3 Formulation of the Problem	21
2.4 The Method of Characteristics and the Canonical Form of the Governing Equations for the Viscoelastic Layer	26
2.5 The Method of Characteristics and the Canonical Form of the Governing Equations for the Orthotropic Layer	34
2.6 Integration of the Canonical Equations for the Viscoelastic Layer	40
2.7 Integration of the Canonical Equations for the Orthotropic Layers	47
2.8 Modification of the Equations for the Boundary and Interface Elements	49

2.9 Ablating Inner Boundary	52
2.10 The Solution Procedure	55
2.11 Numerical Examples and Discussion of the Results	60
 3. THERMOMECHANICAL RESPONSE OF FIBER-REINFORCED CYLINDRICAL COMPOSITES	 76
3.1 Introduction	76
3.2 Basic Equations of the Temperature Rate Dependent Thermoelasticity (TRDTE) for Orthotropic Materials in Cylindrical Composites	77
3.3 Formulation of the Problem	81
3.4 The Method of Characteristics and the Canonical Form of the Governing Equations	84
3.5 Integration of the Canonical Equations	92
3.6 Modification of the Equations for the Boundary and Interface Elements	97
3.7 Numerical Examples and Discussion of the Results	100
 4. THERMOMECHANICAL RESPONSE OF VISCOELASTIC CYLINDERS ENCLOSED IN FIBER-REINFORCED CYLINDRICAL COMPOSITES	 117
4.1 Introduction	117
4.2 Basic Equations of the Generalized Thermo-Viscoelasticity for Isotropic Materials in Cylindrical Composites	118
4.3 Formulation of the Problem	119
4.4 The Method of Characteristics and the Canonical Form of the Governing Equations for the Thermo-Viscoelastic Layer	122
4.5 Integration of the Canonical Equations for the Thermo-Viscoelastic Layer	134

4.6 Modification of the Equations for the Boundary and Interface Elements	140
4.7 Numerical Examples and Discussion of the Results	142
5. CONCLUSIONS	153
REFERENCES.....	157
APPENDICES	
A. METHOD OF CHARACTERISTICS.....	173
B. MANUALS FOR COMPUTER PROGRAMS	177
B.1 Input data file for MECHANICAL	178
B.2 Input data file for MOVING-MECHANICAL.....	179
B.3 Input data file for THERMO-MECHANICAL	180
B.4 Input data file for INVISTHERMO-MECHANICAL.....	181
CURRICULUM VITAE	185

LIST OF FIGURES

FIGURES

2.1. Filament wound fiber-reinforced circular cylindrical composite.	18
2.2. Model of viscoelastic material: standard linear solid.	20
2.3. Network of the characteristic lines on the $(r - t)$ plane.	31
2.4. Typical interior integration element in the viscoelastic layer.....	46
2.5. Description of characteristic lines with a moving inner boundary for the encased viscoelastic cylinder.....	56
2.6. Detailed description of elements T and P on the $(r - t)$ plane.....	57
2.7. Variation of radial pressure applied at the inner surface.	61
2.8. Variation of radial normal stress $-\sigma_{rr} / P_0$ with respect to time \bar{t} at location $\bar{r} = 1.5$ in the viscoelastic layer for non-ablating inner surface.	67
2.9. Variation of circumferential normal stress $\sigma_{\theta\theta} / P_0$ with respect to time \bar{t} at location $\bar{r} = 2.15$ for non-ablating inner surface.	68
2.10. Variation of circumferential normal stress $\sigma_{\theta\theta} / P_0$ with respect to time \bar{t} at location $\bar{r} = 2.15$ for ablating and non ablating inner surfaces.	68

2.11. Variations of non-dimensional stresses with respect to time \bar{t} at location $\bar{r} = 1.25$ for the cylindrical laminate with five generally orthotropic layers.	69
2.12. Variation of radial stress $-\sigma_{rr}^{(v)} / P_0$ with time \bar{t} at location $\bar{r} = 1.5$ in the viscoelastic layer for the ablating and non ablating inner surfaces.	72
2.13. Variation of circumferential stress $-\sigma_{\theta\theta}^{(v)} / P_0$ with time \bar{t} at location $\bar{r} = 1.5$ in the viscoelastic cylinder for non ablating inner surface.	73
2.14. Variation of radial stress $-\sigma_{rr}^{(v)} / P_0$ with time \bar{t} at location $\bar{r} = 2$, the interface between the viscoelastic and first orthotropic layer, for non-ablating inner surface.	73
2.15. Variation of circumferential stress $-\sigma_{\theta\theta}^{(v)} / P_0$ with time \bar{t} at location $\bar{r} = 2$, the interface between the viscoelastic and first orthotropic layer for non-ablating inner surface.	74
2.16. Variation of circumferential stress $\sigma_{\theta\theta}^{(1)} / P_0$ with time \bar{t} at location $\bar{r} = 2$, the interface between the viscoelastic and first orthotropic layer, for non ablating inner surface.	74
2.17. Variation of radial stress $-\sigma_{rr}^{(2)} / P_0$ with time \bar{t} at location $\bar{r} = 2.15$ in the second orthotropic layer for non ablating inner surface.	75
2.18. Variation of circumferential stress $\sigma_{\theta\theta}^{(2)} / P_0$ with time \bar{t} at location $\bar{r} = 2.15$ in the second orthotropic layer for ablating and non-ablating inner surfaces.	75
3.1. Description of the network of characteristic lines for the thermoelastic layered medium.	90

3.2. Typical interior integration element in the orthotropic layer.....	95
3.3. Variation of temperature deviation at the boundary.	103
3.4. Variation of non-dimensional temperature deviation with respect to distance at various non-dimensional times for an unbounded body with a cylindrical hole.	104
3.5. Variation of non-dimensional heat flux with respect to distance at various non-dimensional times for an unbounded body with a cylindrical hole.....	104
3.6. Variation of non-dimensional radial stress with respect to distance at various non-dimensional times for an unbounded body with a cylindrical hole	105
3.7. Variation of radial stress $\bar{\sigma}_{rr}$ with time \bar{t} at $\bar{r} = 1.15$, for the laminate with alternating isotropic layers.	108
3.8. Variation of circumferential stress $\bar{\sigma}_{\theta\theta}$ with time \bar{t} at $\bar{r} = 1.15$, for the laminate with alternating isotropic layers.....	109
3.9. Variation of radial stress $\bar{\sigma}_{rr}$ with time \bar{t} at $\bar{r} = 1.25$, for the laminate with alternating isotropic layers.	109
3.10. Variation of circumferential stress $\bar{\sigma}_{\theta\theta}$ with time \bar{t} at $\bar{r} = 1.25$, for the laminate with alternating isotropic layers.....	110
3.11. Variation of radial normal stress $-\bar{\sigma}_{rr}$ with time \bar{t} at location $\bar{r} = 1.15$ for the laminate with generally orthotropic layers having stacking sequence 30/-30/90/0/90.....	114

3.12. Variation of circumferential normal stress $\bar{\sigma}_{\theta\theta}$ with time \bar{t} at location $\bar{r} = 1.15$, for the laminate with generally orthotropic layers having stacking sequence 30/-30/90/0/90.....	114
3.13. Variation of circumferential normal stress $\bar{\sigma}_{\theta\theta}$ with time \bar{t} at location $\bar{r} = 1.45$ for the laminate with generally orthotropic layers having stacking sequence 30/-30/90/0/90.....	115
3.14. Variation of radial normal stress $-\bar{\sigma}_{rr}$ with time \bar{t} at location $\bar{r} = 1.15$ for the laminate with generally orthotropic layers having stacking sequence 30/-30/30/-30/30.	115
3.15. Variation of circumferential normal stress $\bar{\sigma}_{\theta\theta}$ with time \bar{t} at location $\bar{r} = 1.15$, for the laminate with generally orthotropic layers having stacking sequence 30/-30/30/-30/30.	116
3.16. Variation of circumferential normal stress $\bar{\sigma}_{\theta\theta}$ with time \bar{t} at location $\bar{r} = 1.45$ for the laminate with generally orthotropic layers having stacking sequence 30/-30/30/-30/30.	116
4.1. Network of characteristic lines including viscoelastic layer.	131
4.2. Variation of radial normal stress $\bar{\sigma}_{rr}$ with time \bar{t} at location $\bar{r} = 1.05$, middle of viscoelastic layer.	149
4.3. Variation of circumferential normal stress $\bar{\sigma}_{\theta\theta}$ with time \bar{t} at location $\bar{r} = 1.05$, middle of viscoelastic layer.	149
4.4. Variation of radial normal stress $\bar{\sigma}_{rr}$ with time \bar{t} at location $\bar{r} = 1.15$, middle of first orthotropic layer.....	150

4.5. Variation of circumferential normal stress $\bar{\sigma}_{\theta\theta}$ with time \bar{t} at location $\bar{r} = 1.15$, middle of first orthotropic layer.....	150
4.6. Variation of radial normal stress $\bar{\sigma}_{rr}$ with time \bar{t} at location $\bar{r} = 1.3$, interface between second and third orthotropic layers.	151
4.7. Variation of circumferential normal stress $\bar{\sigma}_{\theta\theta}$ with time \bar{t} at location $\bar{r} = 1.3$ on the side of second layer at the interface between second and third orthotropic layers.	151
4.8. Variation of circumferential normal stress $\bar{\sigma}_{\theta\theta}$ with time \bar{t} at location $\bar{r} = 1.3$ on the side of third layer, at the interface between second and third orthotropic layers.	152
A.1. Position of the singular point.	174

CHAPTER 1

INTRODUCTION

In recent years, the use of advanced composite materials has increased tremendously due to their superior properties. They are found in different areas of applications ranging from space vehicles to sports equipment. As people demand products with superior properties, the use of composites will continue to increase; especially, in the construction of solid propellant rocket motors, space and aircraft vehicles, in which weight is a significant factor. Among composite materials, fiber-reinforced polymer composites found a wide range of applications because of their excellent properties, like high strength-to-weight or stiffness-to-weight ratios and easy manufacturing processes. The analysis of composites, however, is more difficult compared to conventional materials because of the anisotropy and inhomogeneity inherent in these materials.

Many researchers have investigated transient wave propagation through layered media. Most of these works are concentrated on solving elastic problems, but relatively less work is directed to analyzing wave propagation in anisotropic and/or viscoelastic layered media. Early analytical treatment of the subject can be found in Ewing, Jardetzky and Press [1] and in Brekhovskikh [2]. Among more recent books treating harmonic and transient wave propagation in elastic layered media with isotropic and anisotropic layers, we can mention Kennet [3], Tygel and Hubral [4], Van der Hijden [5], Nayfeh [6], Achenbach [7] and Miklowitz [8]. Elegant analytical and numerical techniques based on Green's function formulations, integral transforms, inversion of integral transforms by Cagniard-de Hoop method and asymptotic techniques can be found in these books.

Different methodologies have been employed to study harmonic and transient waves in layered media. Approximate models have been developed and employed which yield satisfactory results when the thickness of the layers are small compared to the wavelengths of the propagating waves, for example, Sun et al. [9], Achenbach et. al. [10], Santosa and Symes [11], Soldatos [12], Noor et al. [13]. Exact methods of elasticity theory have been employed to investigate harmonic wave propagation in multilayered elastic media with isotropic and anisotropic layers which are valid for any wavelength [14-18]. The construction of a steady state Green's function for a laminated circular cylinder is given by Zhuang et al. [19].

Transient axisymmetric wave propagation in weakly coupled layered structures is investigated in [20-21]. Two different computational approaches, one based on the numerical inversion of Fourier and Hankel transforms and the other on finite element method (FEM) are employed in [21]. Rizzi and Doyle [22] developed a spectral element approach based on fast Fourier transform (FFT) and applied it to study transient waves in elastic layered solids. Transfer matrix method was employed by Kundu and Mal [23] to study wave propagation in multilayered solids with isotropic layers and by Mal [24] in laminated composites with anisotropic layers, namely transversely isotropic layers, subjected to periodic surface loads. A multiple transform technique coupled with a matrix method was used to investigate the elastodynamic response of a unidirectional composite laminate to concentrated surface loads in [25-26] and the response of multilayered composite laminates consisting of transversely isotropic layers with arbitrarily oriented symmetry axes to dynamic surface loads in [27].

Compared to the extensive research on wave motion in multilayered elastic media, transient wave propagation in viscoelastic layered media has been investigated relatively less. Approximate theories have been developed by Mengi and Turhan [28] for viscoelastic layered composites with plane layers and by Mengi and Birlik [29] for viscoelastic cylindrical laminated composites. The validity of these approximate theories were assessed by solving a transient [30] and a harmonic wave propagation problem [31]. An analytical method is presented to study the

propagation of plane harmonic waves in an infinite periodically laminated viscoelastic medium in [32]. An exact viscoelastic analogy relation between a periodically layered elastic medium and a homogeneous viscoelastic medium was introduced by Han and Sun in [33]. The problem of reflection and refraction of micropolar elastic waves at a loosely bonded interface between a viscoelastic solid and a micropolar elastic solid is studied by Singh and Kumar [34]. Most of the existing work on transient wave motion in viscoelastic layered media deals with one-dimensional wave propagation normal to the layering [35-37]. Two dimensional transient wave propagation in a viscoelastic sandwich plate was investigated by Nkemzi and Green [38]. Propagation of two-dimensional transient out of plane shear waves in multilayered viscoelastic media and transient waves in viscoelastic cylindrical layered media are investigated by Abu-Alshaikh, Turhan and Mengi [39], [40]. An effective numerical method for solving elastic wave propagation problems in an infinite Timoshenko beam on viscoelastic foundation in time domain was given in [41]. Inhomogeneous plane, monochromatic waves traveling in viscoelastic media are considered in [42].

The method of characteristics has been employed effectively in investigating transient wave propagation problems in layered media. Among many contributions in this area, we can mention those presented in [43-48], which involve investigation of wave propagation in layered elastic cylindrical and spherical media, and infinite elastic media having cylindrical and spherical cavities. The method of characteristics is also employed by Turhan et. al [49-50] in solving problems of viscoelastic layered media with layers modeled as standard linear solid (with one discrete relaxation time). Solution of transient wave propagation in a linear viscoelastic solid with more than one discrete relaxation time is presented by Wegner and Haddow [51]. The same procedure is employed by Wegner [52] in solving waves generated from a spherical cavity in a viscoelastic infinite medium with one and two discrete relaxation times.

Thermal effects are also taken into consideration in many studies in which wave propagation problems are investigated. The conventional thermoelasticity

theory is based, among other constitutive relations, on the classical Fourier's law. The formulation of this theory were laid in the first half of the 19th century [53], but a satisfactory formulation of the dynamical version of the theory, based on firm grounds of irreversible thermodynamics, was presented half a century back [54] to eliminate the paradox inherent in the uncoupled theory that elastic changes have no effect on the temperature. The theory is now proved to be an elegant model for studying coupled effects of elastic and thermal fields, and important contributions, for example of Chadwick [55], Boley and Wiener [56], Carlson [57], Nowacki [58], Parkus [59], Nowinski [60] and Dhaliwal and Singh [61] contain comprehensive accounts of the theory and applications thereof.

The thermoelasticity theory presented in detail in Refs. [53-61] and referred to conventional thermoelasticity (CTE) hereafter, with all its merits, suffer from the deficiency of allowing infinite heat propagation speed contrary to physical observations. During the last four decades, attempts have been made to remove this deficiency on various grounds, and generalized versions of the theory have come into existence. The simplest way of removing the paradox of infinite heat propagation speed present in conventional thermoelasticity is to replace the classical Fourier's law by a generalized conduction equation. We then arrive at a straightforward extension of CTE, each of the equations of this system is hyperbolic type, and consequently no solution of the system can extend to infinity. In what follows, we shall refer to the new theory as extended thermoelasticity, or, briefly, ETE. This theory is often referred to as thermoelasticity with thermal relaxation or thermoelasticity with one relaxation time.

The equations of generalized thermoelasticity with one relaxation time for a homogeneous medium were derived by Lord and Shulman [62]. Dhaliwal and Sherief [63] obtained the corresponding equations for a general anisotropic medium. These equations admit the so-called second sound effect in solids; i.e. they predict finite speeds of propagation for heat and mechanical disturbances.

The half space problem in ETE has been studied by several authors under various boundary conditions. Lord and Shulman [62], Achenbach [64], Norwood and Warren [65], Mengi and Turhan [66], Chandrasekharaiah and Srinath [67] have investigated the cases of step function in stress/strain and/or step function in temperature on the boundary. The problem of an infinitely long solid conducting circular cylinder whose lateral surface is traction free and subjected to known surrounding temperatures in the presence of a uniform magnetic field in the direction of the axis has been investigated by Sherief [68]. Using Laplace transform technique in the solution, as in [68], Sherief and Anwar [69] consider the problem of an infinitely long annular cylinder whose inner and outer surfaces are subjected to known surrounding temperatures and are traction free. The plane wave propagation in a generalized thermo-microstretch solid is investigated in [70]. Sherief and Dhaliwal [71] solved a thermal shock problem; Sherief [72] solved a spherically symmetric problem with a point source. Both of these problems are valid for short times. Sherief and Ezzat have obtained the fundamental solution for thermoelasticity with one relaxation time valid for all times [73]. The uniqueness theorem for the equations of generalized thermoelasticity with one relaxation time, derived by Dhaliwal and Sherief [63], is proved by [74]. The distribution of temperature, displacement and stress in infinite homogeneous transversely isotropic elastic solid having a cylindrical hole has been investigated by taking (i) unit step function in stress and zero temperature change, and (ii) unit step function in temperature and zero stress, at the boundary of the cylindrical hole using Laplace Transform in [75]. Thermal shock on the boundary of a half space is also investigated in [76, 77]. The analysis in the former one is based on the decoupled field equations of generalized thermoelasticity. Equations have been solved with the help of integral transforms. Thermal shock at the surface of a half space is further investigated in [78]. The model of the equations of generalized thermoelasticity with thermal relaxation in an isotropic elastic medium with temperature dependent mechanical properties is established in [79]. At this study, the state space approach is adopted for the solution of one-dimensional problems in the absence or presence of heat sources. State-space approach is also applied for the solutions at [80]. A reciprocal theorem is presented for initial mixed boundary conditions in the framework of the linearized isotropic

thermoelasticity theory of Lord and Shulman in [81]. Eigenvalue approach is applied to the solutions of generalized thermoelasticity with one relaxation time in [82, 83]. A number of thermoelastic wave problems which involve one or two space variables, are treated in a uniform manner, by a system of first order partial differential equations with stress, velocity, heat flow and temperature in [84]. The system of equations are analyzed by the method of characteristics in the study. Nonlinear continuum mechanics techniques are applied to the constitutive equations in [85]. In this study same exact solutions are given to illustrate novel features of the nonlinear theory. For different boundary conditions, in particular for those arising in pulsed laser heating of solids, the exponential stability of the hyperbolic linear system is proved in [86]. In this study, linear and non-linear thermoelastic systems in one space dimension where thermal disturbances modeled propagating as wave like pulses traveling at finite speed using Cattaneo's law for heat conduction is considered.

Only a few authors have considered problems on inhomogenous and/or anisotropic layered media employing generalized thermoelasticity. Mengi and Turhan [87] have made a detailed analysis of problems concerned with inhomogeneous and isotropic half space, and infinite space with spherical and cylindrical cavity, by using the method of characteristics. Kolyano and Shter [88], [89] have derived the governing equations for anisotropic and inhomogeneous medium and studied transverse oscillations of an inhomogeneous and isotropic cantilever beam. Sharma and Sidhu [90] studied propagation of plane harmonic waves in anisotropic generalized thermoelasticity. Propagation of thermoelastic waves in arbitrary anisotropic layered plates and general anisotropic media is investigated in the context of the generalized theory of thermoelasticity in [91] and [92]. The propagation of harmonic waves in a laminated anisotropic plate is studied in [93]. Transient wave propagation in thermoelastic layered composites consisting of alternating isotropic, homogenous, and linearly elastic high strength reinforcing and low strength matrix layers is investigated by Turhan et. al [94] by employing the thermoelasticity theory of Lord and Shulman [62].

Another generalization of the coupled theory of thermoelasticity is known as the thermoelasticity with two relaxation times, which, in other words, is known as temperature rate dependent thermoelasticity. Muller [95] in a review of thermodynamics of thermoelastic solids has proposed an entropy production inequality, with the help of which, he considered restrictions on a class of constitutive equations. A generalization of this inequality was proposed by Green and Laws [96]. Green and Lindsay obtained an explicit version of the constitutive equations in [97]. These equations were also obtained independently by Şuhubi [98]. This theory also predicts finite speeds of propagation as in Lord and Shulman's theory [62]. It differs from the latter in that Fourier's law of heat conduction is not violated if the body under consideration has a center of symmetry. Erbay and Suhubi [99] have studied wave propagation in infinite cylinders employing this version of generalized thermoelasticity with two relaxation times. The dispersion relation is obtained for the case in which the temperature is kept constant on the surface of the cylinder. Ignaczak [100] studied a strong discontinuity wave and obtained a decomposition theorem for this theory [101]. Sherief has obtained the fundamental solutions for generalized thermoelasticity with two relaxation times for point source of heat [102]. In this study, Laplace transform techniques together with the method of potentials are used to obtain the temperature and stress distributions. Sherief, also studied a half space problem employing the equations of generalized thermoelasticity with two relaxation times [103]. In this study, the bounding plane is acted upon by a combination of a thermal and a mechanical shock acting for a finite period of time. Using the theory of linear thermoelasticity proposed by Green and Lindsay [97], Payne and Song [104] treat the thermoelastic problem for a semi-infinite cylinder where the lateral surface of the cylinder is held either at zero temperature and zero displacement, or at zero heat flux and zero traction. The two dimensional thermoelasticity problem for a half space whose surface is traction free and subjected to the effects of heat sources is considered within the context of the theory of thermoelasticity with two relaxation times in [105]. Sherief and Megahed studied the two dimensional axisymmetric problem within the context of the theory of thermoelasticity with two relaxation times in spherical regions [106]. In the study, the general solution is obtained in the Laplace transform domain by using a direct

approach without the use of potential functions. The resulting formulation is utilized to solve a problem for a thick spherical shell. The surface of the shell is taken as traction free and subjected to given axisymmetric temperature distributions. A new time domain boundary element formulation and solution procedure for generalized dynamic coupled thermoelasticity is developed by Polyzos and Beskos [107]. Temperature rate dependent thermoelasticity theory is employed to study the distribution of temperature, deformation and stresses in an infinitely extended isotropic elastic thin plate containing a circular hole for step input at temperature or step input at stress in [108]. Balta and Suhubi developed a theory of nonlocal generalized thermoelasticity within the framework of the nonlocal continuum mechanics [109]. The disturbance due to mechanical and thermal sources in a homogeneous, isotropic, micropolar generalized thermoelastic half-space is investigated in [110]. In the solution, Laplace Fourier transform technique is used. Daneshjoo and Romazani proposed a new mixed finite element formulation to analyze transient coupled thermoelastic problems [111]. The non-classical (Green-Lindsay) coupled model of dynamic thermoelasticity is applied to a laminated composite plate in this study.

In addition to the references cited above, many other authors have employed extensively generalized thermoelasticity theories with one and two relaxation times in harmonic and transient wave propagation problems in nonpolar and micropolar media. Among these, we can mention Refs. [112-121]. A comprehensive survey of the literature on generalized thermoelasticity theories is given in two review papers by Chadrasekharaiah [122-123]. One can also refer to Hetnarski and Ignaczak [124] for a review and presentation of the generalized theories of thermoelasticity.

Compared to the extensive literature on elastic wave propagation in generalized thermoelastic media, relatively less work can be found on transient wave propagation in generalized thermo-viscoelastic media. In the theories of generalized thermo-viscoelasticity, two models have found wide acceptance. In the first model of the equations of generalized thermoviscoelasticity, the relaxation effects of the volume are ignored, and, only, relaxation effects for stress deviators are taken

account. Hence, in this model, viscoelastic constitutive equations of differential or integral type are considered for the stress deviators; whereas, for the spherical stress $\sigma = \sigma_{kk} = \sigma_{11} + \sigma_{22} + \sigma_{33}$, constitutive equation in the same form as that of generalized thermoelasticity theories is considered. The equations of this model with one relaxation time and with two relaxation times are established by Ezzat and coworkers [125-126]. This model has further been developed and has been applied to various problems by different authors among which we can mention [127-129]. In the second model of the equations of generalized thermo-viscoelasticity, the relaxation effects of the volume as well as the relaxation effects for the stress deviators are taken into consideration. The equations of this model for isotropic media are established in [130-131].

In this thesis transient dynamic response of viscoelastic cylinders enclosed in filament wound cylindrical composites is investigated. The filament wound cylindrical composite consists of generally orthotropic elastic layers. A lamina reinforced by unidirectional fibers in which the principal material directions, that is, the fiber direction and the directions normal to the fiber direction coincide with the natural body coordinate axes is said to be a specially orthotropic lamina. In the case of a cylindrical lamina, the natural body coordinate axes are in the axial, circumferential and radial directions. If the fiber direction and the directions normal to it do not coincide with the natural body coordinate axes, the lamina is said to be a generally orthotropic lamina. Thermal effects in addition to mechanical effects are taken into consideration as well. A generalized thermoelasticity theory which incorporates the temperature rate among the constitutive variables and is referred to as temperature rate dependent thermoelasticity is applied to the outer elastic layers; whereas, generalized thermo-viscoelasticity is employed for the inner isotropic viscoelastic layer. These generalized theories predict finite heat propagation speeds.

The body considered in this thesis consists of $n+1$ layers, the inner layer being viscoelastic, while the outer fiber reinforced composite medium consists of n -different generally orthotropic, homogenous and elastic layers. In each ply the fiber orientation may be different. The body is a hollow circular cylinder with a finite

thickness in the radial direction, whereas it extends to infinity in the axial direction. The multilayered medium is subjected to uniform time-dependent dynamic inputs at the inner and/or outer surfaces. The body is assumed to be initially at rest. The layers are assumed to be perfectly bonded to each other. The material of the viscoelastic layer is modeled as standard linear solid.

The case in which the inner surface of the viscoelastic cylinder is a moving boundary is further investigated in this study. This is similar to the solid propellant rocket motor cases. The solid propellant is modeled as a viscoelastic material which in turn is modeled as standard linear solid; whereas, the rocket motorcase is a fiber-reinforced filament wound cylindrical composite. As the propellant burns, the inner surface moves outwards, decreasing the thickness of the viscoelastic layer representing the solid propellant.

The governing field equations of temperature-rate dependent anisotropic thermoelasticity and isotropic thermo-viscoelasticity are applied to the elastic layers and the inner viscoelastic layer, respectively, and the solutions are required to satisfy the continuity conditions at the interfaces of the layers, the boundary conditions at the inner and outer surfaces and the initial conditions.

Method of characteristics is employed to obtain the solutions. This method is suitable because the governing equations are hyperbolic. In the method of characteristics, the governing partial differential equations are transformed into a system of ordinary differential equations each of which is valid along a different family of characteristic lines. These equations are suitable for numerical integration and computer programming. Furthermore different interface, initial and boundary conditions can be handled easily in the method of characteristics. The convergence and stability of the method are well established. Sharp variations in the field variables at the wave fronts can be accommodated in the method. More information about the method can be found in Courant and Hilbert [132]. The method as applied in this thesis, however, is closer to the format applied by Mengi and McNiven [133].

The study is organized as follows: In Chapter 2, dynamic response of viscoelastic cylinders enclosed in filament wound cylindrical composites, with thermal effects neglected, is investigated. The cases of both the ablating and the non-ablating inner surface are considered. In the numerical examples, solid propellant material properties are taken for the inner viscoelastic layer modeled as standard linear solid. The striking effects of solid propellant material properties on the curves denoting the time variations of stresses at different locations are pointed out and discussed. The effects of moving inner boundary are also discussed.

In Chapter 3, thermomechanical response of fiber-reinforced cylindrical composites consisting of only generally orthotropic elastic layers is investigated. In composite material applications, cylindrical laminated composites consisting of all elastic orthotropic layers is very important. Hence, this chapter is devoted to elastic multilayered medium with no inner viscoelastic layer. Thermal effects, in addition to mechanical effects, are taken into consideration as well. A generalized thermoelasticity theory which incorporates the temperature rate among the constitutive variables and is referred to as temperature-rate dependent thermoelasticity theory is employed. This theory is also known as generalized thermoelasticity theory with two relaxation times. In the numerical examples, curves denoting the time variations of stresses at different locations are given for both the case where the thermal effects are neglected and the case where the thermal effects are taken into consideration. The effects of thermal dispersion on the wave profiles are discussed.

In Chapter 4, thermomechanical response of viscoelastic cylinders enclosed in fiber-reinforced cylindrical composites is investigated. The multilayered medium, then consists of n generally orthotropic elastic layers and an isotropic viscoelastic inner layer. Equations of generalized thermoelasticity are applied to the elastic layers; whereas equations of generalized thermo-viscoelasticity, in which relaxation effects of the volume are neglected, are applied to the inner viscoelastic layer. Numerical examples are worked out in which the inner surface of the multilayered body is subjected to uniform time-dependent pressure and uniform time dependent

temperature deviation, while the outer surface is free of surface tractions and temperature deviation is kept zero. The effects of refractions and reflections of waves at the boundaries and at the interfaces of the layers and the effects of geometric and thermal dispersions on the wave profiles are discussed.

The conclusions are presented in Chapter 5. The manual of the computer programs developed in the study are given in Appendix B.

CHAPTER 2

MECHANICAL RESPONSE OF VISCOELASTIC CYLINDERS ENCLOSED IN FIBER-REINFORCED CYLINDRICAL COMPOSITES

2.1 Introduction

In this chapter, dynamic response of viscoelastic cylinders enclosed in filament wound cylindrical composites is investigated. Only mechanical effects are considered in this chapter. The body consists of $n+1$ -layers, the inner layer being viscoelastic, while the outer being fiber-reinforced composite consisting of n -different generally orthotropic, homogeneous and linearly elastic layers. In each ply, the ply orientation angle may be different. The body is a hollow circular cylinder with a finite thickness in the radial direction, whereas it extends to infinity in the axial direction. The multilayered medium is subjected to uniform time-dependent dynamic inputs at the inner and/or outer surfaces. The body is assumed to be initially at rest. The layers are assumed to be perfectly bonded to each other. The material of the viscoelastic layer is modelled as standard linear solid.

The case in which the inner surface of the viscoelastic cylinder is a moving boundary is further investigated in this chapter. This is similar to the solid propellant rocket motor cases. The solid propellant is modelled as a viscoelastic material which in turn is modelled as standard linear solid; whereas, the rocket motor case is a fiber-reinforced filament wound cylindrical composite. As the solid propellant burns, the inner surface moves outwards, decreasing the thickness of the viscoelastic layer representing the solid propellant.

The governing field equations of isotropic viscoelasticity and anisotropic elasticity are applied to the inner viscoelastic layer and each outer elastic layer, respectively, and the solutions are required to satisfy the continuity conditions at the interfaces of the layers, the boundary conditions at the inner and outer surfaces and

the initial conditions.

Method of characteristics is employed to obtain the solutions. Method of characteristics is suitable because the governing equations are hyperbolic. In the method of characteristics, the governing partial differential equations are transformed into a system of ordinary differential equations each of which is valid along a different family of characteristic lines. These equations are suitable for numerical integration and computer programming. Furthermore, different interface, initial and boundary conditions can be handled easily in the method of characteristics. The convergence and stability of the method are well established. Sharp variations in the field variables at the wavefronts can be accommodated in the method of characteristics. Details of the method of characteristics can be found in Courant and Hilbert [132]. The way it is applied in this study, however, is closer to that applied by McNiven and Mengi [133].

2.2 The Fundamental Equations of the Linear Theory of Elasticity for Orthotropic Materials and Viscoelasticity Theory for Isotropic Materials in Cylindrical Coordinates

This part summarizes the basic equations of the theory of linear viscoelasticity and anisotropic elasticity in cylindrical coordinates. These equations are the stress equations of motion, strain-displacement relations and the stress-strain relations for a generally orthotropic elastic material and isotropic viscoelastic material. Derivations can be found in Refs [134-136]. The constitutive equations of orthotropic layers are expressed in the transformed form of stiffness coefficients [137-138].

The stress equations of motion in cylindrical coordinates for a three dimensional body are [134].

$$\frac{\partial \sigma_{rr}}{\partial r} + \frac{1}{r} \frac{\partial \sigma_{r\theta}}{\partial \theta} + \frac{\partial \sigma_{rz}}{\partial z} + \frac{\sigma_{rr} - \sigma_{\theta\theta}}{r} + f_r = \rho \frac{\partial^2 u_r}{\partial t^2} \quad (2.1a)$$

$$\frac{\partial \sigma_{r\theta}}{\partial r} + \frac{1}{r} \frac{\partial \sigma_{\theta\theta}}{\partial \theta} + \frac{\partial \sigma_{\theta z}}{\partial z} + \frac{2}{r} \sigma_{r\theta} + f_\theta = \rho \frac{\partial^2 u_\theta}{\partial t^2} \quad (2.1b)$$

$$\frac{\partial \sigma_{rz}}{\partial r} + \frac{1}{r} \frac{\partial \sigma_{\theta z}}{\partial \theta} + \frac{\partial \sigma_{zz}}{\partial z} + \frac{1}{r} \sigma_{rz} + f_z = \rho \frac{\partial^2 u_z}{\partial t^2}$$

where f_r , f_θ , f_z are the body forces associated with r , θ and z directions, u_r , u_θ and u_z are the displacement components and σ_{rr} is the radial stress, $\sigma_{\theta\theta}$ is the circumferential stress, σ_{zz} is the axial stress and $\sigma_{r\theta}$, σ_{rz} , $\sigma_{\theta z}$ are shear stress components.

Strain-displacement relations can be expressed as

$$\begin{aligned} \varepsilon_{rr} &= \frac{\partial u_r}{\partial r} \\ \varepsilon_{\theta\theta} &= \frac{u_r}{r} + \frac{1}{r} \frac{\partial u_\theta}{\partial \theta} \\ \varepsilon_{zz} &= \frac{\partial u_z}{\partial z} \\ \varepsilon_{r\theta} &= \frac{1}{2} \left(\frac{\partial u_\theta}{\partial r} - \frac{u_\theta}{r} + \frac{1}{r} \frac{\partial u_r}{\partial \theta} \right) \\ \varepsilon_{zr} &= \frac{1}{2} \left(\frac{\partial u_r}{\partial z} + \frac{\partial u_z}{\partial r} \right) \\ \varepsilon_{\theta z} &= \frac{1}{2} \left(\frac{1}{r} \frac{\partial u_z}{\partial \theta} + \frac{\partial u_\theta}{\partial z} \right) \end{aligned} \quad (2.2)$$

where ε_{rr} , $\varepsilon_{\theta\theta}$ and ε_{zz} are the normal strain components associated with r , θ and z directions, and $\varepsilon_{r\theta}$, ε_{rz} , $\varepsilon_{\theta z}$ are the shear strain components.

The stress-strain relations for an orthotropic material in coordinates aligned with the principal material directions can be expressed as [134-136]

$$\begin{aligned}
\sigma_{11} &= C_{11}\varepsilon_{11} + C_{12}\varepsilon_{22} + C_{13}\varepsilon_{33} \\
\sigma_{22} &= C_{21}\varepsilon_{11} + C_{22}\varepsilon_{22} + C_{23}\varepsilon_{33} \\
\sigma_{33} &= C_{31}\varepsilon_{11} + C_{32}\varepsilon_{22} + C_{33}\varepsilon_{33} \\
\sigma_{23} &= 2C_{44}\varepsilon_{23} \\
\sigma_{13} &= 2C_{55}\varepsilon_{13} \\
\sigma_{12} &= 2C_{66}\varepsilon_{12}
\end{aligned} \tag{2.3}$$

where C_{ij} are the stiffnesses in contracted notation. It should be noted that the principal material directions in a fiber reinforced lamina are the fiber direction (1-direction) and the directions normal to the fiber direction (directions - 2 and 3).

In our problem, however, the principal material directions of orthotropy do not coincide with coordinate axes that are geometrically natural to the solution of the problem. In our problem, the natural body coordinates are cylindrical coordinates r, θ and z , where r is the radial coordinate, θ is the polar angle and z is the coordinate in the axial direction of the filament wound cylindrical composite, see Fig. 2.1. Thus, the stress-strain relations are transformed from the principal material directions to the body coordinates (cylindrical coordinates). The results can be expressed as:

$$\begin{aligned}
\sigma_{zz} &= \tilde{C}_{11}\varepsilon_{zz} + \tilde{C}_{12}\varepsilon_{\theta\theta} + \tilde{C}_{13}\varepsilon_{rr} + 2\tilde{C}_{16}\varepsilon_{\theta z} \\
\sigma_{\theta\theta} &= \tilde{C}_{21}\varepsilon_{zz} + \tilde{C}_{22}\varepsilon_{\theta\theta} + \tilde{C}_{23}\varepsilon_{rr} + 2\tilde{C}_{26}\varepsilon_{\theta z} \\
\sigma_{rr} &= \tilde{C}_{31}\varepsilon_{zz} + \tilde{C}_{32}\varepsilon_{\theta\theta} + \tilde{C}_{33}\varepsilon_{rr} + 2\tilde{C}_{36}\varepsilon_{\theta z} \\
\sigma_{r\theta} &= 2\tilde{C}_{36}\varepsilon_{r\theta} + 2\tilde{C}_{45}\varepsilon_{rz}
\end{aligned} \tag{2.4a}$$

$$\begin{aligned}
\sigma_{rz} &= 2\tilde{C}_{45}\epsilon_{r\theta} + 2\tilde{C}_{55}\epsilon_{rz} \\
\sigma_{\theta z} &= \tilde{C}_{16}\epsilon_{zz} + \tilde{C}_{26}\epsilon_{\theta\theta} + \tilde{C}_{36}\epsilon_{rr} + 2\tilde{C}_{66}\epsilon_{\theta z}
\end{aligned} \tag{2.4b}$$

where \tilde{C}_{ij} are the transformed stiffness coefficients for an orthotropic material which can be expressed as,

$$\begin{aligned}
\tilde{C}_{11} &= m^4 C_{11} + 2m^2 n^2 (C_{12} + 2C_{66}) + n^4 C_{22} \\
\tilde{C}_{12} &= n^2 m^2 (C_{11} + C_{22} - 4C_{66}) + (n^4 + m^4) C_{12} \\
\tilde{C}_{13} &= m^2 C_{13} + n^2 C_{23} \\
\tilde{C}_{16} &= nm [m^2 (C_{11} - C_{12} - 2C_{66}) + n^2 (C_{12} - C_{22} + 2C_{66})] \\
\tilde{C}_{22} &= n^4 C_{11} + 2m^2 n^2 (C_{12} + 2C_{66}) + m^4 C_{22} \\
\tilde{C}_{23} &= n^2 C_{13} + m^2 C_{23} \\
\tilde{C}_{26} &= nm [n^2 (C_{11} - C_{12} - 2C_{66}) + m^2 (C_{12} - C_{22} + 2C_{66})] \\
\tilde{C}_{33} &= C_{33} \\
\tilde{C}_{36} &= mn (C_{13} - C_{23}) \\
\tilde{C}_{44} &= m^2 C_{44} + n^2 C_{55} \\
\tilde{C}_{45} &= mn (C_{55} - C_{44}) \\
\tilde{C}_{55} &= n^2 C_{44} + m^2 C_{55} \\
\tilde{C}_{66} &= n^2 m^2 (C_{11} - 2C_{12} + C_{22}) + (n^2 - m^2) C_{66}
\end{aligned} \tag{2.5}$$

and the other \tilde{C}_{ij} are zero.

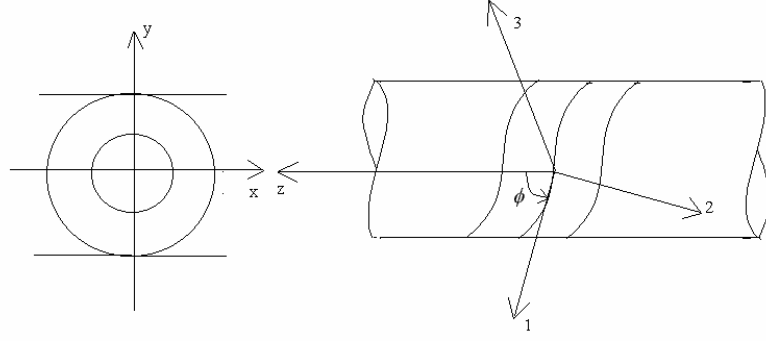


Figure 2.1. Filament wound fiber-reinforced circular cylindrical composite.

In Eqs.(2.5), C_{ij} are the stiffness coefficients referred to the principal material directions, $m = \cos \phi$ and $n = \sin \phi$, where ϕ is the angle between the z-axis and the principal direction 1, the fiber direction, see Fig. 2.1.

The stiffness coefficients, C_{ij} , of an orthotropic material can be expressed in terms of engineering constants associated with the principal material directions as

$$\begin{aligned}
 C_{11} &= \frac{1 - \nu_{23}\nu_{32}}{E_2 E_3 \Delta}, & C_{12} &= \frac{\nu_{21} + \nu_{23}\nu_{31}}{E_1 E_3 \Delta}, \\
 C_{13} &= \frac{\nu_{31} + \nu_{21}\nu_{21}}{E_2 E_3 \Delta}, & C_{21} &= \frac{\nu_{21} + \nu_{23}\nu_{31}}{E_2 E_3 \Delta}, \\
 C_{22} &= \frac{1 - \nu_{13}\nu_{31}}{E_1 E_3 \Delta}, & C_{31} &= \frac{\nu_{31} + \nu_{21}\nu_{32}}{E_2 E_3 \Delta}, \\
 C_{32} &= \frac{\nu_{21} + \nu_{12}\nu_{31}}{E_1 E_3 \Delta}, & C_{33} &= \frac{1 - \nu_{12}\nu_{21}}{E_1 E_2 \Delta}, \\
 C_{44} &= G_{23}, & C_{55} &= G_{13}, \\
 C_{66} &= G_{12}
 \end{aligned} \tag{2.6}$$

where

$$\Delta = \frac{(1 - \nu_{12}\nu_{21} - \nu_{23}\nu_{32} - \nu_{13}\nu_{31} - 2\nu_{21}\nu_{32}\nu_{13})}{E_1 E_2 E_3}$$

and E_1, E_2 and E_3 are Young's moduli in the principal material directions 1, 2, 3, respectively, $\nu_{12}, \nu_{21}, \nu_{13}, \nu_{31}, \nu_{23}, \nu_{32}$ are Poisson's ratios, and G_{31}, G_{23}, G_{12} are the shear moduli in the 1–3, 2–3 and 1–2 planes.

The stress-strain relations for a linear isotropic and homogeneous viscoelastic material in differential equation form are expressed as [133]:

$$P_1(D)\sigma'_{ij} = Q_1(D)\varepsilon'_{ij} \quad (2.7)$$

$$P_2(D)\sigma_{kk} = Q_2(D)\varepsilon_{kk}$$

where

$$P_1(D) = \sum_{k=0}^{n_1} a_k D^k, \quad Q_1(D) = \sum_{k=0}^{m_1} b_k D^k \quad (2.8)$$

$$P_2(D) = \sum_{k=0}^{n_2} c_k D^k, \quad Q_2(D) = \sum_{k=0}^{m_2} d_k D^k$$

In these equations, a_k, b_k, c_k, d_k are specified material constants and $D^k = \frac{\partial^k}{\partial t^k}$. In Eqs. (2.7), σ'_{ij} , ε'_{ij} are the components of stress and strain deviators defined as follows:

$$\sigma'_{ij} = \sigma_{ij} - \frac{1}{3} \delta_{ij} \sigma_{kk} \quad (2.9)$$

$$\varepsilon'_{ij} = \varepsilon_{ij} - \frac{1}{3} \delta_{ij} \varepsilon_{kk}$$

In Eqs. (2.7-2.9), indicial notation is used. In this notation i and j represent the r, θ, z in cylindrical coordinates. A repeated index implies summation. For example, ε_{kk} is equal to the sum of $\varepsilon_{rr}, \varepsilon_{\theta\theta}, \varepsilon_{zz}$ in cylindrical coordinates, that is,

$$\varepsilon_{kk} = \varepsilon_{rr} + \varepsilon_{\theta\theta} + \varepsilon_{zz} \quad (2.10)$$

Furthermore, δ_{ij} is the Kronecker's delta defined as:

$$\delta_{ij} = \begin{cases} 1 & i = j \\ 0 & i \neq j \end{cases} \quad (2.11)$$

Under certain conditions, Eqs. (2.7) can also be written in integral form as:

$$\sigma'_{ij}(\mathbf{r}, t) = G_1(t) \varepsilon'_{ij}(\mathbf{r}, 0) + \int_0^t G_1(t - \tau) \frac{\partial \varepsilon'_{ij}}{\partial \tau}(\mathbf{r}, t) d\tau \quad (2.12)$$

$$\sigma_{kk}(\mathbf{r}, t) = G_2(t) \varepsilon_{kk}(\mathbf{r}, 0) + \int_0^t G_2(t - \tau) \frac{\partial \varepsilon_{kk}}{\partial \tau}(\mathbf{r}, t) d\tau \quad (2.13)$$

where $G_1(t)$ and $G_2(t)$ are shear and bulk relaxations functions, respectively, and \mathbf{r} is the position vector of the particle considered.

In our study, we model the viscoelastic material with standard linear solid. The standard linear solid involves three parameters and can be represented as shown in Fig. 2.

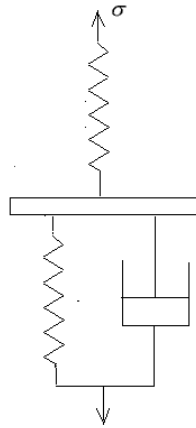


Figure 2.2. Model of viscoelastic material: standard linear solid.

The stress-strain relations in differential form for the standard linear solid are expressed in the same form as given in Eqs. (2.7). The operators, however, are defined as follows:

$$\begin{aligned} P_1(D) &= \sum_{k=0}^1 a_k D^k, & Q_1(D) &= \sum_{k=0}^1 b_k D^k \\ P_2(D) &= \sum_{k=0}^1 c_k D^k, & Q_2(D) &= \sum_{k=0}^1 d_k D^k \end{aligned} \tag{2.14}$$

This completes the summary of the basic equations of viscoelasticity and anisotropic elasticity in cylindrical coordinates.

2.3 Formulation of the Problem

As stated in Section 2.1, viscoelastic cylinders enclosed in filament wound cylindrical composites consisting of n different generally orthotropic, homogenous and linearly elastic fiber-reinforced layers is investigated in this chapter. The body is referred to a cylindrical coordinate system, where the radial distances are measured by the coordinate r . Boundary, initial and interface conditions of the problem imply that the responses of the body are axisymmetrical, that is all the field variables are functions of r and t , only. Moreover, the only nonvanishing displacement component is u_r , that is, the displacement component in the radial direction.

The governing equations for the viscoelastic layer and for a typical fiber-reinforced cylindrical layer will now be given. For the problem considered in this chapter, the components of the displacement field in cylindrical coordinates can be expressed as:

$$u_r = u_r(r, t); \quad u_\theta = u_z = 0 \tag{2.15}$$

For the three-dimensional case, the stress equations of motions in cylindrical coordinates system are given in Section 2.1 by Eqs. (2.1). For the problem considered in this study, these equations for the viscoelastic layer reduce to;

$$\frac{\partial \sigma_{rr}^{(v)}}{\partial r} + \frac{(\sigma_{rr}^{(v)} - \sigma_{\theta\theta}^{(v)})}{r} = \rho_v \frac{\partial^2 u_r^{(v)}}{\partial t^2} \quad (2.16)$$

Equation (2.16) represents the stress equation of motion in the radial direction for the viscoelastic layer. The equations in the θ and z-directions are satisfied identically. In the equation, $\sigma_{rr}^{(v)}$ represents the normal radial stress and $\sigma_{\theta\theta}^{(v)}$ represents the circumferential normal stress. Furthermore, ρ_v is the mass density of the viscoelastic layer and $u_r^{(v)}$ is the displacement component in the r - direction for the viscoelastic layer. In Eq. (2.16), the body forces are taken zero.

The stress equation of motion for the viscoelastic cylinder can be expressed in terms of stress deviators as

$$\frac{\partial}{\partial r} \left(\sigma_{rr}^{(v)'} + \frac{1}{3} \sigma_v^{(v)'} \right) + \frac{\sigma_{rr}^{(v)'} - \sigma_{\theta\theta}^{(v)'}}{r} = \rho_v \frac{\partial^2 u_r^{(v)}}{\partial t^2} \quad (2.17)$$

In Eq. (2.17), $\sigma_{rr}^{(v)'}$, $\sigma_{\theta\theta}^{(v)'}$ are the stress deviators defined in section 2.2 by Eqs. (2.9) and $\sigma_v = \sigma_{kk}^{(v)}$. It should be noted that the subscript v and the superscript v in parentheses denote that the quantity refers to the viscoelastic layer.

For the three-dimensional case, the stress-strain relations of linear isotropic and homogenous viscoelastic material were given by Eqs. (2.7). These equations for the standard linear solid take the following forms:

$$\begin{aligned}
a_0 \sigma_{rr}^{(v)'} + a_1 \frac{\partial \sigma_{rr}^{(v)'}}{\partial t} &= b_0 \varepsilon_{rr}^{(v)'} + b_1 \frac{\partial \varepsilon_{rr}^{(v)'}}{\partial t} \\
a_0 \sigma_{\theta\theta}^{(v)'} + a_1 \frac{\partial \sigma_{\theta\theta}^{(v)'}}{\partial t} &= b_0 \varepsilon_{\theta\theta}^{(v)'} + b_1 \frac{\partial \varepsilon_{\theta\theta}^{(v)'}}{\partial t} \\
c_0 \sigma_v + c_1 \frac{\partial \sigma_v}{\partial t} &= d_0 \varepsilon_v + d_1 \frac{\partial \varepsilon_v}{\partial t}
\end{aligned} \tag{2.18}$$

The strain-displacement relations for the strain deviators $\varepsilon_{rr}^{(v)'}$, $\varepsilon_{\theta\theta}^{(v)'}$ and $\varepsilon_v = \varepsilon_{rr} + \varepsilon_{\theta\theta} + \varepsilon_{zz}$ for the problem considered can be expressed as:

$$\begin{aligned}
\varepsilon_{rr}^{(v)'} &= \frac{1}{3} \left[2 \frac{\partial u_r^{(v)}}{\partial r} - \frac{u_r^{(v)}}{r} \right] \\
\varepsilon_{\theta\theta}^{(v)'} &= \frac{1}{3} \left[2 \frac{u_r^{(v)}}{r} - \frac{\partial u_r^{(v)}}{\partial r} \right] \\
\varepsilon_v &= \frac{\partial u_r^{(v)}}{\partial r} + \frac{u_r^{(v)}}{r}
\end{aligned} \tag{2.19}$$

In writing Eqs. (2.19), we made use of Eqs. (2.2), Eq. (2.9)₂ and the axisymmetrical nature of our problem.

Taking into consideration Eqs. (2.19), we can rewrite Eqs. (2.18) as

$$\begin{aligned}
\frac{a_0}{a_1} \sigma_{rr}^{(v)'} + \frac{\partial \sigma_{rr}^{(v)'}}{\partial t} - \frac{2}{3} \frac{b_0}{a_1} \varepsilon_{rr}^{(v)} + \frac{1}{3} \frac{b_0}{a_1} \frac{u_r^{(v)}}{r} - \frac{2}{3} \frac{b_1}{a_1} \frac{\partial v_r^{(v)}}{\partial r} + \frac{1}{3} \frac{b_1}{a_1} \frac{v_r^{(v)}}{r} &= 0 \\
\frac{a_0}{a_1} \sigma_{\theta\theta}^{(v)'} + \frac{\partial \sigma_{\theta\theta}^{(v)'}}{\partial t} + \frac{1}{3} \frac{b_0}{a_1} \varepsilon_{rr}^{(v)} - \frac{2}{3} \frac{b_0}{a_1} \frac{u_r^{(v)}}{r} + \frac{1}{3} \frac{b_1}{a_1} \frac{\partial v_r^{(v)}}{\partial r} - \frac{2}{3} \frac{b_1}{a_1} \frac{v_r^{(v)}}{r} &= 0 \tag{2.20} \\
\frac{c_0}{c_1} \sigma_v + \frac{\partial \sigma_v}{\partial t} - \frac{d_0}{c_1} \varepsilon_{rr}^{(v)} - \frac{d_0}{c_1} \frac{u_r^{(v)}}{r} - \frac{d_1}{c_1} \frac{\partial v_r^{(v)}}{\partial r} - \frac{d_1}{c_1} \frac{v_r^{(v)}}{r} &= 0
\end{aligned}$$

where

$$\varepsilon_{rr}^{(v)} = \frac{\partial u_r^{(v)}}{\partial r}; \quad v_r^{(v)} = \frac{\partial u_r^{(v)}}{\partial t} \quad (2.21)$$

The stress equation of motion for the outer layers is of the same form as Eq. (2.17). In this case, however, the subscript v and the superscript v in parentheses denoting the viscoelastic layer should be replaced by the subscript and superscript in parentheses characterizing the generally orthotropic elastic layer under consideration. The outer layers are assumed to be homogeneous, generally orthotropic and linearly elastic. Hence, the constitutive equations in terms of stress deviators and displacements for a typical layer can be expressed as,

$$\begin{aligned} \sigma_{rr}' + \left[\frac{1}{3}\tilde{C}_{22} + \frac{1}{3}\tilde{C}_{12} - \frac{2}{3}\tilde{C}_{32} \right] \frac{u_r}{r} + \left[\frac{1}{3}\tilde{C}_{13} + \frac{1}{3}\tilde{C}_{32} - \frac{2}{3}\tilde{C}_{33} \right] \frac{\partial u_r}{\partial r} &= 0 \\ \sigma_{\theta\theta}' + \left[\frac{1}{3}\tilde{C}_{32} + \frac{1}{3}\tilde{C}_{12} - \frac{2}{3}\tilde{C}_{22} \right] \frac{u_r}{r} + \left[\frac{1}{3}\tilde{C}_{33} + \frac{1}{3}\tilde{C}_{13} - \frac{2}{3}\tilde{C}_{23} \right] \frac{\partial u_r}{\partial r} &= 0 \quad (2.22) \\ \sigma - [\tilde{C}_{32} + \tilde{C}_{12} + \tilde{C}_{22}] \frac{u_r}{r} - [\tilde{C}_{33} + \tilde{C}_{23} + \tilde{C}_{13}] \frac{\partial u_r}{\partial r} &= 0 \end{aligned}$$

where $\tilde{C}_{12}, \tilde{C}_{13}, \tilde{C}_{22}, \tilde{C}_{23}, \tilde{C}_{32}, \tilde{C}_{33}$ are the transformed stiffness coefficients for a generally orthotropic material which can be expressed as in Eqs. (2.5) of Section 2.2. Furthermore, σ_{rr}' , $\sigma_{\theta\theta}'$ are stress deviators and $\sigma = \sigma_{rr} + \sigma_{\theta\theta} + \sigma_{zz}$. Differentiating Eqs (2.22) with respect to time, we obtain:

$$\begin{aligned} \frac{\partial \sigma_{rr}'}{\partial t} + \left[\frac{1}{3}\tilde{C}_{22} + \frac{1}{3}\tilde{C}_{12} - \frac{2}{3}\tilde{C}_{32} \right] \frac{v_r}{r} + \left[\frac{1}{3}\tilde{C}_{13} + \frac{1}{3}\tilde{C}_{32} - \frac{2}{3}\tilde{C}_{33} \right] \frac{\partial v_r}{\partial r} &= 0 \\ \frac{\partial \sigma_{\theta\theta}'}{\partial t} + \left[\frac{1}{3}\tilde{C}_{32} + \frac{1}{3}\tilde{C}_{12} - \frac{2}{3}\tilde{C}_{22} \right] \frac{v_r}{r} + \left[\frac{1}{3}\tilde{C}_{33} + \frac{1}{3}\tilde{C}_{13} - \frac{2}{3}\tilde{C}_{23} \right] \frac{\partial v_r}{\partial r} &= 0 \quad (2.23) \\ \frac{\partial \sigma}{\partial t} - [\tilde{C}_{32} + \tilde{C}_{12} + \tilde{C}_{22}] \frac{v_r}{r} - [\tilde{C}_{33} + \tilde{C}_{23} + \tilde{C}_{13}] \frac{\partial v_r}{\partial r} &= 0 \end{aligned}$$

In the above equations v_r is the radial particle velocity of a typical generally orthotropic layer defined as:

$$v_r = \frac{\partial u_r}{\partial t} \quad (2.24)$$

The formulation of the problem is completed by stating the boundary, interface and initial conditions. The boundary conditions at the inner surface $r = a$ and the outer surface $r = c$ can be expressed, respectively, as

$$\sigma_{rr}^{(v)'}(a, t) + \frac{1}{3}\sigma_v(a, t) = -P(t)H(t) \text{ or } v_r^{(v)}(a, t) = V(t)H(t) \quad (2.25)$$

$$\sigma_{rr}^{(n)'}(c, t) + \frac{1}{3}\sigma_n(c, t) = -F(t)H(t) \text{ or } v_r^{(n)}(c, t) = G(t)H(t)$$

where $P(t), V(t), F(t), G(t)$ are prescribed functions of time t , $H(t)$ is the Heaviside

step function, and $v_r^{(v)}, v_r^{(n)} = \left(\frac{\partial u_r^{(v)}}{\partial t}, \frac{\partial u_r^{(n)}}{\partial t} \right)$ are the radial particle velocity

pertaining to the viscoelastic cylinder and the n 'th orthotropic layer. The subscript n and superscript n in parentheses denote that the quantity refers to the outermost orthotropic layer. The layers are assumed to be perfectly bonded to each other. Hence, the interface conditions at the interface $r = b$ between the viscoelastic cylinder and the innermost orthotropic layer, require that,

$$\sigma_{rr}^{(v)'}(b, t) + \frac{1}{3}\sigma_v(b, t) = \sigma_{rr}^{(1)'}(b, t) + \frac{1}{3}\sigma_1(b, t); \quad (2.26)$$

$$u_r^{(v)}(b, t) = u_r^{(1)}(b, t)$$

where the subscript 1 and the superscript 1 in parentheses are used for the quantities referring to the first innermost orthotropic layer.

For a typical interface between the layers designated by F and $F + 1$, Eqs. (2.26) take the form,

$$\sigma_{rr}^{(F)'}(d, t) + \frac{1}{3}\sigma_F(d, t) = \sigma_{rr}^{(F+1)'}(d, t) + \frac{1}{3}\sigma_{F+1}(d, t) \quad (2.27)$$

$$u_r^{(F)}(d, t) = u_r^{(F+1)}(d, t)$$

where the subscript F and superscript F in parenthesis denote the layer which precedes the interface and subscript $F + 1$ and superscript $F + 1$ in parentheses denote the layer which follows the interface. In the above equation, d is the radial coordinate of the interface considered.

The layered body is assumed to be initially at rest; thus, at $t = 0$, we have

$$u_r^{(v)}(r, 0) = v_r^{(v)}(r, 0) = 0; \quad u_r(r, 0) = v_r^{(v)}(r, 0) = 0 \quad (2.28)$$

The formulation of the problem is thus complete. The governing field equations, Eqs. (2.20), (2.21)₂, (2.29-2.30), (2.23), (2.24), (2.52-2.53) are applied to the viscoelastic and orthotropic layers, and the solutions are required to satisfy the boundary conditions at the inner and outer surfaces, Eq. (2.25), the continuity conditions at the interfaces, Eqs. (2.26-2.27), and quiescent initial conditions, Eqs. (2.28). Method of characteristics is employed to obtain the solutions.

2.4 The Method of Characteristics and the Canonical Form of the Governing Equations for the Viscoelastic Layer

In order to apply the method of characteristics, we write the governing equations as a system of first order partial differential equations. For this purpose, we write stress equation of motion, Eq. (2.17), in the form:

$$-\frac{1}{\rho_v} \frac{\partial \sigma_{rr}^{(v)'}}{\partial r} - \frac{1}{3\rho_v} \frac{\partial \sigma_v}{\partial r} - \frac{1}{\rho_v} \frac{\left(\sigma_{rr}^{(v)'} - \sigma_{\theta\theta}^{(v)'} \right)}{r} + \frac{\partial v_r^{(v)}}{\partial t} = 0 \quad (2.29)$$

Furthermore, we have the compatibility equation:

$$\frac{\partial \varepsilon_{rr}^{(v)}}{\partial t} - \frac{\partial v_r^{(v)}}{\partial r} = 0 \quad (2.30)$$

Now, the system of governing first order partial differential equations, Eqs. (2.20), (2.21)₂, (2.29-2.30) can be written in matrix form as:

$$\mathbf{A} \mathbf{U}_{,t} + \mathbf{B} \mathbf{U}_{,r} + \mathbf{C} = \mathbf{0} \quad (2.31)$$

where \mathbf{A} and \mathbf{B} are six by six matrices defined as:

$$\mathbf{A} = \begin{bmatrix} 0 & 1 & 0 & 0 & 0 & 0 \\ 0 & 0 & 1 & 0 & 0 & 0 \\ 0 & 0 & 0 & 1 & 0 & 0 \\ 0 & 0 & 0 & 0 & 1 & 0 \\ 1 & 0 & 0 & 0 & 0 & 0 \\ 0 & 0 & 0 & 0 & 0 & 1 \end{bmatrix} \quad (2.32)$$

$$\mathbf{B} = \begin{bmatrix} 0 & 0 & -\frac{1}{\rho_v} & 0 & -\frac{1}{3\rho_v} & 0 \\ 0 & -\frac{2b_1}{3a_1} & 0 & 0 & 0 & 0 \\ 0 & \frac{b_1}{3a_1} & 0 & 0 & 0 & 0 \\ 0 & -\frac{d_1}{c_1} & 0 & 0 & 0 & 0 \\ 0 & -1 & 0 & 0 & 0 & 0 \\ 0 & 0 & 0 & 0 & 0 & 0 \end{bmatrix} \quad (2.33)$$

and \mathbf{C} and $\mathbf{U}^{(v)}$ are six-dimensional column vectors given as:

$$\mathbf{C} = \begin{bmatrix} -\frac{1}{\rho_v} \frac{\left(\sigma_{rr}^{(v)'} - \sigma_{\theta\theta}^{(v)'} \right)}{r} \\ \frac{a_0}{a_1} \sigma_{rr}^{(v)'} - \frac{2b_0}{3a_1} \varepsilon_{rr}^{(v)} + \frac{1b_0}{3a_1} \frac{u_r^{(v)}}{r} + \frac{1b_1}{3a_1} \frac{v_r^{(v)}}{r} \\ \frac{a_0}{a_1} \sigma_{rr}^{(v)'} - \frac{2b_0}{3a_1} \frac{u_r^{(v)}}{r} + \frac{1b_0}{3a_1} \varepsilon_{rr}^{(v)} - \frac{2b_1}{3a_1} \frac{v_r^{(v)}}{r} \\ \frac{c_0}{c_1} \sigma_v - \frac{d_0}{c_1} \varepsilon_{rr}^{(v)} - \frac{d_0}{c_1} \frac{u_r^{(v)}}{r} - \frac{d_1}{c_1} \frac{v_r^{(v)}}{r} \\ 0 \\ -v_r^{(v)} \end{bmatrix} \quad (2.34)$$

$$\mathbf{U}^{(v)} = \begin{bmatrix} \varepsilon_{rr}^{(v)} \\ v_r^{(v)} \\ \sigma_{rr}^{(v)'} \\ \sigma_{\theta\theta}^{(v)'} \\ \sigma_v \\ u_r^{(v)} \end{bmatrix} \quad (2.35)$$

In Eq. (2.31), $\mathbf{U}^{(v)}$ is the unknown vector and comma denotes partial differentiation:

$$\mathbf{U}_{,t}^{(v)} = \frac{\partial \mathbf{U}^{(v)}}{\partial t}, \quad \mathbf{U}_{,r}^{(v)} = \frac{\partial \mathbf{U}^{(v)}}{\partial r} \quad (2.36)$$

Before we derive the canonical equations from Eq. (2.31), we first establish the characteristic lines along which these equations are valid. The characteristic lines are governed by the characteristic equation [132]

$$\det(\mathbf{B} - V_v \mathbf{A}) = 0 \quad (2.37)$$

where $V_v = \frac{dr}{dt}$ defines the characteristic lines on the $(r-t)$ plane.

In view of Eqs. (2.32-2.33), the characteristic equation, Eq. (2.37), can be expressed as:

$$\det(B - V_v A) = \begin{bmatrix} 0 & -V_v & -\frac{1}{\rho_v} & 0 & -\frac{1}{3\rho_v} & 0 \\ 0 & -\frac{2b_1}{3a_1} & -V_v & 0 & 0 & 0 \\ 0 & \frac{b_1}{3a_1} & 0 & -V_v & 0 & 0 \\ 0 & -\frac{d_1}{c_1} & 0 & 0 & -V_v & 0 \\ -V_v & -1 & 0 & 0 & 0 & 0 \\ 0 & 0 & 0 & 0 & 0 & -V_v \end{bmatrix} =$$

$$-V_v^6 + \left(\frac{2b_1}{3a_1\rho_v} + \frac{d_1}{3c_1\rho_v} \right) V_v^4 = 0 \quad (2.38)$$

The roots of Eq. (2.38) are:

$$V_v^{(1)} = c_v, \quad V_v^{(2)} = -c_v, \quad V_v^{(3)} = V_v^{(4)} = V_v^{(5)} = V_v^{(6)} = 0 \quad (2.39)$$

where

$$c_v = \left[\frac{1}{3\rho_v} \left(\frac{2b_1}{a_1} + \frac{d_1}{c_1} \right) \right]^{1/2} \quad (2.40)$$

$V_v^{(i)}$ are the characteristic values and the characteristic lines are defined as:

$$\begin{aligned}
\frac{dr}{dt} &= V_v^{(1)} = c_v && \text{along } C_v^{(1)} \\
\frac{dr}{dt} &= V_v^{(2)} = -c_v && \text{along } C_v^{(2)} \\
\frac{dr}{dt} &= V_v^{(i)} = 0 \quad (i = 3-6) && \text{along } C_v^{(i)}
\end{aligned} \tag{2.41}$$

Integration of Eq. (2.41) gives the families of characteristic lines $C_v^{(i)}$ ($i = 1-6$) which can be written as:

$$\begin{aligned}
C_v^{(1)} : r - c_v t &= \text{constant} \\
C_v^{(2)} : r + c_v t &= \text{constant} \\
C_v^{(i)} : r &= \text{constant} \quad (i = 3-6)
\end{aligned} \tag{2.42}$$

These families of characteristic lines are shown in the $(r-t)$ plane in Fig. 2.3. We note that $C_v^{(1)}$ describes a family of straight lines with slope c_v , whereas $C_v^{(2)}$ describes a family of straight lines with slope $-c_v$ on the $(r-t)$ plane. Moreover, $C_v^{(i)}$ ($i = 3-6$) describes straight lines parallel to the t -axes, see Fig. 2.3.

In establishing the canonical form of the governing equations, we define the left-hand eigenvectors $L_v^{(i)}$ ($i = 1-6$) corresponding to the characteristic values $V_v^{(i)}$ ($i = 1-6$) as:

$$(\mathbf{B}^T - V_v^{(i)} \mathbf{A}^T) \mathbf{L}_v^{(i)} = \mathbf{0} \quad (i = 1-6) \tag{2.43}$$

where T denotes the transpose.

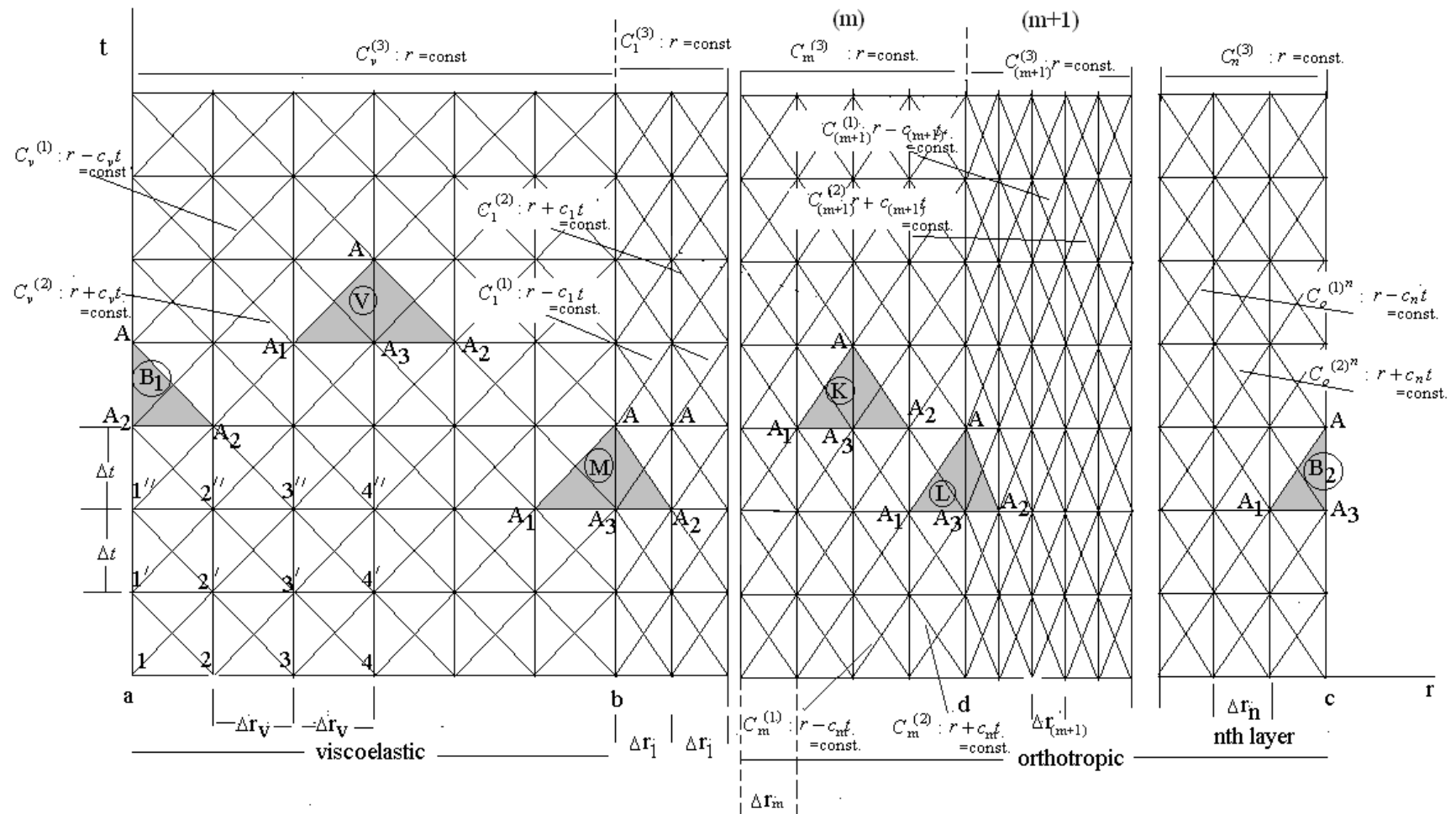


Figure 2.3. Network of the characteristic lines on the $(r-t)$ plane.

Solving Eqs (2.43), in view of Eqs. (2.32-2.33), we can write the left-hand eigenvectors as:

$$\mathbf{L}_v^{(1)} = \begin{bmatrix} \frac{-1}{1} \\ \frac{\rho_v c_v}{0} \\ \frac{1}{3\rho_v c_v} \\ 0 \\ 0 \end{bmatrix}; \quad \mathbf{L}_v^{(2)} = \begin{bmatrix} \frac{-1}{1} \\ \frac{\rho_v c_v}{0} \\ \frac{1}{3\rho_v c_v} \\ 0 \\ 0 \end{bmatrix}; \quad \mathbf{L}_v^{(3)} = \begin{bmatrix} 0 \\ -1 \\ -2 \\ 0 \\ 0 \\ 1 \end{bmatrix}; \quad \mathbf{L}_v^{(4)} = \begin{bmatrix} 0 \\ 0 \\ -1 \\ \frac{b_1 c_1}{3a_1 d_1} \\ 0 \\ 1 \end{bmatrix} \quad (2.44)$$

$$\mathbf{L}_v^{(5)} = \begin{bmatrix} 0 \\ 0 \\ 0 \\ -1 \\ \frac{d_1}{c_1} \\ 1 \end{bmatrix}; \quad \mathbf{L}_v^{(6)} = \begin{bmatrix} 0 \\ 0 \\ 0 \\ 0 \\ 0 \\ 1 \end{bmatrix}$$

The left-hand eigenvectors in Eq. (2.44) are multiplied by arbitrary constants which are not written for the sake of brevity.

The canonical equations can be written as

$$\mathbf{L}_v^{(i)T} \mathbf{A} \frac{d\mathbf{U}^{(v)}}{dt} + \mathbf{L}_v^{(i)T} \mathbf{C} = \mathbf{0} \quad (2.45)$$

which hold along $\frac{dr}{dt} = V_v^{(i)}$ ($i=1-6$). In Eq. (2.45), the superscript T defines transpose, $\frac{d}{dt}$ denotes the total time derivative along the characteristic line and $\mathbf{L}_v^{(i)}$ is the left-hand eigenvector given by Eqs. (2.44). For the derivations of Eqs. (2.37)

and Eqs. (2.45) see Appendix A. By substituting Eqs. (2.44) into Eq. (2.45) and taking into consideration Eqs. (2.32-2.35), we get the canonical equations explicitly as

$$\begin{aligned}
& -\frac{dv_r^{(v)}}{dt} + \frac{1}{\rho_v c_v} \frac{d\sigma_{rr}^{(v)'}}{dt} + \frac{1}{3\rho_v c_v} \frac{d\sigma_v}{dt} - \frac{1}{3\rho_v c_v} \left(\frac{2b_0}{a_1} + \frac{d_0}{c_1} \right) \varepsilon_{rr}^{(v)} - \frac{1}{3\rho_v c_v} \left(\frac{d_1}{c_1} - \frac{b_1}{a_1} \right) \frac{1}{r} v_r^{(v)} \\
& + \frac{1}{\rho_v} \left(\frac{1}{r} + \frac{a_0}{a_1 c_v} \right) \sigma_{rr}^{(v)'} - \frac{1}{\rho_v r} \sigma_{\theta\theta}^{(v)'} + \frac{c_0}{3\rho_v c_v c_1} \sigma_v - \frac{1}{3\rho_v c_v} \left(\frac{d_0}{c_1} - \frac{b_0}{a_1} \right) \frac{1}{r} u_r^{(v)} = 0
\end{aligned}$$

$$\text{along } \frac{dr}{dt} = V_v^{(1)} = c_v \quad (2.46)$$

$$\begin{aligned}
& -\frac{dv_r^{(v)}}{dt} - \frac{1}{\rho_v c_v} \frac{d\sigma_{rr}^{(v)'}}{dt} - \frac{1}{3\rho_v c_v} \frac{d\sigma_v}{dt} + \frac{1}{3\rho_v c_v} \left(\frac{2b_0}{a_1} + \frac{d_0}{c_1} \right) \varepsilon_{rr}^{(v)} + \frac{1}{3\rho_v c_v} \left(\frac{d_1}{c_1} - \frac{b_1}{a_1} \right) \frac{1}{r} v_r^{(v)} \\
& + \frac{1}{\rho_v} \left(\frac{1}{r} - \frac{a_0}{a_1 c_v} \right) \sigma_{rr}^{(v)'} - \frac{1}{\rho_v r} \sigma_{\theta\theta}^{(v)'} - \frac{c_0}{3\rho_v c_v c_1} \sigma_v + \frac{1}{3\rho_v c_v} \left(\frac{d_0}{c_1} - \frac{b_0}{a_1} \right) \frac{1}{r} u_r^{(v)} = 0
\end{aligned}$$

$$\text{along } \frac{dr}{dt} = V_v^{(2)} = -c_v \quad (2.47)$$

$$-\frac{d\sigma_{rr}^{(v)'}}{dt} - 2\frac{d\sigma_{\theta\theta}^{(v)'}}{dt} + \frac{b_1}{a_1} \frac{1}{r} v_r^{(v)} - \frac{a_0}{a_1} \sigma_{rr}^{(v)'} - \frac{2a_0}{a_1} \sigma_{\theta\theta}^{(v)'} + \frac{b_0}{a_1} \frac{1}{x} u_r^{(v)} = 0$$

$$\text{along } \frac{dr}{dt} = V_v^{(3)} = 0 \quad (2.48)$$

$$\begin{aligned}
& -\frac{d\sigma_{rr}^{(v)'}}{dt} - \frac{b_1 c_1}{3d_1 a_1} \frac{d\sigma_v}{dt} + \frac{1}{3a_1} \left(\frac{d_0 b_1}{d_1} - b_0 \right) \varepsilon_{rr}^{(v)} + \frac{b_1}{a_1} \frac{1}{r} v_r^{(v)} - \frac{a_0}{a_1} \sigma_{\theta\theta}^{(v)' } - \frac{b_1 c_0}{3d_1 a_1} \\
& \frac{1}{3a_1} \left(2b_0 + \frac{b_1 d_0}{d_1} \right) \frac{1}{r} u_r^{(v)} = 0
\end{aligned}$$

along $\frac{dr}{dt} = V_v^{(4)} = 0$ (2.49)

$$\begin{aligned}
& -\frac{d\sigma_v}{dt} + \frac{d_1}{c_1} \frac{d\varepsilon_{rr}^{(v)}}{dt} - \frac{c_0}{c_1} \sigma_v + \frac{d_0}{c_1} \varepsilon_{rr}^{(v)} + \frac{d_1}{c_1} \frac{v_r^{(v)}}{r} + \frac{d_0}{c_1} \frac{u_r^{(v)}}{r} = 0
\end{aligned}$$

along $\frac{dr}{dt} = V_v^{(5)} = 0$ (2.50)

$$v_r^{(v)} - \frac{du_r^{(v)}}{dt} = 0$$

along $\frac{dr}{dt} = V_v^{(6)} = 0$ (2.51)

2.5 The Method of Characteristics and the Canonical Form of the Governing Equations for the Orthotropic Layers

The stress equation of motion for a typical orthotropic layer in terms of stress deviators can be written as

$$\frac{\partial \sigma_{rr}'}{\partial r} + \frac{1}{3} \frac{\partial \sigma}{\partial r} + \frac{(\sigma_{rr}' - \sigma_{\theta\theta}')}{r} = \rho \frac{\partial v_r}{\partial t} \quad (2.52)$$

Furthermore, we have the compatibility equation,

$$\frac{\partial \varepsilon_{rr}}{\partial t} - \frac{\partial v_r}{\partial r} = 0 \quad (2.53)$$

Now, the system of the governing first-order partial differential equations, Eqs. (2.23-2.24), (2.52-2.53), for a typical layer can be written in matrix form as

$$\mathbf{H}\mathbf{U}_{,t} + \mathbf{I}\mathbf{U}_{,r} + \mathbf{J} = \mathbf{0} \quad (2.54)$$

where \mathbf{H} and \mathbf{I} are the six-by-six matrices defined as

$$\mathbf{H} = \begin{bmatrix} 0 & 1 & 0 & 0 & 0 & 0 \\ 0 & 0 & 1 & 0 & 0 & 0 \\ 0 & 0 & 0 & 1 & 0 & 0 \\ 0 & 0 & 0 & 0 & 1 & 0 \\ 1 & 0 & 0 & 0 & 0 & 0 \\ 0 & 0 & 0 & 0 & 0 & 1 \end{bmatrix} \quad (2.55)$$

$$\mathbf{I} = \begin{bmatrix} 0 & 0 & \frac{-1}{\rho} & 0 & \frac{-1}{3\rho} & 0 \\ 0 & \left(\frac{1}{3}\tilde{C}_{13} + \frac{1}{3}\tilde{C}_{32} - \frac{2}{3}\tilde{C}_{33} \right) & 0 & 0 & 0 & 0 \\ 0 & \left(\frac{1}{3}\tilde{C}_{33} + \frac{1}{3}\tilde{C}_{13} - \frac{2}{3}\tilde{C}_{23} \right) & 0 & 0 & 0 & 0 \\ 0 & -(\tilde{C}_{33} + \tilde{C}_{23} + \tilde{C}_{13}) & 0 & 0 & 0 & 0 \\ 0 & -1 & 0 & 0 & 0 & 0 \\ 0 & 0 & 0 & 0 & 0 & 0 \end{bmatrix} \quad (2.56)$$

and \mathbf{J} and \mathbf{U} are column vectors given by

$$\mathbf{J} = \begin{bmatrix} -\frac{1}{\rho} \frac{(\sigma'_{rr} - \sigma'_{\theta\theta})}{r} \\ \left(\frac{1}{3}\tilde{C}_{22} + \frac{1}{3}\tilde{C}_{12} - \frac{2}{3}\tilde{C}_{32}\right) \frac{v_r}{r} \\ \left(\frac{1}{3}\tilde{C}_{32} + \frac{1}{3}\tilde{C}_{12} - \frac{2}{3}\tilde{C}_{22}\right) \frac{v_r}{r} \\ -(\tilde{C}_{32} + \tilde{C}_{22} + \tilde{C}_{12}) \frac{v_r}{r} \\ 0 \\ -v_r \end{bmatrix} \quad (2.57)$$

$$\mathbf{U} = \begin{bmatrix} \varepsilon_{rr} \\ v_r \\ \sigma_{rr} \\ \sigma_{\theta\theta} \\ \sigma \\ u_r \end{bmatrix} \quad (2.58)$$

In Eq. (2.54), comma denotes partial differentiation as mentioned previously. Applying the characteristic equation in view of Eqs. (2.55-2.56), we have

$$\det(\mathbf{I} - V\mathbf{H}) = \begin{bmatrix} 0 & -V & \frac{-1}{\rho} & 0 & \frac{-1}{3\rho} & 0 \\ 0 & \left(\frac{1}{3}\tilde{C}_{13} + \frac{1}{3}\tilde{C}_{32} - \frac{2}{3}\tilde{C}_{33}\right) & -V & 0 & 0 & 0 \\ 0 & \left(\frac{1}{3}\tilde{C}_{33} + \frac{1}{3}\tilde{C}_{13} - \frac{2}{3}\tilde{C}_{23}\right) & 0 & -V & 0 & 0 \\ 0 & -(\tilde{C}_{33} + \tilde{C}_{23} + \tilde{C}_{13}) & 0 & 0 & -V & 0 \\ -V & -1 & 0 & 0 & 0 & 0 \\ 0 & 0 & 0 & 0 & 0 & -V \end{bmatrix} =$$

$$V^4 \left(V^2 + \frac{\left(\frac{1}{3}\tilde{C}_{13} + \frac{1}{3}\tilde{C}_{32} - \frac{2}{3}\tilde{C}_{33}\right)}{\rho} - \frac{(\tilde{C}_{33} + \tilde{C}_{23} + \tilde{C}_{13})}{3\rho} \right) = 0 \quad (2.59)$$

The roots of Eq. (2.59) can be obtained as

$$V^{(1)} = c, \quad V^{(2)} = -c, \quad V^{(3)} = V^{(4)} = V^{(5)} = 0 \quad (2.60)$$

where

$$c = \sqrt{\frac{\tilde{C}_{33}}{\rho}} \quad (2.61)$$

The characteristic families of straight lines in the $(r-t)$ plane for a typical orthotropic layer are then defined by:

$$\begin{aligned} \frac{dr}{dt} = V^{(1)} = c & \quad \text{along } C^{(1)} \\ \frac{dr}{dt} = V^{(2)} = -c & \quad \text{along } C^{(2)} \\ \frac{dr}{dt} = V^{(i)} = 0 & \quad \text{along } C^{(i)} \quad (i = 3-6) \end{aligned} \quad (2.62)$$

Integration of Eqs. (2.62) gives the families of characteristic lines $C^{(i)}$ ($i = 1-6$) as:

$$\begin{aligned} C^{(1)} : r - ct &= \text{constant} \\ C^{(2)} : r + ct &= \text{constant} \\ C^{(i)} : r &= \text{constant} \quad (i = 3-6) \end{aligned} \quad (2.63)$$

These families of characteristic lines are shown in the $(r-t)$ plane in Fig. 2.3.

The canonical forms of the governing equations along the characteristic lines can be written as

$$\mathbf{L}^{(i)T} \mathbf{H} \frac{d\mathbf{U}}{dt} + \mathbf{L}^{(i)T} \mathbf{I} = \mathbf{0} \quad \text{along } \frac{dr}{dt} = V^{(i)} \quad i = (1-6) \quad (2.64)$$

where $\mathbf{H}, \mathbf{I}, \mathbf{U}$ are given by Eqs. (2.55, 2.56, 2.58) and $\mathbf{L}^{(i)}$ is the left-hand eigenvector defined by:

$$(\mathbf{I}^T - V^{(i)} \mathbf{H}^T) \mathbf{L}^{(i)} = \mathbf{0} \quad \text{along } C^{(i)} \quad (2.65)$$

Applying Eq. (2.65), the left-hand eigenvectors can be computed as

$$\mathbf{L}^{(1)} = \begin{bmatrix} \frac{-1}{1} \\ \frac{\rho c}{1} \\ \frac{0}{3\rho c} \\ \frac{1}{0} \\ \frac{0}{0} \end{bmatrix}; \mathbf{L}^{(2)} = \begin{bmatrix} \frac{-1}{1} \\ \frac{\rho c}{1} \\ \frac{0}{3\rho c} \\ \frac{-1}{0} \\ \frac{0}{0} \end{bmatrix}; \mathbf{L}^{(3)} = \begin{bmatrix} 0 \\ -1 \\ \left(\frac{1}{3} \tilde{C}_{13} + \frac{1}{3} \tilde{C}_{32} - \frac{2}{3} \tilde{C}_{33} \right) \\ \left(\frac{1}{3} \tilde{C}_{33} + \frac{1}{3} \tilde{C}_{13} - \frac{2}{3} \tilde{C}_{23} \right) \\ 0 \\ 0 \\ 1 \end{bmatrix}; \quad (2.66)$$

$$\mathbf{L}^{(4)} = \begin{bmatrix} 0 \\ 0 \\ -1 \\ -\left(\frac{1}{3} \tilde{C}_{33} + \frac{1}{3} \tilde{C}_{13} - \frac{2}{3} \tilde{C}_{23} \right) \\ \frac{(\tilde{C}_{33} + \tilde{C}_{23} + \tilde{C}_{13})}{0} \\ 0 \\ 1 \end{bmatrix}; \mathbf{L}^{(5)} = \begin{bmatrix} 0 \\ 0 \\ 0 \\ -1 \\ \tilde{C}_{33} + \tilde{C}_{23} + \tilde{C}_{13} \\ 1 \end{bmatrix};; \quad \mathbf{L}^{(6)} = \begin{bmatrix} 0 \\ 0 \\ 0 \\ 0 \\ 0 \\ 1 \end{bmatrix}$$

Since the left-hand eigenvectors of the typical orthotropic layer are found, the canonical equations then can be obtained by applying Eq. (2.64) and taking into consideration Eqs. (2.55-2.58) and Eq. (2.66) . This gives the canonical equations for a typical orthotropic layer as

$$\begin{aligned} \frac{-dv_r}{dt} + \frac{1}{\rho c} \frac{d\sigma_{rr}'}{dt} + \frac{1}{3\rho c} \frac{d\sigma}{dt} + \frac{\sigma_{rr}'}{\rho r} - \frac{\sigma_{\theta\theta}'}{\rho r} - \frac{\tilde{C}_{32}}{\rho c} \frac{v_r}{r} = 0 \\ \text{along } \frac{dr}{dt} = V^{(1)} = c \end{aligned} \quad (2.67)$$

$$\begin{aligned} \frac{-dv_r}{dt} - \frac{1}{\rho c} \frac{d\sigma_{rr}'}{dt} - \frac{1}{3\rho c} \frac{d\sigma}{dt} + \frac{\sigma_{rr}'}{\rho r} - \frac{\sigma_{\theta\theta}'}{\rho r} + \frac{\tilde{C}_{32}}{\rho c} \frac{v_r}{r} = 0 \\ \text{along } \frac{dr}{dt} = V^{(2)} = -c \end{aligned} \quad (2.68)$$

$$\begin{aligned} \frac{-d\sigma_{rr}'}{dt} + \frac{\frac{1}{3}\tilde{C}_{13} + \frac{1}{3}\tilde{C}_{23} - \frac{2}{3}\tilde{C}_{33}}{\frac{1}{3}\tilde{C}_{33} + \frac{1}{3}\tilde{C}_{13} - \frac{2}{3}\tilde{C}_{23}} \frac{d\sigma_{\theta\theta}'}{dt} \\ + \frac{\frac{1}{3}(\tilde{C}_{22}\tilde{C}_{33} - \tilde{C}_{22}\tilde{C}_{13} - \tilde{C}_{33}\tilde{C}_{12} + \tilde{C}_{12}\tilde{C}_{23} + \tilde{C}_{32}\tilde{C}_{13} + \tilde{C}_{32}\tilde{C}_{23})}{\frac{1}{3}\tilde{C}_{33} + \frac{1}{3}\tilde{C}_{13} - \frac{2}{3}\tilde{C}_{23}} \frac{v_r}{r} = 0 \\ \text{along } \frac{dr}{dt} = V^{(3)} = 0 \end{aligned} \quad (2.69)$$

$$\begin{aligned} \frac{-d\sigma_{\theta\theta}'}{dt} + \frac{\frac{2}{3}\tilde{C}_{23} - \frac{1}{3}\tilde{C}_{13} - \frac{1}{3}\tilde{C}_{33}}{\tilde{C}_{23} + \tilde{C}_{13} + \tilde{C}_{33}} \frac{d\sigma}{dt} \\ + \frac{\left(\frac{2}{3}\tilde{C}_{32}\tilde{C}_{13} - \frac{1}{3}\tilde{C}_{22}\tilde{C}_{33} + \frac{1}{3}\tilde{C}_{32}\tilde{C}_{33} - \frac{2}{3}\tilde{C}_{23}\tilde{C}_{22} + \frac{1}{3}\tilde{C}_{13}\tilde{C}_{22} + \tilde{C}_{12}\tilde{C}_{23}\right)}{\tilde{C}_{23} + \tilde{C}_{13} + \tilde{C}_{33}} \frac{v_r}{r} = 0 \\ \text{along } \frac{dr}{dt} = V^{(4)} = 0 \end{aligned} \quad (2.70)$$

$$\begin{aligned} \frac{-d\sigma}{dt} + (\tilde{C}_{33} + \tilde{C}_{23} + \tilde{C}_{13}) \frac{d\varepsilon_{rr}}{dt} + (\tilde{C}_{32} + \tilde{C}_{12} + \tilde{C}_{22}) \frac{v_r}{r} = 0 \\ \text{along } \frac{dr}{dt} = V^{(5)} = 0 \end{aligned} \quad (2.71)$$

$$v_r - \frac{du_r}{dt} = 0$$

$$\text{along } \frac{dr}{dt} = V^{(6)} = 0 \quad (2.72)$$

2.6 Integration of the Canonical Equations for the Viscoelastic Layer

The canonical form of the governing equations for the viscoelastic layers that are valid along the characteristic lines were derived in Section 2.4 and given by Eqs. (2.46-2.51). These equations can be written in matrix form as:

$$\mathbf{E} \frac{d\mathbf{U}^{(v)}}{dt} - \mathbf{F}\mathbf{U}^{(v)} = \mathbf{0} \quad (2.73)$$

where the matrices \mathbf{E} and \mathbf{F} are given as:

$$\mathbf{E} = \begin{bmatrix} 0 & -1 & \frac{1}{\rho_v c_v} & 0 & \frac{1}{3\rho_v c_v} & 0 \\ 0 & -1 & \frac{-1}{\rho_v c_v} & 0 & -\frac{1}{3\rho_v c_v} & 0 \\ 0 & 0 & -1 & -2 & 0 & 0 \\ 0 & 0 & 0 & -1 & -\frac{b_1 c_1}{3d_1 a_1} & 0 \\ \frac{d_1}{c_1} & 0 & 0 & 0 & -1 & 0 \\ 0 & 0 & 0 & 0 & 0 & -1 \end{bmatrix} \quad (2.74)$$

$$F_{11} = \frac{1}{3\rho_v c_v} \left(\frac{2b_0}{a_1} + \frac{d_0}{c_1} \right), \quad F_{12} = \frac{1}{3\rho_v c_v} \left(\frac{d_1}{c_1} - \frac{b_1}{a_1} \right) \frac{1}{r}, \quad (2.75a)$$

$$F_{13} = -\frac{1}{\rho_v} \left(\frac{1}{r} + \frac{a_0}{a_1 c_v} \right), \quad F_{14} = \frac{1}{\rho_v r},$$

$$\begin{aligned}
F_{15} &= -\frac{c_0}{3\rho_v c_v c_1}, & F_{16} &= \frac{1}{3\rho_v c_v} \left(\frac{d_0}{c_1} - \frac{b_0}{a_1} \right) \frac{1}{r}, \\
F_{21} &= -\frac{1}{3\rho_v c_v} \left(\frac{2b_0}{a_1} - \frac{d_0}{c_1} \right), & F_{22} &= -\frac{1}{3\rho_v c_v} \left(\frac{d_1}{c_1} - \frac{b_1}{a_1} \right) \frac{1}{r}, \\
F_{23} &= -\frac{1}{\rho_v} \left(\frac{1}{r} - \frac{a_0}{a_1 c_v} \right), & F_{24} &= \frac{1}{\rho_v r}, \\
F_{25} &= \frac{c_0}{3\rho_v c_v c_1}, & F_{26} &= -\frac{1}{3\rho_v c_v} \left(\frac{d_0}{c_1} - \frac{b_0}{a_1} \right) \frac{1}{r}, \\
F_{32} &= -\frac{b_1}{a_1} \frac{1}{r}, & F_{33} &= \frac{a_0}{a_1}, \\
F_{34} &= \frac{2a_0}{a_1}, & F_{36} &= -\frac{b_0}{a_1} \frac{1}{r}, \\
F_{41} &= -\frac{1}{3a_1} \left(\frac{d_0 b_1}{d_1} - b_0 \right), & F_{42} &= -\frac{b_1}{a_1} \frac{1}{r}, \\
F_{44} &= \frac{a_0}{a_1}, & F_{45} &= \frac{b_1 c_0}{3d_1 a_1}, \\
F_{46} &= -\frac{1}{3a_1} \left(2b_0 + \frac{b_1 d_0}{d_1} \right) \frac{1}{r}, & F_{51} &= -\frac{d_0}{c_1}, \\
F_{52} &= -\frac{d_1}{c_1} \frac{1}{r}, & F_{55} &= \frac{c_0}{c_1}, \\
F_{56} &= -\frac{d_0}{c_1} \frac{1}{r}, & F_{62} &= -1
\end{aligned} \tag{2.75b}$$

all the other $F_{ij} = 0$.

The material constants in the constitutive equations of the standard linear solid given by Eqs. (2.14) can be expressed in terms of the parameters of the shear and bulk moduli which yield more physical insight. To this end, we consider the stress-strain relations for a linear isotropic and homogeneous viscoelastic material in integral

form given in Section 2.2 by Eqs (2.12-2.13). Shear and bulk moduli for the standard linear solid can be written as [133]:

$$G_1(t) = G_{1F} + (G_{10} - G_{1F})e^{-\frac{t}{\tau_1}} \quad (2.76)$$

$$G_2(t) = G_{2F} + (G_{20} - G_{2F})e^{-\frac{t}{\tau_2}}$$

In Eqs. (2.76), the constants τ_1 and τ_2 are the relaxation times of shear and bulk moduli, respectively, and

$$G_{1F} = G_1(\infty), \quad G_{10} = G_1(0) \quad (2.77)$$

$$G_{2F} = G_2(\infty), \quad G_{20} = G_2(0)$$

The constants in Eqs. (2.14) and Eqs. (2.76) are related according to

$$G_{10} = \frac{b_1}{a_1}, \quad G_{1F} = \frac{b_0}{a_0}, \quad \tau_1 = \frac{a_1}{a_0} \quad (2.78)$$

$$G_{20} = \frac{d_1}{c_1}, \quad G_{2F} = \frac{d_0}{c_0}, \quad \tau_2 = \frac{c_1}{c_0}$$

By substituting Eqs. (2.78) into Eqs. (2.74-2.75), we can express the matrices **E** and **F** in terms of the parameters of the shear and bulk moduli of the standard solid as

$$\mathbf{E} = \begin{bmatrix} 0 & -1 & \frac{1}{\rho_v c_v} & 0 & \frac{1}{3\rho_v c_v} & 0 \\ 0 & -1 & -\frac{1}{\rho_v c_v} & 0 & -\frac{1}{3\rho_v c_v} & 0 \\ 0 & 0 & -1 & -2 & 0 & 0 \\ 0 & 0 & 0 & -1 & -\frac{G_{10}}{3G_{20}} & 0 \\ G_{20} & 0 & 0 & 0 & -1 & 0 \\ 0 & 0 & 0 & 0 & 0 & -1 \end{bmatrix} \quad (2.79)$$

$$\begin{aligned} F_{11} &= \frac{1}{3\rho_v c_v} \left(\frac{2G_{1F}}{\tau_1} + \frac{G_{2F}}{\tau_2} \right), & F_{12} &= \frac{1}{3\rho_v c_v} (G_{20} - G_{10}) \frac{1}{r}, \\ F_{13} &= -\frac{1}{\rho_v} \left(\frac{1}{r} + \frac{1}{\tau_1 c_v} \right), & F_{14} &= \frac{1}{\rho_v r}, \\ F_{15} &= -\frac{1}{3\rho_v c_v \tau_2}, & F_{16} &= \frac{1}{3\rho_v c_v} \left(\frac{G_{2F}}{\tau_2} - \frac{G_{1F}}{\tau_1} \right) \frac{1}{r}, \\ F_{21} &= -\frac{1}{3\rho_v c_v} \left(\frac{2G_{2F}}{\tau_1} - \frac{G_{2F}}{\tau_2} \right), & F_{22} &= -\frac{1}{3\rho_v c_v} (G_{20} - G_{10}) \frac{1}{r}, \quad (2.80a) \\ F_{23} &= -\frac{1}{\rho_v} \left(\frac{1}{r} - \frac{1}{\tau_1 c_v} \right), & F_{24} &= \frac{1}{\rho_v r}, \\ F_{25} &= \frac{1}{3\rho_v c_v \tau_2}, & F_{26} &= -\frac{1}{3\rho_v c_v} \left(\frac{G_{2F}}{\tau_2} - \frac{G_{1F}}{\tau_1} \right) \frac{1}{r}, \\ F_{32} &= -\frac{G_{10}}{r}, & F_{33} &= \frac{1}{\tau_1}, \end{aligned}$$

$$\begin{aligned}
F_{34} &= \frac{2}{\tau_1}, & F_{35} &= 0, \\
F_{36} &= -\frac{G_{1F}}{\tau_1} \frac{1}{r}, & F_{41} &= -\frac{1}{3} \left(\frac{G_{10} G_{2F}}{G_{20} \tau_2} - \frac{G_{1F}}{\tau_1} \right), \\
F_{42} &= -\frac{G_{10}}{r}, & F_{44} &= \frac{1}{\tau_1}, \\
F_{45} &= \frac{G_{10}}{3G_{20} \tau_2}, & F_{46} &= -\frac{1}{3} \left(\frac{G_{10}}{G_{20}} \frac{G_{2F}}{\tau_2} + \frac{2G_{1F}}{\tau_1} \right) \frac{1}{r}, \\
F_{51} &= -\frac{G_{2F}}{\tau_2}, & F_{52} &= -G_{20} \frac{1}{r}, \\
F_{55} &= \frac{1}{\tau_2}, & F_{56} &= -\frac{G_{2F}}{\tau_2} \frac{1}{r}, \\
F_{62} &= -1, \\
\text{all the other } F_{ij} &= 0
\end{aligned} \tag{2.80b}$$

where the wave velocity c_v defined by Eq. (2.40) can now be expressed as

$$c_v = \left(\frac{2G_{10} + G_{20}}{3\rho_v} \right)^{\frac{1}{2}} \tag{2.81}$$

The canonical equations, Eqs. (2.73), can be written in a more compact form in indicial notation as:

$$E_{ij} \frac{dU_j^{(v)}}{dt} = F_{ij} U_j^{(v)} \quad (i = 1-6, \quad j = 1-6) \quad (2.82)$$

where a repeated index implies summation over its range. At this stage, it should be pointed out that the numerical procedure starts from the r - axis in the $(r-t)$ plane, and uses the various integration elements shown in Fig. 2.3. A typical interior integration element in the viscoelastic layer shown as element V in Fig. 2.3 is drawn separately in Fig. 2.4. The canonical equations are integrated along the characteristic lines as

$$\int_{A_i}^A E_{ij} \frac{dU_j^{(v)}}{dt} dt = \int_{A_i}^A F_{ij} U_j^{(v)} dt \quad (2.83)$$

where A_i and A are two consecutive points along the characteristic lines $C_v^{(i)}$ ($i = 1-6$), Fig. 2.4. Performing the integration in Eq. (2.83) using the trapezoidal rule, we obtain:

$$E_{ij} \left[U_j^{(v)}(A) - U_j^{(v)}(A_i) \right] = \frac{1}{2} \Delta t \left[F_{ij}(A) U_j^{(v)}(A) + F_{ij}(A_i) U_j^{(v)}(A_i) \right]$$

$$\left[E_{ij} - \frac{1}{2} \Delta t F_{ij}(A) \right] U_j^{(v)}(A) = \left[E_{ij} + \frac{1}{2} \Delta t F_{ij}(A_i) \right] U_j^{(v)}(A_i)$$

or

$$G_{ij}(A) U_j^{(v)}(A) = H_{ij}(A_i) U_j^{(v)}(A_i) \quad (i = 1-6, \quad j = 1-6) \quad (2.84)$$

where

$$G_{ij}(A) = E_{ij} - \frac{1}{2} \Delta t F_{ij}(A) \quad (2.85)$$

$$H_{ij}(A) = E_{ij} + \frac{1}{2} \Delta t F_{ij}(A_i)$$

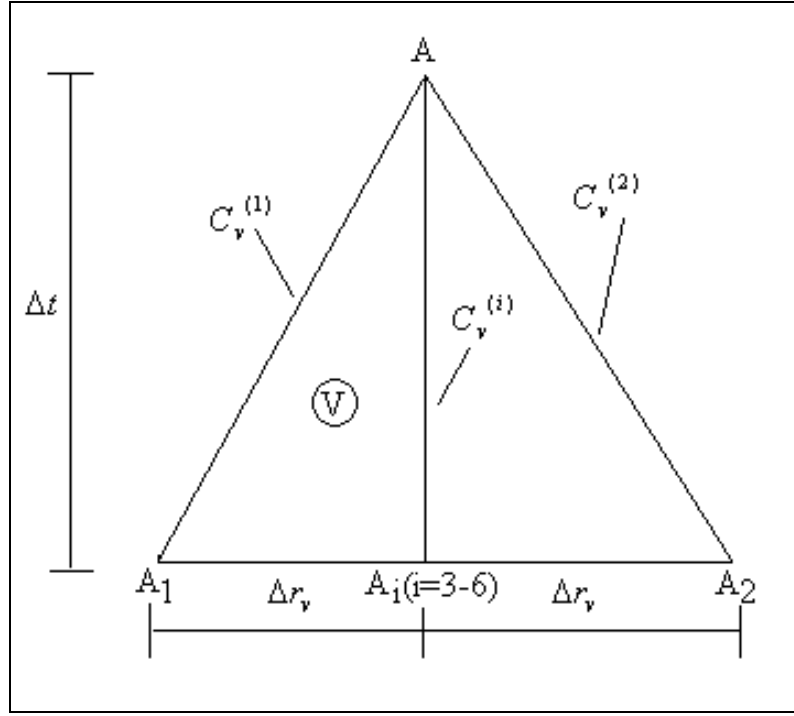


Figure 2.4. Typical interior integration element in the viscoelastic layer.

In Eqs. (2.85), Δt is the time interval between two consecutive points along the characteristic lines $C_v^{(1)}$, $C_v^{(2)}$, $C_v^{(i)}$ ($i = 3-6$), see Figs. (2.3-2.4). Furthermore, in Eqs.(2.84-2.85), a bar under an index implies that summation convention is not applied to that index and $U_j^{(v)}(A)$, $U_j^{(v)}(A_i)$ represents the values of the field variables at point A and A_i , respectively. The elements of E_{ij} and F_{ij} are given in Eqs. (2.79-2.80). Equations (2.84) represent six equations defined by $i = 1-6$, and for each value of the free index i , there is a summation over j which takes the values $j = 1-6$. Thus, when the field variables $U_j^{(v)}$ are known at points A_i ($i = 1-6$), the

values of the field variables $U_j^{(v)}$ at point A can be determined from Eqs. (2.84). In other words, using the triangular mesh shown in Fig. 2.4, the values of the field variables at a specific point along any line parallel to the r -axis in the solution region, see Fig. 2.4, can be found in terms of the known values of the field variables defined at points on the previous line. It is compact and suitable to express the equation in this form for computer programming.

2.7 Integration of the Canonical Equations for the Orthotropic Layers

The canonical form of the governing equations for a typical orthotropic layer derived in Section 2.5 and given by Eqs. (2.67-2.72) can be represented in matrix form as;

$$\mathbf{D} \frac{d\mathbf{U}}{dt} + \mathbf{N}\mathbf{U} = \mathbf{0} \quad (2.86)$$

where the matrices \mathbf{D} and \mathbf{N} are given as;

$$\mathbf{D} = \begin{bmatrix} 0 & -1 & \frac{1}{\rho c} & 0 & \frac{1}{3\rho c} & 0 \\ 0 & -1 & \frac{-1}{\rho c} & 0 & \frac{-1}{3\rho c} & 0 \\ 0 & 0 & -1 & \frac{(\tilde{C}_{13} + \tilde{C}_{23} - 2\tilde{C}_{33})}{(\tilde{C}_{33} + \tilde{C}_{13} - 2\tilde{C}_{23})} & 0 & 0 \\ 0 & 0 & 0 & -1 & \frac{(2\tilde{C}_{23} - \tilde{C}_{13} - \tilde{C}_{33})}{3(\tilde{C}_{23} + \tilde{C}_{13} + \tilde{C}_{33})} & 0 \\ (\tilde{C}_{33} + \tilde{C}_{23} + \tilde{C}_{13}) & 0 & 0 & 0 & -1 & 0 \\ 0 & 0 & 0 & 0 & 0 & -1 \end{bmatrix} \quad (2.87)$$

$$\begin{aligned}
N_{12} &= \frac{\tilde{C}_{32}}{\rho c} \frac{1}{r}, & N_{13} &= \frac{-1}{\rho r}, \\
N_{14} &= \frac{1}{\rho r}, & N_{22} &= \frac{-\tilde{C}_{32}}{\rho c} \frac{1}{r}, \\
N_{23} &= \frac{-1}{\rho r}, & N_{24} &= \frac{1}{\rho r}, \\
N_{32} &= -\frac{(\tilde{C}_{22}\tilde{C}_{33} - \tilde{C}_{22}\tilde{C}_{13} - \tilde{C}_{33}\tilde{C}_{12} + \tilde{C}_{12}\tilde{C}_{23} - \tilde{C}_{32}\tilde{C}_{23} + \tilde{C}_{32}\tilde{C}_{13})}{(\tilde{C}_{33} - 2\tilde{C}_{23} + \tilde{C}_{13})r}, & (2.88) \\
N_{42} &= \frac{-(\tilde{C}_{22}\tilde{C}_{33} + \tilde{C}_{22}\tilde{C}_{13} - \tilde{C}_{23}\tilde{C}_{32} - \tilde{C}_{12}\tilde{C}_{23})}{(\tilde{C}_{33} + \tilde{C}_{23} + \tilde{C}_{13})r}, \\
N_{52} &= \frac{-(\tilde{C}_{32} + \tilde{C}_{22} + \tilde{C}_{12})}{r}, & N_{62} &= 1,
\end{aligned}$$

all the other $N_{ij} = 0$

The unknown vector \mathbf{U} is defined by Eq. (2.58).

The canonical equations valid along the characteristic lines of a typical orthotropic layer can be integrated in a completely analogous manner as those of the viscoelastic layer. We obtain,

$$\begin{aligned}
D_{ij} [U_j(A) - U_j(A_i)] &= \frac{1}{2} \Delta t [N_{ij}(A) U_j(A) + N_{ij}(A_i) U_j(A_i)] \\
\left[D_{ij} - \frac{1}{2} \Delta t N_{ij}(A) \right] U_j(A) &= \left[D_{ij} + \frac{1}{2} \Delta t N_{ij}(A_i) \right] U_j(A_i)
\end{aligned}$$

or

$$S_{ij}U_j(A) = Z_{ij}(A_i)U_j(A_i) \quad (i = 1-6, j = 1-6) \quad (2.89)$$

where

$$S_{ij} = D_{ij} - \frac{1}{2}\Delta t N_{ij}(A) \quad (2.90)$$

$$Z_{ij} = D_{ij} + \frac{1}{2}\Delta t N_{ij}(A_i)$$

In Eqs. (2.90), Δt is the time interval between two consecutive points along the characteristic lines, same as that of the viscoelastic layer, see Fig. 2.3 The elements D_{ij} and N_{ij} are given by Eqs. (2.87-2.88), and U_j defines the components of the unknown vector for a typical orthotropic layer. Furthermore, $U_j(A)$ and $U_j(A_i)$ define the values of U_j at points A and A_i ($i = 1-6$), respectively.

2.8 Modification of the Equations for the Boundary and Interface Elements

For the boundary element ‘B1’, an element on the inner boundary $r = a$ as shown in Fig. 2.3, we should modify Eqs. (2.84) in order to satisfy the boundary conditions.

When the layered body is subjected to time dependent dynamic input at its inner surface, Eqs. (2.25)₁, the integrated canonical equations, Eqs. (2.84), remain the same for $(i = 2-6, j = 1-6)$ whereas, the integrated canonical equation for $(i = 1, j = 1-6)$ should be replaced by the boundary condition

$$\sigma_{rr}^{(v)'}(A) + \frac{1}{3}\sigma_v(A) = -P(A) \quad \text{or} \quad V_r^{(v)}(A) = V(A) \quad (2.91)$$

Now, for the interior element ‘V’, shown in Fig. 2.3, Eqs. (2.84) are capable of determining the values $U_j^{(v)}$ for $(i = 1-6, j = 1-6)$ without any modification.

As for the interface element ‘M’ an element on the interface between the viscoelastic layer and the orthotropic layer labelled as layer 1, we should make use of combining the sets of Eq.(2.84) and Eq. (2.89) together with the interface conditions. The interface conditions require the continuity of the surface tractions and displacements at the interface, that is the stress component $\sigma_{rr}^{(v)}$ of the viscoelastic layer is equal to the stress component $\sigma_{rr}^{(1)}$ of the first orthotropic layer and the particle velocity ($v_r^{(v)}$) of the viscoelastic layer is equal to particle velocity ($v_r^{(1)}$) of the first orthotropic layer at points on the interface. We can write the governing equations for this element as:

$$G_{ij}(A)U_j^{(v)}(A) = H_{ij}(A)U_j^{(v)}(A_i) \quad (i = 1,3,4,5,6; j = 1-6) \quad (2.92)$$

$$S_{ij}U_j^{(1)}(A) = Z_{ij}(A_i)U_j^{(1)}(A_i) \quad (i = 2-6, j = 1-6)$$

supplemented by the interface conditions

$$\sigma_{rr}^{(v)'}(A) + \frac{1}{3}\sigma_v(A) = \sigma_{rr}^{(1)'}(A) + \frac{1}{3}\sigma_1(A) \quad (2.93)$$

and

$$v_r^{(v)}(A) = v_r^{(1)}(A) \quad (2.94)$$

The composite bodies considered in this thesis consist of n different, orthotropic, homogenous and linearly elastic filament wound layers. Equations (2.89) were derived for a typical layer. This typical layer can be considered as the m th layer and all the quantities pertaining to the m th layer will be denoted by subscripts m or superscripts m in parantheses. For a composite case consisting of n layers, m

takes the values $m=1,2,\dots,n$. Thus, the integrated equations for the interior element K in the m th layer can be written as

$$S_{ij}^{(m)} U_j^{(m)}(A) = Z_{ij}^{(m)}(A_i) U_j^{(m)}(A_i) \quad (i=1-6, j=1-6) \quad (2.95)$$

where $S_{ij}^{(m)}$ and $Z_{ij}^{(m)}$ can be obtained from Eqs. (2.90) by simply putting superscripts m in parentheses over all the quantities appearing in these equations. In this thesis, the inner orthotropic layer is assumed to be layer 1 and the outermost orthotropic layer is assumed to be n .

For the boundary element B_2 on the outer surface $r=c$ (see Fig. 2.3), Eqs. (2.89) need to be modified. Equations for $i=1, 3-6$ remain the same, that is

$$S_{ij}^{(n)} U_j^{(n)}(A) = Z_{ij}^{(n)}(A_i) U_j^{(n)}(A_i) \quad (i=1,3,4,5,6; j=1-6) \quad (2.96)$$

whereas, the equation for $i=2$, should be replaced by

$$\sigma_{rr}^{(n)'}(A) + \frac{1}{3} \sigma_{(n)}(A) = -F(A) \quad \text{or} \quad V_r^{(n)}(A) = G(A) \quad (2.97)$$

depending on whether surface tractions or particle velocity is prescribed..

We have another type of element where Eqs. (2.89) need to be modified. These elements which are called the interface elements of orthotropic layers correspond to points A at the interfaces. The number of interfaces depend on the number of layers and since we have n layers, we have $(n-1)$ interfaces which will be denoted by $(L_{12}, L_{23}, \dots, L_{(n-1)(n)})$, see Fig. 2.3. For a point A at the interface between the layers m and $m+1$, element $L_{(m)(m+1)}$, Fig. 2.3, Eqs.(2.89) are modified as

$$S_{ij}^{(m)} U_j^{(m)}(A) = Z_{ij}^{(m)}(A_i) U_j^{(m)}(A_i) \quad (i = 1, 3, 4, 5, 6; j = 1 - 6) \quad (2.98)$$

$$S_{ij}^{(m+1)} U_j^{(m+1)}(A) = Z_{ij}^{(m+1)}(A_i) U_j^{(m+1)}(A_i) \quad (i = 2 - 6; j = 1 - 6)$$

where the superscripts m in paranthesis denote the layer which precedes the interface and $m+1$ denotes the layer which follows the interface. Equations (2.89) for $i = 2$ for m th layer and $i = 1$ for the layer $m+1$ are replaced by the interface conditions requiring the continuity of surface tractions and displacements, which are

$$\sigma_{rr}^{(m)'}(A) + \frac{1}{3} \sigma_m(A) = \sigma_{rr}^{(m+1)'} + \frac{1}{3} \sigma_m(A) \quad (2.99)$$

and

$$v_r^{(m)}(A) = v_r^{(m+1)}(A) \quad (2.100)$$

Thus, modification of the equations for the interface and boundary elements is completed. Equations (2.98–2.100) represent twelve equations to determine the twelve unknowns, $U_j^{(m)}(A)$ and $U_j^{(m+1)}(A)$, pertaining to points on the interface of the layers m and $m+1$.

2.9 Ablating Inner Boundary

In this section, we investigate the case in which the inner surface of the viscoelastic cylinder enclosed in filament wound cylindrical composites is a moving boundary. This is the case in solid propellant rocket motor cases. As the propellant burns, the inner surface moves outwards, decreasing the thickness of the viscoelastic layer representing the solid propellant (see Fig. 2.5). As can be seen from Fig. 2.5, equations for the elements ‘T’ and ‘P’ should be obtained by properly modifying the previously derived equations for the inner and boundary elements of the viscoelastic layer.

In order to find the values of the field variables $U_j^{(v)}$ at points A of the boundary element 'T', we make use of Eqs. (2.84) together with Eq.(2.91). However, the coefficients $G_{ij}(A)$ and $H_{ij}(A_i)$ and the values of the field variables at points A_i , that is $U_j(A_i)$, should be modified properly. For this purpose, the values of G_{ij} ($i = 2 - 6, j = 1 - 6$) at point A should be calculated using the known G_{ij} values of the former and later points (points F and L at Fig. 2.6) with interpolation technique. Formulation of this calculation can be written in equation form as

$$G_{ij}(A) = \frac{G_{ij}(L) - G_{ij}(F)}{\Delta r_v} \Delta r_F + G_{ij}(F) \quad (2.101)$$

where Δr_v and Δr_F are the distances shown in Figs. (2.5-2.6) and $G_{ij}(L)$ and $G_{ij}(F)$ denote the values of G_{ij} at points 'L' and 'F', respectively, Fig. 2.6.

Furthermore, the values of H_{ij} ($i = 2 - 6, j = 1 - 6$) at points 'A₂' and 'A₃' of the element 'T' should be modified using their known values at points 'P'', 'Q' and 'S', see Fig. 2.6. These can be calculated through interpolation as

$$H_{2j}(A_2) = \frac{H_{2j}(S) - H_{2j}(Q)}{\Delta r_v} \Delta r_Q + H_{2j}(Q) \quad (2.102)$$

$$H_{3j}(A_3) = \frac{H_{3j}(Q) - H_{3j}(P')}{\Delta r_{P'Q}} \Delta r_{P'} + H_{3j}(P') \quad (2.103)$$

where $\Delta r_{P'Q}$, Δr_Q , $\Delta r_{P'}$ are the distances shown in Fig. 2.6 and can be calculated as below

$$\Delta r_{p'} = \frac{t + T_{burn}}{2T_{burn}}$$

$$\Delta r_{p'Q} = \Delta r_v - \Delta r_{p'} \quad (2.104)$$

$$\Delta r_Q = 2\Delta r_{p'}$$

In Eqs. (2.104), t is the time corresponding to point A of typical boundary element T and T_{burn} is the burning time of the whole solid propellant. In other words, T_{burn} is the time required to reach zero thickness for viscoelastic layer.

We must further find the values of vector $U_j^{(v)}$ at points A_2 and A_3 of element 'T'. This can be achieved by interpolating known values of the field variables at points 'P', 'Q' and 'S' as shown in Fig. 2.6 and can be written in equation form as

$$U_j^{(v)}(A_2) = \frac{U_j^{(v)}(S) - U_j^{(v)}(Q)}{\Delta r_v} \Delta r_Q + U_j^{(v)}(Q) \quad (2.105)$$

$$U_j^{(v)}(A_3) = \frac{U_j^{(v)}(Q) - U_j^{(v)}(P')}{\Delta r_{p'Q}} \Delta r_{p'} + U_j^{(v)}(P') \quad (2.106)$$

In Eqs. (2.105-2.106), $U_j^{(v)}(P')$, $U_j^{(v)}(Q)$ and $U_j^{(v)}(S)$ denote the values of the field variables $U_j^{(v)}$ at points 'P', 'Q' and 'S', Fig. 2.6.

The modifications of the coefficients and the values of the field variables in Eqs. (2.84) for the inner element 'P' will now be considered. For the element, location of the point A_1 can be seen on Fig. 2.6. As can be seen from the figure, equations of H_{1j} ($j = 1 - 6$) for point A_1 needs modification. This can be done by modifying the time difference and the position values in the equation. For the former one $\Delta t t$ is used instead of Δt after that point. For example $H_{12}(A_1)$ takes the form below

$$H_{12}(A_1) = - \left[1 - \frac{\Delta t t}{6} (G_{20} - G_{10}) \frac{1}{r(A_1)} \right] \quad (2.107)$$

where $\Delta t t$ is the time difference and $r(A_1)$ is the position of the point A_1 of element P as shown in Fig. 2.6 and $\Delta t t$ can be evaluated using the following equation

$$\Delta t t = \Delta P'_Q - \Delta r_{p'} \quad (2.108)$$

Furthermore, the values of $U_j^{(v)}$ for point A_1 of element 'P' should be evaluated by interpolation from known values of the field quantities at points 'W' and 'V' shown in Fig. 2.6. This can be written as

$$U_j^{(v)}(A_1) = \frac{U_j^{(v)}(V) - U_j^{(v)}(W)}{\Delta t} (\Delta t - \Delta t t) + U_j^{(v)}(W) \quad (2.109)$$

where $U_j^{(v)}(V)$ and $U_j^{(v)}(W)$ are the known values of the field variables at points 'V' and 'W', see Fig. 2.6.

For the points A of inner element 'S', Eq. (2.84) do not need any modification.

2.10 The Solution Procedure

At this point, the integration of the canonical equations is completed. Before discussing the numerical examples, we explain below, the numerical procedure in more detail. For this purpose, we refer to the network of characteristic lines, Fig. 2.3.

Our goal is to establish the solution $U_i^{(v)} = (\varepsilon_{rr}^{(v)}, \nu_r^{(v)}, \sigma_{rr}^{(v)}, \sigma_{\theta\theta}^{(v)}, \sigma_v, u_r^{(v)})$ for the viscoelastic layer and $U_i = (\varepsilon_{rr}, \nu_r, \sigma_{rr}, \sigma_{\theta\theta}, \sigma, u_r)$ for the orthotropic layers

Figure 2.5. Description of characteristic lines with a moving inner boundary for the encased viscoelastic cylinder.

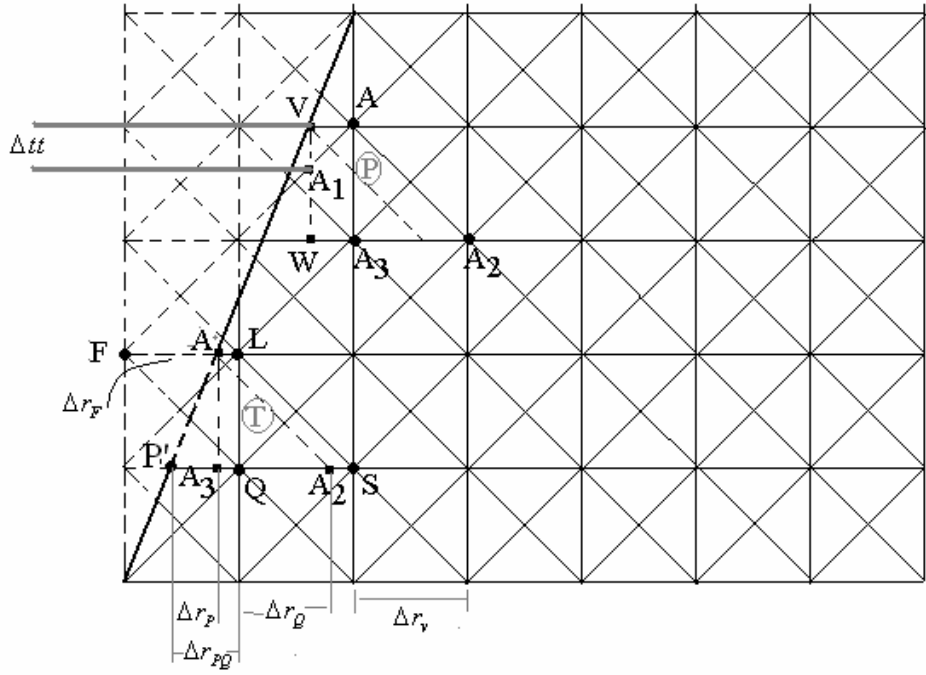


Figure 2.6. Detailed description of elements T and P on the $(r-t)$ plane.

at all points of the network of characteristics lines shown in Fig. 2.3. To achieve this, we start at the origin and proceed along r -axis where the values of, $U_i^{(v)}$, U_i are all equal to zero because of quiescent initial conditions. Then, we proceed into the region by computing $U_i^{(v)}$, U_i at the points of the network with the order 1',2',3',.....1'',2'',3'',....etc(Fig. 2.3).

To explain the numerical procedure, we refer to five different elements, namely, the inner boundary element 'B₁', the inner viscoelastic layer element 'V', the interface element 'M' between viscoelastic layer and first orthotropic layer, the inner orthotropic element 'K', the interface element 'L' between orthotropic layers, and the outer boundary element 'B₂', see Fig. 2.3. Knowing that all the field variables are zero on the r -axis, we start the solution at point 1' which is point A on the boundary $r = a$ and is denoted by element 'B₁' in Fig. 2.3. The analysis of the boundary element 'B₁' involves finding the six components of $U_i^{(v)}$ at the point A in

terms of their values at the points A_2 and A_i ($i = 3 - 6$) and the given boundary condition at the inner surface. The integrated equations giving the values of $U_i^{(v)}$ at the point A are Eqs. (2.84) for ($i = 2 - 6$, $j = 1 - 6$) together with Eq. (2.91) where the inner boundary surface is subjected to uniform time dependent dynamic inputs. As we advance in the $(r - t)$ -plane, we come to an interior point A in the viscoelastic layer which is denoted by element 'V' in Fig. 2.3. Similarly, the analysis for the interior element 'V' involves establishing the six components of $U_i^{(v)}$ at the points A in terms of their values at the points A_1 , A_2 and A_i ($i = 3 - 6$) which at this stage are all known. The equations giving these values were obtained in section 2.6 as Eqs. (2.84). Next element in the solution process is 'M' which represents points A at the interface of the viscoelastic and innermost orthotropic layers. The analysis of this element involves finding the values of $U_i^{(v)}$ and $U_i^{(l)}$, ($i = 1 - 6$), from the integrated canonical equations, Eqs. (2.92) and the interface conditions given by Eqs. (2.93-2.94). Next type of the element in the solution process is, the inner element 'K' in the m th layer and the analysis involves the determination of the values of U_i at the points A in terms of their values at points A_1 , A_2 and A_i ($i = 3 - 6$). This is accomplished by employing Eqs. (2.95). For an interface element 'L' at the interface of layers m and $m+1$, the values of the field variables at point A can be determined from the integrated canonical equations, Eqs. (2.98), together with the interface conditions given by Eqs. (2.99-2.100). Finally, in the analysis for the boundary element 'B₂' at $r = c$, the values of the field variables at point A are determined from Eqs. (2.96-2.97). This completes the description of the numerical procedure to obtain the values of the field variables $U_i^{(v)}$ and U_i ($i = 1 - 6$) at points A of the network of the characteristic lines. For this purpose, a computer program in the FORTRAN language is written and the numerical computations are carried out at the computer.

For the ablating inner boundary solutions, we investigate the problem with two different boundary lines. Equations for the two boundary lines are different from each other because the rates of decrease of the solid rocket propellant for the two

cases are taken different. The equations of these boundary lines in the $(r-t)$ plane can be stated as follows.

$$t = \frac{100}{c_v}(r-a): \quad \text{boundary line BL}_1 \quad (2.110)$$

$$t = \frac{500}{c_v}(r-a): \quad \text{boundary line BL}_2 \quad (2.111)$$

In the first equation, Eq. (2.110), the rate of decrease is the highest while for the last equation, Eq. (2.111), it is the smallest. In other words, Eq. (2.111) has smaller slope with respect to t – *axis* as compared to Eq. (2.110).

Our aim in using two different line equations is, to find $U_j^{(v)}$ ($j=1-6$) and U_j ($j=1-6$) in the viscoelastic cylinder enclosed in filament wound cylindrical composites for two different decreasing rates is to see the effects of the rate of decrease of the thickness of the viscoelastic layer on the stresses in the remaining of the viscoelastic layer and the filament wound cylindrical laminate enclosing the viscoelastic layer. Numerical values for the material properties and the geometric parameters are exactly the same as the numerical values of the examples considered in the non ablating cases.

In the case of an ablating inner boundary, the integrated canonical equations for the boundary element ‘B₁’ and the inner element ‘V’ for some inner points in the immediate vicinity of the ablating boundary need to be modified. This modification was described in some detail in section 2.9. As in the case of non-ablating boundary, we start at the origin and proceed along the r – *axis*, where at all the points the field variables are zero due to quiescent initial conditions. Then, we proceed to point 1’, Fig. 2.5. Point 1’ is a boundary point described by element ‘T’. Hence, we use Eqs. (2.84, 2.91) with the modifications defined by Eqs. (2.101-2.103, 2.105) to find the field quantities at point 1’. Then we proceed to point 2’. This is an interior point in the immediate vicinity described by the interior element ‘P’ and therefore, we use

Eqs. (2.84) with the modifications defined in Eqs. (2.106, 2.107), in order to find the values of the field variables at this point. After finding it, we pass to point $3'$. This is also an interior point, but described by element 'S' and hence we can use Eqs. (2.84) without any modification. We know the values of the field variables at points 2, 3 and 4 and we can find the response of point $3'$. The values of the field variables at points $4'$, $5'$, $6'$, are computed in the same way as that of the non ablating boundary case, employing the same equations with the same elements.

We wrote a computer program for this case and carried out all the computations through the computer. The computer program is written in FORTRAN language as well.

2.11 Numerical Examples and Discussion of the Results

In the numerical examples, the inner surface is assumed to be subjected to a uniform time dependent pressure and the outer surface is free of surface tractions, that is, the boundary conditions, in view of Eqs. (2.25), are

$$\begin{aligned}\sigma_{rr}^{(v)'}(a, t) + \frac{1}{3}\sigma_v(a, t) &= -P(t)H(t) \\ \sigma_{rr}^{(n)'}(c, t) + \frac{1}{3}\sigma_n(c, t) &= 0\end{aligned}\tag{2.112}$$

In the method of characteristics, we are free to choose any time dependency for the applied pressure. In the problems, we choose a step-time variation with an initial ramp, see Fig. 2.7. In this figure, we notice that the applied pressure is zero at $t = 0$, linearly rises to a constant value P_o during a rise time of Δt and remains constant thereafter. The initial ramp in the pressure variation eliminates the complicated circumstances of having first-order discontinuities in the field variables at the wave fronts. Furthermore, it is physically more realistic as a boundary condition than a step time variation without a ramp.

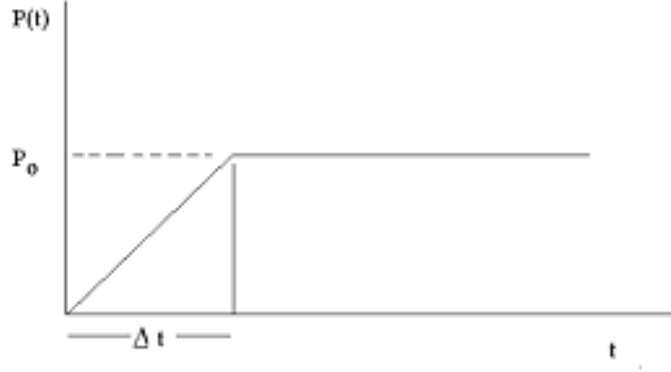


Figure 2.7. Variation of radial pressure applied at the inner surface.

The numerical computations are carried out and the results are displayed in terms of non-dimensional quantities. These non-dimensional quantities are defined as

$$\bar{r} = \frac{r}{a}, \quad \bar{t} = \frac{tc_v}{a}, \quad \bar{c}_v = \frac{c_v}{c_v} = 1$$

$$\bar{\rho}_v = \frac{\rho_v}{\rho_v} = 1, \quad \bar{\rho}_n = \frac{\rho_n}{\rho_v}, \quad \bar{c}_n = \frac{c_n}{c_v}$$

$$(\bar{u}_r^{(v)}, \bar{u}_r^{(n)}) = \left(\frac{u_r^{(v)}}{a}, \frac{u_r^{(n)}}{a} \right), \quad (2.113a)$$

$$(\bar{v}_r^{(v)}, \bar{v}_r^{(n)}) = \left(\frac{v_r^{(v)}}{c_v}, \frac{v_r^{(n)}}{c_v} \right),$$

$$(\bar{E}_1, \bar{E}_2, \bar{E}_3) = \left(\frac{E_1}{\rho_v c_v^2}, \frac{E_2}{\rho_v c_v^2}, \frac{E_3}{\rho_v c_v^2} \right),$$

$$(\bar{\sigma}_{rr}^{(v)'}, \bar{\sigma}_{\theta\theta}^{(v)'}, \bar{\sigma}_v) = \left(\frac{\sigma_{rr}^{(v)'}}{\rho_v c_v^2}, \frac{\sigma_{\theta\theta}^{(v)'}}{\rho_v c_v^2}, \frac{\sigma_v}{\rho_v c_v^2} \right),$$

$$\begin{aligned} \left(\bar{\sigma}_{rr}^{(n)'} , \bar{\sigma}_{\theta\theta}^{(n)'} , \bar{\sigma}_n \right) &= \left(\frac{\sigma_{rr}^{(n)'}}{\rho_v c_v^2} , \frac{\sigma_{\theta\theta}^{(n)'}}{\rho_v c_v^2} , \frac{\sigma_n}{\rho_v c_v^2} \right), \\ \left(\bar{G}_{12}, \bar{G}_{12}, \bar{G}_{23} \right) &= \left(\frac{G_{12}}{\rho_v c_v^2} , \frac{G_{13}}{\rho_v c_v^2} , \frac{G_{23}}{\rho_v c_v^2} \right), \\ \left(\bar{\tau}_1, \bar{\tau}_2 \right) &= \left(\frac{\tau_1 c_v}{a} , \frac{\tau_2 c_v}{a} \right), \end{aligned} \quad (2.113b)$$

$$\left(\bar{G}_{10}, \bar{G}_{20}, \bar{G}_{1F}, \bar{G}_{2F} \right) = \left(\frac{G_{10}}{\rho_v c_v^2} , \frac{G_{20}}{\rho_v c_v^2} , \frac{G_{1F}}{\rho_v c_v^2} , \frac{G_{2F}}{\rho_v c_v^2} \right),$$

$$\bar{a} = \frac{a}{a} = 1, \quad \left(\bar{b}, \bar{c} \right) = \left(\frac{b}{a}, \frac{c}{a} \right)$$

where the non-dimensional quantities are designated by bars. Furthermore, a is the radius of the inner surface and ρ_v, c_v are the mass density and wave velocity of the viscoelastic layer, respectively.

First, several examples will be given to verify the validity, efficiency and effectiveness of the method employed. In the first example of verification, the dynamic response of a viscoelastic cylinder encased in an isotropic, homogeneous and linearly elastic layer is investigated. The viscoelastic and elastic layers are perfectly bonded to each other. The inner surface of the viscoelastic layer is subjected to a uniform time dependent pressure where the time variation is chosen as a step function with an initial ramp, see Fig. 2.7, and the outer surface is free of surface tractions, Eqs (2.112). The encased viscoelastic cylinder is initially at rest. This problem was solved by Turhan and Şen [139] and Şen [144] by employing the method of characteristics. Şen's [144] solution was further verified by the solution of Chou and Greif [43] for a special case. The solution of this problem in our treatment is obtained as a special case of a viscoelastic cylinder encased in a filament wound

fiber-reinforced cylindrical composite consisting of three generally orthotropic layers with stacking sequence -30/0/90 starting from the inner layer. The viscoelastic material is modelled as standart linear solid in this study as well as Refs. [139, 144].

Two different materials (one more viscous) were chosen for the viscoelastic layer. The material properties are taken as Refs. [133, 139]

A) Material 1: (more viscous material properties)

$$\begin{aligned}\bar{G}_{10} &= 0.7; & \bar{G}_{1F} &= 0.14; & \bar{G}_{20} &= 1.6; & \bar{G}_{2F} &= 0.4; \\ \bar{\tau}_1 &= 1.5; & \bar{\tau}_2 &= 2.5; & \bar{\rho} &= 1; & \bar{c}_v &= \frac{c_v}{c_v} = 1\end{aligned}\quad (2.114)$$

B) Material 2: (less viscous material properties)

$$\begin{aligned}\bar{G}_{10} &= 0.7; & \bar{G}_{1F} &= 0.28; & \bar{G}_{20} &= 1.6; & \bar{G}_{2F} &= 0.8 \\ \bar{\tau}_1 &= 3; & \bar{\tau}_2 &= 5; & \bar{\rho} &= 1; & \bar{c}_v &= 1\end{aligned}\quad (2.115)$$

The non-dimensional material properties for the elastic case were taken in [139] as

$$\begin{aligned}\bar{\lambda} &= \frac{\lambda}{\rho_v c_v^2} = 4.57, & \bar{\mu} &= \frac{\mu}{\rho_v c_v^2} = 6.86, \\ \rho_e &= \frac{\rho_e}{\rho_v} = 4, & c_e &= \frac{c_e}{c_v} = 2\end{aligned}\quad (2.116)$$

where λ and μ are Lamé's constants and ρ_e and c_e are the density and particle wave velocities of the isotropic elastic layer.

In our treatment of the problem in this study, we take the material properties of the three generally orthotropic layers the same and such that they represent three identical isotropic elastic layers with the same dimensionless material properties given by Eq. (2.116). The thickness of the layers are chosen such that the total thickness of the multilayered elastic case is the same as the thickness of the elastic layer of Refs. [139,144]. The material properties of the viscoelastic layer in our treatment are taken the same as these given by Eqs. (2.114-2.115). The material properties of the orthotropic layers in our treatment are taken as

$$\bar{E}_1 = \bar{E}_2 = \bar{E}_3 = 11.691; \quad \bar{G}_{12} = \bar{G}_{13} = \bar{G}_{23} = 3.96 \quad (2.117)$$

$$\nu_{23} = \nu_{32} = \nu_{31} = \nu_{13} = \nu_{21} = \nu_{12} = 0.3$$

The geometric properties of the case cylinders of Refs. [139,144] and those considered in this treatment are

$$\bar{a} = 1; \quad \bar{b} = 2; \quad \bar{c} = 2.3 \quad (2.118)$$

The curves for denoting the variations of the non-dimensional radial normal stress $-\sigma_{rr}^{(v)} / P_0$ with the dimensionless time $\bar{t} = tc_v / a$ at the location $\bar{r} = r / a = 1.5$ and the non- dimensional circumferential normal stress $\sigma_{\theta\theta} / P_0$ with $\bar{t} = tc_v / a$ at location $\bar{r} = 2.15$ for nonablating inner surface are given in Figs. (2.8, 2.9), respectively. Location $\bar{r} = 1.5$ is in the viscoelastic layer, whereas $\bar{r} = 2.15$ is in the outer elastic case. The curves for viscoelastic material 1 obtained from Refs. [139,144] and those obtained in this study as a special case are almost identical and they are given as the same curves in Figs. (2.8, 2.9). The curves for viscoelastic material 2 are not given in Refs. [139,144]. They are given in this study to show the effects of viscosity of the viscoelastic layer. Material 2 is less viscous than material 1

and this is revealed in the curves by a slower attenuation of the stress levels due to material internal friction. The case of ablating inner surface defined by

$$\bar{t} = 500(\bar{r} - 1): \quad \text{boundary line BL}_2 \quad (2.119)$$

is considered in Fig. 2.10. The curves in this figure denote the time variations of $\sigma_{\theta\theta} / P_0$ at the location $\bar{r} = 2.15$ in the outer elastic layer for both the ablating and non-ablating inner surfaces. The curves are for viscoelastic material 1. The curves of Refs. [139,144] and these obtained in this study coincide and they are shown as one curve in Fig. 2.10. These excellent agreements verify the validity of our solutions.

In the second example of verification, transient dynamic response of a multilayered medium consisting of five generally orthotropic layers with the stacking sequence 30/-30/90/0/90 is considered. A uniform pressure with a stepwise time variation as shown in Fig. 2.7, is applied on the inner surface and the outer boundary is free of surface tractions. This problem was solved by Turhan and Ghaith [140] which was verified, for a special case, by the solution of Chou and Greif [43]. The numerical computations are carried out for T300/5208 graphite/epoxy composite with the non dimensional properties

$$\bar{E}_1 = \frac{E_1}{C_{33}} = 0.817,$$

$$\bar{E}_2 = \bar{E}_3 = \frac{E_2}{C_{33}} = \frac{E_3}{C_{33}} = 0.644, \quad (2.120a)$$

$$\bar{G}_{12} = G_{13} = \frac{G_{12}}{C_{33}} = \frac{G_{13}}{C_{33}} = 0.0338,$$

$$\bar{G}_{23} = \frac{G_{23}}{C_{33}} = 0.035,$$

$$\nu_{12} = \nu_{13} = 0.238, \quad \nu_{23} = 0.49$$

$$\bar{a} = 1, \quad \bar{b} = 1.5, \quad (2.120b)$$

$$\bar{h}_i = 0.1 \quad (i = 1-5), \quad \bar{\rho}_i = 1 \quad (i = 1-5)$$

This problem is solved in this study by modifying our computer program to include only the generally orthotropic layers without the viscoelastic layer. The solution obtained in this study is exactly the same as that given in Ref. [140] and the curves giving the time variations of the non-dimensional radial and circumferential normal stresses at location $\bar{r} = 1.25$ are given in Fig. 2.11.

We now present some results for the case of viscoelastic cylinders encased in filament wound fiber-reinforced cylindrical composites which is the basic problem investigated in this chapter. The inner surface is subjected to a uniform time dependent pressure and the outer surface is free of surface tractions, that is, the boundary conditions are given by Eqs (2.112). The pressure function $P(t)$ has a step-time variation with an initial ramp as shown in Fig. 2.7. The body is assumed to be initially at rest; hence, the initial conditions are as given in Eqs. (2.28). The layers are assumed to be perfectly bonded to each other, and therefore, the interface conditions are as defined by Eqs. (2.26-2.27). The multilayered body consists of a viscoelastic layer whose material is modeled as standard linear solid and three generally orthotropic elastic layers with stacking sequence -30/0/90 starting from the inner layer. The numerical computations are carried out using solid propellant material properties for inner viscoelastic layer and S2 glass/epoxy composite material properties for orthotropic elastic outer layers [141-142]. The non-dimensional material properties then can be written as

A) Propellant properties

$$\bar{G}_{10} = 0.006; \quad \bar{G}_{1F} = 0.002; \quad \bar{G}_{20} = 2.988; \quad (2.121)$$

$$\bar{G}_{2F} = 0.805; \quad \bar{\tau}_1 = 1.4; \quad \bar{\tau}_2 = 3.8; \quad \bar{\rho}_v = 1;$$

B) S2 glass/epoxy properties

$$\nu_{23} = \nu_{32} = 0.33; \quad \nu_{31} = \nu_{13} = \nu_{21} = \nu_{12} = 0.236;$$

$$\bar{G}_{23} = 20.786; \quad \bar{G}_{13} = \bar{G}_{12} = 19.591 \quad (2.122)$$

$$\bar{E}_1 = 163.693; \quad \bar{E}_2 = \bar{E}_3 = 54.564$$

$$\bar{\rho} = 1.588$$

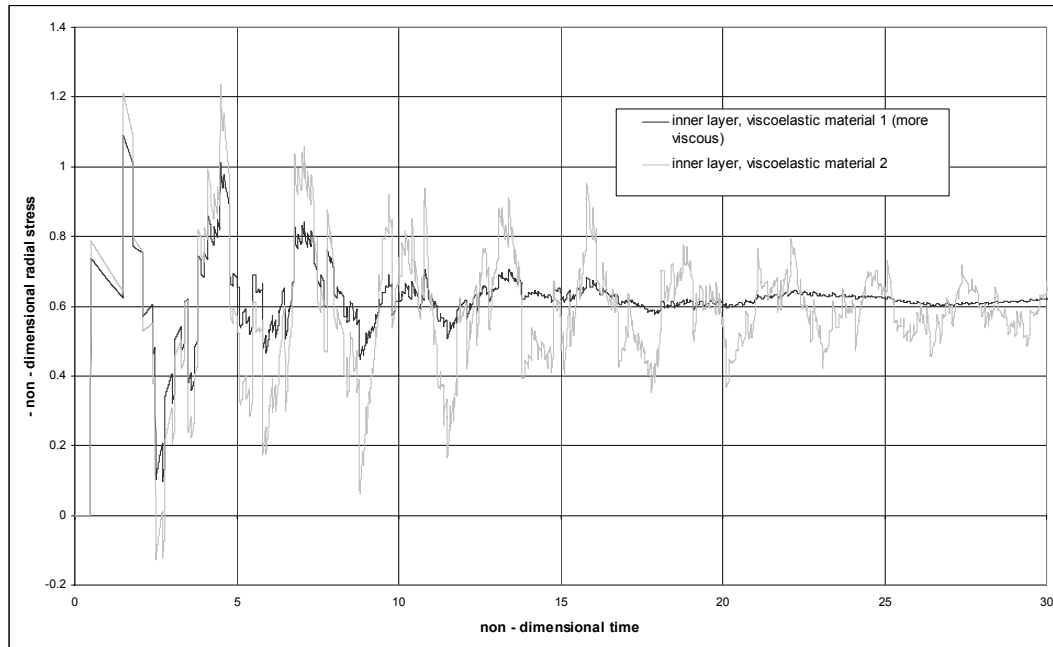


Figure 2.8. Variation of radial normal stress $-\sigma_{rr}/P_0$ with time \bar{t} at location $\bar{r} = 1.5$ in the viscoelastic layer for non-ablating inner surface.

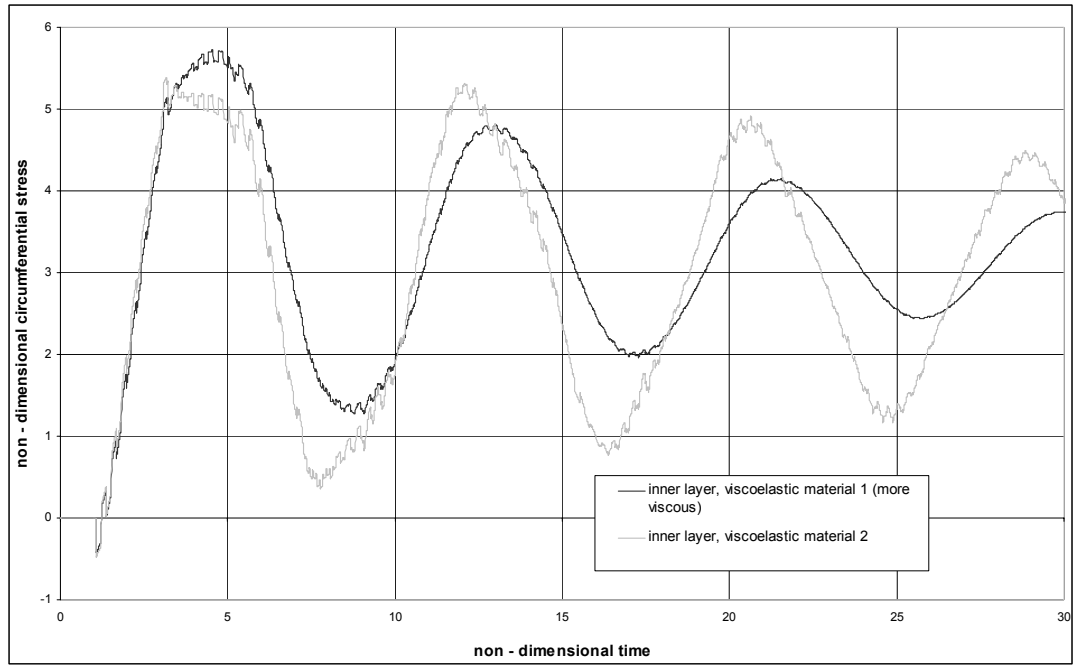


Figure 2.9. Variation of circumferential normal stress $\sigma_{\theta\theta} / P_0$ with time \bar{t} at location $\bar{r} = 2.15$ for non-ablating inner surface.

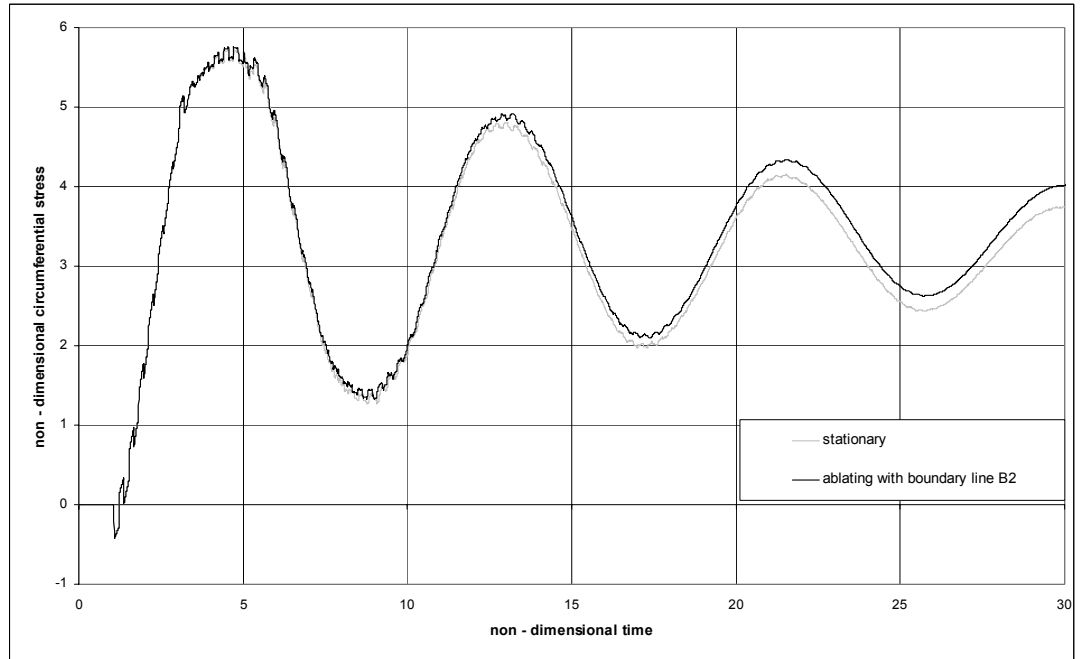


Figure 2.10. Variation of circumferential normal stress $\sigma_{\theta\theta} / P_0$ with time \bar{t} at location $\bar{r} = 2.15$ for ablating and non ablating inner surfaces.

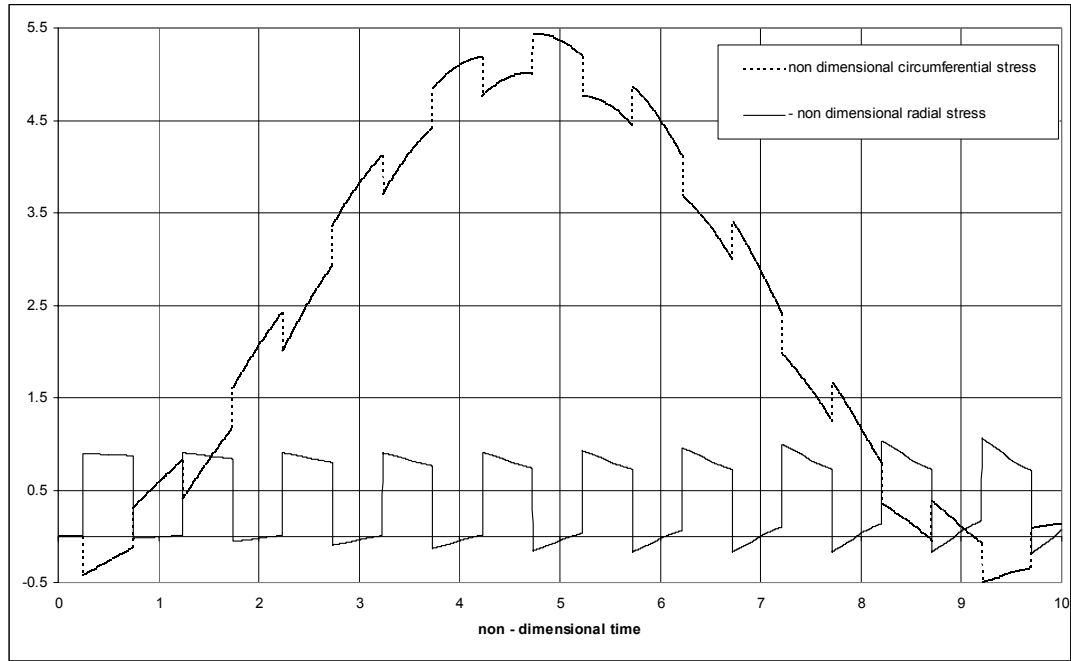


Figure 2.11. Variations of non-dimensional stresses with time \bar{t} at location $\bar{r} = 1.25$ for the cylindrical laminate with five generally orthotropic layers.

The numerical results are illustrated in curves in Figs. (2.12-2.18). In Fig. 2.12, the variation of $-\sigma_{rr}^{(v)} / P_0$ with time \bar{t} at the location $\bar{r} = 1.5$ is displayed. In the figure, three curves are given, one for the stationary inner surface and the other two for ablating inner boundaries. Equations of ablating inner boundary lines in the $(\bar{r} - \bar{t})$ plane are given by Eqs. (2.110, 2.111). The curves denote the effects of reflections at the inner ($\bar{r} = 1$), and outer ($\bar{r} = 2.3$) boundaries, and reflections and transmissions at the interfaces of the layers. Furthermore, the curves denote the effects of material internal friction due to the fact that the body is four layered and first layer is viscoelastic. The effect of geometric dispersion is also apparent in the curves. The pattern of sudden increases and decreases in the stress levels is due to the arrival of reflected, re-reflected and transmitted waves generated at the inner and outer boundaries and the interfaces between the viscoelastic and elastic orthotropic layers. We note that the mass densities and wave velocities of all the orthotropic elastic plies are the same, hence reflections at the interfaces between orthotropic layers are not

distinctive in the curves. In the values of stress levels up and down, we can also see the effects of viscoelasticity and the cylindrical geometry of the layered body. If the four layers were made of elastic materials with the same properties and the geometry of the body were plane instead of cylinder, the jumps in the stress levels would be equal to 1 and dimensionless stress levels would be either 0 or 1 which is a well known fundamental result in wave propagation. In the curves of Fig. 2.12, we see that the non-dimensional radial stress $-\sigma_{rr}^{(v)} / P_0$ reaches values as high as 2. This is quite striking. Normally, the radial stress does not reach that high values in ordinary elastic or viscoelastic layers. The reason it is so high here is due to the distinguished properties of the solid propellant which is quite close to being incompressible. We also note that the radial stress is compressive in the time range considered. This is also a desirable situation for smooth combustion of the propellant. The curves for the ablating inner boundary cases show similar features especially in the neighborhood of the time of arrival of the disturbance. As time passes on, differences in the curves become more distinct. This is due to the differences in the rates of decrease of the thickness of the viscoelastic layer. The curve with the bold color is for the boundary line B2 defined by the equation $\bar{t} = 500(\bar{r} - 1)$. When we compare this curve with the curve having a solid line and grey color which is for the stationary inner boundary, curves differ very little from each other. On the other hand, the curve for the boundary line B1 defined by the equation $\bar{t} = 100(\bar{r} - 1)$ deviates more significantly for large times from that of the stationary inner boundary case. Thus, naturally, as the rate of decrease gets larger, the differences in the curves increase.

Fig. 2.14 shows the variation of the non-dimensional stress $-\sigma_{rr}^{(v)} / P_0$ with time \bar{t} at location $\bar{r} = 2$ (interface). The curve in this figure exhibits similar features as those of Fig. 2.12. We note that the peak stress levels get smaller for the problem as we go away from the inner surface ($\bar{r} = 1$), see Figs. (2.12, 2.14). This is due to the material internal friction and geometric dispersion.

Figures (2.13, 2.15) denote the variations of the non-dimensional circumferential normal stress $-\sigma_{\theta\theta}^{(v)} / P_0$ with time \bar{t} at points $\bar{r} = 1.5$ and 2 (interface),

respectively, of the multilayered medium. These curves reveal similar trends. The effects of reflections at the boundaries, reflections and transmissions from interface between viscoelastic and first orthotropic layer, internal friction and body geometry are exhibited in these curves, as well. We note from these curves that $\sigma_{\theta\theta}^{(v)} / P_0$ is overwhelmingly negative. Furthermore, we note that the trend and the values of the stress levels for $\sigma_{\theta\theta}^{(v)} / P_0$ are very similar to those of $\sigma_{rr}^{(v)} / P_0$ at the locations and time ranges considered. This is due to the incompressible nature of the propellant. We also note from the two figures that, the peak levels of the stress $\sigma_{\theta\theta}^{(v)} / P_0$ are higher at location $\bar{r} = 1.5$ than at $\bar{r} = 2$. This is due to the internal friction in the viscoelastic layer and geometric dispersion.

Figures (2.16, 2.18) show the variations of the circumferential normal stress $\sigma_{\theta\theta}^{(1)} / P_0$ and $\sigma_{\theta\theta}^{(2)} / P_0$ with time \bar{t} at locations $\bar{r} = 2$ (interface) and 2.15, respectively. These figures display similar trends. We note from the figures that the major stress in the orthotropic layers is $\sigma_{\theta\theta} / P_0$ which may assume values as high as 11 for $\bar{r} = 2$ (interface) and 18 for $\bar{r} = 2.15$. At the interface $\bar{r} = 2$, we note that the circumferential normal stress $\sigma_{\theta\theta} / P_0$ suffers discontinuities. It may reach values as high as 11 in the orthotropic side, whereas in the viscoelastic side of the interface it remains less than 2, see Figs. (2.15, 2.16). We further note that $\sigma_{\theta\theta} / P_0$ for orthotropic layers is basically tensile, whereas in the viscoelastic layer which represents a solid propellant, it is basically compressive. The circumferential stress being compressive in the viscoelastic layer is a desired situation for solid propellants. In addition to the stationary inner boundary curve, Fig. 18 includes two different ablating boundary curves as well. It is seen from the figure that the curves for the stationary surface and ablating boundary surface denoted as BL_2 differ little from each other. This is because BL_2 defined by equation $\bar{t} = 500(\bar{r} - 1)$ in the $(\bar{r} - \bar{t})$ -plane is a slowly moving boundary. However, the curve pertaining to the boundary BL_1 represented by equation $\bar{t} = 100(\bar{r} - 1)$, deviate more significantly from the curve

related to the stationary boundary. This is because ablating boundary BL_1 is a fast moving boundary.

Finally, Fig. 17 displays the variation of radial normal stress $-\sigma_{rr}^{(2)} / P_0$ with respect to time \bar{t} at location $\bar{r} = 2.15$. This curve also denotes the effects of reflections and transmissions at the boundaries and interfaces. Jumps in the stress levels decrease as time \bar{t} increases. This is due to body geometry and viscoelasticity of the first layer. When we compare this figure to the non-ablating curve of Fig. 12, the differences are due to the position of the location considered. Since the point is close to the outer boundary and the interface, the jumps at the stress levels are more frequent in this figure compared to the curve of the non-ablating case of Fig. 12. This is also due to the fact that wave velocity in the orthotropic layer is nearly seven times to that in the viscoelastic layer and the thickness of the orthotropic layers is one-tenth of that of the viscoelastic layer.

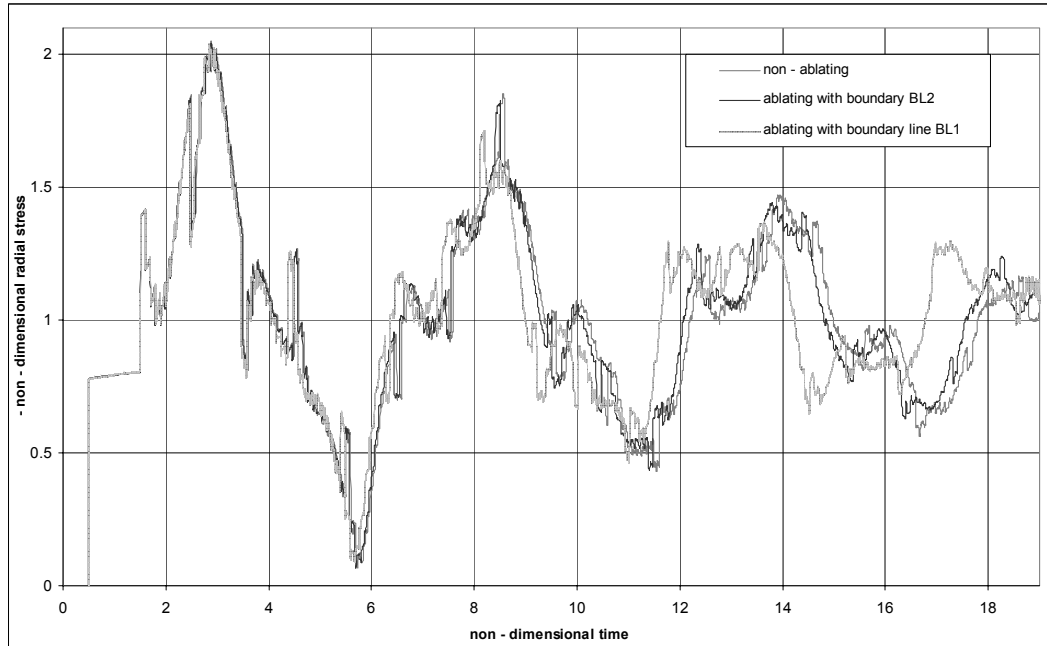


Figure 2.12. Variation of radial stress $-\sigma_{rr}^{(v)} / P_0$ with time \bar{t} at location $\bar{r} = 1.5$ in the viscoelastic layer for the ablating and non-ablating inner surfaces.

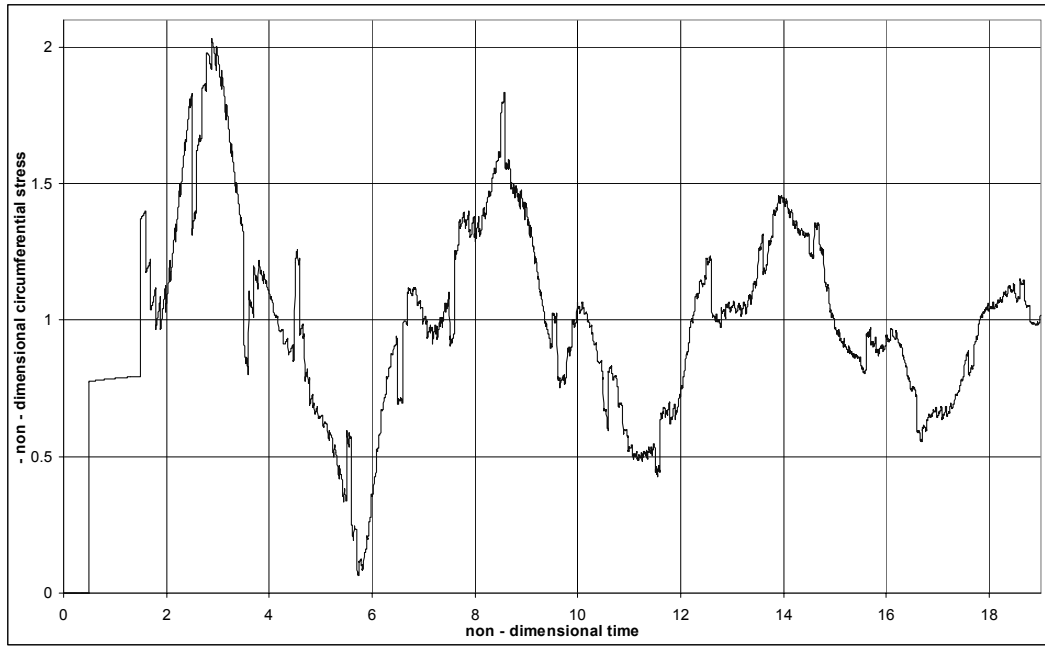


Figure 2.13. Variation of circumferential stress $-\sigma_{\theta\theta}^{(v)}/P_0$ with time \bar{t} at location $\bar{r} = 1.5$ in the viscoelastic cylinder for non-ablating inner surface.

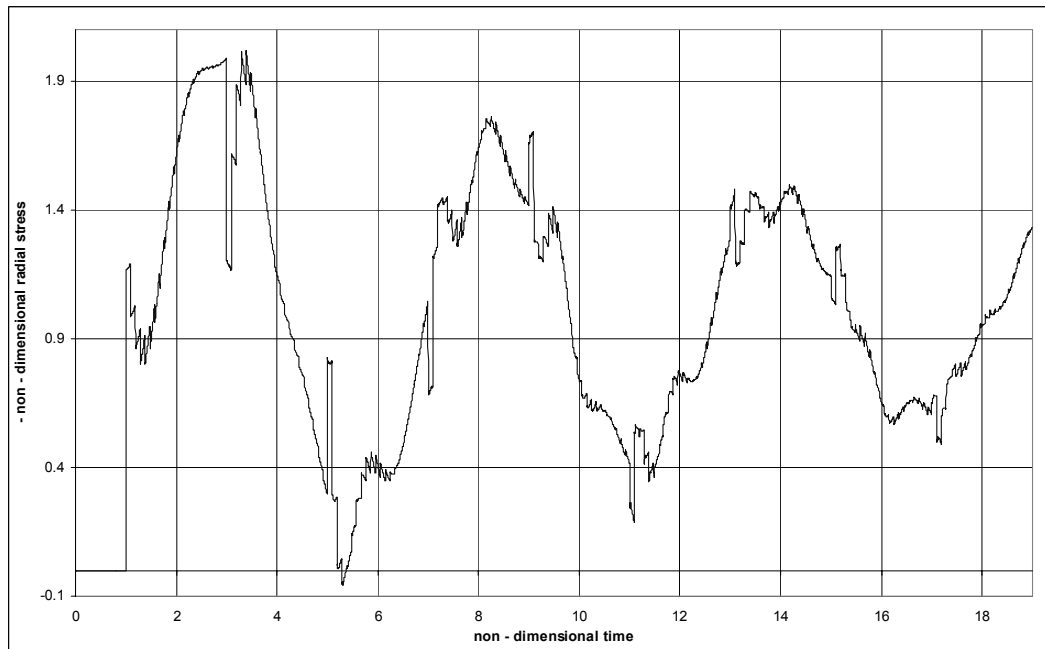


Figure 2.14. Variation of radial stress $-\sigma_{rr}^{(v)}/P_0$ with time \bar{t} at location $\bar{r} = 2$, the interface between the viscoelastic and first orthotropic layer, for non-ablating inner surface.

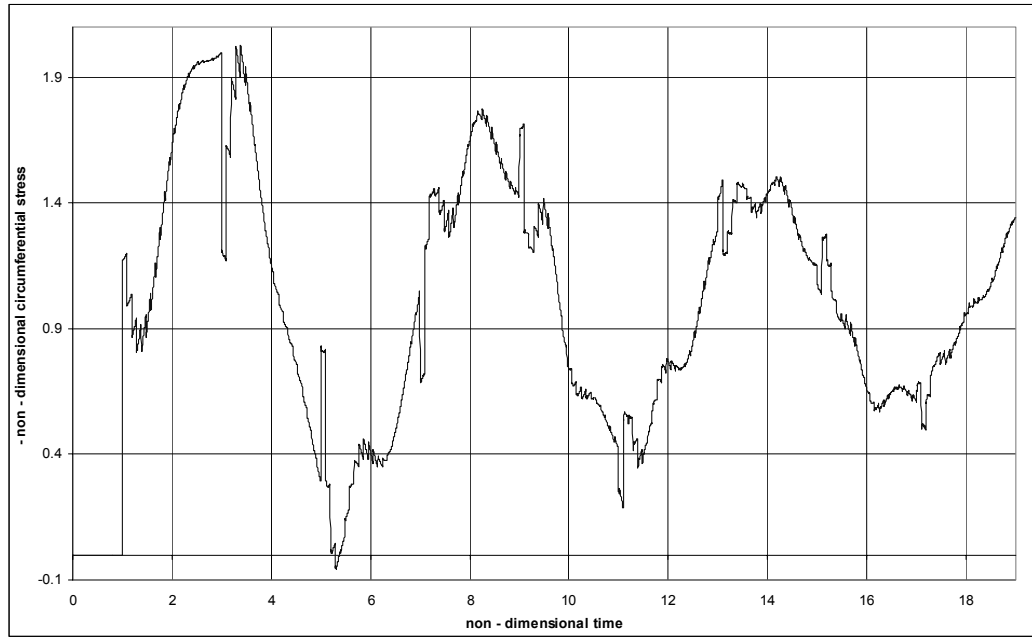


Figure 2.15. Variation of circumferential stress $-\sigma_{\theta\theta}^{(v)}/P_0$ with time \bar{t} at location $\bar{r} = 2$, the interface between the viscoelastic and first orthotropic layer for non-ablating inner surface.

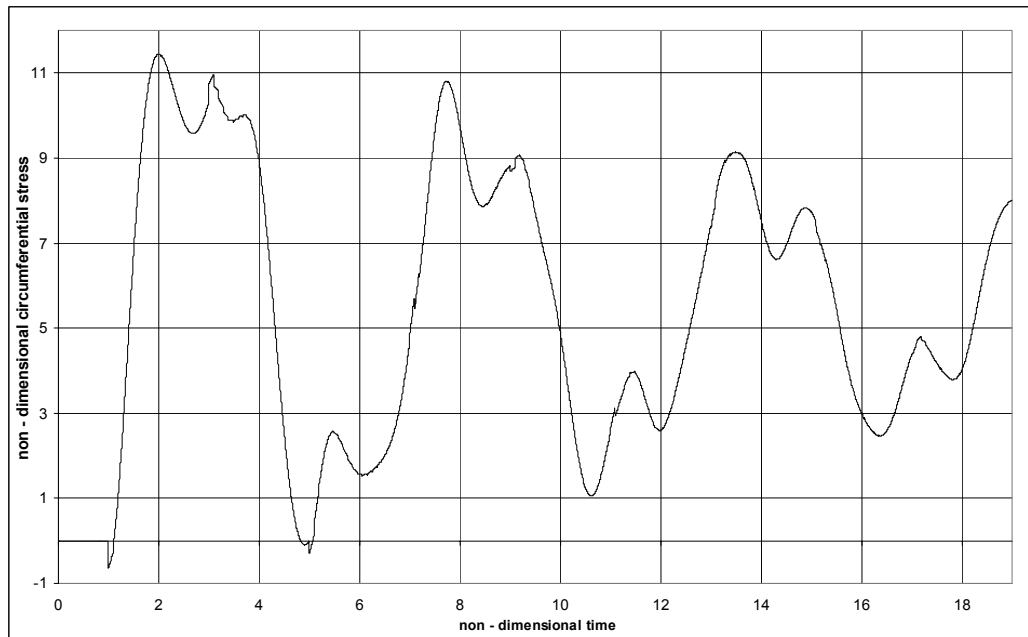


Figure 2.16. Variation of circumferential stress $\sigma_{\theta\theta}^{(1)}/P_0$ with time \bar{t} at location $\bar{r} = 2$, the interface between the viscoelastic and first orthotropic layer, for non-ablating inner surface.

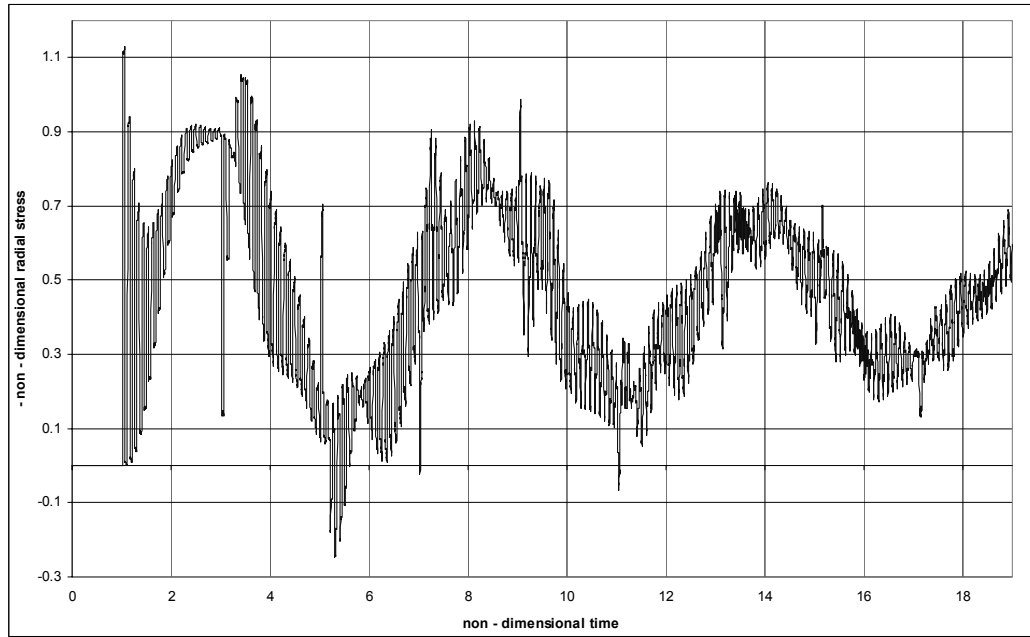


Figure 2.17. Variation of radial stress $-\sigma_{rr}^{(2)}/P_0$ with time \bar{t} at location $\bar{r} = 2.15$ in the second orthotropic layer for non-ablating inner surface.

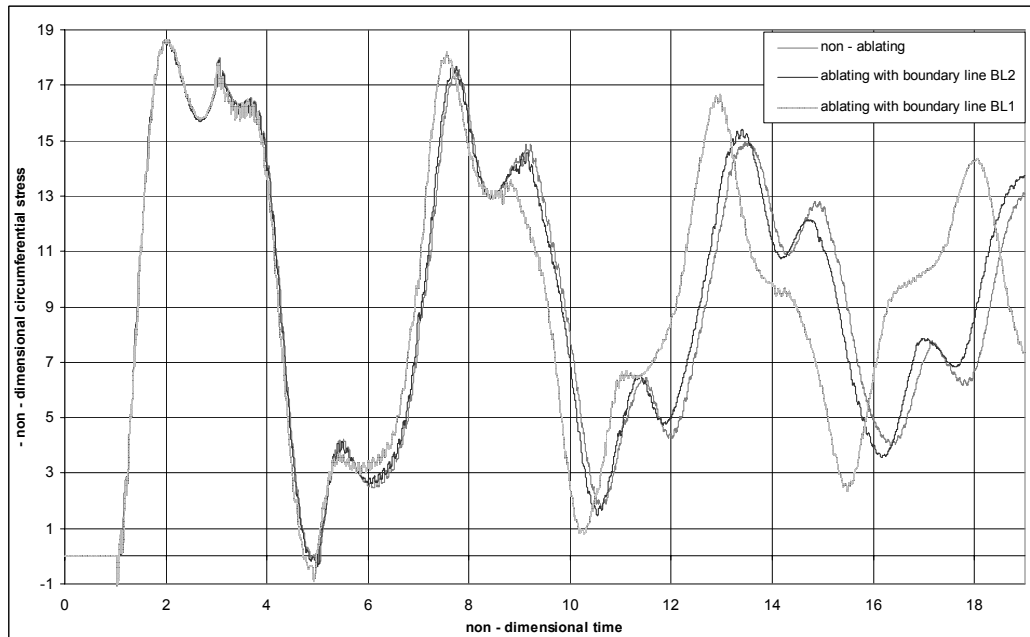


Figure 2.18. Variation of circumferential stress $\sigma_{\theta\theta}^{(2)}/P_0$ with time \bar{t} at location $\bar{r} = 2.15$ in the second orthotropic layer for ablating and non-ablating inner surfaces.

CHAPTER 3

THERMOMECHANICAL RESPONSE OF FIBER-REINFORCED CYLINDRICAL COMPOSITES

3.1 Introduction

In this chapter, transient dynamic response of filament wound cylindrical composites will be investigated. Thermal effects, in addition to mechanical effects, are taken into consideration as well. A generalized thermoelasticity theory which incorporates the temperature rate among the constitutive variables and is referred to as temperature-rate dependent thermoelasticity theory is employed. This theory predicts finite heat propagation speeds. This theory has been developed and used in many steady state and transient wave propagation problems, among which we can cite [97-121]. An exhaustive review of the literature on these theories known as thermoelasticity with second sound is given in Ref. [122-124].

The body considered in this chapter consist of n-different generally orthotropic, homogeneous and elastic layers. In each ply, the ply orientation angle may be different. The body is a hollow circular cylinder with a finite thickness in the radial direction, whereas it extends to infinity in the axial direction. The multilayered medium is subjected to uniform time-dependent dynamic inputs at the inner and/or outer surfaces. The body is assumed to be initially at rest. The layers are assumed to be perfectly bonded to each other.

The governing field equations of anisotropic temperature rate dependent thermoelasticity will be applied to each layer and the solutions are required to satisfy the continuity conditions at the interfaces of the layers, the boundary conditions at the inner and outer surfaces and the initial conditions. In the following parts of this chapter, governing field equations are explained briefly.

Method of characteristics is employed to obtain the solutions. Method of characteristics is suitable for this thermoelastic problem as well, because the governing equations of the temperature rate dependent thermoelasticity are hyperbolic unlike those of classical thermoelasticity.

3.2 Basic Equations of the Temperature Rate Dependent Thermoelasticity (TRDTE) for Orthotropic Materials in Cylindrical Coordinates

This part summarizes the basic equations of temperature rate dependent thermoelasticity (TRDTE) for orthotropic materials. Equations for the anisotropic TRDTE with no symmetry are obtained from Chandrasekharaiah [122] and more information can be obtained from this reference.

Constitutive equations of TRDTE together with the energy equation for homogenous and anisotropic materials for the three-dimensional body in Cartesian coordinates can be written as [122];

$$\begin{aligned}\sigma_{ij} &= C_{ijkl} \varepsilon_{kl} - \beta_{ij} (T + \alpha \dot{T}) \\ \rho S &= (\rho c / T_0) (T + \alpha_0 \dot{T}) - \left(\frac{c_i}{T_0} \right) T_{,i} + \beta_{ij} \varepsilon_{ij} \\ q_i &= -(c_i \dot{T} + k_{ij} T_{,j}) \\ q_{i,i} &= \rho (R - \dot{S} T_0)\end{aligned}\tag{3.1}$$

In Eqs. (3.1), T is the temperature deviation from the initial uniform reference temperature T_0 , ie, $T = T' - T_0$, where T' is the absolute temperature. Also, C_{ijkl} is the elasticity tensor, β_{ij} is the thermoelasticity tensor, k_{ij} is the thermal conductivity tensor and c is the specific heat per unit mass, in the isothermal state. Further, q_i is the heat flux, S is the entropy per unit mass and $\alpha, \alpha_0, \alpha_1, \sigma_2, c_i$ are new material constants not encountered in classical thermoelasticity (CTE). Furthermore, the last

of Eqs. (3.1) is the energy equation in which R is the intensity of the internal heat source per unit mass. In addition to these, following symmetry conditions hold good;

$$C_{ijkl} = C_{klij} = C_{jikl} = C_{ijlk}, \quad \beta_{ij} = \beta_{ji}, \quad k_{ij} = k_{ji} \quad (3.2)$$

We note that, in Eqs. (3.1-3.2), indicial notation is used and from now on, the rules pertaining to its use will be employed, otherwise it will be indicated.

For an orthotropic material with three orthogonal planes of symmetry the second rank symmetric thermoelasticity tensor β_{ij} takes the form;

$$[\beta] = \begin{bmatrix} \beta_{11} & 0 & 0 \\ 0 & \beta_{22} & 0 \\ 0 & 0 & \beta_{33} \end{bmatrix} \quad (3.3)$$

This is the form referred to the principal material directions 1, 2 and 3. The transformed thermoelasticity tensor components referred to the body coordinates r, θ, z (cylindrical coordinates, see Fig. 2.1) can be expressed as;

$$\begin{aligned} \beta_{zz} &= m^2 \beta_{11} + n^2 \beta_{22} \\ \beta_{\theta\theta} &= n^2 \beta_{11} + m^2 \beta_{22} \\ \beta_{rr} &= \beta_{33} \\ \beta_{\theta z} &= mn\beta_{11} - mn\beta_{22} \end{aligned} \quad (3.4)$$

where $m = \cos \phi$, $n = \sin \phi$ and ϕ is the angle between the z -axis and the principal material direction 1, the fiber direction, see Fig. 2.1.

The symmetric thermal conductivity tensor k_{ij} has six independent components for an anisotropic material with no symmetry. However, for an orthotropic material with

three orthogonal planes of symmetry, the thermal conductivity tensor referred to the principal material directions takes the form below.

$$[\mathbf{k}] = \begin{bmatrix} k_{11} & 0 & 0 \\ 0 & k_{22} & 0 \\ 0 & 0 & k_{33} \end{bmatrix} \quad (3.5)$$

The transformed thermal conductivity tensor components referred to the body coordinates r, θ, z can be expressed as;

$$\begin{aligned} k_{zz} &= m^2 k_{11} + n^2 k_{22} \\ k_{\theta\theta} &= n^2 k_{11} + m^2 k_{22} \\ k_{rr} &= k_{33} \\ k_{\theta z} &= mnk_{11} - mnk_{22} \end{aligned} \quad (3.6)$$

Furthermore, it can be shown that the material constants c_i in Eqs. (3.1)₂, (3.1)₃ are zero for an orthotropic material having three orthogonal planes of symmetry.

Thus, the equations for a generally orthotropic thermoelastic layer can be written in cylindrical coordinates as;

constitutive equations for stress components

$$\begin{aligned} \sigma_{zz} &= \tilde{C}_{11}\epsilon_{zz} + \tilde{C}_{12}\epsilon_{\theta\theta} + \tilde{C}_{13}\epsilon_{rr} + 2\tilde{C}_{16}\epsilon_{\theta z} - \beta_{zz}(T + \alpha\dot{T}) \\ \sigma_{\theta\theta} &= \tilde{C}_{21}\epsilon_{zz} + \tilde{C}_{22}\epsilon_{\theta\theta} + \tilde{C}_{23}\epsilon_{rr} + 2\tilde{C}_{26}\epsilon_{\theta z} - \beta_{\theta\theta}(T + \alpha\dot{T}) \\ \sigma_{rr} &= \tilde{C}_{31}\epsilon_{zz} + \tilde{C}_{32}\epsilon_{\theta\theta} + \tilde{C}_{33}\epsilon_{rr} + 2\tilde{C}_{36}\epsilon_{\theta z} - \beta_{rr}(T + \alpha\dot{T}) \end{aligned} \quad (3.7a)$$

$$\sigma_{r\theta} = 2\tilde{C}_{36}\varepsilon_{r\theta} + 2\tilde{C}_{45}\varepsilon_{rz}$$

$$\sigma_{rz} = 2\tilde{C}_{45}\varepsilon_{r\theta} + 2\tilde{C}_{55}\varepsilon_{rz} \quad (3.7b)$$

$$\sigma_{\theta z} = \tilde{C}_{16}\varepsilon_{zz} + \tilde{C}_{26}\varepsilon_{\theta\theta} + \tilde{C}_{36}\varepsilon_{rr} + 2\tilde{C}_{66}\varepsilon_{\theta z} - \beta_{\theta z}(T + \alpha\dot{T})$$

where \tilde{C}_{ij} are the transformed stiffness coefficients for a generally orthotropic material, see Eqs. (2.5),

constitutive equation for the entropy dencity

$$\rho S = (\rho c / T_0)(T + \alpha_0 \dot{T}) + \beta_{zz}\varepsilon_{zz} + \beta_{\theta z}\varepsilon_{z\theta} + \beta_{\theta z}\varepsilon_{\theta z} + \beta_{\theta\theta}\varepsilon_{\theta\theta} + \beta_{rr}\varepsilon_{rr} \quad (3.8)$$

energy equation

$$\frac{1}{r} \frac{\partial}{\partial r}(r q_r) + \frac{1}{r} \frac{\partial q_\theta}{\partial \theta} + \frac{\partial q_z}{\partial z} = \rho(R - \dot{S}T_0) \quad (3.9)$$

Fourier law of heat conduction

$$q_r = -k_{rr} \frac{\partial T}{\partial r}$$

$$q_\theta = -k_{\theta\theta} \frac{1}{r} \frac{\partial T}{\partial \theta} - k_{\theta z} \frac{\partial T}{\partial z} \quad (3.10)$$

$$q_z = -k_{z\theta} \frac{1}{r} \frac{\partial T}{\partial \theta} - k_{zz} \frac{\partial T}{\partial z}$$

This completes the summary of the basic equations of temperature-rate dependent thermoelasticity in cylindrical coordinates for generally orthotropic materials.

3.3 Formulation of the Problem

As stated in Section 3.1, transient dynamic response of filament wound cylindrical composites consisting of n different generally orthotropic, homogenous, thermoelastic layers is investigated in this chapter. The body is referred to a cylindrical coordinate system where the radial distances are measured by the coordinate r . Boundary, initial and interface conditions of the problem dictate that the responses of the body are axisymmetrical, that is all the field variables are functions of r and t , only. Moreover, the only non-vanishing displacement component is u_r , that is, the displacement component in the radial direction.

For the three dimensional case, the stress equations of motions in cylindrical coordinates are given in Section 2.2 by Eqs. (2.1). For the problem considered in this study, these equations for a typical layer can be expressed in the form,

$$\frac{1}{\rho} \frac{\partial \sigma_{rr}}{\partial r} + \frac{(\sigma_{rr} - \sigma_{\theta\theta})}{r} = \rho \frac{\partial^2 u_r}{\partial t^2} \quad (3.10)$$

where the body forces are taken zero.

For the three dimensional case, the constitutive equations for stress components of orthotropic thermoelastic materials were given by Eqs. (3.7). In our problem, these equations for the relevant stress components σ_{rr} and $\sigma_{\theta\theta}$ take the following forms for the typical orthotropic layer:

$$\sigma_{rr} - \tilde{C}_{32} \frac{u_r}{r} - \tilde{C}_{33} \frac{\partial u_r}{\partial r} + \beta_{rr} (T + \alpha \dot{T}) = 0 \quad (3.11)$$

$$\sigma_{\theta\theta} - \tilde{C}_{22} \frac{u_r}{r} - \tilde{C}_{23} \frac{\partial u_r}{\partial r} + \beta_{rr} (T + \alpha \dot{T}) = 0$$

Fourier law of heat conduction, the constitutive equation for the entropy density and the energy equation for our axi-symmetrical problem, can be written, respectively, in view of Eqs. (3.8 – 3.9) as.

$$q_r + k_{rr} \frac{\partial T}{\partial r} = 0$$

$$\frac{q_r}{r} + \frac{\partial q_r}{\partial r} + \rho \dot{S} T_0 = 0 \quad (3.12)$$

$$\rho S - \beta_{\theta\theta} \frac{u_r}{r} - \beta_{rr} \frac{\partial u_r}{\partial r} - \frac{\rho c}{T_0} (T + \alpha_0 \dot{T}) = 0$$

where the internal heat source R is taken zero.

Differentiating Eqs. (3.11), (3.12)₁ and (3.12)₃ with respect to t , and eliminating \dot{S} from the energy equation, Eq. (3.12)₃, we obtain

$$\frac{\partial \sigma_{rr}}{\partial t} - \tilde{C}_{32} \frac{v_r}{r} - \tilde{C}_{33} \frac{\partial v_r}{\partial r} + \beta_{rr} \phi + \alpha \beta_{rr} \frac{\partial \phi}{\partial t} = 0$$

$$\frac{\partial \sigma_{\theta\theta}}{\partial t} - \tilde{C}_{22} \frac{v_r}{r} - \tilde{C}_{23} \frac{\partial v_r}{\partial r} + \beta_{rr} \phi + \alpha \beta_{rr} \frac{\partial \phi}{\partial t} = 0$$

(3.13)

$$\frac{1}{T_0} \frac{q_r}{r} + \frac{1}{T_0} \frac{\partial q_r}{\partial r} + \beta_{\theta\theta} \frac{v_r}{r} + \beta_{rr} \frac{\partial v_r}{\partial r} + \frac{\rho c}{T_0} \phi + \frac{\rho c}{T_0} \alpha_0 \frac{\partial \phi}{\partial t} = 0$$

$$\frac{\partial q_r}{\partial t} + k_{rr} \frac{\partial \phi}{\partial r} = 0$$

where

$$\phi = \frac{\partial T}{\partial t}; \quad v_r = \frac{\partial u_r}{\partial t} \quad (3.14)$$

The formulation of the problem is completed by stating the boundary, interface and initial conditions. The boundary conditions involve both mechanical and thermal parts. At each point of the boundary surface, surface tractions or displacements and temperature deviations or heat fluxes should be prescribed. Thus the boundary conditions at the inner surface, $r = a$ can be expressed as

$$\begin{aligned} \sigma_{rr}(a,t) = -P(t)H(t) \quad \text{or} \quad V_r(a,t) = V(t)H(t) \quad \text{and} \\ T(a,t) = T^*(t)H(t) \quad \text{or} \quad q_r(a,t) = Q(t)H(t) \end{aligned} \quad (3.15)$$

and at the outer surface $r = b$ as

$$\begin{aligned} \sigma_{rr}(b,t) = -F(t)H(t) \quad \text{or} \quad V_r(b,t) = V^*(t)H(t) \quad \text{and} \\ T(b,t) = t^*(t)H(t) \quad \text{or} \quad q_r(b,t) = Q^*(t)H(t) \end{aligned} \quad (3.16)$$

where $P(t)$, $V(t)$, $T^*(t)$, $Q(t)$, $F(t)$, $V^*(t)$, $t^*(t)$, $Q^*(t)$ are prescribed functions of t and $H(t)$ is the Heaviside step function.

Since the bodies are assumed to be initially at rest, all the field variables are zero at $t = 0$. The layers of the bodies are assumed to be perfectly bonded to each other. Hence, the interface conditions imply that the normal stress σ_{rr} , the displacement component u_r , the temperature deviation T and the heat flux q_r are continuous across the interfaces of the layers.

The formulation of the problem is thus complete. The governing field equations, Eqs. (3.13), (3.14), (3.10) are applied to each layer and the solutions are required to satisfy the continuity conditions at the interfaces, the boundary conditions at the inner and outer surfaces Eqs. (3.15-3.16) and zero initial conditions. Method of characteristics is employed to obtain the solution.

3.4 The Method of Characteristics and the Canonical Form of the Governing Equations

In order to apply the method of characteristics, we write the governing equations as a system of first-order, partial differential equations. The system of the governing first order partial differential equations, Eqs. (3.13), (3.14), (3.10) can be written in matrix form for a typical orthotropic layer as:

$$\mathbf{P}\mathbf{U}_{,t} + \mathbf{Q}\mathbf{U}_{,r} + \mathbf{R} = \mathbf{0} \quad (3.17)$$

where \mathbf{P} and \mathbf{Q} are seven by seven matrices defined as:

$$\mathbf{P} = \begin{bmatrix} \alpha\beta_{rr} & 0 & 1 & 0 & 0 & 0 & 0 \\ \alpha\beta_{\theta\theta} & 0 & 0 & 1 & 0 & 0 & 0 \\ \frac{\rho c}{T_o} \alpha_0 & 0 & 0 & 0 & 0 & 0 & 0 \\ 0 & 0 & 0 & 0 & 1 & 0 & 0 \\ 0 & -1 & 0 & 0 & 0 & 0 & 0 \\ 0 & 0 & 0 & 0 & 0 & 0 & 1 \\ 0 & 0 & 0 & 0 & 0 & 1 & 0 \end{bmatrix} \quad (3.18)$$

$$\mathbf{Q} = \begin{bmatrix} 0 & -\tilde{C}_{33} & 0 & 0 & 0 & 0 & 0 \\ 0 & -\tilde{C}_{23} & 0 & 0 & 0 & 0 & 0 \\ 0 & \beta_{rr} & 0 & 0 & \frac{1}{T_0} & 0 & 0 \\ k_{rr} & 0 & 0 & 0 & 0 & 0 & 0 \\ 0 & 0 & \frac{1}{\rho} & 0 & 0 & 0 & 0 \\ 0 & 0 & 0 & 0 & 0 & 0 & 0 \\ 0 & 0 & 0 & 0 & 0 & 0 & 0 \end{bmatrix} \quad (3.19)$$

and \mathbf{R} and \mathbf{U} are seven dimensional column vectors given as:

$$\mathbf{R} = \begin{bmatrix} -\tilde{C}_{32} \frac{v_r}{r} + \beta_{rr} \phi \\ -\tilde{C}_{22} \frac{v_r}{r} + \beta_{\theta\theta} \phi \\ \frac{1}{T_o} \frac{q_{rr}}{r} + \beta_{\theta\theta} \frac{v_r}{r} + \frac{\rho c}{T_o} \phi \\ 0 \\ \frac{1}{\rho} \left(\frac{\sigma_{rr} - \sigma_{\theta\theta}}{x} \right) \\ -v_r \\ -\phi \end{bmatrix} \quad (3.20)$$

$$\mathbf{U} = \begin{bmatrix} \phi \\ v_r \\ \sigma_{rr} \\ \sigma_{\theta\theta} \\ q_r \\ T \\ u_r \end{bmatrix} \quad (3.21)$$

In Eq. (3.17), \mathbf{U} is the unknown vector and comma denotes partial differentiation:

$$\mathbf{U}_{,t} = \frac{\partial \mathbf{U}}{\partial t}, \quad \mathbf{U}_{,r} = \frac{\partial \mathbf{U}}{\partial r} \quad (3.22)$$

Before we derive the canonical equations from Eq. (3.17), we first establish the characteristic lines along which these equations are valid. The equation governing the characteristic lines can be written as

$$\det(\mathbf{Q} - V\mathbf{P}) = 0 \quad (3.23)$$

where $V = \frac{dr}{dt}$ defines the characteristic lines on the $(r-t)$ plane.

In view of Eqs. (3.18-3.19), the characteristics equation, Eq. (3.23), is expressed as:

$$\det(\mathbf{I} - V\mathbf{H}) = \begin{bmatrix} -V\alpha\beta_{rr} & -\tilde{C}_{33} & -V & 0 & 0 & 0 & 0 \\ -V\alpha\beta_{rr} & -\tilde{C}_{23} & 0 & -V & 0 & 0 & 0 \\ -\frac{V\rho c\alpha_0}{T_0} & \beta_{rr} & 0 & 0 & \frac{1}{T_0} & 0 & 0 \\ k_{rr} & 0 & 0 & 0 & -V & 0 & 0 \\ 0 & -V & \frac{1}{\rho} & 0 & 0 & 0 & 0 \\ 0 & 0 & 0 & 0 & 0 & 0 & -V \\ 0 & 0 & 0 & 0 & 0 & -V & 0 \end{bmatrix} = 0 \quad (3.24)$$

$$V^3 \frac{(V^2\alpha\beta_{rr}^2T_0 - V^2c\alpha_0^2\rho\tilde{C}_{33} + V^4c\alpha_0\rho^2 + k_{rr}\tilde{C}_{33} - k_{rr}V\rho)}{\rho T_0} = 0 \quad (3.25)$$

The roots of Eq. (3.25) can be obtained as:

$$V^{(1)} = c_1, \quad V^{(2)} = -c_1, \quad V^{(3)} = c_2, \quad V^{(4)} = -c_2 \quad (3.26)$$

$$V^{(5)} = V^{(6)} = V^{(7)} = 0$$

where

$$c_1 = \frac{1}{2\rho c\alpha_0} \sqrt{-2c\alpha_0 \left(\frac{\rho k_{rr} - \beta_{rr}^2\alpha T_0 + \tilde{C}_{33}\rho c\alpha_0}{k_{rr}^2\rho^2 - 2k_{rr}\rho\beta_{rr}^2\alpha_o T_0 - 2\tilde{C}_{33}k_{rr}\rho^2 c\alpha_0 + \beta_{rr}^4\alpha^2 T_0^2} + \sqrt{-2\beta_{rr}^2\alpha T_0\tilde{C}_{33}\rho c\alpha_0 + \rho^2\tilde{C}_{33}^2 c^2\alpha_0^2} \right)} \quad (3.27a)$$

$$c_2 = \frac{1}{2\rho c \alpha_0} \sqrt{-2c \alpha_0 \left(\frac{\rho k_{rr} - \beta_{rr}^2 \alpha T_0 + \tilde{C}_{33} \rho c \alpha_0}{\sqrt{k_{rr}^2 \rho^2 - 2k_{rr} \rho \beta_{rr}^2 \alpha_o T_0 - 2\tilde{C}_{33} k_{rr} \rho^2 c \alpha_0 + \beta_{rr}^4 \alpha^2 T_0^2}} - \sqrt{-2\beta_{rr}^2 \alpha T_0 \tilde{C}_{33} \rho c \alpha_0 + \rho^2 \tilde{C}_{33}^2 c^2 \alpha_0^2} \right)} \quad (3.27b)$$

$V^{(i)}$ ($i = 1 - 7$) are the characteristic values and the characteristic lines are defined as:

$$\begin{aligned} \frac{dr}{dt} = V^{(1)} = c_1 & \quad \text{along } C^{(1)} \\ \frac{dr}{dt} = V^{(2)} = -c_1 & \quad \text{along } C^{(2)} \\ \frac{dr}{dt} = V^{(3)} = c_2 & \quad \text{along } C^{(3)} \\ \frac{dr}{dt} = V^{(4)} = -c_2 & \quad \text{along } C^{(4)} \\ \frac{dr}{dt} = V^{(5)} = V^{(6)} = V^{(7)} = 0 & \quad \text{along } C^{(5)} \end{aligned} \quad (3.28)$$

Integration of Eq. (3.28) gives the families of characteristic lines $C^{(i)}$ $i = (1 - 7)$ as;

$$\begin{aligned} C^{(1)} : r - c_1 t &= \text{constant} \\ C^{(2)} : r + c_1 t &= \text{constant} \\ C^{(3)} : r - c_2 t &= \text{constant} \\ C^{(4)} : r + c_2 t &= \text{constant} \\ C^{(i)} : r &= \text{constant} \quad (i = 5 - 7) \end{aligned} \quad (3.29)$$

These families of characteristic lines are shown in the $(r-t)$ plane in Fig. 3.1. We note that $C^{(1)}$ and $C^{(3)}$ describe families of straight lines with slopes c_1 and c_2 , respectively, while $C^{(2)}$ and $C^{(4)}$ describe families with slopes $-c_1$ and $-c_2$, on the $(r-t)$ plane. Moreover, $C^{(i)}$ ($i = 5-7$) describes straight lines parallel to the t -axis, see Fig. 3.1.

The canonical forms of the governing equations along the characteristic lines can be written similar to Eqs. (2.64) as:

$$\mathbf{L}^{(i)T} \mathbf{P} \frac{d\mathbf{U}}{dt} + \mathbf{L}^{(i)T} \mathbf{Q} = \mathbf{0} \quad \text{along} \quad \frac{dr}{dt} = V^{(i)} \quad i = (1-7) \quad (3.30)$$

where $\mathbf{P}, \mathbf{Q}, \mathbf{U}$ are given by Eqs. (3.18, 3.19, 3.21) and $\mathbf{L}^{(i)}$ is the left-hand eigenvector which, similar to Eq. (2.65), is defined as:

$$(\mathbf{Q}^T - V^{(i)} \mathbf{P}^T) \mathbf{L}^{(i)} = 0 \quad \text{along} \quad C^{(i)} \quad (i = 1-7) \quad (3.31)$$

Applying Eq. (3.31), the left-hand eigenvectors can be computed as

$$\mathbf{L}^{(1)} = \begin{bmatrix} 1 \\ 0 \\ \frac{\tilde{C}_{33} - \rho c_1^2}{\beta_{rr}} \\ \frac{1}{T_0 c_1} \left(\frac{\tilde{C}_{33} - \rho c_1^2}{\beta_{rr}} \right) \\ \rho c_1 \\ 0 \\ 0 \end{bmatrix}, \quad \mathbf{L}^{(2)} = \begin{bmatrix} 1 \\ 0 \\ \frac{\tilde{C}_{33} - \rho c_1^2}{\beta_{rr}} \\ \frac{-1}{T_0 c_1} \left(\frac{\tilde{C}_{33} - \rho c_1^2}{\beta_{rr}} \right) \\ -\rho c_1 \\ 0 \\ 0 \end{bmatrix} \quad (3.32a)$$

$$\mathbf{L}^{(3)} = \begin{bmatrix} 1 \\ 0 \\ \frac{\tilde{C}_{33} - \rho c_2^2}{\beta_{rr}} \\ \frac{1}{T_0 c_2} \left(\frac{\tilde{C}_{33} - \rho c_2^2}{\beta_{rr}} \right) \\ \rho c_2 \\ 0 \\ 0 \end{bmatrix}, \quad \mathbf{L}^{(4)} = \begin{bmatrix} 1 \\ 0 \\ \frac{\tilde{C}_{33} - \rho c_2^2}{\beta_{rr}} \\ \frac{-1}{T_0 c_2} \left(\frac{\tilde{C}_{33} - \rho c_2^2}{\beta_{rr}} \right) \\ -\rho c_2 \\ 0 \\ 0 \end{bmatrix} \quad (3.32b)$$

$$\mathbf{L}^{(5)} = \begin{bmatrix} -\frac{\tilde{C}_{23}}{\tilde{C}_{33}} \\ \frac{\tilde{C}_{23}}{\tilde{C}_{33}} \\ 1 \\ 0 \\ 0 \\ 0 \\ 0 \\ 0 \end{bmatrix}, \quad \mathbf{L}^{(6)} = \begin{bmatrix} -\frac{\tilde{C}_{23}}{\tilde{C}_{33}} \\ \frac{\tilde{C}_{23}}{\tilde{C}_{33}} \\ 1 \\ 0 \\ 0 \\ 0 \\ 1 \\ 0 \end{bmatrix}, \quad \mathbf{L}^{(7)} = \begin{bmatrix} -\frac{\tilde{C}_{23}}{\tilde{C}_{33}} \\ \frac{\tilde{C}_{23}}{\tilde{C}_{33}} \\ 1 \\ 0 \\ 0 \\ 0 \\ 0 \\ 1 \end{bmatrix}$$

Since the left-hand eigenvectors of the orthotropic layers are found, then the canonical equations can be obtained by applying Eg. (3.30) and taking into consideration Eqs. (3.18-3.20). Performing the matrix products, we get the following set of canonical equations:

$$\begin{aligned} & \left(\alpha \beta_{rr} + \frac{(\tilde{C}_{33} - \rho c_1^2) \rho c}{\beta_{rr} T_0} \alpha_0 \right) \frac{d\phi}{dt} + \frac{1}{T_0 c_1} \frac{(\tilde{C}_{33} - \rho c_1^2)}{\beta_{rr}} \frac{dq_r}{dt} + \frac{d\sigma_{rr}}{dt} \\ & - \rho_o c_1 \frac{dv_r}{dt} + \left(-\tilde{C}_{32} + \beta_{\theta\theta} \frac{(\tilde{C}_{33} - \rho c_1^2)}{\beta_{rr}} \right) \frac{v_r}{r} + \frac{1}{T_0} \frac{(\tilde{C}_{33} - \rho c_1^2)}{\beta_{rr}} \frac{q_r}{r} + \left(\frac{\rho c (\tilde{C}_{33} - \rho c_1^2)}{T_0 \beta_{rr}} + \beta_{rr} \right) \phi \\ & + c_1 \frac{(\sigma_{rr} - \sigma_{\theta\theta})}{r} = 0 \end{aligned}$$

along $\frac{dr}{dt} = V^{(1)} = c_1$ (3.33)

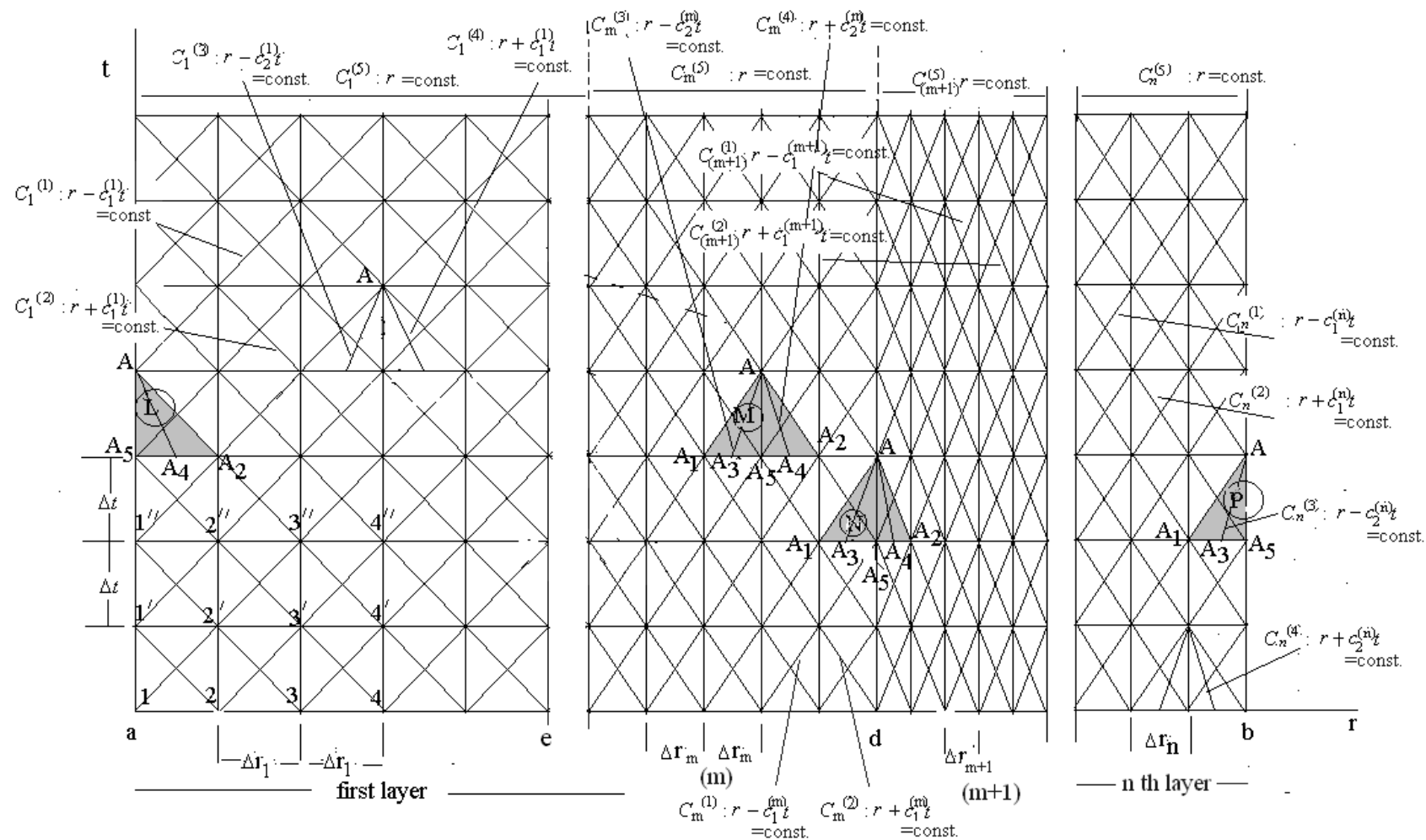


Figure 3.1. Description of the network of characteristic lines for the thermoelastic layered medium.

$$\begin{aligned}
& \left(\alpha \beta_{rr} + \frac{(\tilde{C}_{33} - \rho c_1^2) \rho}{\beta_{rr}} \frac{1}{T_0} \alpha_0 \right) \frac{d\phi}{dt} - \frac{1}{T_0 c_1} \frac{(\tilde{C}_{33} - \rho c_1^2)}{\beta_{rr}} \frac{dq_r}{dt} + \frac{d\sigma_{rr}}{dt} \\
& + \rho c_1 \frac{dv_r}{dt} + \left(-\tilde{C}_{32} + \beta_{\theta\theta} \frac{(\tilde{C}_{33} - \rho c_1^2)}{\beta_{rr}} \right) \frac{v_r}{r} + \frac{1}{T_0} \frac{(\tilde{C}_{33} - \rho c_1^2)}{\beta_{rr}} \frac{q_r}{r} + \left(\frac{\rho}{T_0} \frac{(\tilde{C}_{33} - \rho c_1^2)}{\beta_{rr}} + \beta_{rr} \right) \phi \\
& - c_1 \frac{(\sigma_{rr} - \sigma_{\theta\theta})}{r} = 0
\end{aligned}$$

along $\frac{dr}{dt} = V^{(2)} = -c_1$ (3.34)

$$\begin{aligned}
& \left(\alpha \beta_{rr} + \frac{(\tilde{C}_{33} - \rho c_2^2) \rho}{\beta_{rr}} \frac{1}{T_0} \alpha_0 \right) \frac{d\phi}{dt} + \frac{1}{T_0 c_2} \frac{(\tilde{C}_{33} - \rho c_2^2)}{\beta_{rr}} \frac{dq_r}{dt} + \frac{d\sigma_{rr}}{dt} \\
& - \rho c_2 \frac{dv_r}{dt} + \left(-\tilde{C}_{32} + \beta_{\theta\theta} \frac{(\tilde{C}_{33} - \rho c_2^2)}{\beta_{rr}} \right) \frac{v_r}{r} + \frac{1}{T_0} \frac{(\tilde{C}_{33} - \rho c_2^2)}{\beta_{rr}} \frac{q_r}{r} + \left(\frac{\rho}{T_0} \frac{(\tilde{C}_{33} - \rho c_2^2)}{\beta_{rr}} + \beta_{rr} \right) \phi \\
& + c_2 \frac{(\sigma_{rr} - \sigma_{\theta\theta})}{r} = 0
\end{aligned}$$

along $\frac{dr}{dt} = V^{(3)} = c_2$ (3.35)

$$\begin{aligned}
& \left(\alpha \beta_{rr} + \frac{(\tilde{C}_{33} - \rho c_2^2) \rho}{\beta_{rr}} \frac{1}{T_0} \alpha_0 \right) \frac{d\phi}{dt} - \frac{1}{T_0 c_2} \frac{(\tilde{C}_{33} - \rho c_2^2)}{\beta_{rr}} \frac{dq_r}{dt} + \frac{d\sigma_{rr}}{dt} \\
& + \rho c_2 \frac{dv_r}{dt} + \left(-\tilde{C}_{32} + \beta_{\theta\theta} \frac{(\tilde{C}_{33} - \rho c_2^2)}{\beta_{rr}} \right) \frac{v_r}{r} + \frac{1}{T_0} \frac{(\tilde{C}_{33} - \rho c_2^2)}{\beta_{rr}} \frac{q_r}{r} + \left(\frac{\rho}{T_0} \frac{(\tilde{C}_{33} - \rho c_2^2)}{\beta_{rr}} + \beta_{rr} \right) \phi \\
& - c_2 \frac{(\sigma_{rr} - \sigma_{\theta\theta})}{r} = 0
\end{aligned}$$

along $\frac{dr}{dt} = V^{(4)} = -c_2$ (3.36)

$$\begin{aligned}
& \left(\alpha \beta_{\theta\theta} - \frac{\tilde{C}_{23}}{\tilde{C}_{33}} \alpha \beta_{rr} \right) \frac{d\phi}{dt} + \left(\tilde{C}_{32} \frac{\tilde{C}_{23}}{\tilde{C}_{33}} - \tilde{C}_{22} \right) \frac{v_r}{r} - \frac{\tilde{C}_{23}}{\tilde{C}_{33}} \frac{d\sigma_{rr}}{dt} + \frac{d\sigma_{\theta\theta}}{dt} + \left(\beta_{\theta\theta} - \frac{\tilde{C}_{23}}{\tilde{C}_{33}} \beta_{rr} \right) \phi = 0
\end{aligned}$$

along $\frac{dr}{dt} = V^{(5)} = 0$ (3.37)

$$\begin{aligned}
& \left(\alpha \beta_{\theta\theta} - \frac{\tilde{C}_{23}}{\tilde{C}_{33}} \alpha \beta_{rr} \right) \frac{d\phi}{dt} + \left(\tilde{C}_{32} \frac{\tilde{C}_{23}}{\tilde{C}_{33}} - \tilde{C}_{22} \right) \frac{v_r}{r} - \frac{\tilde{C}_{23}}{\tilde{C}_{33}} \frac{d\sigma_{rr}}{dt} + \frac{d\sigma_{\theta\theta}}{dt} + \left(\beta_{\theta\theta} - \frac{\tilde{C}_{23}}{\tilde{C}_{33}} \beta_{rr} \right) \phi \\
& + \frac{du_r}{dt} - v_r = 0
\end{aligned}$$

along $\frac{dr}{dt} = V^{(6)} = 0$ (3.38)

$$\begin{aligned}
& \left(\alpha \beta_{\theta\theta} - \frac{\tilde{C}_{23}}{\tilde{C}_{33}} \alpha \beta_{rr} \right) \frac{d\phi}{dt} + \left(\tilde{C}_{32} \frac{\tilde{C}_{23}}{\tilde{C}_{33}} - \tilde{C}_{22} \right) \frac{v_r}{r} - \frac{\tilde{C}_{23}}{\tilde{C}_{33}} \frac{d\sigma_{rr}}{dt} + \frac{d\sigma_{\theta\theta}}{dt} + \left(\beta_{\theta\theta} - \frac{\tilde{C}_{23}}{\tilde{C}_{33}} \beta_{rr} - 1 \right) \phi \\
& + \frac{dT}{dt} = 0
\end{aligned}$$

along $\frac{dr}{dt} = V^{(7)} = 0$ (3.39)

3.5 Integration of the Canonical Equations

The canonical form of the governing equations for the typical orthotropic layer which are given Eqs (3.33-3.39) can be represented in matrix form as;

$$\mathbf{D} \frac{d\mathbf{U}}{dt} - \mathbf{N}\mathbf{U} = \mathbf{0} \quad (3.40)$$

where the matrices \mathbf{D} and \mathbf{N} are given as;

$$\begin{aligned}
D_{11} &= -\alpha \beta_{rr} + \left(\frac{\tilde{C}_{33} - \rho c_1^2}{\beta_{rr}} \right) \frac{\rho c_1}{T_0} \alpha, & D_{12} &= -\rho c_1, \\
D_{13} &= 1, & D_{15} &= \frac{1}{T_0 c_1} \left(\frac{\tilde{C}_{33} - \rho c_1^2}{\beta_{rr}} \right) \quad (3.41a) \\
D_{21} &= -\alpha \beta_{rr} + \left(\frac{\tilde{C}_{33} - \rho c_1^2}{\beta_{rr}} \right) \frac{\rho c_1}{T_0} \alpha, & D_{22} &= \rho c_1,
\end{aligned}$$

$$D_{23} = 1,$$

$$D_{31} = -\alpha\beta_{rr} + \left(\frac{\tilde{C}_{33} - \rho c_2^2}{\beta_{rr}} \right) \frac{\rho c_1}{T_0} \alpha,$$

$$D_{33} = 1,$$

$$D_{41} = -\alpha\beta_{rr} + \left(\frac{\tilde{C}_{33} - \rho c_2^2}{\beta_{rr}} \right) \frac{\rho c_1}{T_0} \alpha,$$

$$D_{43} = 1,$$

$$D_{51} = \alpha\beta_{rr} \frac{\tilde{C}_{23}}{\tilde{C}_{33}} + \alpha\beta_{\theta\theta},$$

$$D_{54} = 1,$$

$$D_{63} = \frac{\tilde{C}_{23}}{C_{33}}$$

$$D_{67} = 1,$$

$$D_{73} = -\frac{\tilde{C}_{23}}{\tilde{C}_{33}},$$

$$D_{76} = 1,$$

all the other $D_{ij} = 0$

$$N_{11} = -\left(\frac{\rho c}{T_0} \frac{(\tilde{C}_{33} - \rho c_1^2)}{\beta_{rr}} + \beta_{rr} \right),$$

(3.42a)

$$N_{12} = -\left(-\tilde{C}_{32} + \frac{\beta_{\theta\theta}}{\beta_{rr}} (\tilde{C}_{33} - \rho c_1^2) \right) \frac{1}{r},$$

$$D_{25} = \frac{1}{T_0 c_1} \frac{(\tilde{C}_{33} - \rho c_1^2)}{\beta_{rr}}$$

$$D_{32} = -\rho c_2,$$

$$D_{35} = \frac{1}{T_0 c_2} \frac{(\tilde{C}_{33} - \rho c_2^2)}{\beta_{rr}},$$

$$D_{42} = \rho c_2,$$

$$D_{45} = -\frac{1}{T_0 c_2} \frac{(\tilde{C}_{33} - \rho c_2^2)}{\beta_{rr}},$$

$$D_{53} = -\frac{\tilde{C}_{23}}{\tilde{C}_{33}}, \quad (3.41b)$$

$$D_{61} = \alpha\beta_{rr} \frac{\tilde{C}_{23}}{\tilde{C}_{33}} + \alpha\beta_{\theta\theta},$$

$$D_{64} = 1,$$

$$D_{71} = \alpha\beta_{rr} \frac{\tilde{C}_{23}}{\tilde{C}_{33}} + \alpha_2 \beta_{\theta\theta}$$

$$D_{74} = 1,$$

$$\begin{aligned}
N_{13} &= -\frac{c_1}{r}, & N_{14} &= \frac{c_1}{r}, \\
N_{15} &= -\frac{(\tilde{C}_{33} - \rho c_1^2)}{\beta_{rr} T_0} \frac{1}{r}, & N_{17} &= 0, \\
N_{21} &= -\left(\frac{\rho}{T_o} \frac{(\tilde{C}_{33} - \rho c_1^2)}{\beta_{rr}} \right) \frac{1}{r}, & N_{23} &= -\frac{c_1}{r}, \\
N_{22} &= -\left(-\tilde{C}_{32} + \frac{\beta_{\theta\theta}}{\beta_{rr}} (\tilde{C}_{33} - \rho c_1^2) \right) \frac{1}{r}, & N_{24} &= -\frac{c_1}{r}, \\
N_{25} &= -\frac{(\tilde{C}_{33} - \rho c_1^2)}{\beta_{rr} T_0} \frac{1}{r}, & N_{31} &= -\left(\frac{\rho}{T_0} \frac{(\tilde{C}_{33} - \rho c_2^2)}{\beta_{rr}} + \beta_{rr} \right), \\
N_{32} &= -\left(-\tilde{C}_{32} + \frac{\beta_{\theta\theta}}{\beta_{rr}} (\tilde{C}_{33} - \rho c_2^2) \right) \frac{1}{r}, & N_{33} &= -\frac{c_2}{r}, \quad (3.42b) \\
N_{34} &= \frac{c_2}{r}, & N_{35} &= -\frac{(\tilde{C}_{33} - \rho c_2^2)}{\beta_{rr} T_0} \frac{1}{r}, \\
N_{41} &= -\left(\frac{\rho}{T_o} \frac{(\tilde{C}_{33} - \rho c_2^2)}{\beta_{rr}} \right) \frac{1}{r}, & N_{43} &= \frac{c_2}{r}, \\
N_{42} &= -\left(-\tilde{C}_{32} + \frac{\beta_{\theta\theta}}{\beta_{rr}} (\tilde{C}_{33} - \rho c_2^2) \right) \frac{1}{r}, & N_{44} &= -\frac{c_2}{r}, \\
N_{45} &= -\frac{(\tilde{C}_{33} - \rho c_2^2)}{\beta_{rr} T_0} \frac{1}{r}, & N_{51} &= -\left(\beta_{\theta\theta} - \beta_{rr} \frac{\tilde{C}_{23}}{\tilde{C}_{33}} \right), \\
N_{52} &= -\left(\tilde{C}_{32} \frac{\tilde{C}_{23}}{\tilde{C}_{33}} - \tilde{C}_{22} \right) \frac{1}{r}, & N_{61} &= -\left(\beta_{\theta\theta} - \beta_{rr} \frac{\tilde{C}_{23}}{\tilde{C}_{33}} \right), \\
N_{62} &= -\left(\tilde{C}_{32} \frac{\tilde{C}_{23}}{\tilde{C}_{33}} - \tilde{C}_{22} \right) \frac{1}{r} + 1, & N_{71} &= -\left(\beta_{\theta\theta} - \beta_{rr} \frac{\tilde{C}_{23}}{\tilde{C}_{33}} - 1 \right), \\
N_{72} &= -\left(\tilde{C}_{32} \frac{\tilde{C}_{23}}{\tilde{C}_{33}} - \tilde{C}_{22} \right) \frac{1}{r},
\end{aligned}$$

all the other $N_{ij} = 0$.

and the unknown vector \mathbf{U} is given by Eq. (3.21).

The integration of the canonical equation along the characteristic lines of a typical layer can be done in exactly the same way as was done in Chapter 2 through Eqs. (2.82-2.85). The integrated equations thus obtained are

$$S_{ij}U_j(A) = Z_{ij}(A_i)U_j(A_i) \quad (i = 1-7, j = 1-7) \quad (3.43)$$

where

$$S_{ij} = D_{ij} - \frac{1}{2} \Delta t N_{ij}(A) \quad (3.44)$$

$$Z_{ij} = D_{ij} + \frac{1}{2} \Delta t N_{ij}(A_i)$$

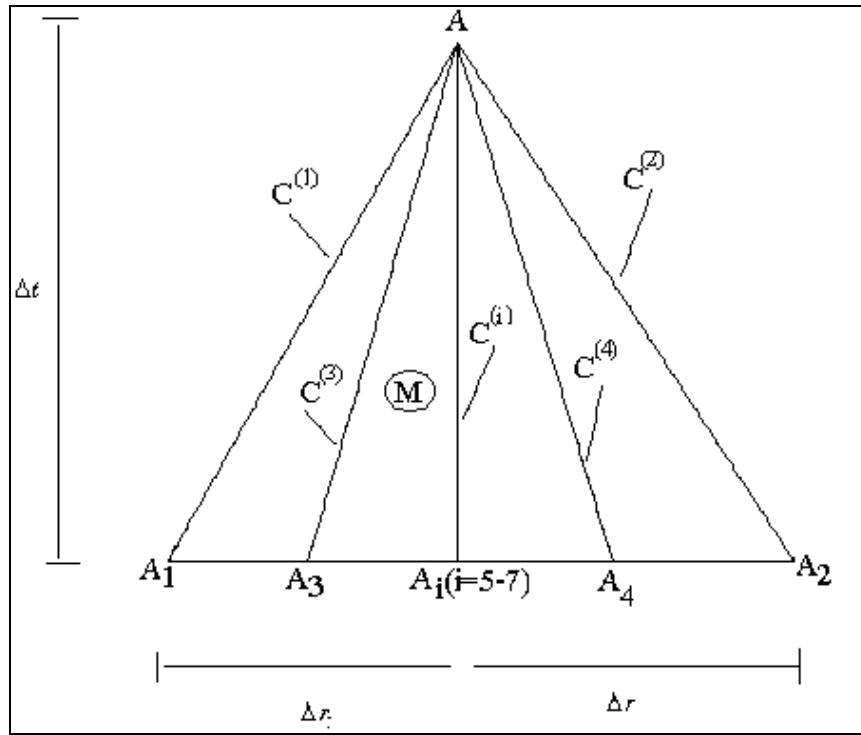


Figure 3.2. Typical interior integration element in the orthotropic layer.

In Eqs. (3.44), Δt is the time interval between two consecutive points along the characteristic lines $C^{(i)}$ ($i = 1-7$), see Figs. (3.1-3.2). Furthermore, in Eqs.(3.43-

3.44), a bar under an index implies that summation convention is not applied to that index and $U_j(A)$, $U_j(A_i)$ represents the values of the field variables at points A and A_i , respectively. To compute the values of field variables at A_3 and A_4 in terms of the values of the field variables at points A_1 , A_5 and A_2 , we use a linear interpolation between A_1 and A_5 , and A_2 and A_5 , (see Fig. 3.1). This gives

$$U_j(A_3) = \frac{U_j(A_5) - U_j(A_1)}{\Delta r} \Delta r_{a1} + U_j(A_1) \quad (3.45)$$

$$U_j(A_4) = \frac{U_j(A_2) - U_j(A_5)}{\Delta r} \Delta r_{a5} + U_j(A_5)$$

where Δr is the distance between two consecutive vertical straight lines in $(r-t)$ plane for the typical layer. Furthermore, Δr_{a1} and Δr_{a5} are define as,

$$\Delta r_{a1} = \Delta r - c_2 \Delta T \quad (3.46)$$

$$\Delta r_{a5} = c_2 \Delta T$$

The elements of D_{ij} and N_{ij} are given in Eqs.(3.41-3.42). Equations (3.43) represent seven equations defined by $i = 1 - 7$, and for each value of the free index i , there is a summation over j which takes the values $(j = 1 - 7)$. Thus, when the field variables U_j are known at points A_i ($i = 1 - 7$), the values of the field variables U_j at point A can be determined from Eqs. (3.43). In other words, using the triangular mesh shown in Fig. 3.2, the values of the field variables at a specific point along any line parallel to the r – axis in the solution region, see Fig. 3.1, can be found in terms of the known values of the field variables defined at points on the previous line. It is compact and suitable to express the equations in this form for computer programming.

3.6 Modification of the Equations for the Boundary and Interface Elements

The integrated canonical equations, Eqs. (3.43), are valid for interior points represented by interior elements, e.g., element M, see Fig. 3.1. For points on the boundaries and at the interfaces, these equations need to be modified.

For the boundary point “L” on the inner surface $r = a$, Fig. 3.1, the integrated canonical equations, Eqs. (3.43), remain the same for $i = 2, 4 - 7; j = 1 - 7$, whereas, the integrated canonical equations for $i = 1, 3; j = 1 - 7$ should be replaced by the boundary conditions, Eqs. (3.15),

$$\begin{aligned} \sigma_{rr}^{(1)}(A) = -P(A) \quad \text{or} \quad V_r^{(1)}(A) = V(A) \quad \text{and} \\ T_1(A) = T^*(A) \quad \text{or} \quad q_r^{(1)}(A) = Q(A) \end{aligned} \quad (3.47)$$

depending on whether the surface tractions or particle velocities and temperature deviations or heat fluxes are prescribed on the inner surface $r = a$. The subscript 1 and superscript 1 in parentheses denote that the quantities refer to layer 1, the innermost layer.

Let us recall that the composite bodies considered in this chapter consist of n different, orthotropic, homogeneous and thermoelastic fiber reinforced layers. Equations (3.43) were derived for a typical layer. This typical layer can be considered as the m th layer and all the quantities pertaining to the m th layer will be denoted by subscripts m or superscripts m in parentheses. For a body consisting of n layers, m takes the values $m=1, 2, \dots, n$. Thus, the integrated equations for the interior element M in the m th layer (see Fig. 3.1) can be written as

$$S_{ij}^{(m)} U_j^{(m)}(A) = Z_{ij}^{(m)}(A_i) U_j^{(m)}(A_i) \quad (i = 1 - 7, j = 1 - 7) \quad (3.48)$$

where $S_{ij}^{(m)}$ and $Z_{ij}^{(m)}$ can be obtained from Eqs. (3.44) by simply putting superscripts m in parentheses over all the quantities appearing in the equation. In this thesis, the innermost orthotropic layer is assumed to be layer 1 and the outermost orthotropic layer is assumed to be n .

Equations (3.43) should be modified for the outer boundary element “P”, as well. In this case, integrated canonical equations, Eqs. (3.43), remain same for $i = 1, 3, 5 - 7; j = 1 - 7$, that is,

$$S_{ij}^{(n)} U_j^{(n)}(A) = Z_{ij}^{(n)}(A_i) U_j^{(n)}(A_i) \quad i = 1, 3, 5 - 7; j = 1 - 7 \quad (3.49)$$

whereas, the equations for $i = 2, 4; j = 1 - 7$ should be replaced by,

$$\sigma_{rr}^{(n)}(A) = -F(A) \quad \text{or} \quad V_r^{(n)}(A) = V^*(A) \quad \text{and} \quad (3.50)$$

$$T_n(A) = t^*(A) \quad \text{or} \quad q_r^{(n)}(A) = Q^*(A)$$

depending on what is prescribed on the outer boundary $r = b$.

We have another type of element where Eqs. (3.43) need to be modified. These elements which are called the interface elements correspond to points A at the interfaces. The number of interfaces depend on the number of layers and since we have n layers, we have $(n-1)$ interfaces which will be denoted by $(N_{12}, N_{23}, \dots, N_{(n-1)(n)})$, see Fig.3.1. For a point A at the interface between the layers m and $m+1$, element $N_{(m)(m+1)}$, Fig. 3.1, Eqs.(3.43) are modified as

$$S_{ij}^{(m)} U_j^{(m)}(A) = Z_{ij}^{(m)}(A_i) U_j^{(m)}(A_i) \quad i = 1, 3, 5 - 7; j = 1 - 7 \quad (3.51)$$

$$S_{ij}^{(m+1)} U_j^{(m+1)}(A) = Z_{ij}^{(m+1)}(A_i) U_j^{(m+1)}(A_i) \quad i = 2, 4, 5 - 7, j = 1 - 7$$

where the superscripts m denote the layer which precedes the interface and $m+1$ denotes the layer which follows the interface. Equations (3.43) for $i = 2, 4$ for m th layer and $i = 1, 3$ for the layer $m+1$ are replaced by the interface conditions requiring the continuity of radial stress, σ_{rr} , particle wave velocity, v_r , temperature deviation, T , and heat flux, q_r . These conditions can be expressed as,

$$\begin{aligned}\sigma_{rr}^{(m)}(A) &= \sigma_{rr}^{(m+1)}(A) \\ v_r^{(m)}(A) &= v_r^{(m+1)}(A) \\ T_m(A) &= T_{m+1}(A) \\ q_r^{(m)}(A) &= q_r^{(m+1)}(A)\end{aligned}\tag{3.52}$$

Thus, modification of the equations for the interface and boundary elements is completed. Equations (3.51–3.52) represent fourteen equations to determine the fourteen unknowns, $U_j^{(m)}(A)$ and $U_j^{(m+1)}(A)$, pertaining to points on the interface of the layers m and $m+1$.

The solution procedure is exactly the same as that explained in Section 2.10. We establishing the solution $U_i = (\phi, v_r, \sigma_{rr}, \sigma_{\theta\theta}, q_r, T, u_r)$ at all points of the network of characteristic lines shown in Fig. 3.1. We start at the origin, proceed along the r –axis and advance into the solution region determining the values of U_i at the points of the network with the order $1', 2', 3', \dots, 1'', 2'', 3'', \dots$ etc, see Fig. 3.1. In this process, we employ the integrated canonical equations for the boundary element ‘L’, interior element ‘M’, interface element ‘N’, and the outer boundary element ‘P’, Fig. 3.1. These equations are discussed in detail above. For this purpose, a computer program in the FORTRAN language is written and the numerical computations are carried out at the computer.

3.7 Numerical Examples and Discussion of the Results

In the numerical examples involving the multilayered medium, it has been assumed that the inner surface, $r = a$, is subjected to a uniform pressure and a uniform temperature deviation, while the outer surface $r = b$ is free of surface tractions and kept at zero temperature deviation. Thus, the boundary conditions at the inner ($r = a$) and outer ($r = b$) surfaces can be expressed, respectively, as

$$\begin{aligned}\sigma_{rr}(a, t) &= -P(t)H(t), & T(a, t) &= T^*(t)H(t) \text{ or } T(a, t) = 0 \\ \sigma_{rr}(b, t) &= 0, & T(b, t) &= 0\end{aligned}\tag{3.53}$$

In the method of characteristics, we are free to choose any time dependency for the applied pressure and temperature deviation. In the problems, we choose a step-time variation with an initial ramp, see Fig. 2.7 and Fig. 3.3. In the figures, we notice that the applied pressure and temperature deviation are zero at $t = 0$, linearly rises to a constant value P_0 and T_0 , respectively, during a rise time of Δt and remain constant thereafter. The initial ramp in the pressure variation and temperature deviation eliminates the complicated circumstances of having first-order discontinuities in the field variables at the wave fronts and it is physically more realistic.

The numerical computations are carried out and the results are displayed in terms of non-dimensional quantities. These non-dimensional quantities are defined as

$$\begin{aligned}\bar{\rho} &= \frac{\rho}{\rho_1}, & \bar{v} &= \frac{v}{c_L^{(1)}}, & \bar{t} &= \frac{tc_L^{(1)}}{a} \\ (\bar{E}_1, \bar{E}_2, \bar{E}_3) &= \left(\frac{E_1}{\rho_1 c_L^{(1)2}}, \frac{E_2}{\rho_1 c_L^{(1)2}}, \frac{E_3}{\rho_1 c_L^{(1)2}} \right), & \bar{c} &= c \frac{T_0}{c_L^{(1)2}}\end{aligned}\tag{3.54a}$$

$$\begin{aligned} (\bar{G}_{12}, \bar{G}_{13}, \bar{G}_{23}) &= \left(\frac{G_{12}}{\rho_1 c_L^{(1)2}}, \frac{G_{13}}{\rho_1 c_L^{(1)2}}, \frac{G_{23}}{\rho_1 c_L^{(1)2}} \right), & \bar{r} &= \frac{r}{a}, \\ (\bar{\sigma}_{rr}, \bar{\sigma}_{\theta\theta}) &= \left(\frac{\sigma_{rr}}{\rho c_L^2}, \frac{\sigma_{\theta\theta}}{\rho c_L^2} \right), & \bar{u}_r &= \frac{u_r}{a}, \end{aligned} \quad (3.54b)$$

$$(\bar{c}_1, \bar{c}_2) = \left(\frac{c_1}{c_L^{(1)}}, \frac{c_2}{c_L^{(1)}} \right), \quad \bar{k}_{rr} = k_{rr} \frac{T_0}{\rho_1 c_L^{(1)3} a},$$

$$(\bar{\beta}_{11}, \bar{\beta}_{22}, \bar{\beta}_{33}) = \left(\frac{\beta_{11} T_0}{\rho_1 c_L^{(1)2}}, \frac{\beta_{22} T_0}{\rho_1 c_L^{(1)2}}, \frac{\beta_{33} T_0}{\rho_1 c_L^{(1)2}} \right), \quad \bar{T} = \frac{T}{T_0},$$

$$\bar{\alpha} = \frac{\alpha c_L^{(1)}}{a}, \quad \bar{q}_r = \frac{q_r}{\rho_1 c_L^3}, \quad \bar{\alpha}_0 = \frac{\alpha_0 c_L^{(1)}}{a}$$

where $c_L^{(1)} = \sqrt{\frac{C_{33}^{(1)}}{\rho_1}}$ in Eqs. (3.54) is the uncoupled mechanical longitudinal wave speed in layer 1 and the non-dimensional quantities are shown by putting bars over them. Furthermore, a is the radius of the inner surface and ρ_1 is the mass density of the innermost layer 1.

First, an example of verification will be given. In this example, a whole space containing a cylindrical hole is considered. A uniform pressure is applied on the surface of the cylindrical hole, and the transient dynamic response of the whole space is investigated by employing the TRDTE theory. The boundary conditions on the cylindrical surface $r = a$ are taken as

$$\sigma_{rr}(a, t) = -P_0 H(t); \quad T(a, t) = 0 \quad (3.55)$$

where P_0 is a constant and $H(t)$ is the Heaviside unit step function. The body is initially unstressed, at rest and at a constant reference temperature T_0 . The whole space is isotropic, homogenous and linearly elastic. This problem was solved by Harmain, Wegner and Haddow [120] by employing the method of characteristics. The solution of this problem in our treatment is obtained as a special case of the general multilayered problem. The computer program developed in this thesis for multilayered medium consisting of n generally orthotropic layers is employed. By suitably choosing the material constants and the geometric parameters of the orthotropic layers, the solution for the homogenous isotropic whole space containing a cylindrical whole is obtained as a special case. The non-dimensional material properties of the orthotropic layers in our treatment, which gives the same material properties as chosen in [120] for the isotropic whole space, are taken as

$$\begin{aligned}
\bar{\rho} &= \frac{\rho}{\rho} = 1, & \bar{k}_{rr} &= k_{rr} \frac{T_0}{\rho c_L^3 ag} = 0.0003192, \\
\bar{E}_1 &= \bar{E}_2 = \bar{E}_3 = \frac{E_1}{\rho c_L^2} = \frac{E_2}{\rho c_L^2} = \frac{E_3}{\rho c_L^2} = 0.675, \\
\bar{G}_{12} &= \bar{G}_{23} = \bar{G}_{13} = \frac{G_{12}}{\rho c_L^2} = \frac{G_{23}}{\rho c_L^2} = \frac{G_{13}}{\rho c_L^2} = 0.254, \\
\bar{\nu}_{23} &= \bar{\nu}_{32} = \bar{\nu}_{31} = \bar{\nu}_{13} = \bar{\nu}_{21} = \bar{\nu}_{12} = 0.33, & \bar{a} &= \frac{a}{ag} = 322700 \\
\bar{\beta}_{11} &= \bar{\beta}_{22} = \bar{\beta}_{33} = \frac{\beta_{11} T_0}{\rho c_L^2} = \frac{\beta_{22} T_0}{\rho c_L^2} = \frac{\beta_{33} T_0}{\rho c_L^2} = 0.015, \\
\bar{c} &= c \frac{T_0}{c_L^2} = 0.007, & \bar{\alpha} &= \alpha \frac{c_L}{ag} = 0.01,
\end{aligned} \tag{3.56a}$$

$$\bar{\alpha}_0 = \alpha_0 \frac{c_L}{ag} = 0.01, \quad \bar{r} = \frac{r}{ag} \quad (3.56b)$$

where $c_L = \sqrt{\frac{(2\mu + \lambda)}{\rho}} = \sqrt{\frac{C_{33}}{\rho}}$ is the uncoupled mechanical longitudinal wave speed, and the constant g is a non-dimensional scaling parameter used by Harmain, Wegner and Haddow [120] to present the results for times several order of magnitude larger than the relaxation time constant. Furthermore, the constant non-dimensional uniform pressure applied at the cylindrical surface is taken as $\bar{P}_0 = 0.001$.

The variations of non-dimensional temperature deviation \bar{T} , non-dimensional heat flux \bar{q} and non-dimensional radial stress $\bar{\sigma}_{rr}$ with dimensionless $\bar{r} = r/ag$ at times $\bar{t} = 0.2, 0.4, 0.6, 0.8, 1.0$ are given in Figs. (3.4-3.6), respectively. As seen from Figs. (3.4-3.6), the curves of Harmain, Wegner and Haddow [120] coincide with the curves obtained from our treatment.

We shall now present some results for multilayered media consisting of generally orthotropic layers. In the first example investigated, we consider a cylindrical laminate consisting of alternating isotropic layers, which we denote as layers 1 and 2. The laminate consists of five layers with the sequence 1/2/1/2/1 starting from the innermost layer. The material properties of the orthotropic layers are chosen such that they represent isotropic layers. The non-dimensional properties are taken as,

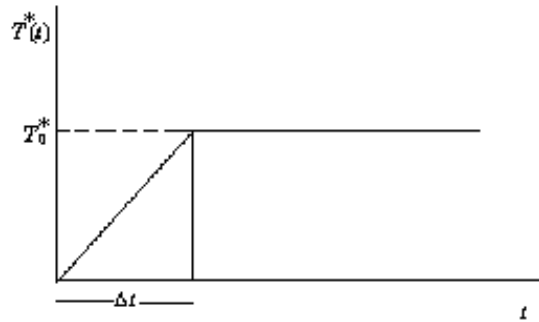


Figure 3.3. Variation of temperature deviation at the boundary.

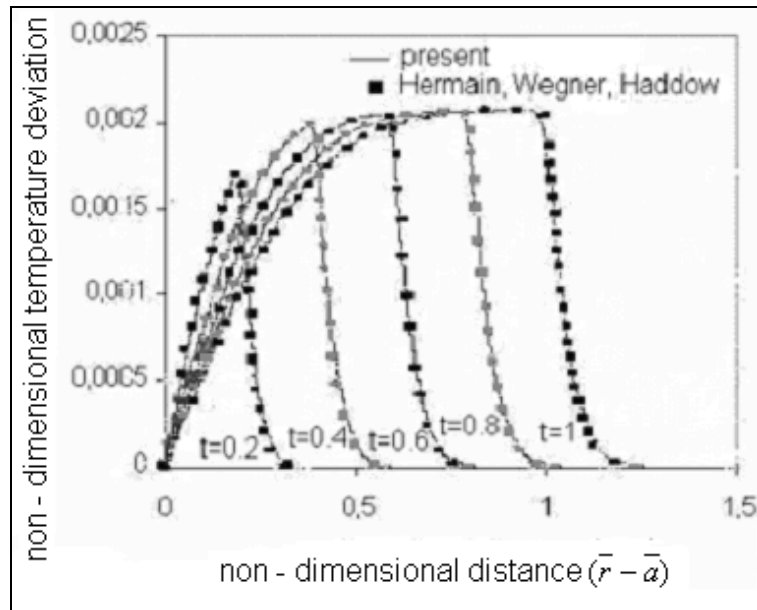


Figure 3.4. Variation of non-dimensional temperature deviation with respect to distance at various non-dimensional times for an unbounded body with a cylindrical hole.

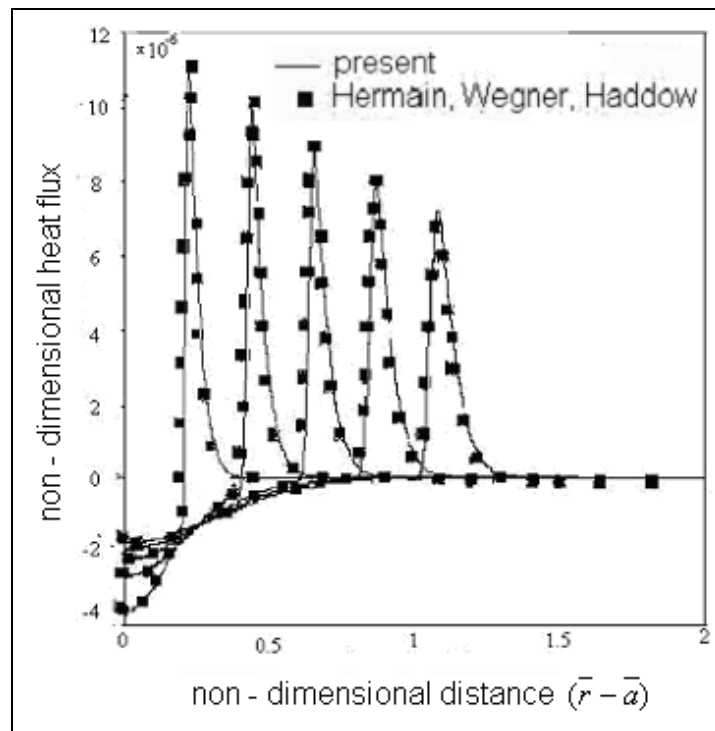


Figure 3.5. Variation of non-dimensional heat flux with respect to distance at various non-dimensional times for an unbounded body with a cylindrical hole

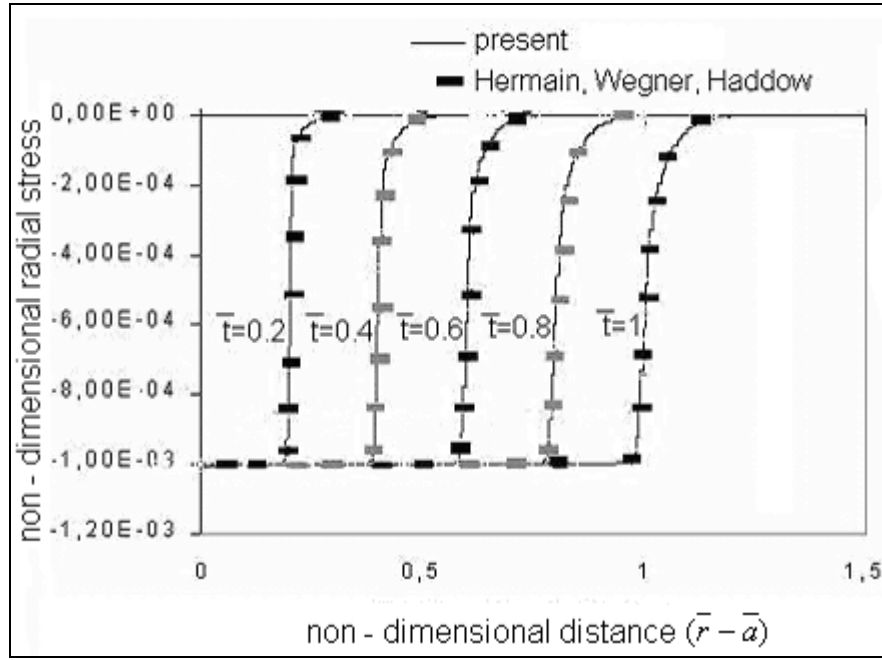


Figure 3.6. Variation of non-dimensional radial stress with respect to distance at various non-dimensional times for an unbounded body with a cylindrical hole.

$$\bar{\rho}_1 = 1,$$

$$\bar{E}_1^{(1)} = E_1^{(2)} = E_1^{(3)} = 0.675,$$

$$\bar{G}_{12}^{(1)} = \bar{G}_{23}^{(1)} = \bar{G}_{13}^{(1)} = 0.254,$$

$$\nu_{23}^{(1)} = \nu_{32}^{(1)} = \nu_{31}^{(1)} = \nu_{13}^{(1)} = \nu_{21}^{(1)} = \nu_{12}^{(1)} = 0.33, \quad (3.57a)$$

$$\bar{a} = 1, \quad \bar{k}_{rr}^{(1)} = 6.569 \times 10^{-10}, \quad \bar{c}^{(1)} = 0.005,$$

$$\bar{\beta}_{11}^{(1)} = \beta_{22}^{(1)} = \beta_{33}^{(1)} = 0.003,$$

$$\bar{\alpha}^{(1)} = \alpha_0^{(1)} = 0.00000002316,$$

$$\bar{\rho}_2 = \frac{\rho_2}{\rho_1} = 0.872,$$

$$\bar{E}_1^{(2)} = E_2^{(2)} = E_3^{(2)} = 1.038,$$

$$\bar{G}_{12}^{(2)} = \bar{G}_{23}^{(2)} = \bar{G}_{13} = 0.39,$$

$$\nu_{23}^{(2)} = \nu_{32}^{(2)} = \nu_{31}^{(2)} = \nu_{13}^{(2)} = \nu_{21}^{(2)} = \nu_{12}^{(2)} = 0.33, \quad (3.57b)$$

$$\bar{\beta}_{11}^{(2)} = \bar{\beta}_{22}^{(2)} = \bar{\beta}_{33}^{(2)} = 0.003,$$

$$\bar{c}^{(2)} = 0.006, \quad \bar{k}_{rr}^{(2)} = 3.941 \times 10^{-10},$$

$$\bar{\alpha}^{(2)} = \bar{\alpha}_0^{(2)} = 0.00000002316,$$

In Eqs. (3.57), the non dimensional quantities are shown by putting bars over them, and subscripts 1 and 2 or superscripts 1 and 2 in parentheses, respectively, denote that the quantities belong to layer 1 or 2.

Furthermore, the non dimensional thickness of the layers are equal to $\bar{h}_1 = \bar{h}_2 = 0.1$, and the network of characteristic lines used in the numerical analysis is defined by $\Delta \bar{t} = 0.00025$. In the examples, the boundary conditions are as given by Eqs. (3.53). The applied pressure at the inner surface $\bar{r} = \bar{a} = 1$ is a step function with an initial ramp as given in Fig. 2.7. It is zero at $\bar{t} = 0$, then linearly rises to a constant value $\bar{P}_0 = 0.001$ during a rise time of $\Delta \bar{t} = 0.00025$ after which it remains constant. The applied temperature at the inner surface is either a step function with an initial ramp as given in Fig. 3.3 with $\bar{T}_0 = 0.08$ or 0.3 or it is zero. This is expressed explicitly in

each figure. In all cases, the outer surface $\bar{r} = \bar{b}$ is free of surface tractions and the temperature deviation is kept zero.

Results of the numerical computations are given in Figs. (3.7-3.10). The curves are given for the cases when the thermal effects are neglected and when they are taken into account, which in the sequel are described as non-thermal and thermoelastic solutions, respectively. Variations of the non dimensional stress $-\bar{\sigma}_{rr}$ with time \bar{t} at location $\bar{r} = 1.15$ is given in Fig. 3.7. The curves denote clearly the dispersion caused by the thermal effects in the wave profiles. In the curve representing the non thermal solution in which thermal effects are neglected, the sudden changes in the stress levels correspond to the arrivals of reflected and refracted waves from the interfaces and boundaries of the composite body at the position considered. In the thermoelastic solutions in which thermal effects are taken into account, the curves display a similar character. However, due to the thermal dispersion, the sudden changes in the elastic solution now become smoothly varying curves. The maximum values of the radial normal stress for thermoelastic solutions increase as inner temperature deviation increases, especially for higher non-dimensional times. The radial stress remains mostly compressive both in non thermal and thermoelastic solutions. This is especially the case for thermoelastic solutions.

The curves of Fig. 3.8 display the variations of the dimensionless normal stress $\bar{\sigma}_{\theta\theta}$ with \bar{t} at $\bar{r} = 1.15$, the middle of the second layer of the multilayered media. The normal circumferential stress is basically tensile; whereas, for short durations of time, it may become compressive as seen in Fig. 3.8. In addition to the solutions obtained by employing the TRDTE theory, the elastic solutions with thermal effects neglected are also given in the figure. We further note that the effects of thermal changes are more significant for the circumferential stress and the circumferential stresses are much higher than the normal stresses.

The curves of Fig. 3.9 show the variations of the non-dimensional radial stress $-\bar{\sigma}_{rr}$ with time \bar{t} at location $\bar{r} = 1.25$. These curves display similar features as those of

Fig. 3.7. In addition to the effects of reflections and refractions from the interfaces and boundaries and thermal dispersion, we can see the effects of geometric attenuation in these curves as well. The maximum levels of the stresses in the curves of Fig. 3.9 are considerably lower than those of Fig. 3.7, because the location $\bar{r} = 1.25$ compared to $\bar{r} = 1.15$ is further away from the inner boundary. In fact maximum value of $-\bar{\sigma}_{rr}$ in the curves of Fig. 3.9 is approximately 0.0011, whereas it reaches values as high as 0.0015 in Fig. 3.7.

In the curves of Fig. 3.10, the variations of the dimensionless circumferential normal stress $\bar{\sigma}_{\theta\theta}$ with \bar{t} at the location $\bar{r} = 1.25$, which corresponds to the middle of the third layer from the inner surface, are displayed. These curves show similar trends as those in in Fig. 3.8. The maximum stress levels are much lower. The effects of thermal dispersion seem to be relatively more pronounced in these curves then those of Fig. 3.8.

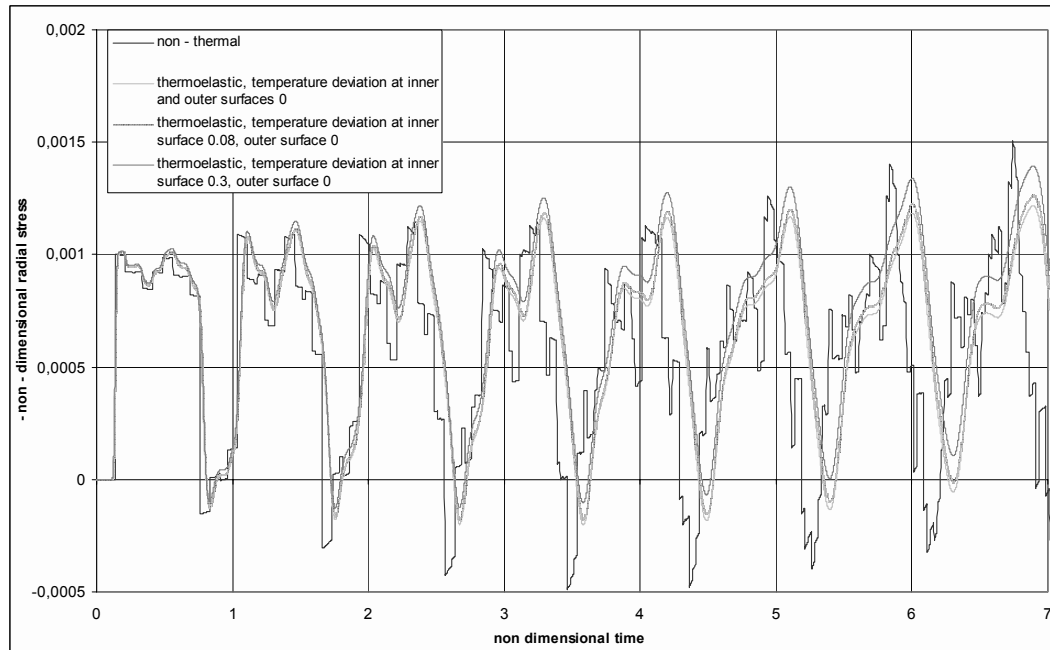


Figure 3.7. Variation of radial stress $\bar{\sigma}_{rr}$ with time \bar{t} at $\bar{r} = 1.15$, for the laminate with alternating isotropic layers.

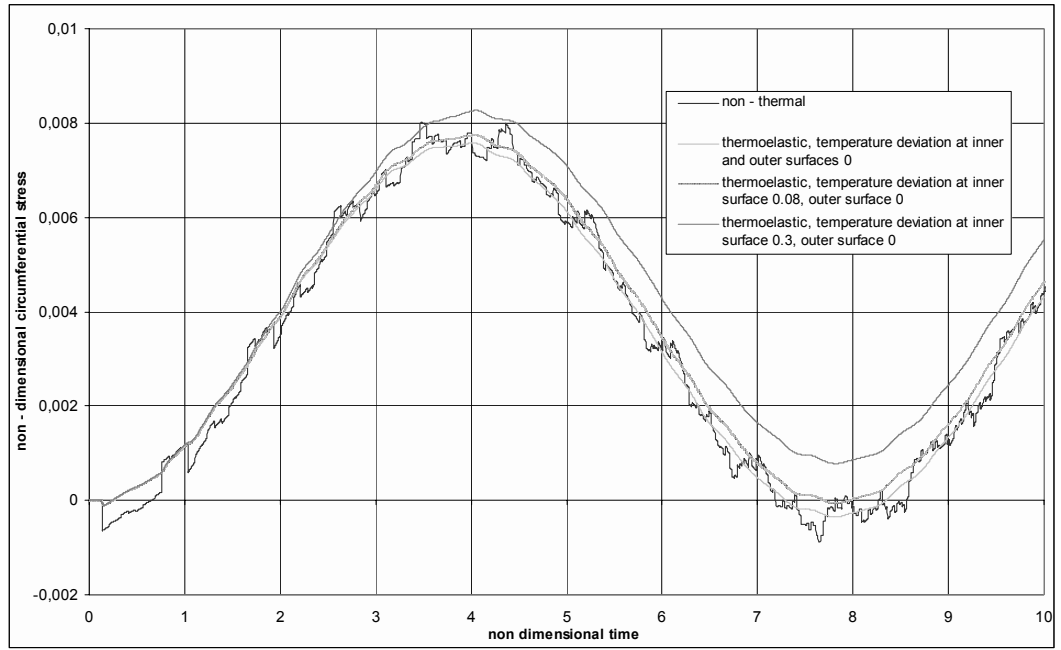


Figure 3.8. Variation of circumferential stress $\bar{\sigma}_{\theta\theta}$ with time \bar{t} at $\bar{r} = 1.15$, for the laminate with alternating isotropic layers.

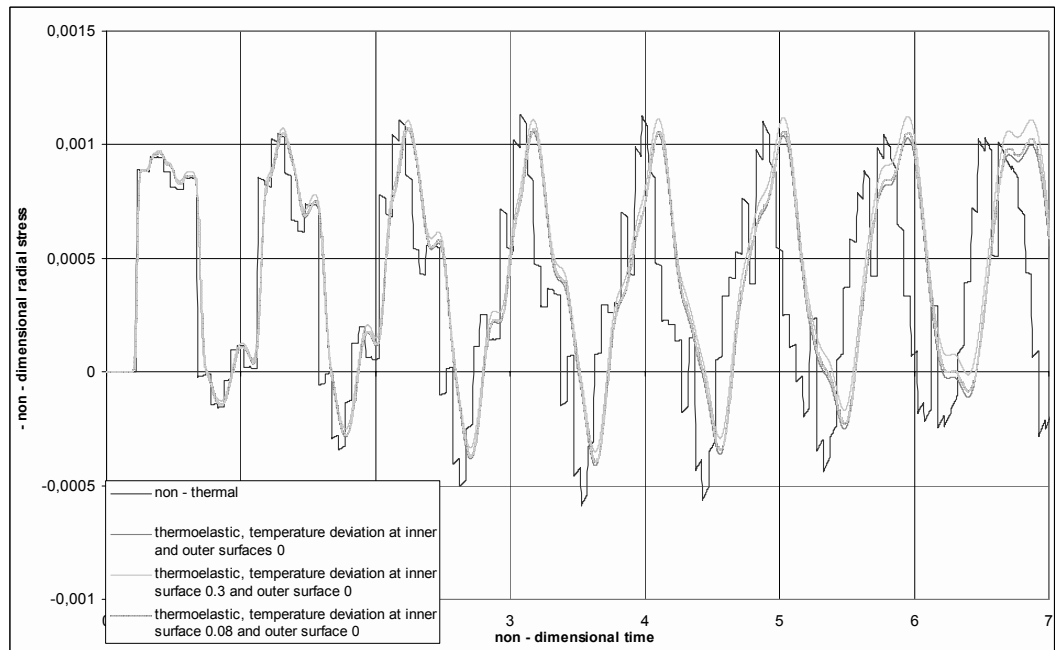


Figure 3.9. Variation of radial stress $\bar{\sigma}_{rr}$ with time \bar{t} at $\bar{r} = 1.25$, for the laminate with alternating isotropic layers.

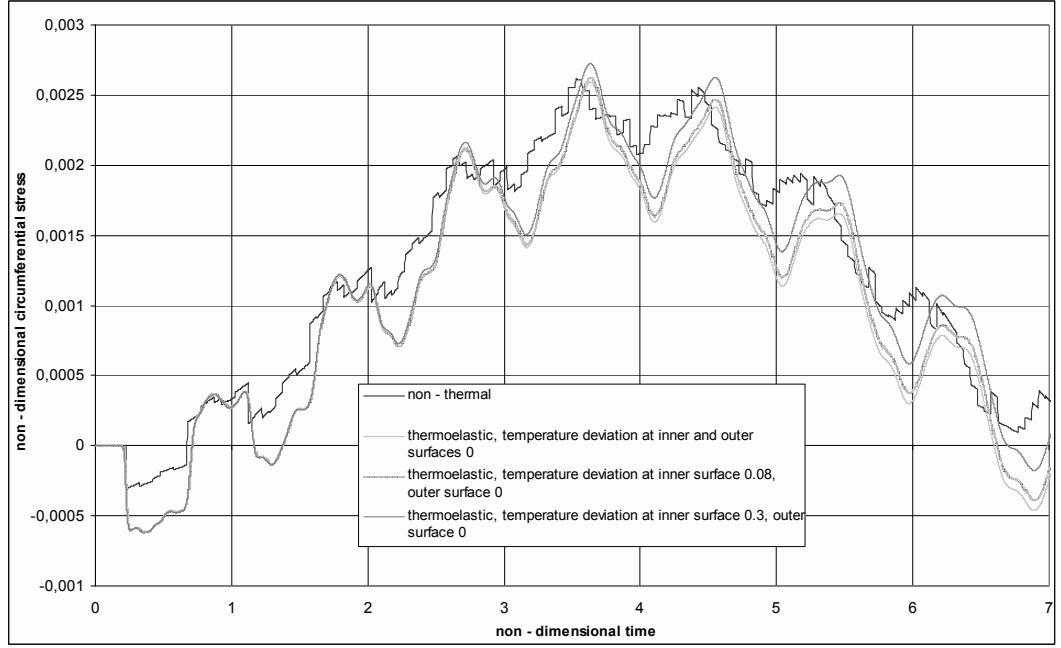


Figure 3.10. Variation of circumferential stress $\bar{\sigma}_{\theta\theta}$ with \bar{t} at $\bar{r}=1.25$, for the laminate with alternating isotropic layers.

Next, we shall investigate an example involving a filament wound fiber-reinforced cylindrical composite which is the basic problem investigated in this chapter. The boundary conditions given by Eqs. (3.53) are considered with the pressure function $P(t)$ and temperature deviation $T(t)$ given as in Fig. 2.7 and Fig. 3.3. The multilayered bodies considered consist of five generally orthotropic elastic layers with stacking sequence 30/-30/90/0/90 and 30/-30/30/-30/30 starting from the innermost layer. The numerical computations are carried out using S2 glass/epoxy material properties for generally orthotropic layers [141]. The non-dimensional material properties then can be written as

$$\begin{aligned} \bar{\rho} &= 1, & \bar{T}_0 &= 1, & \bar{c} &= 0.027 \\ & & & & & (3.58a) \\ (\bar{E}_1, \bar{E}_2, \bar{E}_3) &= (2.323, 0.787, 0.787), \end{aligned}$$

$$(\bar{G}_{12}, \bar{G}_{13}, \bar{G}_{23}) = (0.278, 0.278, 0.295),$$

$$\bar{k}_{rr} = 6.943 \times 10^{-9}$$

$$(\bar{\beta}_{11}, \bar{\beta}_{22}, \bar{\beta}_{33}) = (0.024, 0.015, 0.015) \quad (3.58b)$$

$$\bar{\alpha} = 0.00000001585, \quad \bar{\alpha}_0 = 0.00000001585$$

$$\nu_{23} = \nu_{32} = 0.33,$$

$$\nu_{31} = \nu_{13} = \nu_{21} = \nu_{12} = 0.236$$

Furthermore, the non-dimensional thicknesses of the layers are equal to $\bar{h}_i = 0.1$ $i = (1-5)$, and the network of characteristic lines used in the numerical analysis is defined by $\bar{\Delta t} = 0.00025$. The applied pressure at the inner surface $\bar{r} = \bar{a} = 1$ given in Fig. 2.7 is zero at $\bar{t} = 0$, then linearly rises to a constant value $\bar{P}_0 = 0.001$ during a rise time of $\bar{\Delta t} = 0.00025$, after which it remains constant.

Results of the numerical computations are given in the form of curves in Figs. (3.11-3.16) The curves are given for the cases when the thermal effects are neglected and when they are taken into account.

The temperature deviation prescribed at $\bar{r} = 1$ is a step function with an initial ramp, see Fig. (3.3), with $\bar{T}_0 = 0.00, 0.01, 0.02$ or 0.04 . This is pointed out explicitly in each figure. In all cases, the outer surface $\bar{r} = \bar{b} = 1.5$ is free of surface tractions and temperature deviation is zero.

Variation of the non-dimensional stress $-\bar{\sigma}_{rr}$ with time \bar{t} at location $\bar{r} = 1.15$ for a multilayered body having stacking sequence 30/-30/90/0/90 is shown in Fig. 3.11. The curves of Fig. 3.11, correspond to non-thermal and three thermoelastic solutions, in which the temperature deviations at the inner surface are 0.00, 0.01 and 0.02 while

the outer surface temperature deviation kept zero. The curves denote clearly the dispersion caused by the thermal effects in the wave profiles. In the curve representing the solution in which thermal effects are neglected, the sudden changes in the stress levels correspond to the arrivals of reflected and refracted waves from the interfaces and boundaries of the composite body at the position considered. In the thermoelastic solutions in which thermal effects are taken into account, the curves display a similar character. However, due to the thermal dispersion, the sudden changes in the non-thermal solution now become smoothly varying curves. There is considerable difference between the non-thermal solution and the solutions when thermal effects are taken into account even in the case when the temperature deviations at the inner and outer boundary surfaces are kept at zero. We note that these differences become more apparent as time passes. Furthermore, the differences are larger as the temperature deviation prescribed at the inner surface gets higher. We also note that the radial stress remains basically compressive.

Figure 3.12 displays the variations of the dimensionless normal stress $\bar{\sigma}_{\theta\theta}$ with \bar{t} for a multilayered body having stacking sequence 30/-30/90/0/90 at the location $\bar{r} = 1.25$ which represents the middle of the third layer of the laminate. The normal circumferential stress is basically tensile; whereas, for short durations of time after the arrival of the wave front at the location considered, it may become compressive as seen in Fig. 3.12. The curves represent the non-thermal solution together with the thermoelastic solutions in which the dimensionless temperature deviations at the inner surface take the values 0.00, 0.01, 0.04. The curves display similar features. However, due to thermal dispersion, the sudden changes in the non-thermal solution become smoothly varying curves in the thermoelastic solutions. The differences between non-thermal and thermoelastic curves are smaller for small inner surface temperature deviations. Higher temperature deviations at the inner surface yield thermoelastic curves which differ more significantly from the non-thermal one, especially for larger times. We further note that the circumferential normal stress is the dominant stress for the laminate, since it reaches nearly four times higher stress values than the radial one.

The curves of Fig. 3.13 show the variations of the dimensionless normal stress $\bar{\sigma}_{\theta\theta}$ with \bar{t} for a multilayered body having stacking sequence 30/-30/90/0/90 at $\bar{r} = 1.45$, which corresponds to the middle of the fifth orthotropic layer. The curves of the non-thermal solution together with the thermoelastic solutions where the temperature deviation at the inner surface are 0.0 and 0.04 are shown in the figure. The curves display similar trends as those of Fig. 3.12.

Variation of the non-dimensional stress $-\bar{\sigma}_{rr}$ with time \bar{t} at location $\bar{r} = 1.15$ for a multilayered body having stacking sequence 30/-30/30/-30/30 is shown in Fig. 3.14. The curves of the non-thermal solution together with the thermoelastic solutions where the temperature deviations at the inner surface are 0.00, 0.01 and 0.02 are shown in the figure. The curves display similar trends as those of Fig. 3.11. The curves of the figure have smaller maximum stress values relative to the curves of Fig. 3.11.

Figures (3.15-3.16) show the variations of the dimensionless normal stress $\bar{\sigma}_{\theta\theta}$ with \bar{t} at locations $\bar{r} = 1.15$ and $\bar{r} = 1.45$, for a multilayered body having stacking sequence 30/-30/30/-30/30. The curves of the non-thermal solution together with the thermoelastic solutions where the temperature deviations at the inner surface are 0.0, 0.01 and 0.04 are shown in the figure. The curves display similar trends as those of Fig. 3.12 and Fig. 3.13. Effects of geometric attenuation can be seen in these figures since the curves of Fig. 3.16 reach smaller stress values than those of Fig. 3.15. When we compare the curves of Figures 3.12 and 3.13, however, we see that the stress levels at $\bar{r} = 1.45$ are higher than those at $\bar{r} = 1.15$ in spite of geometric attenuation. This is because of the effects of the stacking sequence of the layers. Even though all the other properties are the same, the stacking sequence in Figs. (3.12-3.13) is 30/-30/90/0/90; whereas, in Figs. (3.15-3.16), it is 30/-30/30/-30/30. This shows that the effects of stacking sequence on the wave profiles can be quite significant.

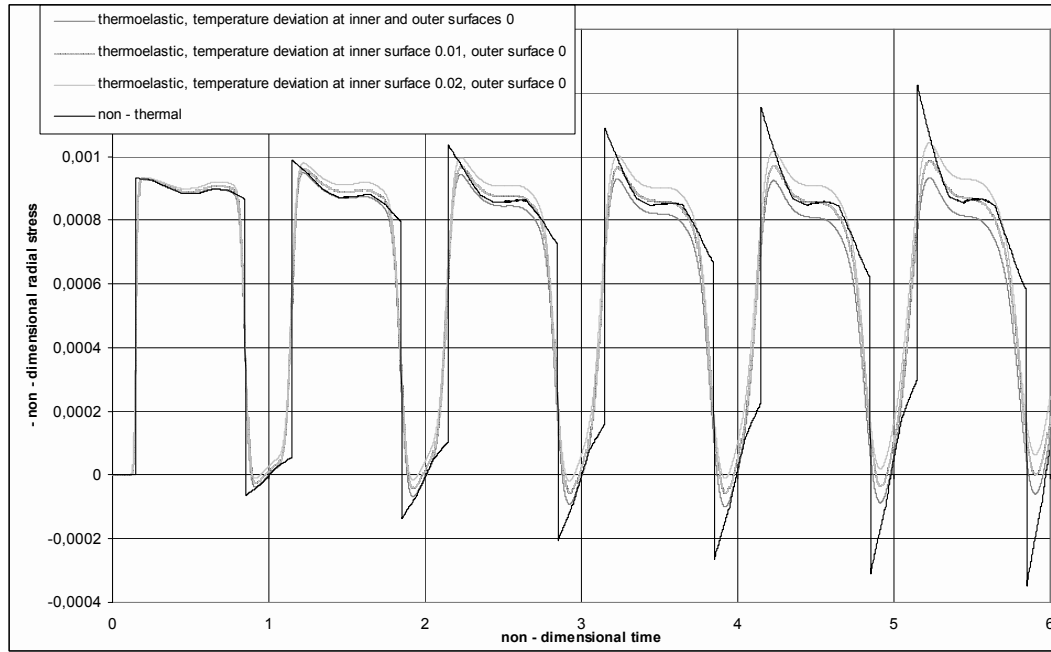


Figure 3.11. Variation of radial normal stress $-\bar{\sigma}_{rr}$ with time \bar{t} at location $\bar{r} = 1.15$, for the laminate with generally orthotropic layers having stacking sequence 30/-30/90/0/90.

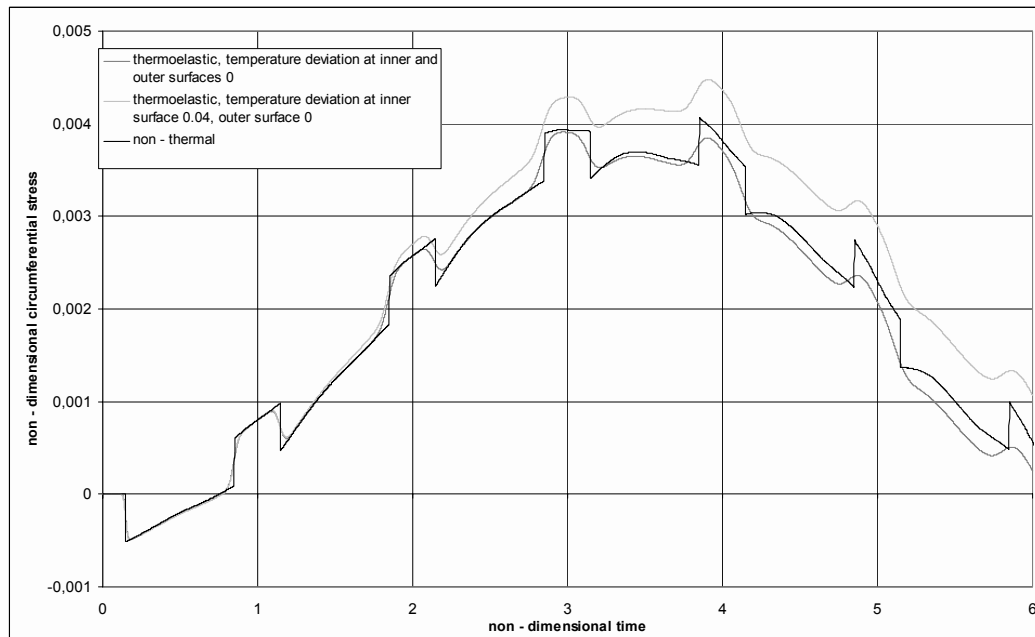


Figure 3.12. Variation of circumferential normal stress $\bar{\sigma}_{\theta\theta}$ with time \bar{t} at location $\bar{r} = 1.15$, for the laminate with generally orthotropic layers having stacking sequence 30/-30/90/0/90.

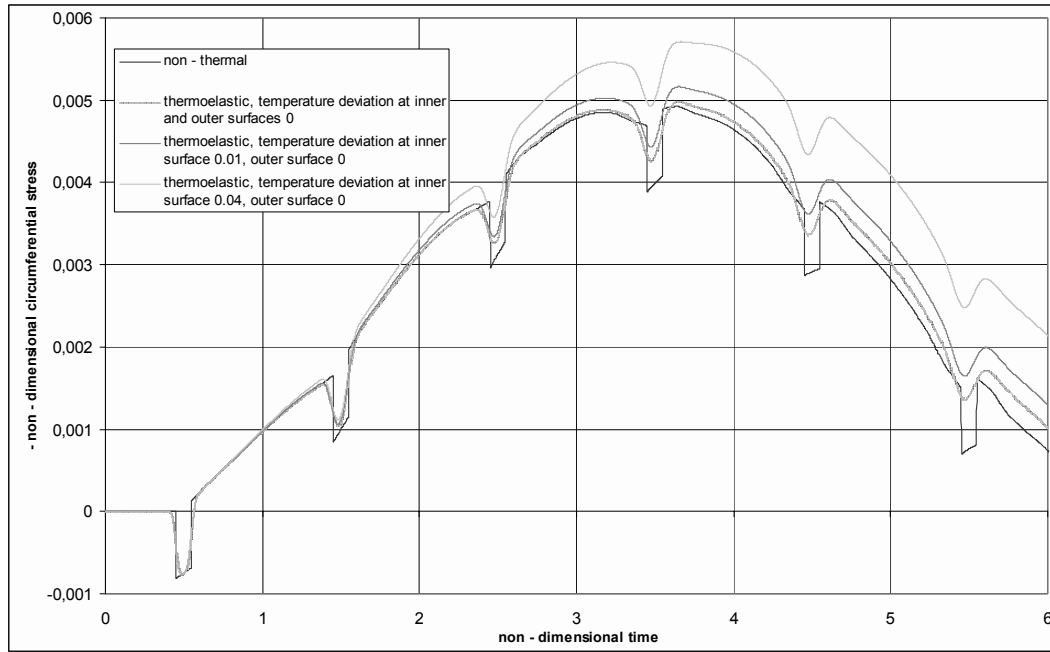


Figure 3.13. Variation of circumferential normal stress $\bar{\sigma}_{\theta\theta}$ with time \bar{t} at location $\bar{r} = 1.45$, for the laminate with generally orthotropic layers having stacking sequence 30/-30/90/0/90.

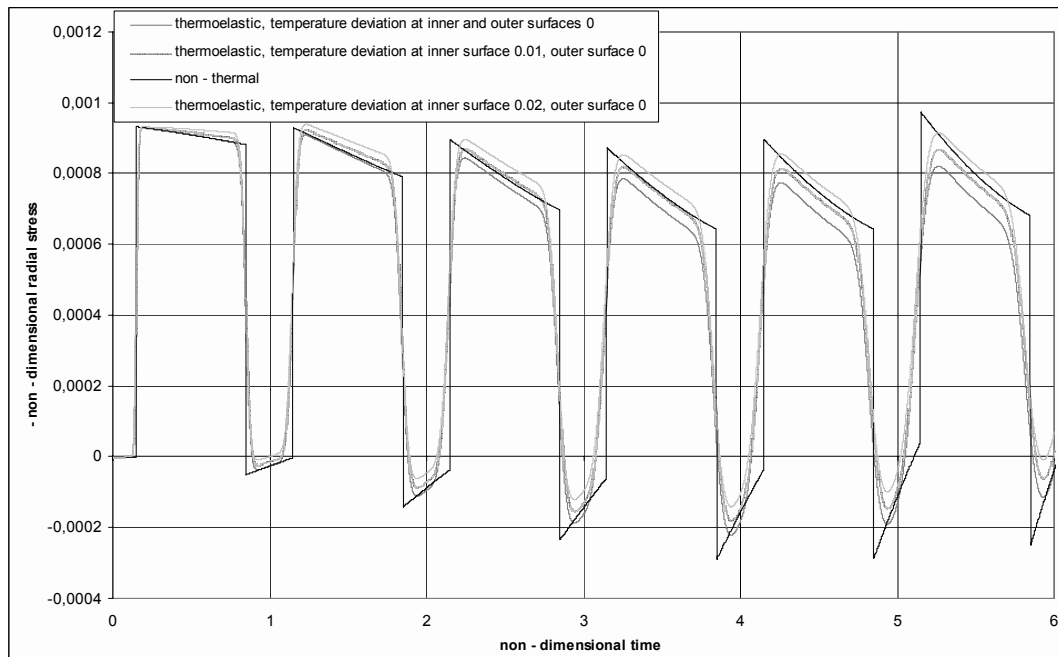


Figure 3.14. Variation of radial normal stress $-\bar{\sigma}_{rr}$ with time \bar{t} at location $\bar{r} = 1.15$, for the laminate with generally orthotropic layers having stacking sequence 30/-30/30/-30/30.

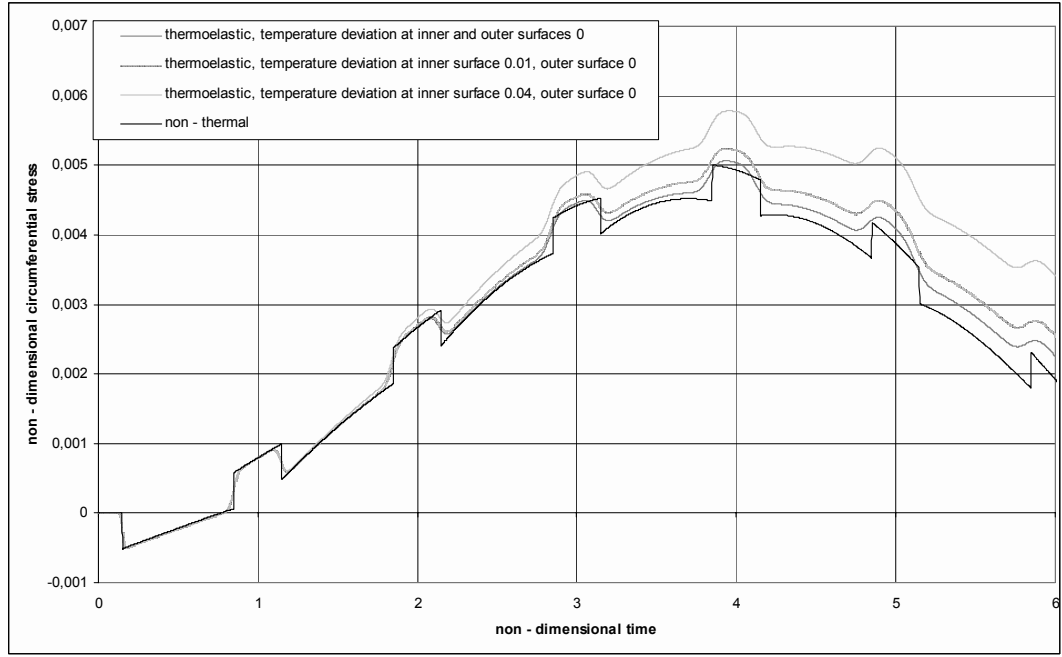


Figure 3.15. Variation of circumferential normal stress $\bar{\sigma}_{\theta\theta}$ with time \bar{t} at location $\bar{r} = 1.15$, for the laminate with generally orthotropic layers having stacking sequence 30/-30/30/-30/30.

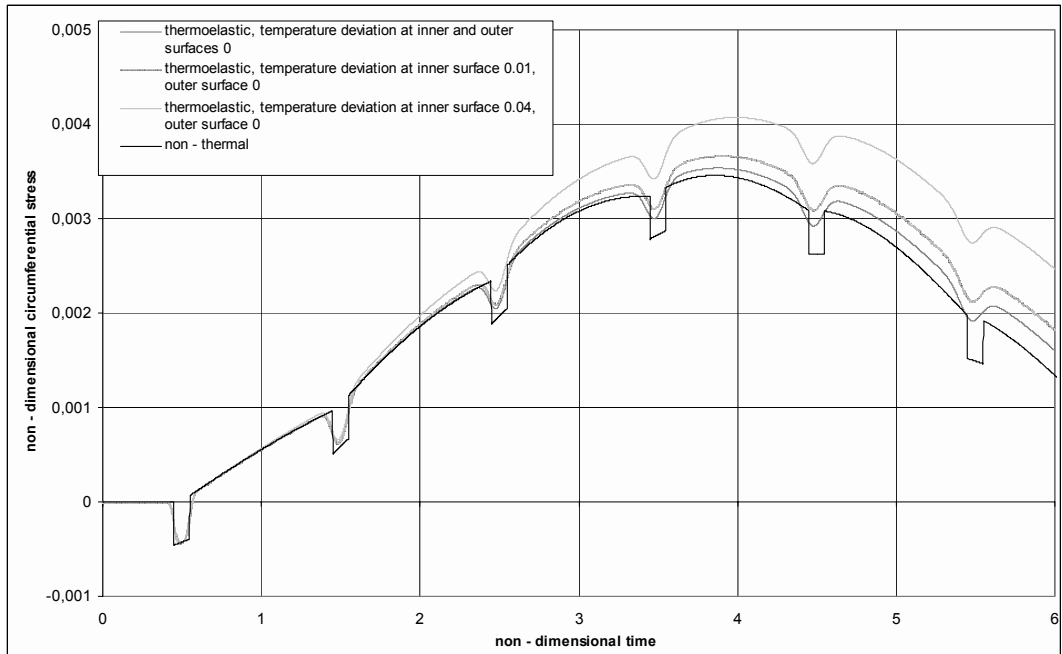


Figure 3.16. Variation of circumferential normal stress $\bar{\sigma}_{\theta\theta}$ with respect to time \bar{t} at location $\bar{r} = 1.45$ for the laminate with generally orthotropic layers having stacking sequence 30/-30/30/-30/30.

CHAPTER 4

THERMOMECHANICAL RESPONSE OF VISCOELASTIC CYLINDERS ENCLOSED IN FIBER-REINFORCED CYLINDRICAL COMPOSITES

4.1 Introduction

In this chapter, transient dynamic response of viscoelastic cylinders enclosed in filament wound cylindrical composites will be investigated. Thermal effects, in addition to the mechanical effects, are taken into consideration as in the previous chapter.

The body considered in this chapter consists of $n+1$ -layers, the inner layer being isotropic, homogenous and linearly viscoelastic, while the outer part being fiber-reinforced composite consisting of n -different generally orthotropic, homogeneous and linearly elastic layers. In each ply, the ply orientation angle may be different. The body is a hollow circular cylinder with a finite thickness in the radial direction, whereas it extends to infinity in the axial direction. The multilayered medium is subjected to uniform time-dependent dynamic inputs at the inner and/or outer surfaces. The body is assumed to be initially at rest. The layers are assumed to be perfectly bonded to each other.

The governing field equations of generalized thermo-viscoelasticity with two relaxation times is applied to the inner viscoelastic layer in addition to the application of the governing field equations of generalized anisotropic thermoelasticity to the outer layers and the solutions are required to satisfy the continuity conditions at the interfaces of the layers, the boundary conditions at the inner and outer surfaces and the initial conditions. In the following section of this chapter, governing field equations of generalized viscoelasticity are explained briefly [125-131]. Governing equations of the generalized anisotropic thermoelasticity applied to the outer layers are already discussed in detail in the previous chapter.

Similar to Chapter 2 and Chapter 3, method of characteristics is employed to obtain the solutions. Method of characteristics is suitable because the governing equations are hyperbolic

4.2 Basic Equations of the Generalized Thermo-Viscoelasticity for Isotropic Materials in Cylindrical Coordinates

In this section, we summarize the basic equations of generalized thermo-viscoelasticity with two relaxation times for isotropic materials as applied to the viscoelastic layer considered in this study. In our treatment in this chapter, we take the constitutive equations for the stress deviators σ'_{ij} as in Eq. (2.7)₁ in differential equation form with $P_1(D)$ and $Q_1(D)$ defined by Eq. (2.14)₁ or as in Eq. (2.12) in integral form where the shear modulus $G_1(t)$ is given by Eq. (2.76)₁. These are the constitutive equations for stress deviators in terms of strain deviators for standard linear solid. Assuming that the relaxation effects of the volume properties of the material are ignored, we can write for the general theory of thermo-viscoelasticity with two relaxation times

$$\sigma_v = 3K \left[\varepsilon_v - 3\alpha_T^{(v)} (T_v - T_0 + \alpha_v \dot{T}_v) \right] \quad (4.1)$$

where $\sigma_v = \sigma_{kk}^{(v)}$ and K is the bulk modulus defined in terms of Lamé's constant λ and μ as $K = \lambda + \frac{2}{3}\mu$. Furthermore, $\alpha_T^{(v)}$ is the coefficient of linear thermal expansion and subscript v and the superscript v in parentheses denote that the quantity refers to the viscoelastic layer, same as in Chapter 2. Other parameters in Eq. (4.1) are the same as defined in the previous chapters. Generalized thermo-viscoelasticity is a relatively new subject which is not treated widely in the literature yet. Taking the constitutive equations as described above is quite new.

In the case of isotropic thermo-viscoelastic materials, Eqs. (3.1)_{2,3,4} reduce to,

$$\begin{aligned}
\rho_v S_v &= (\rho_v c_v / T_0) (T_v + \alpha_0^{(v)} \dot{T}_v) + \beta_v \varepsilon_v \\
q_i^{(v)} &= -k_v T_{,i} \\
q_{i,i}^{(v)} &= \rho_v (R - \dot{S}_v T_0)
\end{aligned} \tag{4.2}$$

We note that in the above equations, indicial notation is used as was done in the previous chapters when it was appropriate.

This completes the summary of the basic equations of generalized thermo-viscoelasticity as applied to the viscoelastic layer considered in this study.

4.3 Formulation of the Problem

The body is referred to a cylindrical coordinate system where the radial distances are measured by the coordinate r . As in Chapters 2 and 3 boundary, initial and interface conditions of the problem require the responses of the body to be axisymmetrical. Thus all the field variables are functions of r and t only, and the only non-vanishing displacement component is u_r , that is the displacement component in the radial direction. The constitutive equations for the stress deviators σ'_{ij} given by (2.7)₁ and (2.14)₁ for the three-dimensional case now reduce to Eqs. (2.20)_{1,2} for the axisymmetrical problem investigated in this chapter. The constitutive equation for $\sigma_v = \sigma_{kk}^{(v)}$ given by Eq. (4.1) for the three-dimensional case takes the following form for the axisymmetrical problem:

$$\sigma_v - 3K \frac{\partial u_r^{(v)}}{\partial r} - 3K \frac{u_r^{(v)}}{r} + 9K \alpha_T^{(v)} T + 9K \alpha_T^{(v)} \alpha_v \frac{\partial T}{\partial t} = 0 \tag{4.3}$$

In writing Eq. (4.1), we used Eq. (2.19)₃ for the dilatation $\varepsilon_v = \varepsilon_{kk}^{(v)}$. For our axisymmetrical problem, Eqs. (4.2) take the forms:

$$\rho_v S_v - \beta_v \frac{u_r^{(v)}}{r} - \beta_v \frac{\partial u_r^{(v)}}{\partial r} - \frac{\rho_v c_v}{T_0} (T + \alpha_0^{(v)} \dot{T}) = 0$$

$$q_r^{(v)} + k_v \frac{\partial T_v}{\partial r} = 0 \quad (4.4)$$

$$\frac{q_r^{(v)}}{r} + \frac{\partial q_r^{(v)}}{\partial r} + \rho_v \dot{S}_v T_0 = 0$$

In preparation for the application of method of characteristics, we differentiate Eq. (4.3) with respect to t , and obtain

$$\frac{\partial \sigma_v}{\partial t} - 3K \frac{\partial v_r^{(v)}}{\partial r} - 3K \frac{v_r^{(v)}}{r} + 9K \alpha_T^{(v)} \phi_v + 9K \alpha_T^{(v)} \alpha_v \frac{\partial \phi_v}{\partial t} = 0 \quad (4.5)$$

where

$$\phi_v = \frac{\partial T_v}{\partial t} \quad (4.6)$$

Differentiating Eq. (4.4)₁ with respect to time t and eliminating \dot{S}_v from Eq. (4.4)₃, we get

$$\begin{aligned} & \frac{1}{T_0} \frac{q_r^{(v)}}{r} + \frac{1}{T_0} \frac{\partial q_r^{(v)}}{\partial r} + 3K \alpha_T^{(v)} \frac{\partial v_r^{(v)}}{\partial r} + 3K \alpha_T^{(v)} \frac{v_r^{(v)}}{r} + \frac{\rho_v c_v}{T_0} \phi_v \\ & + \frac{\rho_v c_v}{T_0} \alpha_0^{(v)} \frac{\partial \phi_v}{\partial t} = 0 \end{aligned} \quad (4.7)$$

where in the above equations $v_r^{(v)} = \frac{\partial u_r^{(v)}}{\partial t}$ is the particle velocity of the viscoelastic layer which was defined in Chapter 2 by Eq. (2.21)₂. The stress equation of motion for the viscoelastic layer is the same as Eq. (2.29) in Chapter 2. We also have a compatibility equation between the normal strain $\varepsilon_{rr}^{(v)}$ and particle velocity $v_r^{(v)}$ which is given by Eq. (2.30). The formulation of the governing field equations for the thermo-viscoelastic layer is now complete. These are Eqs. (2.20)_{1,2}, (2.21)₂, (2.29-2.30), (4.5), (4.6), (4.4)₂ and (4.7) involving the field variables $\varepsilon_{rr}^{(v)}$, $v_r^{(v)}$, $\sigma_{rr}^{(v)}$, $\sigma_{\theta\theta}^{(v)}$, σ_v , $u_r^{(v)}$, ϕ_v , $q_r^{(v)}$ and T_v , i.e., nine equations with nine unknown field variables. The governing field equations for a typical generally orthotropic thermoelastic layer are the same as those given Chapter 3, i.e., Eqs. (3.10) and (3.13-3.14). These equations represent seven equations with seven unknown field variables ϕ , v_r , σ_{rr} , $\sigma_{\theta\theta}$, q_r , T and u_r for each orthotropic layer.

The formulation of the problem is completed by stating the boundary, interface and initial conditions. As boundary conditions, surface tractions or displacements and temperature deviations or heat fluxes can be prescribed at the boundary surfaces. Thus, the boundary conditions at the inner surface, $r = a$, can be expressed as

$$\sigma_{rr}^{(v)}(a,t) + \frac{1}{3}\sigma_v(a,t) = -P(t)H(t) \quad \text{or} \quad V_r^{(v)}(a,t) = V(t)H(t) \quad \text{and} \quad (4.8)$$

$$T_v(a,t) = T^*(t)H(t) \quad \text{or} \quad q_r^{(v)}(a,t) = Q(t)H(t)$$

and at the outer surface $r = b$ as

$$\sigma_{rr}^{(n)}(b,t) + \frac{1}{3}\sigma_v(a,t) = -F(t)H(t) \quad \text{or} \quad V_r^{(n)}(b,t) = V^*(t)H(t) \quad \text{and} \quad (4.9)$$

$$T_n(b,t) = t^*(t)H(t) \quad \text{or} \quad q_r^{(n)}(b,t) = Q^*(b,t)H(t)$$

where $P(t)$, $V(t)$, $T^*(t)$, $Q(t)$, $F(t)$, $V^*(t)$, $t^*(t)$ and $Q^*(t)$ are prescribed functions of t and $H(t)$ is the Heaviside step function. Furthermore, subscript v and superscript v in parentheses refer to the viscoelastic layer and subscript n and superscript n in parentheses refer to the outermost orthotropic layer, that is, the layer adjacent to the outer boundary surface.

Since the bodies are assumed to be initially at rest, all the field variables are zero at $t = 0$. The layers of the bodies are assumed to be perfectly bonded to each other. Hence, the interface conditions imply that the normal stress σ_{rr} , the displacement component u_r , the temperature deviation T and the heat flux q_r are continuous across the interfaces of the layers.

The formulation of the problem is thus complete. The governing field equations, Eqs. (2.20)_{1,2}, (2.21)₂, (2.29-2.30), (4.4)₂, (4.5), (4.6) and (4.7) are applied to the viscoelastic layer and Eqs. (3.13), (3.14), (3.10) are applied to the orthotropic elastic layers, and the solutions are required to satisfy the boundary conditions at the inner and outer surfaces, Eq. (4.8, 4.9), the continuity conditions at the interfaces and quiescent initial conditions. Method of characteristics is employed to obtain the solution. Application of method of characteristics to the governing field equations of the viscoelastic layer will be explained in this chapter in the next section. For orthotropic layers, application of the method of characteristics and integration of the canonical equations along the characteristic lines are the same as in Chapter 3.

4.4 The Method of Characteristics and the Canonical Form of the Governing Equations for the Thermo-Viscoelastic Layer

In order to apply the method of characteristics, we write the governing equations as a system of first order, partial differential equations. The system of the governing first order partial differential equations, Eqs. (2.20)_{1,2}, (2.21)₂, (2.29-2.30), (4.4)₂, (4.5), (4.6) and (4.7) can be written in matrix form as:

$$\mathbf{A}\mathbf{U}_{,t}^{(v)} + \mathbf{B}\mathbf{U}_{,r}^{(v)} + \mathbf{C} = \mathbf{0} \quad (4.10)$$

where \mathbf{A} and \mathbf{B} are nine by nine matrices defined as:

$$\mathbf{A} = \begin{bmatrix} 0 & -1 & 0 & 0 & 0 & 0 & 0 & 0 & 0 \\ 0 & 0 & 1 & 0 & 0 & 0 & 0 & 0 & 0 \\ 0 & 0 & 0 & 1 & 0 & 0 & 0 & 0 & 0 \\ 0 & 0 & 0 & 0 & 1 & 0 & 9K\alpha_T^{(v)}\alpha_v & 0 & 0 \\ 0 & 0 & 0 & 0 & 0 & 0 & \frac{\rho_v c_v \alpha_0^{(v)}}{T_0} & 0 & 0 \\ 0 & 0 & 0 & 0 & 0 & 0 & 0 & 1 & 0 \\ 1 & 0 & 0 & 0 & 0 & 0 & 0 & 0 & 0 \\ 0 & 0 & 0 & 0 & 0 & 1 & 0 & 0 & 0 \\ 0 & 0 & 0 & 0 & 0 & 0 & 0 & 0 & 1 \end{bmatrix} \quad (4.11)$$

$$\mathbf{B} = \begin{bmatrix} 0 & 0 & \frac{1}{\rho_v} & 0 & \frac{1}{3\rho_v} & 0 & 0 & 0 & 0 \\ 0 & -\frac{2b_1}{3a_1} & 0 & 0 & 0 & 0 & 0 & 0 & 0 \\ 0 & \frac{1b_1}{3a_1} & 0 & 0 & 0 & 0 & 0 & 0 & 0 \\ 0 & -3K & 0 & 0 & 0 & 0 & 0 & 0 & 0 \\ 0 & 3K\alpha_T^{(v)} & 0 & 0 & 0 & 0 & 0 & \frac{1}{T_0} & 0 \\ 0 & 0 & 0 & 0 & 0 & 0 & k_v & 0 & 0 \\ 0 & -1 & 0 & 0 & 0 & 0 & 0 & 0 & 0 \\ 0 & 0 & 0 & 0 & 0 & 0 & 0 & 0 & 0 \\ 0 & 0 & 0 & 0 & 0 & 0 & 0 & 0 & 0 \end{bmatrix} \quad (4.12)$$

and \mathbf{C} and $\mathbf{U}^{(v)}$ are nine-dimensional column vectors given as:

$$\mathbf{C} = \begin{bmatrix} \frac{1}{\rho_v} \frac{r}{r} \left(\sigma_{rr}^{(v)'} - \sigma_{\theta\theta}^{(v)'} \right) \\ \frac{a_0}{a_1} \sigma_{rr}^{(v)'} - \frac{2}{3} \frac{b_0}{a_1} \varepsilon_{rr}^{(v)} + \frac{1}{3} \frac{b_0}{a_1} \frac{u_r^{(v)}}{r} + \frac{1}{3} \frac{b_1}{a_1} \frac{v_r^{(v)}}{r} \\ \frac{a_0}{a_1} \sigma_{\theta\theta}^{(v)'} - \frac{2}{3} \frac{b_0}{a_1} \frac{u_r^{(v)}}{r} + \frac{1}{3} \frac{b_0}{a_1} \varepsilon_{rr}^{(v)} - \frac{2}{3} \frac{b_1}{a_1} \frac{v_r^{(v)}}{r} \\ -3K \frac{v_r^{(v)}}{r} + 9K \alpha_T^{(v)} \phi_v \\ \frac{1}{T_0} \frac{q_r^{(v)}}{r} + 3K \alpha_T^{(v)} \frac{v_r^{(v)}}{r} + \frac{\rho_v c_v}{T_0} \phi_v \\ 0 \\ 0 \\ -v_r^{(v)} \\ -\phi_v \end{bmatrix} \quad (4.13)$$

$$\mathbf{U}^{(v)} = \begin{bmatrix} \varepsilon_{rr}^{(v)} \\ v_r^{(v)} \\ \sigma_{rr}^{(v)'} \\ \sigma_{\theta\theta}^{(v)'} \\ \sigma_v^{(v)} \\ u_r^{(v)} \\ \phi_v \\ q_r^{(v)} \\ T_v \end{bmatrix} \quad (4.14)$$

In Eq. (4.10) $\mathbf{U}^{(v)}$ is the unknown vector and comma denotes partial differentiation as defined in Eq. (2.36).

Before we derive the canonical equations from Eq. (4.10), we first establish the characteristic lines along which these equations are valid. The characteristic lines are governed by the characteristic equation (2.37).

In view of Eqs. (4.11-4.12), the characteristic equation, Eq. (2.37), can be expressed as:

$$\det(\mathbf{B} - V_v \mathbf{A}) = \begin{bmatrix} 0 & V_v & \frac{1}{\rho_v} & 0 & \frac{1}{3\rho_v} & 0 & 0 & 0 & 0 \\ 0 & -\frac{2}{3} \frac{b_1}{a_1} & -V_v & 0 & 0 & 0 & 0 & 0 & 0 \\ 0 & \frac{1}{3} \frac{b_1}{a_1} & 0 & -V_v & 0 & 0 & 0 & 0 & 0 \\ 0 & -3K & 0 & 0 & -V_v & 0 & -9K\alpha_T^{(v)}\alpha_v V_v & 0 & 0 \\ 0 & 3K\alpha_T^{(v)} & 0 & 0 & 0 & 0 & -\frac{\rho_v c_v \alpha_0^{(v)}}{T_0} V_v & \frac{1}{T_0} & 0 \\ 0 & 0 & 0 & 0 & 0 & 0 & k_v & -V_v & 0 \\ -V_v & -1 & 0 & 0 & 0 & 0 & 0 & 0 & 0 \\ 0 & 0 & 0 & 0 & 0 & -V_v & 0 & 0 & 0 \\ 0 & 0 & 0 & 0 & 0 & 0 & 0 & 0 & -V_v \end{bmatrix} =$$

$$\begin{aligned} & \left(\frac{\rho_v c_v \alpha_0^{(v)}}{T_0} \right) V^9 - \left(\frac{k_v}{T_0} + \frac{2}{3} \frac{b_1}{a_1} \frac{c_v \alpha_0^{(v)}}{T_0} + \frac{K c_v \alpha_0^{(v)}}{T_0} + \frac{9K^2 \alpha_T^{(v)^2} \alpha_v}{\rho_v} \right) V^7 \\ & + \left(\frac{2}{3} \frac{b_1}{a_1} \frac{k_v}{\rho_v} \frac{1}{T_0} + \frac{K k_v}{\rho_v T_0} \right) V^5 = 0 \end{aligned} \quad (4.15)$$

The roots of Eq. (4.15) are:

$$V_v^{(1)} = c_1^{(v)}, \quad V_v^{(2)} = -c_1^{(v)}, \quad V_v^{(3)} = c_2^{(v)}, \quad V_v^{(4)} = -c_2^{(v)} \quad (4.16)$$

$$V_v^{(5)} = V_v^{(6)} = V_v^{(7)} = V_v^{(8)} = V_v^{(9)} = 0$$

where

$$c_1^{(v)} = \frac{\sqrt{6}}{6\rho_v \sqrt{c_v \alpha_0^{(v)}}} \left[\sqrt{\frac{3\rho_v k_r^{(v)} + 2G_{10}\rho_v c_v \alpha_0^{(v)} + 3K\rho_v c_v \alpha_0^{(v)} + 27K^2 \alpha_T^{(v)^2} \alpha_v T_0}{9k_r^{(v)^2} \rho_v^2 - 12\rho_v^2 k_r^{(v)} G_{10} c_v \alpha_0^{(v)} - 18\rho_v^2 k_r^{(v)} K c_v \alpha_0^{(v)} + 162\rho_v k_r^{(v)} K^2 \alpha_T^{(v)^2} \alpha_v T_0 + 4G_{10}^2 \rho_v^2 c_v^2 \alpha_0^{(v)^2} + 12G_{10}\rho_v^2 c_v^2 \alpha_0^{(v)^2} K + 108G_{10}\rho_v c_v \alpha_0^{(v)} K^2 \alpha_T^{(v)^2} \alpha_v T_0 + 9K^2 \rho_v^2 c_v^2 \alpha_0^{(v)^2} + 162K^3 \rho_v c_v \alpha_0^{(v)} \alpha_T^{(v)^2} \alpha_v T_0 + 729K^4 \alpha_T^{(v)^4} \alpha_v^{(2)} T_0^2}} \right] + \left[\begin{array}{l} \\ \\ \\ \\ \end{array} \right] \quad (4.17)$$

$$c_2^{(v)} = \frac{\sqrt{6}}{6\rho_v \sqrt{c_v \alpha_0^{(v)}}} \left[\sqrt{\frac{3\rho_v k_r^{(v)} + 2G_{10}\rho_v c_v \alpha_0^{(v)} + 3K\rho_v c_v \alpha_0^{(v)} + 27K^2 \alpha_T^{(v)^2} \alpha_v T_0}{9k_r^{(v)^2} \rho_v^2 - 12\rho_v^2 k_r^{(v)} G_{10} c_v \alpha_0^{(v)} - 18\rho_v^2 k_r^{(v)} K c_v \alpha_0^{(v)} + 162\rho_v k_r^{(v)} K^2 \alpha_T^{(v)^2} \alpha_v T_0 + 4G_{10}^2 \rho_v^2 c_v^2 \alpha_0^{(v)^2} + 12G_{10}\rho_v^2 c_v^2 \alpha_0^{(v)^2} K + 108G_{10}\rho_v c_v \alpha_0^{(v)} K^2 \alpha_T^{(v)^2} \alpha_v T_0 + 9K^2 \rho_v^2 c_v^2 \alpha_0^{(v)^2} + 162K^3 \rho_v c_v \alpha_0^{(v)} \alpha_T^{(v)^2} \alpha_v T_0 + 729K^4 \alpha_T^{(v)^4} \alpha_v^{(2)} T_0^2}} \right] - \left[\begin{array}{l} \\ \\ \\ \\ \end{array} \right]$$

where Eq. (2.78)₁, is used to express the wave velocities in terms of G_{10} , a parameter of shear modulus, instead of a_1 and b_1 , and the bulk modulus K , in addition to other material parameters appearing in the expressions.

$V_v^{(i)}$ are the characteristic values and the characteristic lines are defined as:

$$\begin{aligned} \frac{dr}{dt} &= V_v^{(1)} = c_1^{(v)} && \text{along } C_v^{(1)} \\ \frac{dr}{dt} &= V_v^{(2)} = -c_1^{(v)} && \text{along } C_v^{(2)} \\ \frac{dr}{dt} &= V_v^{(3)} = c_2^{(v)} && \text{along } C_v^{(3)} \end{aligned} \quad (4.18a)$$

$$\frac{dr}{dt} = V_v^{(4)} = -c_2^{(v)} \quad \text{along } C_v^{(4)} \quad (4.18b)$$

$$\frac{dr}{dt} = V_v^{(i)} = 0 \quad \text{along } C_v^{(i)} \quad (i = 5 - 9)$$

Integration of Eq. (4.18) gives the families of characteristic lines $C^{(i)}$ $i = (1 - 9)$ as;

$$\begin{aligned} C_v^{(1)} : r - c_1^{(v)} t &= \text{constant} \\ C_v^{(2)} : r + c_1^{(v)} t &= \text{constant} \\ C_v^{(3)} : r - c_2^{(v)} t &= \text{constant} \\ C_v^{(4)} : r + c_2^{(v)} t &= \text{constant} \\ C_v^{(i)} : r &= \text{constant} \quad (i = 5 - 9) \end{aligned} \quad (4.19)$$

These families of characteristic lines are shown in the $(r - t)$ plane in Fig. 4.1. We note that $C_v^{(1)}$ and $C_v^{(3)}$ describe families of straight lines with slopes $c_1^{(v)}$ and $c_2^{(v)}$, respectively, whereas $C_v^{(2)}$ and $C_v^{(4)}$ describe families of straight lines with slopes $-c_1^{(v)}$ and $-c_2^{(v)}$, on the $(r - t)$ plane. Moreover, $C_v^{(i)}$ ($i = 5 - 9$) describe straight lines parallel to the $t - axis$, see Fig. 4.1.

In establishing the canonical equations, we define the left-hand eigenvectors $\mathbf{L}_v^{(i)}$ ($i = 1 - 9$) corresponding to the characteristic values $V_v^{(i)}$ ($i = 1 - 9$) as

$$(\mathbf{B}^T - V_v^{(i)} \mathbf{A}^T) \mathbf{L}_v^{(i)} = \mathbf{0} \quad (i = 1 - 9) \quad (4.20)$$

Solving Eqs (4.20), in view of Eqs. (4.11-4.12), we can write the left-hand eigenvectors as:

$$\begin{aligned}
\mathbf{L}^{(1)} &= \begin{bmatrix} \frac{1}{\rho_v c_1^{(v)}} \\ 0 \\ \frac{1}{3\rho_v c_1^{(v)}} \\ -\frac{1}{3K\alpha_T^{(v)}} \left[c_1^{(v)} - \frac{2}{3} \frac{b_1}{a_1} \frac{1}{\rho_v c_1^{(v)}} - \frac{K}{\rho_v c_1^{(v)}} \right] \\ -\frac{1}{T_0 c_1^{(v)}} \frac{1}{3K\alpha_T^{(v)}} \left[c_1^{(v)} - \frac{2}{3} \frac{b_1}{a_1} \frac{1}{\rho_v c_1^{(v)}} - \frac{K}{\rho_v c_1^{(v)}} \right] \\ 0 \\ 0 \\ 0 \end{bmatrix}, \\
\mathbf{L}^{(2)} &= \begin{bmatrix} \frac{-1}{\rho_v c_1^{(v)}} \\ 0 \\ \frac{-1}{3\rho_v c_1^{(v)}} \\ \frac{1}{3K\alpha_T^{(v)}} \left[c_1^{(v)} - \frac{2}{3} \frac{b_1}{a_1} \frac{1}{\rho_v c_1^{(v)}} - \frac{K}{\rho_v c_1^{(v)}} \right] \\ -\frac{1}{T_0 c_1^{(v)}} \frac{1}{3K\alpha_T^{(v)}} \left[c_1^{(v)} - \frac{2}{3} \frac{b_1}{a_1} \frac{1}{\rho_v c_1^{(v)}} - \frac{K}{\rho_v c_1^{(v)}} \right] \\ 0 \\ 0 \\ 0 \end{bmatrix}, \\
\mathbf{L}^{(3)} &= \begin{bmatrix} \frac{1}{\rho_v c_2^{(v)}} \\ 0 \\ \frac{1}{3\rho_v c_2^{(v)}} \\ -\frac{1}{3K\alpha_T^{(v)}} \left[c_2^{(v)} - \frac{2}{3} \frac{b_1}{a_1} \frac{1}{\rho_v c_2^{(v)}} - \frac{K}{\rho_v c_2^{(v)}} \right] \\ -\frac{1}{T_0 c_2^{(v)}} \frac{1}{3K\alpha_T^{(v)}} \left[c_2^{(v)} - \frac{2}{3} \frac{b_1}{a_1} \frac{1}{\rho_v c_2^{(v)}} - \frac{K}{\rho_v c_2^{(v)}} \right] \\ 0 \\ 0 \\ 0 \end{bmatrix},
\end{aligned} \tag{4.21a}$$

$$\mathbf{L}^{(4)} = \begin{bmatrix} \frac{1}{-1} \\ \frac{-1}{\rho_v c_2^{(v)}} \\ 0 \\ \frac{-1}{3\rho_v c_2^{(v)}} \\ \frac{1}{3K\alpha_T^{(v)}} \left[c_2^{(v)} - \frac{2}{3} \frac{b_1}{a_1} \frac{1}{\rho_v c_2^{(v)}} - \frac{K}{\rho_v c_2^{(v)}} \right] \\ -\frac{1}{T_0 c_2^{(v)}} \frac{1}{3K\alpha_T^{(v)}} \left[c_2^{(v)} - \frac{2}{3} \frac{b_1}{a_1} \frac{1}{\rho_v c_2^{(v)}} - \frac{K}{\rho_v c_2^{(v)}} \right] \\ 0 \\ 0 \\ 0 \end{bmatrix},$$

$$\mathbf{L}^{(5)} = \begin{bmatrix} 0 \\ \frac{1}{2} \\ \frac{1}{2} \\ 1 \\ 0 \\ 0 \\ 0 \\ 0 \\ 0 \\ 0 \end{bmatrix}, \quad \mathbf{L}^{(6)} = \begin{bmatrix} 0 \\ -\frac{9}{2} \frac{a_1}{b_1} K \\ 0 \\ 1 \\ 0 \\ 0 \\ 0 \\ 0 \\ 0 \\ 0 \end{bmatrix}, \quad \mathbf{L}^{(7)} = \begin{bmatrix} 0 \\ \frac{3}{2} \frac{a_1}{b_1} \\ 0 \\ 0 \\ 0 \\ 0 \\ 1 \\ 0 \\ 0 \\ 0 \end{bmatrix} \quad (4.21b)$$

$$\mathbf{L}^{(8)} = \begin{bmatrix} 0 \\ 0 \\ 0 \\ 0 \\ 0 \\ 0 \\ 0 \\ 0 \\ 1 \\ 0 \end{bmatrix}, \quad \mathbf{L}^{(9)} = \begin{bmatrix} 0 \\ 0 \\ 0 \\ 0 \\ 0 \\ 0 \\ 0 \\ 0 \\ 0 \\ 1 \end{bmatrix}$$

The left-hand eigenvectors in Eq. (4.21) are multiplied by arbitrary constants as in the previous chapters which are not written for the sake of brevity.

The canonical equations can be written as in Eq. (2.45) which hold along $\frac{dr}{dt} = V_v^{(i)}$ ($i = 1-9$). In this case, however, $\mathbf{L}_v^{(i)}$ is the left-hand eigenvector given by Eqs. (4.21). By substituting Eqs. (4.21) into Eq. (2.45) and taking into consideration Eqs. (4.11 - 4.14), we get the canonical equations explicitly as

$$\begin{aligned}
& -\frac{dv_r^{(v)}}{dt} + \frac{1}{\rho_v c_1^{(v)}} \frac{d\sigma_{rr}^{(v)'}}{dt} + \frac{1}{3\rho_v c_1^{(v)}} \frac{d\sigma_v}{dt} \\
& + \left(\frac{3K\alpha_T^{(v)}\alpha_v}{\rho_v c_1^{(v)}} - \frac{\rho_v c_v \alpha_0^{(v)}}{3K\alpha_T^{(v)}T_0} \left(c_1^{(v)} - \frac{2}{3} \frac{b_1}{a_1} \frac{1}{\rho_v c_1^{(v)}} - \frac{K}{\rho_v c_1^{(v)}} \right) \right) \frac{d\phi_v}{dt} \\
& - \frac{1}{T_0 c_1^{(v)}} \frac{1}{3K\alpha_T^{(v)}} \left(c_1^{(v)} - \frac{2}{3} \frac{b_1}{a_1} \frac{1}{\rho_v c_1^{(v)}} - \frac{K}{\rho_v c_1^{(v)}} \right) \frac{dq_r^{(v)}}{dt} \\
& + \left(\frac{1}{3\rho_v c_1^{(v)}} \frac{b_1}{a_1} - \frac{K}{\rho_v c_1^{(v)}} - \left(c_1^{(v)} - \frac{2}{3} \frac{b_1}{a_1} \frac{1}{\rho_v c_1^{(v)}} - \frac{K}{\rho_v c_1^{(v)}} \right) \right) \frac{v_r^{(v)}}{r} - \frac{2}{3} \frac{b_0}{a_1} \frac{1}{\rho_v c_1^{(v)}} \mathcal{E}_{rr}^{(v)} \\
& + \left(\frac{3K\alpha_T^{(v)}}{\rho_v c_1^{(v)}} - \frac{\rho_v c_v}{3K\alpha_T^{(v)}T_0} \left(c_1^{(v)} - \frac{2}{3} \frac{b_1}{a_1} \frac{1}{\rho_v c_1^{(v)}} - \frac{K}{\rho_v c_1^{(v)}} \right) \right) \phi_v \\
& - \frac{1}{3K\alpha_T^{(v)}T_0} \left(c_1^{(v)} - \frac{2}{3} \frac{b_1}{a_1} \frac{1}{\rho_v c_1^{(v)}} - \frac{K}{\rho_v c_1^{(v)}} \right) \frac{q_r^{(v)}}{r} \\
& + \left(\frac{1}{\rho_v r} + \frac{1}{\rho_v c_1^{(v)}} \frac{a_0}{a_1} \right) \sigma_{rr}^{(v)'} - \frac{1}{\rho_v r} \sigma_{\theta\theta}^{(v)'} + \frac{1}{3\rho_v c_1^{(v)}} \frac{b_0}{a_1} \frac{u_r^{(v)}}{r} = 0
\end{aligned}$$

$$\text{along } \frac{dr}{dt} = V_v^{(1)} = c_1^{(v)} \quad (4.22)$$

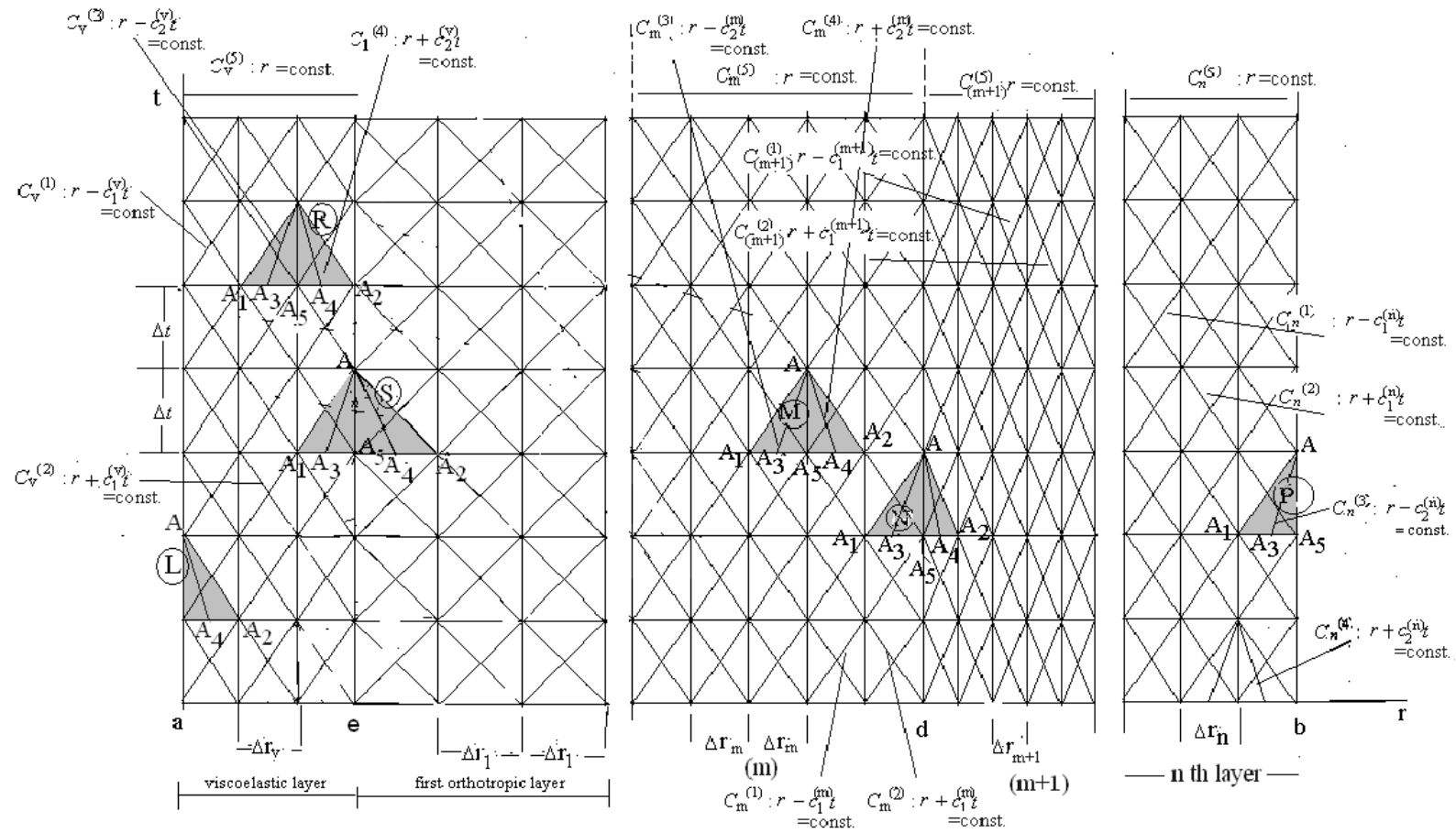


Figure 4.1. Network of characteristic lines for the multilayered medium with inner viscoelastic layer.

$$\begin{aligned}
& -\frac{dv_r^{(v)}}{dt} - \frac{1}{\rho_v c_1^{(v)}} \frac{d\sigma_{rr}^{(v)'}}{dt} - \frac{1}{3\rho_v c_1^{(v)}} \frac{d\sigma_v}{dt} \\
& - \left(\frac{3K\alpha_T^{(v)}\alpha_v}{\rho_v c_1^{(v)}} - \frac{\rho_v c_v \alpha_0^{(v)}}{3K\alpha_T^{(v)}T_0} \left(c_1^{(v)} - \frac{2}{3} \frac{b_1}{a_1} \frac{1}{\rho_v c_1^{(v)}} - \frac{K}{\rho_v c_1^{(v)}} \right) \right) \frac{d\phi^{(v)}}{dt} \\
& - \frac{1}{T_0 c_1^{(v)}} \frac{1}{3K\alpha_T^{(v)}} \left(c_1^{(v)} - \frac{2}{3} \frac{b_1}{a_1} \frac{1}{\rho_v c_1^{(v)}} - \frac{K}{\rho_v c_1^{(v)}} \right) \frac{dq_r^{(v)}}{dt} \\
& - \left(\frac{1}{3\rho_v c_1^{(v)}} \frac{b_1}{a_1} - \frac{K}{\rho_v c_1^{(v)}} - \left(c_1^{(v)} - \frac{2}{3} \frac{b_1}{a_1} \frac{1}{\rho_v c_1^{(v)}} - \frac{K}{\rho_v c_1^{(v)}} \right) \right) \frac{v_r^{(v)}}{r} + \frac{2}{3} \frac{b_0}{a_1} \frac{1}{\rho_v c_1^{(v)}} \varepsilon_{rr}^{(v)} \\
& - \left(\frac{3K\alpha_T^{(v)}}{\rho_v c_1^{(v)}} - \frac{\rho_v c_v}{3K\alpha_T^{(v)}T_0} \left(c_1^{(v)} - \frac{2}{3} \frac{b_1}{a_1} \frac{1}{\rho_v c_1^{(v)}} - \frac{K}{\rho_v c_1^{(v)}} \right) \right) \phi^{(v)} \\
& + \frac{1}{3K\alpha_T^{(v)}T_0} \left(c_1^{(v)} - \frac{2}{3} \frac{b_1}{a_1} \frac{1}{\rho_v c_1^{(v)}} - \frac{K}{\rho_v c_1^{(v)}} \right) \frac{q_r^{(v)}}{r} \\
& + \left(\frac{1}{\rho_v r} - \frac{1}{\rho_v c_1^{(v)}} \frac{a_0}{a_1} \right) \sigma_{rr}^{(v)'} - \frac{1}{\rho_v r} \sigma_{\theta\theta}^{(v)'} - \frac{1}{3\rho_v c_1^{(v)}} \frac{b_0}{a_1} \frac{u_r^{(v)}}{r} = 0
\end{aligned}$$

$$\text{along } \frac{dr}{dt} = V_v^{(2)} = -c_1^{(v)} \quad (4.23)$$

$$\begin{aligned}
& -\frac{dv_r^{(v)}}{dt} + \frac{1}{\rho_v c_2^{(v)}} \frac{d\sigma_{rr}^{(v)'}}{dt} + \frac{1}{3\rho_v c_2^{(v)}} \frac{d\sigma_v}{dt} \\
& + \left(\frac{3K\alpha_T^{(v)}\alpha_v}{\rho_v c_2^{(v)}} - \frac{\rho_v c_v \alpha_0^{(v)}}{3K\alpha_T^{(v)}T_0} \left(c_2^{(v)} - \frac{2}{3} \frac{b_1}{a_1} \frac{1}{\rho_v c_2^{(v)}} - \frac{K}{\rho_v c_2^{(v)}} \right) \right) \frac{d\phi_v}{dt} \\
& - \frac{1}{T_0 c_2^{(v)}} \frac{1}{3K\alpha_T^{(v)}} \left(c_2^{(v)} - \frac{2}{3} \frac{b_1}{a_1} \frac{1}{\rho_v c_2^{(v)}} - \frac{K}{\rho_v c_2^{(v)}} \right) \frac{dq_r^{(v)}}{dt} \\
& + \left(\frac{1}{3\rho_v c_2^{(v)}} \frac{b_1}{a_1} - \frac{K}{\rho_v c_2^{(v)}} - \left(c_2^{(v)} - \frac{2}{3} \frac{b_1}{a_1} \frac{1}{\rho_v c_2^{(v)}} - \frac{K}{\rho_v c_2^{(v)}} \right) \right) \frac{v_r^{(v)}}{r} - \frac{2}{3} \frac{b_0}{a_1} \frac{1}{\rho_v c_2^{(v)}} \varepsilon_{rr}^{(v)} \\
& + \left(\frac{3K\alpha_T^{(v)}}{\rho_v c_2^{(v)}} - \frac{\rho_v c_v}{3K\alpha_T^{(v)}T_0} \left(c_2^{(v)} - \frac{2}{3} \frac{b_1}{a_1} \frac{1}{\rho_v c_2^{(v)}} - \frac{K}{\rho_v c_2^{(v)}} \right) \right) \phi_v \\
& - \frac{1}{3K\alpha_T^{(v)}T_0} \left(c_2^{(v)} - \frac{2}{3} \frac{b_1}{a_1} \frac{1}{\rho_v c_2^{(v)}} - \frac{K}{\rho_v c_2^{(v)}} \right) \frac{q_r^{(v)}}{r} \\
& + \left(\frac{1}{\rho_v r} + \frac{1}{\rho_v c_2^{(v)}} \frac{a_0}{a_1} \right) \sigma_{rr}^{(v)'} - \frac{1}{\rho_v r} \sigma_{\theta\theta}^{(v)'} + \frac{1}{3\rho_v c_1^{(v)}} \frac{b_0}{a_1} \frac{u_r^{(v)}}{r} = 0
\end{aligned}$$

$$\text{along } \frac{dr}{dt} = V_v^{(3)} = c_2^{(v)} \quad (4.24)$$

$$\begin{aligned}
& -\frac{dv_r^{(v)}}{dt} - \frac{1}{\rho_v c_2^{(v)}} \frac{d\sigma_{rr}^{(v)'}}{dt} - \frac{1}{3\rho_v c_2^{(v)}} \frac{d\sigma_v}{dt} \\
& - \left(\frac{3K\alpha_T^{(v)}\alpha_v}{\rho_v c_2^{(v)}} - \frac{\rho_v c_v \alpha_0^{(v)}}{3K\alpha_T^{(v)}T_0} \left(c_2^{(v)} - \frac{2b_1}{3a_1} \frac{1}{\rho_v c_2^{(v)}} - \frac{K}{\rho_v c_2^{(v)}} \right) \right) \frac{d\phi_v}{dt} \\
& - \frac{1}{T_0 c_2^{(v)}} \frac{1}{3K\alpha_T^{(v)}} \left(c_2^{(v)} - \frac{2b_1}{3a_1} \frac{1}{\rho_v c_2^{(v)}} - \frac{K}{\rho_v c_2^{(v)}} \right) \frac{dq_r^{(v)}}{dt} \\
& - \left(\frac{1}{3\rho_v c_2^{(v)}} \frac{b_1}{a_1} - \frac{K}{\rho_v c_2^{(v)}} - \left(c_2^{(v)} - \frac{2b_1}{3a_1} \frac{1}{\rho_v c_2^{(v)}} - \frac{K}{\rho_v c_2^{(v)}} \right) \right) \frac{v_r^{(v)}}{r} + \frac{2b_0}{3a_1} \frac{1}{\rho_v c_2^{(v)}} \varepsilon_{rr}^{(v)} \\
& - \left(\frac{3K\alpha_T^{(v)}}{\rho_v c_2^{(v)}} - \frac{\rho_v c_v}{3K\alpha_T^{(v)}T_0} \left(c_2^{(v)} - \frac{2b_1}{3a_1} \frac{1}{\rho_v c_2^{(v)}} - \frac{K}{\rho_v c_2^{(v)}} \right) \right) \phi_v \\
& + \frac{1}{3K\alpha_T^{(v)}T_0} \left(c_2^{(v)} - \frac{2b_1}{3a_1} \frac{1}{\rho_v c_2^{(v)}} - \frac{K}{\rho_v c_2^{(v)}} \right) \frac{q_r^{(v)}}{r} \\
& + \left(\frac{1}{\rho_v r} - \frac{1}{\rho_v c_2^{(v)}} \frac{a_0}{a_1} \right) \sigma_{rr}^{(v)'} - \frac{1}{\rho_v r} \sigma_{\theta\theta}^{(v)'} - \frac{1}{3\rho_v c_2^{(v)}} \frac{b_0}{a_1} \frac{u_r^{(v)}}{r} = 0
\end{aligned}$$

$$\text{along } \frac{dr}{dt} = V_v^{(4)} = -c_2^{(v)} \quad (4.25)$$

$$\frac{1}{2} \frac{d\sigma_{rr}^{(v)'}}{dt} + \frac{d\sigma_{\theta\theta}^{(v)'}}{dt} + \frac{1}{2} \frac{a_0}{a_1} \sigma_{rr}^{(v)'} + \frac{a_0}{a_1} \sigma_{\theta\theta}^{(v)'} - \frac{1}{2} \frac{b_0}{a_1} \frac{u_r^{(v)}}{r} - \frac{1}{2} \frac{b_1}{a_1} \frac{v_r^{(v)}}{r} = 0$$

$$\text{along } \frac{dr}{dt} = V_v^{(5)} = 0 \quad (4.26)$$

$$\begin{aligned}
& -\frac{9a_1}{2b_1} K \frac{d\sigma_{rr}^{(v)'}}{dt} + \frac{d\sigma_v}{dt} + 9K\alpha_T^{(v)}\alpha_v \frac{d\phi^{(v)}}{dt} - \frac{9a_0}{2b_1} K \sigma_{rr}^{(v)'} - \frac{3b_0}{2b_1} K \frac{u_r^{(v)}}{r} - \frac{9}{2} K \frac{v_r^{(v)}}{r} \\
& + \frac{3b_0}{b_1} K \varepsilon_{rr}^{(v)} + 9K\alpha_T^{(v)}\phi_v = 0
\end{aligned}$$

$$\text{along } \frac{dr}{dt} = V_v^{(6)} = 0 \quad (4.27)$$

$$\frac{3}{2} \frac{a_1}{b_1} \frac{d\sigma_{rr}^{(v)'}}{dt} + \frac{d\varepsilon_{rr}^{(v)}}{dt} - \frac{3}{2} \frac{a_0}{b_1} \sigma_{rr}^{(v)'} + \frac{b_0}{b_1} \varepsilon_{rr}^{(v)} - \frac{1}{2} \frac{b_0}{b_1} \frac{u_r^{(v)}}{r} - \frac{1}{2} \frac{v_r^{(v)}}{r}$$

along $\frac{dr}{dt} = V_v^{(7)} = 0$ (4.28)

$$\frac{du_r^{(v)}}{dt} - v_r^{(v)} = 0$$

along $\frac{dr}{dt} = V_v^{(8)} = 0$ (4.29)

$$\frac{dT}{dt} - \phi_v = 0$$

along $\frac{dr}{dt} = V_v^{(9)} = 0$ (4.30)

4.5 Integration of the Canonical Equations for the Thermo-Viscoelastic Layer

The canonical form of the governing equations for the thermo-viscoelastic layer which are given by Eqs (4.22-4.30) can be represented in matrix form as in Eq. (2.73) where in this case the matrices **E** and **F** are given as:

$$E_{12} = -1,$$

$$E_{15} = \frac{1}{3\rho_v c_1^{(v)}},$$

(4.31a)

$$E_{17} = \left[\frac{3K\alpha_T^{(v)}\alpha_v}{\rho_v c_1^{(v)}} - \frac{\rho_v c_v \alpha_0^v}{3K\alpha_T^{(v)}T_0} \left(c_1^{(v)} - \frac{2}{3} \frac{b_1}{a_1} \frac{1}{\rho_v c_1^{(v)}} - \frac{K}{\rho_v c_1^{(v)}} \right) \right],$$

$$E_{18} = -\frac{1}{T_0 c_1^{(v)}} \frac{1}{3K\alpha_T^{(v)}} \left(c_1^{(v)} - \frac{2}{3} G_{10} \frac{1}{\rho_v c_1^{(v)}} - \frac{K}{\rho_v c_1^{(v)}} \right),$$

$$E_{22} = -1, \quad E_{23} = \frac{1}{\rho_v c_1^{(v)}},$$

$$E_{25} = -\frac{1}{3\rho_v c_1^{(v)}},$$

$$E_{27} = -\left[\frac{3K\alpha_T^{(v)}\alpha_v}{\rho_v c_1^{(v)}} - \frac{\rho_v c_v \alpha_0^v}{3K\alpha_T^{(v)}T_0} \left(c_1^{(v)} - \frac{2}{3}G_{10} \frac{1}{\rho_v c_1^{(v)}} - \frac{K}{\rho_v c_1^{(v)}} \right) \right],$$

$$E_{28} = -\frac{1}{T_0 c_1^{(v)}} \frac{1}{3K\alpha_T^{(v)}} \left(c_1^{(v)} - \frac{2}{3}G_{10} \frac{1}{\rho_v c_1^{(v)}} - \frac{K}{\rho_v c_1^{(v)}} \right),$$

$$E_{32} = -1, \quad E_{33} = \frac{1}{\rho_v c_2^{(v)}}, \quad (4.31b)$$

$$E_{35} = \frac{1}{3\rho_v c_2^{(v)}},$$

$$E_{37} = \left[\frac{3K\alpha_T^{(v)}\alpha_v}{\rho_v c_2^{(v)}} - \frac{\rho_v c_v \alpha_0^v}{3K\alpha_T^{(v)}T_0} \left(c_2^{(v)} - \frac{2}{3}G_{10} \frac{1}{\rho_v c_2^{(v)}} - \frac{K}{\rho_v c_2^{(v)}} \right) \right],$$

$$E_{38} = -\frac{1}{T_0 c_2^{(v)}} \frac{1}{3K\alpha_T^{(v)}} \left(c_2^{(v)} - \frac{2}{3}G_{10} \frac{1}{\rho_v c_2^{(v)}} - \frac{K}{\rho_v c_2^{(v)}} \right),$$

$$E_{42} = -1, \quad E_{43} = -\frac{1}{\rho_v c_2^{(v)}}$$

$$E_{45} = -\frac{1}{3\rho_v c_2^{(v)}},$$

$$\begin{aligned}
E_{47} &= - \left[\frac{3K\alpha_T^{(v)}\alpha_v}{\rho_v c_2^{(v)}} - \frac{\rho_v c_v \alpha_0^v}{3K\alpha_T^{(v)}T_0} \left(c_2^{(v)} - \frac{2}{3}G_{10} \frac{1}{\rho_v c_2^{(v)}} - \frac{K}{\rho_v c_2^{(v)}} \right) \right] \\
E_{48} &= - \frac{1}{T_0 c_2^{(v)}} \frac{1}{3K\alpha_T^{(v)}} \left(c_2^{(v)} - \frac{2}{3}G_{10} \frac{1}{\rho_v c_2^{(v)}} - \frac{K}{\rho_v c_2^{(v)}} \right) \\
E_{53} &= \frac{1}{2}, & E_{54} &= 1, \\
E_{63} &= -\frac{9}{2} \frac{1}{G_{10}} K, & E_{65} &= 1, \\
E_{67} &= 9K\alpha_T^{(v)}\alpha_v, & E_{71} &= 1, \\
E_{73} &= \frac{3}{2} \frac{1}{G_{10}}, & E_{99} &= 1
\end{aligned} \tag{4.31c}$$

all the other $E_{ij} = 0$.

$$\begin{aligned}
F_{11} &= \frac{2}{3} \frac{G_{1F}}{\tau_1} \frac{1}{\rho_v c_1^{(v)}}, \\
F_{12} &= - \left[\frac{1}{3\rho_v c_1^{(v)}} G_{10} - \frac{K}{\rho_v c_1^{(v)}} - \left(c_1^{(v)} - \frac{2}{3}G_{10} \frac{1}{\rho_v c_1^{(v)}} - \frac{K}{\rho_v c_1^{(v)}} \right) \right] \frac{1}{r}, \\
F_{13} &= - \left(\frac{1}{\rho_v r} + \frac{1}{\rho_v c_1^{(v)}} \frac{1}{\tau_1} \right), & F_{14} &= \frac{1}{\rho_v r}, \\
F_{16} &= - \frac{1}{3\rho_v c_1^{(v)}} \frac{G_{1F}}{\tau_1} \frac{1}{r}, \\
F_{17} &= - \left[\frac{3K\alpha_T^{(v)}}{\rho_v c_1^{(v)}} - \frac{\rho_v c_v}{3K\alpha_T^{(v)}T_0} \left(c_1^{(v)} - \frac{2}{3}G_{10} \frac{1}{\rho_v c_1^{(v)}} - \frac{K}{\rho_v c_1^{(v)}} \right) \right],
\end{aligned} \tag{4.32a}$$

$$\begin{aligned}
F_{18} &= \frac{1}{3K\alpha_T^{(v)}T_0} \left(c_1^{(v)} - \frac{2}{3}G_{10} \frac{1}{\rho_v c_1^{(v)}} - \frac{K}{\rho_v c_1^{(v)}} \right) \frac{1}{r}, \\
F_{21} &= -\frac{2}{3} \frac{1}{\rho_v c_1^{(v)}} \frac{G_{1F}}{\tau_1}, \\
F_{22} &= \left[\frac{1}{3\rho_v c_1^{(v)}} G_{10} - \frac{K}{\rho_v c_1^{(v)}} - \left(c_1^{(v)} - \frac{2}{3}G_{10} \frac{1}{\rho_v c_1^{(v)}} - \frac{K}{\rho_v c_1^{(v)}} \right) \right] \frac{1}{r}, \\
F_{23} &= -\left(\frac{1}{\rho_v r} - \frac{1}{\rho_v c_1^{(v)}} \frac{1}{\tau_1} \right), \quad F_{24} = \frac{1}{\rho_v r}, \\
F_{26} &= \frac{1}{3\rho_v c_1^{(v)}} \frac{G_{1F}}{\tau_1} \frac{1}{r}, \\
F_{27} &= \left[\frac{3K\alpha_T^{(v)}}{\rho_v c_1^{(v)}} - \frac{\rho_v c_v}{3K\alpha_T^{(v)}T_0} \left(c_1^{(v)} - \frac{2}{3}G_{10} \frac{1}{\rho_v c_1^{(v)}} - \frac{K}{\rho_v c_1^{(v)}} \right) \right] \\
F_{28} &= -\frac{1}{3K\alpha_T^{(v)}T_0} \left(c_1^{(v)} - \frac{2}{3}G_{10} \frac{1}{\rho_v c_1^{(v)}} - \frac{K}{\rho_v c_1^{(v)}} \right) \frac{1}{r} \quad (4.32b) \\
F_{31} &= \frac{2}{3} \frac{G_{1F}}{\tau_1} \frac{1}{\rho_v c_2^{(v)}} \\
F_{32} &= -\left[\frac{1}{3\rho_v c_2^{(v)}} G_{10} - \frac{K}{\rho_v c_2^{(v)}} - \left(c_2^{(v)} - \frac{2}{3}G_{10} \frac{1}{\rho_v c_2^{(v)}} - \frac{K}{\rho_v c_2^{(v)}} \right) \right] \frac{1}{r}, \\
F_{33} &= -\left(\frac{1}{\rho_v r} + \frac{1}{\rho_v c_2^{(v)}} \frac{1}{\tau_1} \right), \quad F_{34} = \frac{1}{\rho_v r}, \\
F_{35} &= 0, \quad F_{36} = -\frac{1}{3\rho_v c_2^{(v)}} \frac{G_{1F}}{\tau_1} \frac{1}{r},
\end{aligned}$$

$$\begin{aligned}
F_{37} &= - \left[\frac{3K\alpha_T^{(v)}}{\rho_v c_2^{(v)}} - \frac{\rho_v c_v}{3K\alpha_T^{(v)}T_0} \left(c_2^{(v)} - \frac{2}{3}G_{10} \frac{1}{\rho_v c_2^{(v)}} - \frac{K}{\rho_v c_2^{(v)}} \right) \right], \\
F_{38} &= \frac{1}{3K\alpha_T^{(v)}T_0} \left(c_2^{(v)} - \frac{2}{3}G_{10} \frac{1}{\rho_v c_2^{(v)}} - \frac{K}{\rho_v c_2^{(v)}} \right) \frac{1}{r}, \\
F_{41} &= - \frac{2}{3} \frac{1}{\rho_v c_2^{(v)}} \frac{G_{1F}}{\tau_1}, \\
F_{42} &= \left[\frac{1}{3\rho_v c_2^{(v)}} G_{10} - \frac{K}{\rho_v c_2^{(v)}} - \left(c_2^{(v)} - \frac{2}{3}G_{10} \frac{1}{\rho_v c_2^{(v)}} - \frac{K}{\rho_v c_2^{(v)}} \right) \right] \frac{1}{r}, \\
F_{43} &= - \left(\frac{1}{\rho_v r} - \frac{1}{\rho_v c_2^{(v)}} \frac{1}{\tau_1} \right), \quad F_{44} = \frac{1}{\rho_v r}, \\
F_{46} &= - \frac{1}{3\rho_v c_2^{(v)}} \frac{G_{1F}}{\tau_1} \frac{1}{r}, \tag{4.32c} \\
F_{47} &= \left[\frac{3K\alpha_T^{(v)}}{\rho_v c_2^{(v)}} - \frac{\rho_v c_v}{3K\alpha_T^{(v)}T_0} \left(c_2^{(v)} - \frac{2}{3}G_{10} \frac{1}{\rho_v c_2^{(v)}} - \frac{K}{\rho_v c_2^{(v)}} \right) \right], \\
F_{48} &= - \frac{1}{3K\alpha_T^{(v)}T_0} \left(c_2^{(v)} - \frac{2}{3}G_{10} \frac{1}{\rho_v c_2^{(v)}} - \frac{K}{\rho_v c_2^{(v)}} \right) \frac{1}{r}, \\
F_{52} &= \frac{1}{2} G_{10} \frac{1}{r}, \quad F_{53} = - \frac{1}{2} \frac{1}{\tau_1}, \\
F_{54} &= - \frac{1}{\tau_1}, \quad F_{56} = \frac{1}{2} \frac{G_{1F}}{\tau_1} \frac{1}{r}, \\
F_{61} &= - \frac{3G_{1F}}{G_{10}} K, \quad F_{62} = \frac{9}{2} K \frac{1}{r}, \\
F_{63} &= \frac{9}{2} \frac{1}{\tau_1 G_{10}} K, \quad F_{66} = \left(\frac{3}{2} \frac{G_{1F}}{G_{10}} \frac{1}{\tau_1} K \right) \frac{1}{r},
\end{aligned}$$

$$\begin{aligned}
F_{71} &= -\frac{G_{1F}}{G_{10}} \frac{1}{\tau_1}, & F_{72} &= \frac{1}{2} \frac{1}{r}, \\
F_{73} &= \frac{3}{2} \frac{1}{\tau_1 G_{10}}, & F_{76} &= \frac{1}{2} \frac{G_{1F}}{G_{10}} \frac{1}{\tau_1} \frac{1}{r}, \\
F_{82} &= 1, & F_{97} &= 1, \\
\text{all the other } F_{ij} &= 0
\end{aligned} \tag{4.32d}$$

The unknown vector $\mathbf{U}^{(v)}$ can be written as Eq. (4.14).

Applying the same mathematical operations as in Eqs. (2.82-2.83), we obtain the integrated canonical equations along the characteristic lines for the thermo-viscoelastic layer as

$$G_{ij}(A)U_j^{(v)}(A) = H_{ij}(A_i)U_j^{(v)}(A_i) \quad (i=1-9, j=1-9) \tag{4.33}$$

where

$$G_{ij}(A) = E_{ij} - \frac{1}{2} \Delta t F_{ij}(A) \tag{4.34}$$

$$H_{ij}(A_i) = E_{ij} + \frac{1}{2} \Delta t F_{ij}(A_i)$$

In Eqs. (4.34), Δt is the time interval between two consecutive points along the characteristic lines $C_v^{(i)}$ ($i=1-9$), see Fig. 4.1. Furthermore, in Eqs.(4.33 - 4.34), a bar under an index implies that summation convention is not applied to that index

and $U_j^{(v)}(A)$, $U_j^{(v)}(A_i)$ represent the values of the field variables at points A and A_i , respectively, as in the previous chapters.

To compute the values of field variables at A_3 and A_4 , we use a linear interpolation between the points A_1 and A_5 and A_2 and A_5 (see Fig. 4.1) using Eqs. (3.45) by simply putting subscript v or superscript v in parentheses on the related elements.

The elements of E_{ij} and F_{ij} are given in Eqs.(4.31-4.32). Equations (4.33) represent nine equations defined by $i = 1-9$, and for each value of the free index i , there is a summation over j which takes the values ($j = 1-9$). Thus, when the field variables U_j are known at points A_i ($i = 1-9$), the values of the field variables U_j at point A can be determined from Eqs. (4.33). In other words, the values of the field variables at a specific point along any line parallel to the r -axis in the solution region, see Fig. 4.1, can be found in terms of the known values of the field variables defined at points on the previous line. It is compact and suitable to express the equations in this form for computer programming.

For the orthotropic layers of the problem considered in this chapter, canonical forms of the equations, integrated forms of the equations along the characteristic lines are the same as those of Chapter 3. These are Eqs. (3.33 – 3.39) and Eqs. (3.43). These equations are not rewritten here for the sake of brevity.

4.6 Modification of the Equations for the Boundary and Interface Elements

Equations (3.43) and Eqs. (4.33) are valid for the interior points of the layers of the multilayered body and should be modified for points A on the boundaries and interfaces. The modified form of Eqs. (3.43) for the interfaces between the orthotropic layers and outer boundary element are the same as those of Eqs. (3.49-3.52).

For points A on the inner boundary, which is denoted by the element “L” in Fig. 4.1, the integrated canonical equations, Eqs. (4.33), remain the same for $i = 2, 4 - 9; j = 1 - 9$, whereas, the integrated canonical equations for $i = 1, 3; j = 1 - 9$ should be replaced by the boundary conditions on the inner surface $r = a$:

$$\sigma_{rr}^{(v)'}(A) + \frac{1}{3}\sigma_v(A) = -P(A) \quad \text{or} \quad V_r(A) = V(A) \quad \text{and} \quad (4.35)$$

$$T_v(A) = T^*(A) \quad \text{or} \quad q_r^{(v)}(A) = Q(A)$$

As for the interface element ‘S’, an element on the interface between the viscoelastic layer and the orthotropic layer labeled as layer 1, we should make use of combining the sets of Eq.(3.43) and Eq. (4.33) together with the interface conditions. The interface conditions require the continuity of the surface tractions, displacements, heat flux and temperature at the interface. For the interface element ‘S’, then the integrated canonical equations, Eqs. (3.43) remain the same for $i = 1, 3, 5 - 7$, whereas, Eqs. (4.33) remain the same for $i = 2, 4, 5 - 9$; thus, we have

$$G_{ij}(A)U_j^{(v)}(A) = H_{ij}(A_i)U_j^{(v)}(A_i) \quad i = 1, 3, 5 - 9; j = 1 - 9 \quad (4.36)$$

$$S_{ij}^{(1)}U_j^{(1)}(A) = Z_{ij}^{(1)}(A_i)U_j^{(1)}(A_i) \quad i = 2, 4, 5 - 7, j = 1 - 7$$

Equations (3.43) for $i = 2, 4$ and Eqs. (4.33) for $i = 1, 3$ should be replaced by the interface conditions

$$\sigma_{rr}^{(v)'}(A) + \frac{1}{3}\sigma_v(A) = \sigma_{rr}^{(1)}(A)$$

$$v_r^{(v)}(A) = v_r^{(1)}(A) \quad (4.37a)$$

$$T_v(A) = T_1(A)$$

$$q_r^{(v)}(A) = q_r^{(1)}(A) \quad (4.37b)$$

Thus, modification of the equations for the interface and boundary elements is completed. Equations (4.36–4.37) represent sixteen equations to determine the sixteen unknowns, $U_j^{(v)}(A)$ and $U_j^{(1)}(A)$ $j = (1-16)$, pertaining to points on the interface between the viscoelastic layer and first orthotropic layer.

Without getting into details, the numerical procedure employed here is of the same form as that employed in the previous chapters.

4.7 Numerical Examples and Discussion of the Results

In the numerical examples, it is assumed that the inner surface $r = a$ is subjected to a uniform time dependent pressure and a uniform temperature deviation and the outer surface $r = b$ is free of surface tractions and the temperature deviation is kept at zero, that is, the boundary conditions are

$$\begin{aligned} \sigma_{rr}^{(v)'}(a, t) + \frac{1}{3}\sigma_v(a, t) &= -P(t)H(t), \quad T_v(a, t) = T^*(t)H(t) \\ \sigma_{rr}^{(n)}(b, t) &= 0, \quad T_n(b, t) = 0 \end{aligned} \quad (4.38)$$

In the method of characteristics, we are free to choose any time dependency for the applied pressure and temperature deviation. In the examples, we choose a step-time variation with an initial ramp, see Figs. (2.7, 3.3). In the figures, we notice that the applied pressure and temperature deviation are zero at $t = 0$, linearly rise to constant values P_0 and T_0^* , respectively, during a rise time of Δt and remain constant thereafter. The initial ramp in the pressure variation and temperature deviation eliminates the complicated circumstances of having first-order discontinuities in the field variables at the wave fronts.

The numerical computations are carried out and the results are displayed in terms of non-dimensional quantities. These non-dimensional quantities are defined as

$$\bar{r} = \frac{r}{a}, \quad \bar{t} = \frac{tc_0}{a}, \quad \bar{u}_r = \frac{u_r}{a}$$

$$\bar{u}_r^{(v)} = \frac{u_r^{(v)}}{a}, \quad \bar{v}_r^{(v)} = \frac{v_r^{(v)}}{c_0}, \quad \bar{\rho}_v = \frac{\rho_v}{\rho_v} = 1$$

$$\bar{v}_r = \frac{v_r}{c_0}, \quad \bar{\rho} = \frac{\rho}{\rho_v}$$

$$(\bar{E}_1, \bar{E}_2, \bar{E}_3) = \left(\frac{E_1}{\rho_v c_0^2}, \frac{E_2}{\rho_v c_0^2}, \frac{E_3}{\rho_v c_0^2} \right),$$

$$(\bar{\sigma}_{rr}, \bar{\sigma}_{\theta\theta}) = \left(\frac{\sigma_{rr}}{\rho_v c_0^2}, \frac{\sigma_{\theta\theta}}{\rho_v c_0^2} \right), \quad (4.39a)$$

$$(\bar{\sigma}_{rr}^{(v)'}, \bar{\sigma}_{\theta\theta}^{(v)'}, \bar{\sigma}_v) = \left(\frac{\sigma_{rr}^{(v)'}}{\rho_v c_0^2}, \frac{\sigma_{\theta\theta}^{(v)'}}{\rho_v c_0^2}, \frac{\sigma_v}{\rho_v c_0^2} \right)$$

$$(\bar{G}_{12}, \bar{G}_{13}, \bar{G}_{23}) = \left(\frac{G_{12}}{\rho_v c_0^2}, \frac{G_{13}}{\rho_v c_0^2}, \frac{G_{23}}{\rho_v c_0^2} \right),$$

$$(\bar{\tau}_1, \bar{\tau}_2) = \left(\frac{\tau_1 c_0}{a}, \frac{\tau_2 c_0}{a} \right),$$

$$(\bar{G}_{10}, \bar{G}_{1F}, K) = \left(\frac{G_{10}}{\rho_v c_0^2}, \frac{G_{1F}}{\rho_v c_0^2}, \frac{K}{\rho_v c_0^2} \right),$$

$$(\bar{q}_r, \bar{q}_r^{(v)}) = \left(\frac{q_r}{\rho_v c_0^3}, \frac{q_r^{(v)}}{\rho_v c_0^3} \right),$$

$$(\bar{\beta}_{11}, \bar{\beta}_{22}, \bar{\beta}_{33}) = \left(\frac{\beta_{11} T_0}{\rho_v c_0^2}, \frac{\beta_{22} T_0}{\rho_v c_0^2}, \frac{\beta_{33} T_0}{\rho_v c_0^2} \right),$$

$$(\bar{\alpha}, \bar{\alpha}_0) = \left(\frac{\alpha c_0}{a}, \frac{\alpha_0 c_0}{a} \right),$$

$$(\bar{\alpha}_v, \bar{\alpha}_0^{(v)}) = \left(\frac{\alpha_v c_0}{a}, \frac{\alpha_0^{(v)} c_0}{a} \right),$$

(4.39b)

$$\bar{T}_0 = \frac{T_0}{T_0} = 1, \quad \bar{T} = \frac{T}{T_0},$$

$$\bar{c} = \frac{c T_0}{\rho_v c_0^2}, \quad \bar{c}_v = \frac{c_v T_0}{\rho_v c_0^2},$$

$$\bar{k}_{rr} = k_{rr} \frac{T_0}{\rho_v c_0^3 a}, \quad \bar{k}_v = k_v \frac{T_0}{\rho_v c_0^3 a}, \quad \bar{\alpha}_T^{(v)} = \alpha_T^{(v)} T_0$$

$$(\bar{c}_1, \bar{c}_2) = \left(\frac{c_1}{c_0}, \frac{c_2}{c_0} \right)$$

where $c_0 = \sqrt{\frac{1}{3\rho_v}(2G_{10} + 3K)}$ is the uncoupled mechanical longitudinal wave speed for viscoelastic layer and a bar over the elements designates non-dimensional quantities. Furthermore, a is the radius of the inner surface and ρ_v is the mass density of the typical viscoelastic layer.

We now present some results for the response of viscoelastic cylinders enclosed in filament wound fiber- reinforced cylindrical composites. The multilayered body is subjected to boundary conditions given by Eqs. (4.38) with $P(t)$ and $T^*(t)$ defined as in Figs. (2.7,3.3); it is initially at rest and the layers are perfectly bonded to each other. The body consists of three generally orthotropic elastic layers with stacking sequence -45/90/30 starting from the first orthotropic layer and one viscoelastic innermost layer. The non-dimensional material properties are taken as

$$(\bar{G}_{10}, \bar{G}_{1F}, K) = (0.857, 0.735, 0.429)$$

$$\bar{\rho}_v = 1, \quad \bar{\alpha}_T^{(v)} = 0.008,$$

$$\bar{\alpha}_v = \bar{\alpha}_0^{(v)} = 0.00000001844$$

$$\bar{c}_v = 0.022, \quad \bar{\tau}_1 = 3688000$$

$$(\bar{k}_v, \bar{k}_{rr}) = (4.549 \times 10^{-9}, 5.958 \times 10^{-9})$$

$$\bar{\rho}_i = 1.35 \quad i = (1-3), \quad \bar{T}_0 = 1, \quad \bar{c} = 0.02 \quad (4.40a)$$

$$(\bar{E}_1, \bar{E}_2, \bar{E}_3) = (2.318, 0.785, 0.785),$$

$$(\bar{G}_{12}, \bar{G}_{13}, \bar{G}_{23}) = (0.277, 0.277, 0.294),$$

$$(\bar{\beta}_{11}, \bar{\beta}_{22}, \bar{\beta}_{33}) = (0.024, 0.015, 0.015)$$

$$\bar{\alpha} = 0.00000001585, \quad \bar{\alpha}_0 = 0.00000001585$$

$$\nu_{23} = \nu_{32} = 0.33, \quad (4.40b)$$

$$\nu_{31} = \nu_{13} = \nu_{21} = \nu_{12} = 0.236$$

The thicknesses of the viscoelastic layer and the orthotropic layers are all equal to $h_i = 0.1$ ($i = 1 - 3$), and the network of characteristic lines used in the numerical analysis is defined by $\overline{\Delta t} = 0.0002$. The applied pressure at inner surface is zero at $\bar{t} = 0$, then linearly rises to a constant value $\bar{P}_0 = 0.001$ during a rise time of $\overline{\Delta t} = 0.0002$ after which it remains constant. The applied temperature deviation at the inner surface is taken as $\bar{T}_0^* = 0.08$.

Results of the numerical computations are given in Figs. (4.2-4.8). The curves are given for the cases when the thermal effects are neglected and when they are taken into account, which in the sequel are described as non-thermal and thermal solutions, respectively.

Variations of the non-dimensional stress $-\bar{\sigma}_{rr}$ with time \bar{t} at location $\bar{r} = 1.05$, corresponding to the middle of the viscoelastic layer, are displayed in Fig. 4.2. The curves denote the effects of reflections at the inner ($\bar{r} = 1$), and outer ($\bar{r} = 1.4$) boundaries, and reflections and transmissions at the interfaces of the layers. Figure 4.2 includes two curves, one is for the non-thermal solution and the other is for the solution where thermal effects are taken into consideration. The curves of Fig. 4.2 denote clearly the dispersion caused by the thermal effects in the wave profiles. In the curve representing the non-thermal solution, the sudden changes in the stress levels correspond to the arrivals of reflected and refracted waves from the interfaces and boundaries of the composite body at the position considered. In the thermal solution, the curves display a similar character. However, due to the thermal dispersion, the sudden changes, in the non-thermal solution now become smoothly varying curves (see Fig. 4.2). The maximum values of the radial normal stresses are smaller in the thermal solution than in the non-thermal solution. The radial stress

remains mostly compressive. From Fig. 4.2, one sees that the disturbances propagate faster when thermal effects are taken into consideration.

Figure 4.3 shows the variations of the dimensionless normal stress $\bar{\sigma}_{\theta\theta}$ with \bar{t} at the location 1.05, middle of the viscoelastic layer of the multilayered medium. The normal circumferential stress remains tensile for thermal and non-thermal solutions except short duration, near the time of arrival of the wave front. Thermal solution displays a similar character with non-thermal one. However, due to the thermal dispersion, the sudden changes in the non-thermal solution now become smoothly varying curve. For the position considered, thermal effects are significant for the circumferential stress. Different from the radial stress trend, circumferential stress levels are higher for some non-dimensional time intervals in the thermal solution. Furthermore, we note from the figure that, circumferential stress is the significant stress for the layer and position considered, since it reaches nearly three and a half times higher stress values than the radial one.

Figure 4.5 shows the variations of the dimensionless normal stress $\bar{\sigma}_{\theta\theta}$ with time \bar{t} at the location $\bar{r}=1.15$, the middle of the first orthotropic layer. We note that circumferential normal stress reaches higher values in the first orthotropic layer than those in the viscoelastic layer. Figure 4.5 includes non-thermal solution, as well as the thermal solution with temperature deviation at the inner boundary taken as 0.08. Due to the thermal dispersion, the sudden changes in the non thermal solution now become smoothly varying curves as in the curves of previous figures. The sudden changes in the stress levels due to reflections and refractions are more distinct and significant in these curves compared to the curves of Fig. 4.3. The fact that the circumferential normal stress is the dominant stress is more valid for the elastic orthotropic layer which can be seen from the comparison of the curves of Figs. (4.5, 4.4)

In Fig. 4.4, the variation of radial stress $\bar{\sigma}_{rr}$ with time \bar{t} at location $\bar{r}=1.15$ is given. The curves of Fig. 4.4 display similar features as those of Fig. 4.2. The sudden changes in the stress levels due to reflections and refractions of waves at the

boundaries and interfaces in the non-thermal solution leave their places to smoothly varying curves in the thermal solution due to thermal dispersion. The radial stress $\bar{\sigma}_{rr}$ in the curves of Fig. 4.4 may assume tensile values as well; whereas, in the curves of Fig. 4.2, it was primarily compressive. The maximum values of the radial normal stress are smaller in the thermal solution than in the non thermal solution. We note from the curves in Fig. 4.4 that the disturbances propagate faster when thermal effects are taken into consideration.

Figures (4.6-4.8) display the time variations of the radial normal stress $\bar{\sigma}_{rr}$ and circumferential normal stress $\bar{\sigma}_{\theta\theta}$ at the interface between second and third orthotropic layers. The radial stress $\bar{\sigma}_{rr}$ is continuous across the interface and its time variation at the location $\bar{r}=1.3$ is given in Fig. 4.6; whereas, $\bar{\sigma}_{\theta\theta}$ is discontinuous across the interface and its time variations at the points just before and just after the interface, i.e., at $\bar{r}=1.3-0$ and $\bar{r}=1.3+0$ are shown in Figs. (4.7, 4.8), respectively. The curves in these figures display similar trends as the curves in the previous figures. The sudden changes in the stress levels in the non-thermal solutions are more distinct and pronounced in these curves and they are smoothed out in the case of thermal solutions. The radial stresses assume tensile stresses as well and the extreme stress levels are smaller in the thermal case, Fig. 4.6. The circumferential stress $\bar{\sigma}_{\theta\theta}$ suffers considerable jumps at the interface which may reach values twice as high, see Figs. (4.7, 4.8).

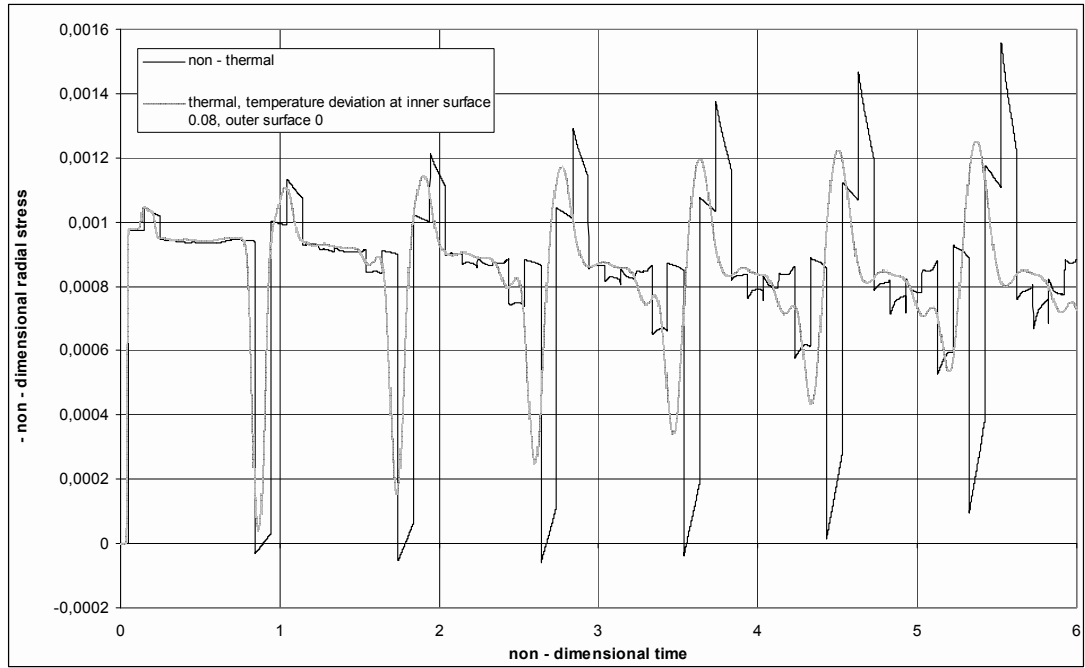


Figure 4.2. Variation of radial normal stress $\bar{\sigma}_{rr}$ with time \bar{t} at location $\bar{r} = 1.05$, middle of viscoelastic layer.

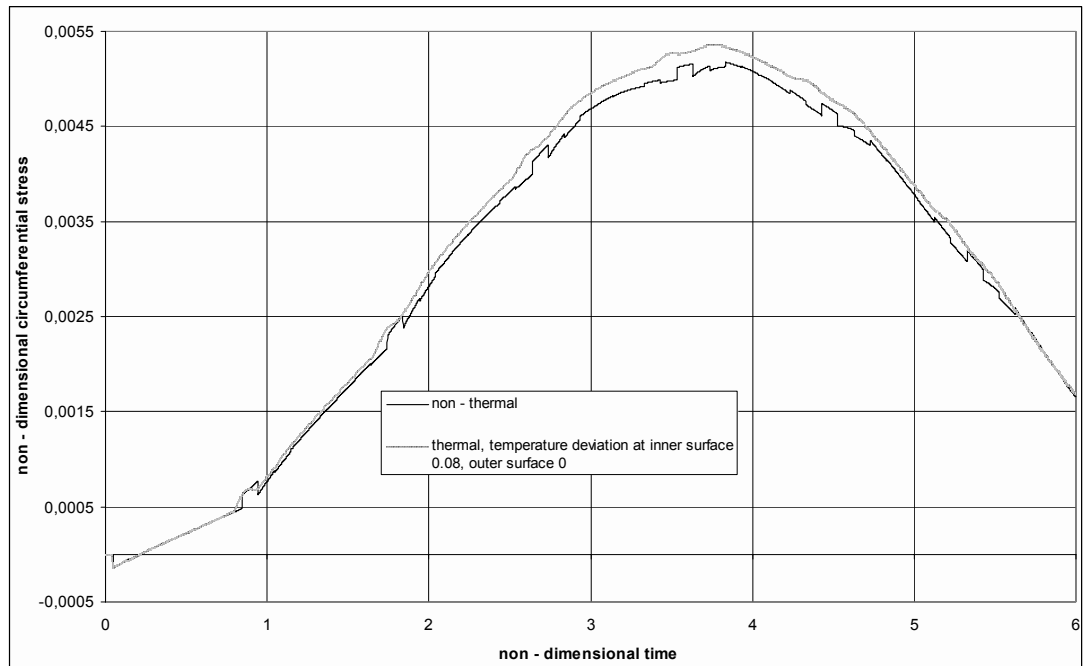


Figure 4.3. Variation of circumferential normal stress $\bar{\sigma}_{\theta\theta}$ with time \bar{t} at location $\bar{r} = 1.05$, middle of viscoelastic layer.

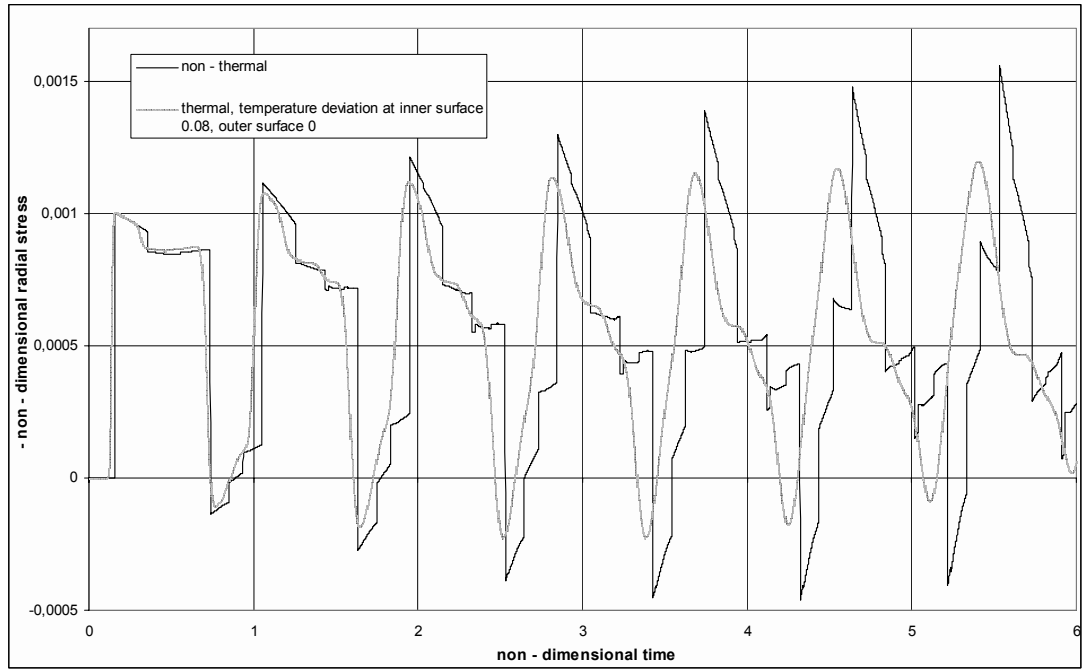


Figure 4.4. Variation of radial normal stress $\bar{\sigma}_{rr}$ with time \bar{t} at location $\bar{r} = 1.15$, middle of first orthotropic layer.

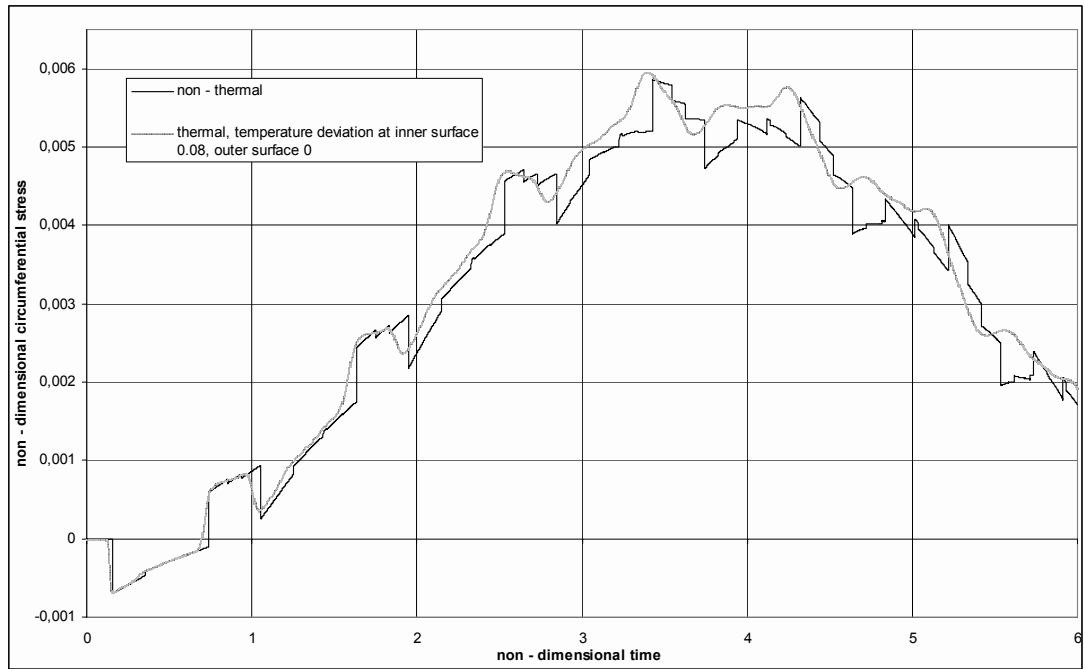


Figure 4.5. Variation of circumferential normal stress $\bar{\sigma}_{\theta\theta}$ with time \bar{t} at location $\bar{r} = 1.15$, middle of first orthotropic layer.

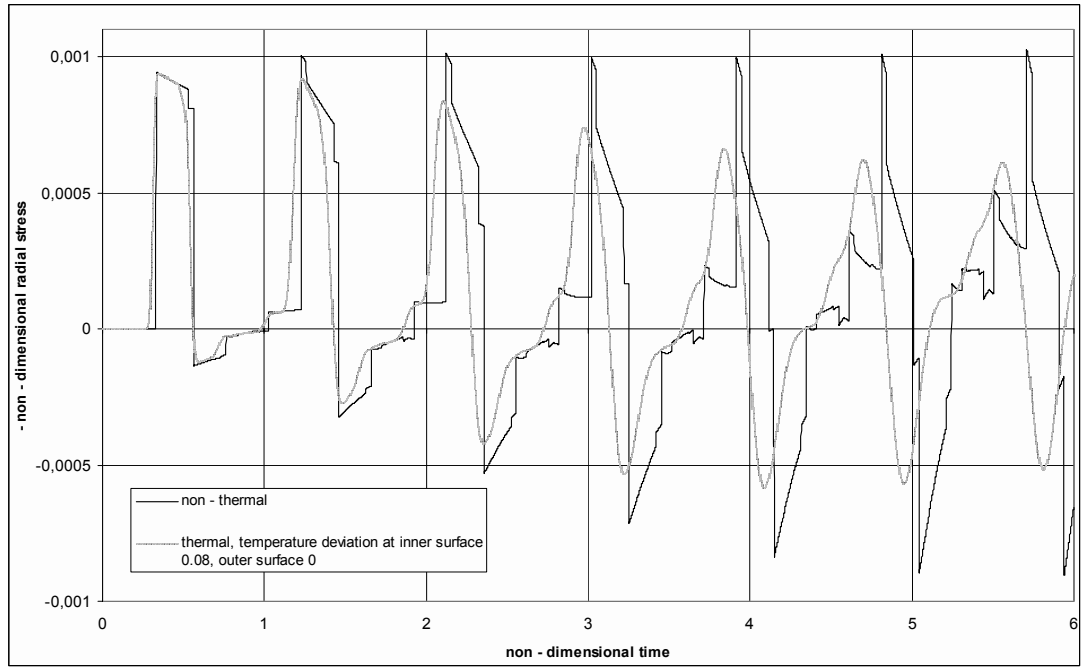


Figure 4.6. Variation of radial normal stress $\bar{\sigma}_{rr}$ with time \bar{t} at location $\bar{r} = 1.3$, interface between second and third orthotropic layers.

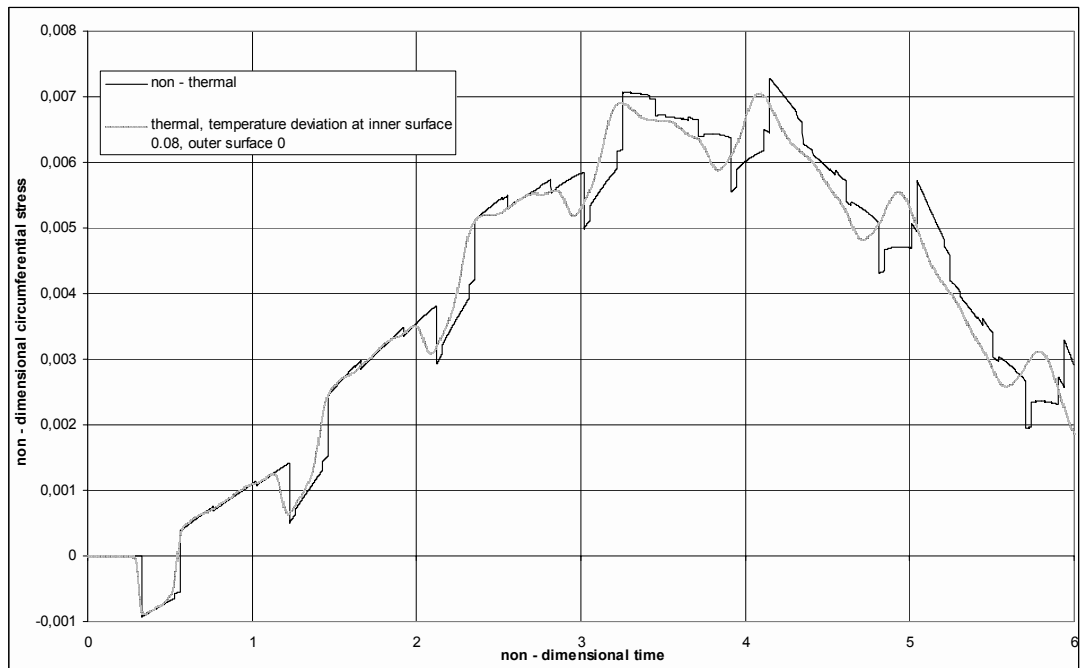


Figure 4.7. Variation of circumferential normal stress $\bar{\sigma}_{\theta\theta}$ with time \bar{t} at location $\bar{r} = 1.3$ on the side of second layer at the interface between second and third orthotropic layers.

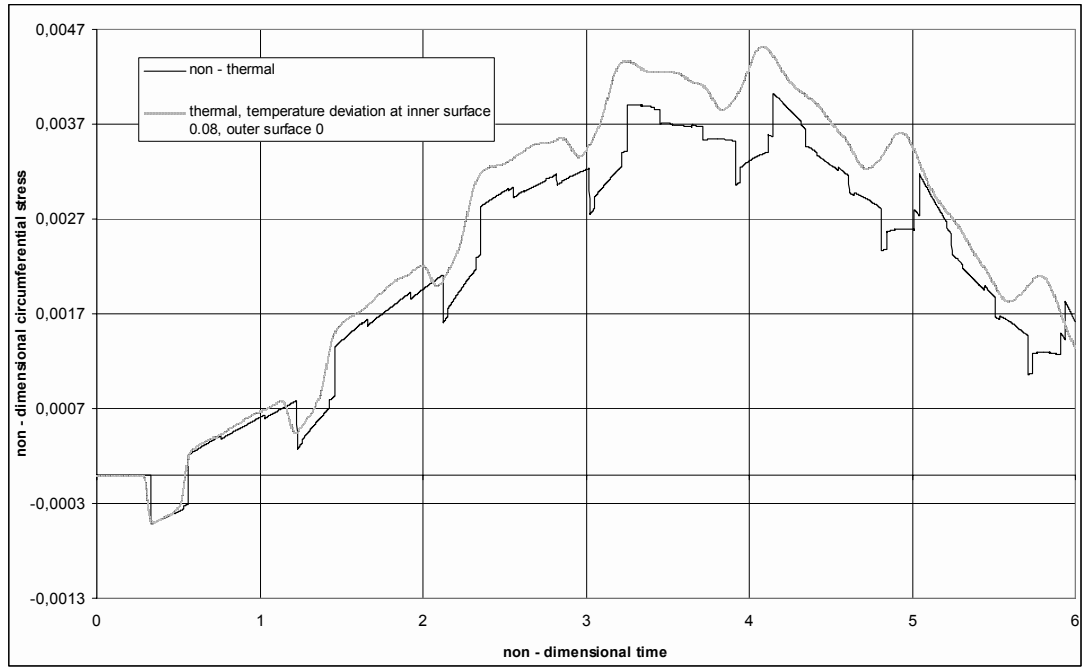


Figure 4.8. Variation of circumferential normal stress $\bar{\sigma}_{\theta\theta}$ with time \bar{t} at location $\bar{r} = 1.3$ on the side of third layer, at the interface between second and third orthotropic layers.

CHAPTER 5

CONCLUSIONS

In this thesis, transient dynamic response of viscoelastic cylinders enclosed in filament wound cylindrical composites is investigated. The multilayered medium consists of $n+1$ layers, the inner layer being viscoelastic, while the outer fiber reinforced cylindrical laminate consists of n -different generally orthotropic, homogeneous and linearly elastic layers. The problems investigated in this thesis can be grouped under three categories. In the first category, presented in Chapter 2, transient dynamic response of the viscoelastic cylinder enclosed in filament wound cylindrical laminate, with thermal effects neglected, is investigated. In the numerical examples, the inner surface is subjected to a uniform pressure which varies in time as a step function with an initial ramp, and the outer surface is free of surface tractions. Solid propellant material properties are used for the viscoelastic layer. Curves displaying the variations of the nondimensional radial stress σ_{rr}/P_0 and circumferential normal stress $\sigma_{\theta\theta}/P_0$ with time \bar{t} at different locations in the inner viscoelastic and outer elastic layers show striking properties. At points in the viscoelastic layer, both σ_{rr}/P_0 and $\sigma_{\theta\theta}/P_0$ are compressive, their values and variations are very close to each other and they reach values as high as -2. At points in the outer generally orthotropic layers and in the time interval considered, however, σ_{rr}/P_0 is basically compressive and $\sigma_{\theta\theta}/P_0$ is basically tensile. The highest levels of σ_{rr}/P_0 are around -1, whereas $\sigma_{\theta\theta}/P_0$ may reach values as high as 18. This striking difference in the trends of the time variations of the stresses σ_{rr}/P_0 and $\sigma_{\theta\theta}/P_0$ in the inner viscoelastic and outer orthotropic layers is due to the propellant material properties of the viscoelastic layer. The fact that the normal stresses in the viscoelastic layer are compressive is a desired property for solid propellants. The case of ablating inner surface is investigated as well. This is an important advantage of the method of characteristics. Handling of a moving boundary, which may be a

formidable task in many methods of solution, can be achieved without much difficulty in the method of characteristics. Furthermore, for verification purposes, solutions are obtained for two special cases and the results are compared with those already existing in the literature and excellent agreements are found.

In the second category of problems, presented in Chapter 3, the thermomechanical response of fiber-reinforced cylindrical composites consisting of n generally orthotropic linearly elastic layers is investigated. Thermal effects, in addition to the mechanical effects, are taken into consideration as well. A generalized thermoelasticity theory which incorporates the temperature rate among the constitutive variables is employed. This theory is known as temperature-rate dependent thermoelasticity (TRDTE) theory or generalized thermoelasticity with two relaxation times. This theory predicts finite speeds for thermal disturbances. In the numerical examples, uniform time dependent pressure and temperature deviation varying in time as step function with initial ramp are applied at the inner surface, and the outer surface is free of surface tractions and kept at zero temperature deviation. The numerical results are displayed in curves showing the variations of normal stresses $\bar{\sigma}_{rr}$ and $\bar{\sigma}_{\theta\theta}$ with time at different locations in the cylindrical laminate. Curves where thermal effects are neglected are also given in the figures. The curves clearly reveal the effects of reflections and refractions of waves from the boundary surfaces and the interfaces of the layers. The sharp changes in the stress levels in the non-thermal solution are smoothed out in the thermal solutions due to thermal dispersion. The effects of the stacking sequence of the layers and the effects of geometric dispersion on the wave profiles are also apparent. The stress levels decrease as we go away from the inner surface due to geometric dispersion; but in some cases, due to the stacking sequence of the layers, the stress levels at further points are higher than at points closer to the inner surface. The generalized thermoelasticity theory employed in this thesis is a linear theory; hence, it is valid for small temperatures deviations. The curves reveal that the effects of thermal dispersion may be significant even for small temperature deviations prescribed at the inner surface, especially for large times after the arrival of the waves.

A verification example solved as a special case of the general formulation presented in this thesis is compared with the solution existing in the literature and it is shown that the two solutions are almost identical. This verification example shows that generalized thermoelasticity theory employed in this thesis describes accurately the response for very short times and for very small distances.

In the third category of problems, presented in Chapter 4, the transient dynamic response of an isotropic viscoelastic layer enclosed in a fiber-reinforced cylindrical laminate consisting of n generally orthotropic elastic layers is investigated. The elastic layers are governed by the equations of generalized thermo-viscoelasticity in which relaxation effects of the volume are neglected. Generalized thermo-viscoelasticity is a relatively new subject which is not treated widely in the literature yet. The constitutive equations as employed in this thesis are quite new. Numerical results displayed in curves are given for the cases when the thermal effects are neglected and when they are taken into account which are described as non-thermal and thermal solutions, respectively. The boundary conditions considered are similar to the ones considered in the second category of problems. The curves show the time variations of $\bar{\sigma}_{rr}$ and $\bar{\sigma}_{\theta\theta}$ at different locations and they reveal that disturbances propagate faster when thermal effects are taken into consideration. Radial stress in the inner viscoelastic layer is basically compressive; whereas, in the outer orthotropic layers, it may assume tensile values as well. The dominant stress is the circumferential normal stress in both the viscoelastic and the elastic layers; but the ratio of the maximum levels of the circumferential stress to radial stress is higher in the orthotropic elastic layers than in the viscoelastic layer. Thermal dispersion smoothes out the distinct sudden changes in the stress levels of the non-thermal solutions and this is more apparent in the radial stress variations. The effects of reflections, refractions, and the effects of stacking sequence of the elastic layers are similar to those in the previous problems.

Four computer programs are written in this thesis. The first computer program handles the problems discussed in the first category with non-ablating inner surface, Chapter 2. In the second program, the first program is modified to take care

of the ablating inner boundary. The third program handles the transient dynamic response of filament wound cylindrical laminates consisting of n generally orthotropic thermoelastic layers, problems in the second category, Chapter 3. Finally, the last computer program handles the problems discussed under the third category, Chapter 4.

As a final comment for future research, this work can be extended to two-dimensional problems in multilayered elastic, and/or viscoelastic media by employing a technique which combines the method of characteristics with the Fourier transform, for example.

REFERENCES

- [1] Ewing, W. M., Jardetsky, W.S. and Press, F., Elastic Waves in Layered Media, McGraw-Hill, New York (1957).
- [2] Brekhovskikh, L. M., Waves in Layered Media, Academic Press, New York (1960).
- [3] Kennet, B. L. N., Seismic Wave Propagation in Stratified Media, Cambridge U. P., Cambridge, UK (1983).
- [4] Tygel, M., Hubral, P., Transient Waves in Layered Media, Elsevier Press, Amsterdam (1987).
- [5] Van der Hijden, J. H. M. T., Propagation of Transient Elastic Waves in Stratified Anisotropic Media, Amsterdam: North Holland (1987).
- [6] Nayfeh, A. H. , Wave Propagation in Layered Anisotropic Media, Amsterdam: North Holland (1995).
- [7] Achenbach, J. D., Wave Propagation in Elastic Solids, North Holland, New York (1987).
- [8] Miklowitz, J., The Theory of Elastic Waves and Wave Guides, North-Holland, New York (1984).
- [9] Sun, C. T., Achenbach, J. D. and Herrmann, G., “*Continuum Theory for a Laminated Medium*”, ASME Journal of Applied Mechanics, 35, 467(1968).

- [10] Achenbach J. D., Sun, C. T. and Herrmann G., “*On the Vibrations of a Laminated Body*”, ASME Journal of Applied Mechanics, 35, 689(1968).
- [11] Santosa, F., Symes, W. W., “*A Dispersive Effective Medium for Wave Propagation in Periodic Composites*”, SIAM :J. Appl. Math., 51, 984(1991).
- [12] Soldatos, K. P., “*On the Theories Used for the Wave Propagation in Laminated Composite Thin Elastic Shells*”, J. Appl. Math. Phys. (ZAMP), 36, 120(1985).
- [13] Noor, A. K., Burton, N. S., Peters, J. M., “*Assessment of Computational Models for Multilayered Composite Cylinders*”, Int. J. Solids Struct., 27, 1269(1991).
- [14] Delph, T. J., Herrmann, G., Kaul, R. K., “*Harmonic Wave Propagation in a Periodically Layered Infinite Elastic Body: Plane Strain, Analytical Results*”, ASME J. Appl. Mech., 46, 113(1979).
- [15] Delph, T. J., Herrmann, G., Kaul, R. K., “*Harmonic Wave Propagation in a Periodically Layered Infinite Elastic Body: Plane Strain, Numerical Results*”, ASME J. Appl. Mech., 47, 531(1980).
- [16] Braga, A. M. B., Herrmann, G., “*Floquet Waves in Anisotropic Periodically Layered Composites*”, J. Acoust. Soc. Am., 91, 1211(1992).
- [17] Liu, G. R., Tani, J., Watanabe, K., Ohyoshi, T., “*Lamb Wave Propagation in Anisotropic Laminates*”, ASME J. Appl. Mech., 57, 923(1990).
- [18] Marcus, S., Mead, D. J., “*Axisymmetric and Asymmetric Wave Motion in Orthotropic Cylinders*”, J. Sound Vib., 181(1), 127(1995).
- [19] Zhuang, W., Shah, A. H., Dong, S. B., “*Elastodynamic Green’s function for laminated anisotropic circular cylinders*”, J. Appl. Mech., 66, 665(1999).

- [20] Cetinkaya, C., Vakakis, A. F., “*Transient Axisymmetric Stress Wave Propagation in Weakly Coupled Layered Structures*”, J. of Sound and Vib., 182, 283(1995).
- [21] Cetinkaya, C., Brown, J., Mohammed, A. A. F. and Vakakis, A. F. “*Near Field Transient Axisymmetric Waves in Layered Structures: Effects of Weak Coupling*”, Int. J. Numer. Math. in Engrg., 40, 1639(1997).
- [22] Rizzi, S. A., Doyle, J. F., “*A Spectral Element Approach to Wave Motion in Layered Solids*”, J. Vib. Acoust., 114, 569(1992).
- [23] Kundu, T., Mal, A. K., “*Elastic Waves in a Multilayered Solid Due to a Dislocation Source*”, Wave Motion., 7, 459(1985).
- [24] Mal, A. K., “*Wave Propagation in Layered Composite Laminates Under Periodic Surface Loads*”, Wave Motion., 10, 257(1988).
- [25] Mal, A. K. and Lih, S. S., “*Elastodynamic Response of a Unidirectional Composite Laminate to Concentrated Surface Loads, Part I*”, ASME J. Appl. Mech., 59, 878(1992).
- [26] Mal, A. K. and Lih, S. S., “*Elastodynamic Response of a Unidirectional Composite Laminate to Concentrated Surface Loads, Part II*”, ASME J. Appl. Mech., 59, 887(1992).
- [27] Lih, S. S., Mal, A. K., “*Response of Multilayered Composite Laminates to Dynamic Surface Loads*”, Composites Part B., 27B, 633(1996).
- [28] Mengi, Y., Turhan, D., “*A Higher Order Dynamic Theory for Viscoelastic Plates and Layered Composites*”, J. Sound Vib., 92, 311(1984).

- [29] Mengi, Y., Birlik, G. A., “*A Refined Dynamic Theory for Viscoelastic Cylindrical Shells and Cylindrical Laminated Composites, Part I: General Theory*”, J. Sound Vib., 130(1), 55(1989).
- [30] Birlik, G, Mengi, Y., “*Transient Wave Propagation in a Viscoelastic Layered Composite – an Approximate Theory*”, J. Sound Vib., 112(1), 141(1987).
- [31] Mengi, Y., Birlik, G. A., “*A Refined Dynamic Theory for Viscoelastic Cylindrical Shells and Cylindrical Laminated Composites, Part 2: An Application*”, J. Sound Vib., 130(1), 69(1989).
- [32] Naciri, T., Navi, P., Granacher, O., “*On Harmonic Wave Propagation in Multilayered Viscoelastic Media*”, Int. J. Mech. Sci., 32(3), 225(1990).
- [33] Han C., Sun C. T., “*Attenuation of Stress Wave Propagation in Periodically Layered Elastic Media*”, J. Sound Vib., 243(4), 747(2001).
- [34] Singh, B., Kumar, R., “*Reflection and Refraction of Micropolar Elastic Waves at a Loosely Bonded Interface Between Viscoelastic Solid and Micropolar Elastic Solid*”, Int. J. Engng. Sci., 36(2), 101(1998).
- [35] Ting, T. C. T., Mukunoki, I., “*A Theory of Viscoelastic Analogy for Wave Propagation Normal to the Layering of a Layered Medium*”, ASME J. Appl. Mech., 46(2), 329(1979).
- [36] Ting, T. C. T., “*The Effects of Dispersion and Dissipation on Wave Propagation in Viscoelastic Layered Composites*”, Int. J. Solids Struct., 16(10), 903(1980).
- [37] Jiang, L., Haddow, J. B., “*A Finite Element Solution of Plane Wave Propagation in Inhomogenous Linear Viscoelastic Solids*”, J. Sound Vib., 184(3), 429(1995).

- [38] Nkemzi, D., Green, W. A., “*Transient Wave Propagation in a Viscoelastic Sandwich Plate*”, Acta Mech., 102, 167(1994).
- [39] Abu-Alshaikh, I., Turhan, D, Mengi, Y. “*Propagation of Transient Out-of-Plane Shear Waves in Viscoelastic Layered Media*”, Int. J. Mech Sci., 43, 2911(2001).
- [40] Abu-Alshaikh, I., Turhan, D, Mengi, Y. “*Transient Waves in Viscoelastic Cylindrical Layered Media*”, European J. Mech. A/Solids, 21, 811(2002).
- [41] Liu, T., Li, Q., “*Transient Elastic Wave Propagation in an Infinite Timoshenko Beam on Viscoelastic Foundation*”, Int. J. Solids Structures, 40, 3211(2003).
- [42] Caviglia, G., Morro, A., Pagani, E., “*Inhomogenous Waves in Viscoelastic Media*”, Wave Motion, 12, 143(1990).
- [43] Chou, S. C., Greif, R., “*Numerical Solution of Stress Waves in Layered Media*”, AIAA Journal, 6(6), 123(1968).
- [44] Chou, P. C., Koenig, H. A., “*A Uniform Approach to Cylindrical and Spherical Elastic Waves by Method of Characteristics*”, J. Appl. Mech, 33, 159(1966).
- [45] Haddow, J. B., Mioduchowski, A., “*Analysis of Expansion of Spherical Cavity in Unbounded Hyperelastic Medium by Method of Characteristics*”, Acta Mechanica, 23, 15(1975).
- [46] Mioduchowski, A., Moodie, T. B. and Haddow, J. B., “*Waves from Suddenly Punched Hole in Finitely Stretched Elastic Sheet*”, ASME J. Appl. Mech., 45, 83(1978).

- [47] Mioduchowski, A., Haddow, J. B., “*Sudden Pressurization of a Cylindrical Cavity of Oval Section*”, *Acta Mechanica*, 40, 49(1981).
- [48] Moodie, T. B., Mioduchowski, A., Haddow, J. B., Tait, R. J., “*Elastic Waves Generated by Loading Applied to Spherical Cavity*”, *Acta Mechanica*, 40, 49(1981).
- [49] Turhan, D. and Calayir, Y., “*Transient Dynamic Response of Viscoelastic Layered Composites*”, *Structural Dynamics: Recent Advances* (Ed. by Petyt, M., Wolfe, H. F. and Mei, C.), London: Elsevier Applied Science, 353(1991).
- [50] Turhan, D. and Alshaikh, I. A., “*Transient Shear Wave Propagation in Periodically Layered Media, Photonic Band Gaps and Localization*”, (Ed. by Soukoulis, C. M.), Plenum Press, New York, 479(1993).
- [51] Wegner, J. L. and Haddow, J. B., “*A Note on Plane Wave Propagation in a Linear Viscoelastic Solid*”, *Int. J. Engng. Sci*, 27, 1545(1989).
- [52] Wegner, J. L., “*Propagation of Waves from a Spherical Cavity in an Unbounded Linear Viscoelastic Solid*”, *Int. J. Engng. Sci*, 31, 493(1993).
- [53] Duhamel, J. M. C., “*Second Memoire Sur Les Phenomes Thermomechaniques*”, *J. Ecole Polytech*, 15, 1(1837).
- [54] Biot, M. A., “*Thermoelasticity and Irreversible Thermodynamics*”, *J. Appl. Phys.*, 27, 240(1956).
- [55] Chadwick, P., “*Thermoelasticity. The Dynamic theory, in Progress in Solid Mechanics*”, Hill, R. and Sneddon, I. N., Eds., North-Holland, Amsterdam, 1, 263(1960).

- [56] Boley, B. A. and Weiner, J. H., Theory of Thermal Stresses, Wiley, New York 1960.
- [57] Carlson, D. E., Linear Thermoelasticity, in Encyclopedia of Physics, Vol. 6 a/2, Springer-Verlag, Vienna 1972.
- [58] Nowacki, W., Dynamic Problems of Thermoelasticity, Noordhoff, Leyden 1975.
- [59] Parkus, H., Thermoelasticity, 2 nd ed., Chapter 5, Springer-Verlag, New York 1976.
- [60] Nowinski, J. L., Theory of Thermoelasticity with Applications, Noordhoff, Alphen Aan Den Rijn 1978.
- [61] Dhaliwal, R. S. and Singh, A., Dynamic Coupled Thermoelasticity, Hindustan Publishing Co, Delphi 1980.
- [62] Lord, H. W. and Shulman, Y., “*A generalized Dynamical Theory of Thermoelasticity*” J. Mech. Phys. Solids, 15, 299(1967).
- [63] Dhaliwal, R. S. and Sherief, H. H., “*Generalized Thermoelasticity for Anisotropic Media*” Quart Appl. Math., 38, 1(1980).
- [64] Achenbach, J. D., “*The Influence of Heat Conduction on Propagating Stress Jumps*”, J. Mech. Phys. Solids, 16, 273(1968).
- [65] Norwood, F. R. and Warren, W. R., “*Wave Propagation in the Generalized Dynamical Theory of Thermoelasticity*”, Quart J. Mech Appl. Math., 22, 283(1969).

- [66] Mengi, Y., Turhan, D., “*The Influence of Retardation Time of the Heat Flux on Pulse Propagation*”, ASME J. Appl. Mech., 45, 433(1978).
- [67] Chandrasekharaiah, D. S., Srinath, K. S., “*One Dimensional Waves in a Thermoelastic Half Space without Energy Dissipation*”, Int. J. Eng. Sci., 34(13), 1447(1996).
- [68] Sherief, H. H., “*Problem in Electro Magneto Thermoelasticity for an Infinitely Long Solid Conducting Circular Cylinder with Thermal Relaxation*”, Int. J. Eng. Sci., 7, 1137(1994).
- [69] Sherief, H. H. and Anwar M. N., “*A Problem in Generalized Thermoelasticity for an Infinitely Long Annular Cylinder*”, Int. J. Eng. Sci., 26(3), 301(1988).
- [70] Singh, B., Kumar, R., “*Wave Propagation in Generalized Thermo-microstretch Elastic Solid*”, Int. J. Eng. Sci., 36, 891(1998).
- [71] Sherief, H. H. and Dhaliwal R. S., “*Generalized One Dimensional Thermal Shock Problem for Small Times*”, J. Thermal Stresses, 4, 407(1981).
- [72] Sherief, H. H., J. Thermal Stresses, 9, 151(1984).
- [73] Sherief, H. H. and Ezzat M., J. Thermal Stresses, 17, 75(1984).
- [74] Sherief, H. H., “*On Uniqueness and Stability in Generalized Thermoelasticity*”, Quaterly of Applied Mathematics, XLIV(4), 773(1987).
- [75] Sharma, J. N., “*Transient Generalized Thermoelastic Waves in Transversely Isotropic Medium with a Cylindrical Hole*”, Int. J. Eng. Sci., 25(4), 463(1987).

- [76] Sharma, J. N., “*Some Considerations on Generalized Thermoelasticity*”, Int. J. Eng. Sci., 25, 1387(1987).
- [77] El-Magraby, N. M., Yossef, H. M., “*State Space Approach to Generalized Thermoelastic Problem with Thermomechanical Shock*”, Applied Mathematics and Computation, 156, 577(2004).
- [78] Sherief, H. H., Helmy, K. A., “*A Two Dimensional Problem for a Half-Space in Magneto-Thermoelasticity with Thermal Relaxation*”, Int. J. Eng. Sci., 40, 587(2002).
- [79] Ezzat, M. A., Karamany, A. S., Sumin, A.A, “*The Dependence of the Modulus of Elasticity on Reference Temperature in Generalized Thermoelasticity with Thermal Relaxation*”, Applied Mathematics and Computation, 147, 169(2004).
- [80] He, T., Tioni X., Shen, Y. P., “*State Space Approach to one Dimensional Thermal Shock Problem for a Semi-Infinite Piezoelectric Rod*”, Int. J. Eng. Sci., 40, 1081(2001).
- [81] Massalas, C. V., “*A Reciprocal Theorem in Generalized Thermoelasticity Proposed by Lord and Shulman*”, Lett. Appl. Eng. Sci., 23(6), 685(1985).
- [82] Sinha M., Bera, R. K., “*Eigenvalue Approach to Study the Effect of Rotation and Relaxation Time in Generalized Thermoelasticity*”, Computers and Mathematics with Applications, 46, 783(2003).
- [83] Baksı, A., Kumar, B. R., Debnath, L., “*Eigenvalue Approach to Study the Effect of Rotation and Relaxation Time in Two Dimensional Problems of Generalized Thermoelasticity*”, Int. J. Eng. Sci., 42, 1573(2004).

- [84] Sumi, N., “*Numerical Solutions of Thermoelastic Wave Problems by the Method of Characteristics*”, J. Thermal Stresses, 24, 509(2001).
- [85] Fox, N., “*Generalized Thermoelasticity*”, Int. J. Eng. Sci., 7, 437(1969).
- [86] Rocke, R., “*Thermoelasticity with Second Sound - Exponential Stability in Linear and Non Linear 1-D*”, Mathematical Methods in the applied Sciences, 25, 409(2001).
- [87] Mengi, Y., Turhan, D., “*Transient Response of Inhomogenous Thermoelastic Media to a Dynamic Input*”, Z. Angew Math. Physic., 29, 561(1978).
- [88] Kolyano, Yu. M., and Shter, E. I., “*Thermoelasticity of Nonhomogenous Medium*”, J. Eng. Phys., 38, 695(1980).
- [89] Kolyano, Yu. M., and Shter, E. I., “*Application of the Variational Principle to the Solution of Generalized Coupled Problems in Thermoelasticity of Inhomogenous Media*”, J. Eng. Phys., 42, 84(1982).
- [90] Sharma, J. N. and Sidha, R. S., “*On the Propagation of Plane Harmonic Waves in Anisotropic Generalized Thermoelasticity*”, Int. J. Eng. Sci., 24(9), 1511(1986).
- [91] Verma K. L., “*On the Propagation of Waves in Layered Anisotropic Media in Generalized Thermoelasticity*”, Int. J. Eng. Sci., 40, 2077(2002).
- [92] Verma K. L., Hasake, N. “*Wave Propagation in Plates of General Anisotropic Media in Generalized Thermoelasticity*”, Int. J. Eng. Sci., 39, 1739(2001).

- [93] Hawwa, M. A. and Nayfeh A. H., “*The General Problem of Thermoelastic Waves in Anisotropic Periodically Laminated Composites*”, Composites Engineering, 5(12), 1499(1995).
- [94] Turhan D., Celep, Z., Edden, Z. I. K., “*Transient Wave Propagation in Layered Media Conducting Heat*”, Journal of Sound and Vibration, 144(2), 247(1991).
- [95] Müller, I., “*The Coldness, a Universal Function in Thermoelastic Bodies*”, Arch. Rat. Mech. Anal., 41, 319(1971).
- [96] Green, A. E., and Laws, N., “*On the Entropy Production Inequality*”, Arch. Rat. Mech. Anal., 45, 47(1972).
- [97] Green, A. E., and Lindsay, K. A., “*Thermoelasticity*”, J. Elast., 2, 1(1972).
- [98] Suhubi, E. S., Thermoelastic Solids, in Continuum Physics, A. C. Eringen, Ed., Academic, New York, 2, 191(1975).
- [99] Erbay, S., Şuhubi, E. S., “*Longitudinal Wave Propagation in a Generalized Thermoelastic Cylinder*”, J. Thermal Stresses , 9, 279(1986).
- [100] Ignaczac, J. Thermal Stresses, 8, 25(1985).
- [101] Ignaczac J., “*Decomposition Theorem for Thermoelasticity with Finite Wave Speeds*” J. Thermal Stresses, 1, 41(1978).
- [102] Sherief, H. H., “*Fundamental solution for Thermoelasticity with Two Relaxation Times*”, Int. J. Eng. Sci., 30(7), 861(1992).
- [103] Sherief, H. H., “*A Thermomechanical Shock Problem for Thermoelasticity with Two Relaxation Times*”, Int. J. Eng. Sci., 32(2), 313(1994).

- [104] Payne, L. E., Song, J. C., “*Growth and Decay in Generalized Thermoelasticity*”, Int. J. Eng. Sci., 40, 385(2002).
- [105] Sherief, H. H., Megahed, F. A., “*A Two Dimensional Thermoelasticity Problem for a Half Space Subjected to Heat Sources*”, Int. J. Solids and Structures, 36, 1369(1999).
- [106] Sherief, H. H., Megahed, F. A., “*Two Dimensional Problems for Thermoelasticity with to Relaxation Times in Spherical Regions Under Axisymmetric Distributions*”, Int. J. Eng. Sci., 37, 299(1999).
- [107] Polyzos, D., Beskos, D. E., “*A New Time Domain Boundary Element formulation for Generalized Dynamic Coupled Thermoelasticity*”, Eng. Analy. with Boundary Elements, 22, 111(1998).
- [108] Choudhuri, S. K. R., Chatterjee, G., “*Radially Symmetric Temperature Rate Dependent Thermoelastic Wave Propagation in an Infinitely Extended Thin Plate Containing a Circular Hole*”, Int. J. Eng. Sci., 27(3), 251(1989).
- [109] Balta, F., Şuhubi, E. S., “*Theory of Nonlocal Generalized Theory*”, Int. J. Eng. Sci., 15, 579(1977).
- [110] Kumar, R., Deswal, S., “*Mechanical and Thermal Sources in a Micropolar Generalized Thermoelastic Medium*”, J. Sound Vib., 239(3), 467(2001).
- [111] Daneshjoo, K., Romazani, M., “*Coupled Thermoelasticity in Laminated Composite Plates Based on Green-Lindsay Model*”, Composite Structures, 55, 387(2002).
- [112] Sharma, J. N., Pathania, V., “*Generalized Thermoelastic Waves in Anisotropic Plates Sandwiched Between Liquid Layers*”, J. Sound Vib., 278, 383(2004).

- [113] Sharma, J. N., Pathania, V., “*Generalized Thermoelastic Wave Propagation in Circumferential Direction of Transversely Isotropic Cylindrical Curved Plates*”, J. Sound Vib., 281, 1117(2005).
- [114] Sharma, J. N., Sidha, R. S., “*On the Propagation of Plane Harmonic Waves in Anisotropic Generalized Thermoelasticity*”, Int. J. Eng. Sci., 24(9), 1511(1986).
- [115] Misra, J. C., Chottopadhyay, N. C., Chakravorty A., “*Study of Thermoelastic Wave Propagation in a Half Space Using GN Theory*”, J. Thermal Stresses, 23, 327(2000).
- [116] Strunin, D. V., Melnik, R. V. N., Roberts A. J., “*Coupled Thermomechanical Waves in Hyperbolic Thermoelasticity*”, J. Thermal Stresses, 24, 121(2001).
- [117] El-Karamany A. S., Ezzat, M. A., “*Analytical Aspects in Boundary Integral Equation Formulation for the Generalized Linear Micropolar Thermoelasticity*”, Int. J. of Mechanical Sciences, 46, 389(2004).
- [118] Singh, B., Kumar, R., “*Reflection of Plane Waves from the Flat Boundary of a Micropolar Generalized Thermoelastic Half-Space*”, Int. J. Eng. Sci., 36, 865(1998).
- [119] Wegner, J. L., Haddow J. B., “*Linear Thermoelasticity, Second Sound and the Entropy Inequality*”, Wave Motion, 18, 67(1993).
- [120] Hermain G. A., Wegner J. L., Su, J., Haddow J. B., “*Coupled Radially Symmetric Linear Thermoelasticity*”, Wave Motion, 25, 385(1997).
- [121] Singh, B., “*Reflection of Plane Sound Wave from a Micropolar Generalized Thermoelastic Solid Half Space*”, J. Sound Vib., 235(4), 685(2000).

- [122] Chandrasekharaiah, D., S., "Thermoelasticity with Second Sound:A Review", Appl. Mech. Re., 39(3), 355(1986).
- [123] Chandrasekharaiah, D., S., "Hyperbolic Thermoelasticity:A review of Recent Literature", Appl. Mech. Rev., 51, 707(1998).
- [124] Hetnarski, R., B, Ignazak, J., "Generalized Thermoelasticity", J. Thermal Stresses, 22, 451(1999).
- [125] Ezzat, M., El-Karamany, A., Samaan, A., "State Space formulation to Generalized Thermoviscoelasticity with Thermal Relaxation", J. Thermal Stresses, 24, 823(2001).
- [126] Ezzat, M. A., Othman, M. I., El-Karamany, A. S., "*State Space Approach to Two-Dimensional Generalized Thermo-Viscoelasticity with Two-Relaxation Times*", Int. J. Eng. Sci., 40, 1251(2002).
- [127] El-Karamany, A. S., Ezzat, M. A., "*Boundary Integral Equation Formulation for the Generalized Thermoviscoelasticity with Two Relaxation Times*", Applied Mathematics and Computation, 151, 347(2004).
- [128] Ezzat, M. A., El-Karamany, A. M. S., "*The Uniqueness and Reciprocity Theorems for Generalized Thermo-Viscoelasticity with Two Relaxation Times*", Int. J. Eng. Sci., 40, 1275(2002).
- [129] El-Karamany, A. S., Ezzat, M. A., "*Thermal Shock Problem in Generalized Thermo-Viscoelasticity under Four Theories*", Int. J. Eng. Sci., 42, 649(2004).
- [130] Ezzat, M. A., El-Karamany, A. S., "*The Relaxation Effects of Volume Properties of Viscoelastic Material in Generalized Thermoelasticity*", Int. J. Eng. Sci., 41, 2281(2003).

- [131] Aouadi, M., El-Karamany, A. S., “*The Relaxation Effects of Volume Properties in Two-Dimensional Generalized Thermo-Viscoelastic Problem*”, Applied Mathematics and Computation, 151, 689(2004).
- [132] Courant, R and Hilbert, D., “*Method of Mathematical Physics*”, Vol. 2, Interscience New York, (1966).
- [133] McNiven, H.D. and Mengi, Y., “*Propagation of Transient Cylindrical Waves in an Infinite Viscoelastic Body*”, Int. J. Solids Structures, 7, 979(1971).
- [134] Sokolnikoff, I.S., “*Mathematical Theory of Elasticity*”, Second Edition, McGraw-Hill (1956).
- [135] Fung, Y. C., Foundations of Solid Mechanics, Prentice-Hall (1965).
- [136] Timoshenko, S. P. and Goodier, J.N., Theory of Elasticity, Third Edition, McGraw-Hill (1970).
- [137] Tsai, S. W., Theory of Composite Design, Thick Composites, Dayton (1992).
- [138] Herakovich, C. T., Mechanics of Fibrous Composites, John Wiley and Sons (1998).
- [139] Turhan, D. and Şen, Ö., “*Transient Wave Propagation in Encased Viscoelastic Cylinders*”, Fifth International Conference on Mathematical and Numerical Aspects of Wave Propagation, 202(2000).
- [140] Turhan, D. and Ghaith M., “*Transient Wave Propagation in Filament Wound Cylindrical Composites*”, Fourth International Conference on Mathematical and Numerical Aspects of Wave Propagation, 459(1998).

- [141] Kamran, D. and Ramezani M., “Coupled Thermoelasticity in Laminated Composite Plates Based on Green-Lindsay Model”, *Composite Structures*, 55, 387(2002).
- [142] Thangjitham, S. and Heller, R. A., “*Stress Response of Rocket Motors to Environmental Thermal Loads*”, *J. Spacecraft*, 23, 519(1986).
- [143] Herakovich, C. T., “*Influence of Layer Thickness on the Strength of Angle-Ply Laminates*”, *J. Composite Materials*, 16, 216(1982).
- [144] Şen, Ö., Transient Dynamic Response of Encased Viscoelastic Cylinders, M.S. Thesis, Department of Engineering Sciences ,1998.

APPENDIX A

METHOD OF CHARACTERISTICS

In this appendix, the derivations of the basic equations used in the method of characteristics, namely, the characteristic equation and the canonical equations will be given. Let the system of governing 1-D partial differential equations be given in matrix form as

$$\mathbf{A}\mathbf{U}_{,t} + \mathbf{B}\mathbf{U}_{,x} + \mathbf{C} = \mathbf{0} \quad (\text{A.1})$$

where \mathbf{A} and \mathbf{B} are (mxm) square matrices, \mathbf{C} is an m dimensional vector and \mathbf{U} is m-dimensional unknown vector

$$\mathbf{U} = (U_1, U_2, U_3, \dots, U_m)^T \quad (\text{A.2})$$

The unknown field variables $U_1, U_2, U_3, \dots, U_m$ are functions of the space variable x and the time variable t . The system of governing equations, Eq. (A.1), is assumed to be linear, i.e., \mathbf{A} and \mathbf{B} are functions of x and t only and \mathbf{C} is a linear function of \mathbf{U} , i.e.,

$$\mathbf{C} = \mathbf{D}\mathbf{U} + \mathbf{E} \quad (\text{A.3})$$

where \mathbf{D} is an (mxm) matrix and \mathbf{E} is m-dimensional vector both of which are functions of x and t , only. Furthermore, comma denotes partial differentiation in

Eq. (A.1), i.e., $U_{,t} = \frac{\partial U}{\partial t}$ and $U_{,x} = \frac{\partial U}{\partial x}$.

Let $x=x(t)$ define the equation of the singular point (wave front) at which the field variables and/or their derivatives may suffer discontinuities. The plot of $x(t)$ is given in Fig. A.1. If f denotes a function of x and t , the jump of $f(x,t)$ at the singular point is defined and denoted as

$$[f] = f^+ - f^- \quad (\text{A.4})$$

where the supercripts $+$ and $-$ denote the values of the function on the disturbed and undisturbed sides of the singular point, respectively.

Now, assume that U is continuous and the first derivatives of U are discontinuous on the singular point $x=x(t)$, i.e., $[U] = 0$, $[U_{,t}] \neq 0$, $[U_{,x}] \neq 0$ on $x=x(t)$.

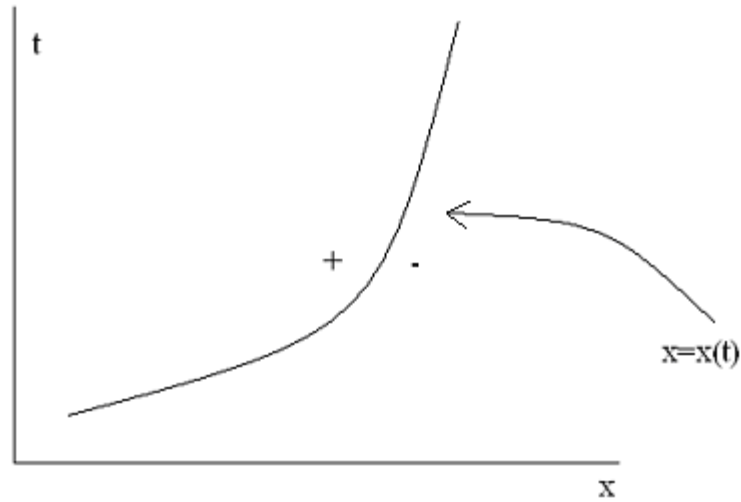


Figure A.1. Position of the singular point.

Writing Eq. (A.1) on positive and negative sides of $x=x(t)$, noting that A , B and C are continuous on $x=x(t)$, and taking the difference, we obtain on $x=x(t)$

$$\mathbf{A}[\mathbf{U}_{,t}] + \mathbf{B}[\mathbf{U}_{,x}] = \mathbf{0} \quad (\text{A.5})$$

The kinematical condition of compatibility gives on $x=x(t)$

$$\left[\frac{\partial \mathbf{U}}{\partial t} \right] = -V \left[\frac{\partial \mathbf{U}}{\partial x} \right] \quad (\text{A.6})$$

where V denotes the propagation velocity of the singular point (wave front). Substituting Eq. (A.6) into Eq. (A.5), we get

$$(\mathbf{B} - V\mathbf{A})\mathbf{W} = \mathbf{0} \quad (\text{A.7})$$

where $\mathbf{W} = [\mathbf{U}_{,x}]$. This is an eigenvalue problem and \mathbf{W} is the eigenvector and V is the eigenvalue. For non trivial solution

$$\det(\mathbf{B} - V\mathbf{A}) = 0 \quad (\text{A.8})$$

Equation (A.8) is called the characteristic equation. Solving the equation we find m roots (characteristic values), i.e, $V^{(i)} = (V^{(1)}, V^{(2)}, V^{(3)}, \dots, V^{(m)})$. If the roots are real then the system is called hyperbolic and each $V^{(i)}$ corresponds to i^{th} family of characteristic curves $C^{(i)}$. This characteristic family can be determined by solving the following equation:

$$C^{(i)} : \frac{dx}{dt} = V^{(i)} \longrightarrow x = x^{(i)}(\alpha^{(i)}, t) \quad \text{for} \quad i = 1, 2, \dots, m \quad (\text{A.9})$$

where $\alpha^{(i)}$ are integration constants. The family of the curves $C^{(1)}, C^{(2)}, \dots, C^{(m)}$ constitutes the characteristic manifold.

Now, we shall put Eq. (A.1) into canonical form. For this purpose, we define the left hand eigenvector $\mathbf{L}^{(i)}$ corresponding to $V^{(i)}$ as

$$\mathbf{L}^{(i)T} (\mathbf{B} - V^{(i)} \mathbf{A}) = \mathbf{0} \quad (i = 1 - m) \quad (\text{A.10})$$

or

$$(\mathbf{B}^T - V^{(i)} \mathbf{A}^T) \mathbf{L}^{(i)} = \mathbf{0} \quad (i = 1 - m) \quad (\text{A.11})$$

Pre-multiply Eq. (A.1) by $\mathbf{L}^{(i)T}$ ($i=1-m$) and substituting

$$\mathbf{L}^{(i)T} \mathbf{B} = V^{(i)} \mathbf{L}^{(i)T} \mathbf{A} \quad i = (1 - m) \quad (\text{A.12})$$

from Eq. (A.10), we can write

$$\mathbf{L}^{(i)T} \mathbf{A} (\mathbf{U}_{,t} + V^{(i)} \mathbf{U}_{,x}) + \mathbf{L}^{(i)T} \mathbf{C} = \mathbf{0} \quad \text{on} \quad C^{(i)} \quad (\text{A.13})$$

Noting that $V^{(i)} = \frac{dx}{dt}$ and the quantity in paranthesis in Eq. (A.13) is equal to $\frac{d\mathbf{U}}{dt}$,

we can write

$$\mathbf{L}^{(i)T} \mathbf{A} \frac{d\mathbf{U}}{dt} + \mathbf{L}^{(i)T} \mathbf{C} = \mathbf{0} \quad (\text{A.14})$$

which holds along $(dx/dt) = V^{(i)}$ ($i = 1 - m$). Eqs. (A.14) are called the canonical equations. In these equations d/dt denotes the total time derivative along the characteristic lines. Thus, through the application of the method of characteristics, the system of governing partial differential equations, Eqs. (A.1), is transformed into a system of ordinary differential equations., Eqs. (A.14), each of which is valid along a different family of characteristic lines.

APPENDIX B

MANUALS FOR COMPUTER PROGRAMS

In this study, four program are written in order to perform the calculations discussed in Chapter 2, 3 and 4, respectively. One is for the mechanical response of viscoelastic cylinders enclosed in filament wound cylindrical composites called MECHANICAL. Second is the modified form of MECHANICAL calculating the field variables for ablating inner boundary case. This second program is called MOVING-MECHANICAL. Third program is called THERMO-MECHANICAL and calculates field variables for n-layered filament wound cylindrical composites. The last program is for the thermomechanical response of viscoelastic cylinders enclosed in filament wound cylindrical composites. This program is called INVISTHERMO-MECHANICAL. The programs have similar structure and contain parts with the following functions:

INPUT: Reads the input file “INP”, writes geometric and material properties of each layer in the output file “out”.

MATRIX: Evaluates the matrices G_{ij} and H_{ij} , Eq. (2.84), Eq. (4.33), S_{ij} and Z_{ij} , Eq. (2.89), Eq. (3.43).

VECTORSOLVE: Evaluates the vector $H_{ij}U_j(A_i)$, Eq. (2.84), Eq. (4.33), $Z_{ij}U_j(A_i)$, Eq. (2.89), Eq. (3.43) and call sabroutine sol.

SUBROUTINE SOL: Solves the system of complex linear equations at every point A of the solution region.

OUT: Write the field variables in the output files 'OUT'.

B1. Input data file for MECHANICAL

The program MECHANICAL is written for non-ablating problem in Chapter 2. The input file of this program is composed of the following parts:

PO, RO, RO1

XA, DX1, DX, DT

TAU1, TAU2

G10, G1F, G20, G2F

JMAX'

ANG1, ANG2, ANG3

NU23, NU32, NU31, NU13, NU21

NU12, G23, G13, G12, E2

E3, E1

The parameters can be defined as follows;

PO: inner pressure

RO: density of viscoelastic layer

RO1: density of the orthotropic layers

XA: inner radius of the body

DX1: increment in the r-axis for the viscoelastic layer

DX: increment in the r-axis for the orthotropic layers

DT: increment in the t-axis

TAU1: relaxation time for shear moduli

TAU2: relaxation time for bulk moduli

G10: initial shear relaxation moduli

G1F: final shear relaxation moduli

G20: initial bulk relaxation moduli

G2F: final bulk relaxation moduli

JMAX: number of increments

ANG1, ANG2, ANG3: ply angles of the orthotropic layers

NU23, NU32, NU31, NU13, NU21, NU12: Poisson's ratios of orthotropic layers

G23, G13, G12: Shear moduli of orthotropic layers

E2, E3, E1: Young moduli of orthotropic layers in principal material directions

B2. Input data file for MOVING-MECHANICAL

The program MOVING-MECHANICAL is written for ablating problem in Chapter 2. The input file of this program is composed of the parts containing previous section. In addition to this parameters program needs parameter called “SLOPE”, that is the slope of the ablating boundary line.

B3 Input data file for THERMO-MECHANICAL:

The program THERMO-MECHANICAL is written for the problems in Chapter 3. The input file of this program is composed of the following parts:

XA, DX, DT, PO

TETO, TETA, JMAX

INANG, INANG1, INANG2, INANG3, INANG4

NU23, NU32, NU31, NU13, NU21

NU12, G23, G13, G12, E2

E3, E1

RO, KOND, AF, AFO

BT1, BT2, BT3, Cp

The parameters can be defined as follows;

XA: inner radius of the body

DX: increment in the r-axis for the layers

DT: increment in the t-axis

PO: inner pressure

TETO: initial uniform temperature

TETA: temperature deviation from the initial uniform temperature T_0

JMAX: number of increments

INANG, INANG1, INANG2, INANG3, INANG4: ply angles of the orthotropic layers

NU23, NU32, NU31, NU13, NU21, NU12: Poisson's Ratios of orthotropic layers

G23, G13, G12: Shear moduli of orthotropic layers

E2, E3, E1: Young moduli of orthotropic layers in principal material directions

KOND: conductivity of first orthotropic layer

B4 Input data file for INVISTHERMO-MECHANICAL:

The program INVISTHERMO-MECHANICAL is written for the problems in Chapter 4. The input file of this program is composed of the following parts:

XA, DT

TETO, JMAX, PO

TETA

DX1, KONDV

G10, G1F, RO1

AFT1, AF1, Cp1, AFO1

BULK1

TAU1

DX

INANG, INANG1, INANG2

NU23, NU32, NU31, NU13, NU21, NU12

G23, G13, G12, E2

E3, E1

RO, AF, AFO

BT1, BT2, BT3, Cp

KOND

The parameters can be defined as follows;

XA: inner radius of the body

DT': increment in the t-axis

TETO: initial uniform temperature

JMAX: number of increments

PO: inner pressure

TETA: temperature deviation from the initial uniform temperature T_0

DX1: increment in the r-axis for the viscoelastic layers

KONDV: conductivity of viscoelastic layer

G10: initial shear relaxation moduli for viscoelastic layer

G1F: final shear relaxation moduli for viscoelastic layer

RO1 density of inner viscoelastic layer

AFT1 thermal expansion coefficient of viscoelastic layer

AF1, AFO1: thermal relaxation times for viscoelastic layer

Cp1: specific heat for viscoelastic layer

BULK1: bulk moduli for viscoelastic layer

TAU1: relaxation time for shear moduli for viscoelastic layer

DX: increment in the r-axis for the orthotropic layers

INANG, INANG1, INANG2: ply angles of the orthotropic layers.

NU23, NU32, NU31, NU13, NU21, NU12: Poisson's Ratios of orthotropic layers

G23, G13, G12: Shear moduli of orthotropic layers

E2, E3, E1: Young moduli of orthotropic layers in principal material directions

RO: density of orthotropic layers

AF, AFO: thermal relaxation times for orthotropic layers

BT1, BT2, BT3: Elements of thermoelasticity tensor.

Cp: specific heat for orthotropic layers

KOND: conductivity of orthotropic layers

CURRICULUM VITAE

PERSONAL INFORMATION :

Surname : ŞEN

Name : Özge

Date of birth : 10 October 1972

Place of birth : Ankara - TURKEY

Nationality : Turkish

Permanent address : Güneş Sitesi 5. Blok No:8
Yaşamkent Mah./Çayyolu
Ankara ,TURKEY Tel: +90 (312) 242 05 66
Mobile Tel: +90 (532) 223 88 06

Work address : TÜBİTAK-SAGE
Turkish Scientific & Technical Research Council
Defense Industries Research & Development Institute
P.K. 16, 06261 Mamak – ANKARA / TURKEY
Tel: +90 (312) 590 91 33
Fax: +90 (312) 590 91 48-49
E-mail: osen@sage.tubitak.gov.tr

Marital status : Married

PROFESSION:

Physics, B.Sc., Engineering Science, M.Sc., METU

EDUCATION :

<i><u>School</u></i>	<i><u>Years/Diploma, Subject</u></i>
<i><u>Primary School</u></i>	
Hamdullah Suphi İlkokulu Emek, Ankara, TÜRKİYE	1978 – 1983 (Primary School Diploma)
<i><u>Secondary School</u></i>	
Bahçelievler Ortaokulu Emek, Ankara, TÜRKİYE	1983 – 1986 (Secondary School Diploma)
<i><u>High School</u></i>	
Cumhuriyet Lisesi Emek, Ankara, TÜRKİYE	1986 – 1989 (High School Diploma /in math. & science division)
<i><u>University</u></i>	
METU Department of Physics İnönü Blv., Ankara, TÜRKİYE	1989 – 1994 (B.Sc. , Solid State Physics)
METU Department of Engineering Sciences İnönü Blv., Ankara, TÜRKİYE	1995 – 1998 (M.Sc. , “Computational Mechanics”, Transient Dynamic Response of Encased Viscoelastic Cylinders)

METU	1999 – 2005
Department of Mechanical Engineering	(Phd. , “Computational Mechanics”, Transient
İnönü Blv., Ankara, TÜRKİYE	Dynamic Response of Viscoelastic Cylinders Enclosed in Filament Wound Cylindrical Composites)

LANGUAGE SKILLS :

Native Language : Turkish
Other Languages : English

PUBLICATIONS:

- Ö. Şen, Transient Dynamic Response of Encased Viscoelastic Cylinders, MSc Thesis, Department of Engineering Sciences, METU, September 1998.
- Ö. Şen, Failure Analysis of Solid Propellant Rocket Motor Nozzle, ANSYS Users Seminar, October 1999.
- D. Turhan, Ö. Şen, Transient Wave Propagation in Encased Viscoelastic Cylinders, SIAM 2000, pp. 202-207.
- Ö. Şen, D. Turhan, Dynamic Response of Viscoelastic Cylinders Enclosed in Filament Wound Cylindrical Composites, EUROMECH 2003, pp. 87 Abstract Booklet.

TECHNICAL TRAINING AND SEMINERS :

- Viscoelasticity and Viscoplasticity -Relaxation Processes in Glass-, Anton Matzenmiller, Institut für Mechanik of the Fachbereich 15 University Gesamthochschule Kassel Mönchebergstr. 7 34109 Kassel, October 1999, METU, ANKARA, TURKEY.
- Engineering Knowledge in Crack Initiation and Growth in Metallic and Composite Materials, Dr. Bob CARLSON, Georgia Institute of Technology, June, 19 2001, TAI, ANKARA, TURKEY.
- French-Turkish Symposium on Composite Materials, November, 26-27 2001, İTÜ Maden Fakültesi, İSTANBUL, TURKEY.
- Basic Quality Concepts & Institution Culture
TÜSSİDE Gebze, Kocaeli, TURKEY, March-2002
- Heat Transfer Analysis for defense, aerospace and electronic Industries and Infrared Radiation Signature, Ralph Habig, Thermo-Analytic Inc. September 20 2002, METU, ANNKARA, TURKEY
- Strain Gage Seminar– BİAS Engineering – 2003, TÜBİTAK_SAGE, ANKARA, TURKEY
- Passive Thermal Control – Dr. Mehmet ARIK, Dr. Ad Delil, Dr. Volodymyr Baturkin, Dr. Boris KOSOY, September 22-24 2003, ANTALYA, TURKEY.
- PAT 301-302 Seminar –Bias Engineering – 2004, TÜBİTAK-SAGE, ANKARA TURKEY.

WORK EXPERIENCE :

<i>Organization</i>	<i>Years</i>	<i>Job</i>
<i>METU</i>		
Department of Civil Engineering İnönü Blv., Ankara, TÜRKİYE	Aug. 1995 – Sep. 1998	Research Assistant

<i>Organization</i>	<i>Years</i>	<i>Job</i>
<i>TÜBİTAK-SAGE</i>		
Structure Mechanics Ankara, TÜRKİYE	Sep. 1998 –	Senior Research Engineer

COMPUTER EXPERIENCE:

<i>Mathematical Software:</i>	Matlab, Mathcad vs.
<i>Technical Software:</i>	ANSYS, MARC, PATRAN, NASTRAN,
AUTOCAD	
<i>Programming Language:</i>	FORTRAN, PASCAL.
<i>Graphical Software:</i>	Photoshop, Paint Shop Pro
<i>Project Management Software:</i>	MS Project